THE MEASUREMENT AND INTERPRETATION OF SMALL STRAIN STIFFNESS OF SOILS

by

Vojkan Jovičić

A Thesis submitted for the Degree of
Doctor of Philosophy

THE CITY UNIVERSITY
Civil Engineering Department

February 1997

To my parents Života and Dušanka and to my wife Nataša

CONTENTS

LIST OF TABLES

LIST OF FIGURES

ACKNOWLEDGEMENTS

The four years I spent at City University were challenging, demanding and productive. In short, a great time. To do research in an environment in which the opinions are openly discussed and new ideas are encouraged is a privilege for which I am indebted to Professor John Atkinson in general and in particular as he made my initial stay at City possible. The last three years of the research, which makes up the content of this thesis, has been funded by EPSRC to whom I am grateful for their support.

I would like to thank to my advisor Dr Matthew Coop for his constant encouragement and support throughout the project, in particularly in the laboratory where his assistance was the most valuable. In terms of consultancies these included Sunday morning wake up calls from the laboratory when yet another high pressure test went wrong and long conversations over long distances.

I would also like to thank Dr Sarah Stallebrass who supervised my work on finite element analyses for her friendly support during all these years and Professor Neil Taylor for his support and comments which arrived, somehow, when they have been needed the most. Special thoughts go to Dr Colin Abbiss for fruitful discussions and friendship we shared in the last two years. I would like to thank warmly Mr Keith Osborne, Mr Reg Allen and especially Mr Lloyd Martika who used their technical skills to help me through the most difficult bit, that is, to bridge the gap between ideas and reality.

DECLARATION

I grant powers of discretion to the University Librarian to allow this thesis to be copied in whole or in part without further reference to me. This permission covers only single copies made for study purposes, subjected to normal conditions of acknowledgement.

ABSTRACT

The measurement of soil stiffness at very small strains (G_{max}) has been carried out under both dynamic and continuous loading in the triaxial apparatus up to high stresses. A new system of LVDTs has been used to measure axial strain locally during continuous loading while dynamic stiffnesses were measured using bender elements. Using the two methods good agreement was found between the stiffnesses at 0.0001% strain for two different materials.

Bender elements measure the propagation time of shear waves through a soil sample so that the value of G_{max} can be determined. The design of the bender element configuration in the triaxial apparatus has been improved so that the reduction in the electrical noise resulted in a high quality of received signal. Bender elements were also incorporated into high pressure triaxial cells and were used to test very stiff soils for the first time. Theoretical studies and dynamic finite element analyses are presented which have been carried out to develop more objective criteria for the determination of G_{max}. Several techniques have been proposed for simple and direct measurement of the arrival time of the shear wave to an accuracy of $\pm 1\%$.

The thesis presents the results of bender element tests examining the variation of G_{max} for sands, which is then related to the stiffness at larger strains determined under continuous loading using the new system of LVDTs. Three sands with very different geological origins were tested over a wide range of stresses allowing a general framework for stiffnesses to be established. The interpretation of the results is based on the correct normalisation of the data by which means unique relationships have been derived for each soil. The framework demonstrates that the confining stress and volumetric state relative to the normal compression line are the principal controlling factors of stiffness as they would be for clays. However, the framework distinguishes that for sands the means of arriving at its initial volume stress state are also important, in particular whether this is by overconsolidation or compaction.

The thesis also presents results of bender element tests examining the anisotropy of G_{max} of both natural and reconstituted clays. The work investigates both the stress induced and inherent components of G_{max} anisotropy related to an axi-symmetric stress state or cross anisotropy of the soil fabric. The results show that the stress induced anisotropy of soils is generally small for an axi-symmetric stress state while significant inherent anisotropy was found in natural London clay. The same degree of inherent anisotropy has been reproduced by anisotropic straining of reconstituted London clay suggesting that the inherent anisotropy is a variable factor related to the strain history. The rate of change was, however, found to be very small so that when an isotropic stress regime was applied the G_{max} anisotropy persisted long after the plastic strain increments became isotropic.

Finally, finite element analyses were carried out using the 3 SKH model (Stallebrass, 1990b) to investigate the influence of G_{max} on calculated ground movements. The analyses consisted of parametric studies of the stress-strain behaviour of a triaxial sample, the load deflection behaviour of a foundation and the ground movements around a tunnel. Although constrained by the limitations of the model the analyses offer an insight into the behaviour which can be also important for a general understanding of the behaviour of real soils. The studies highlighted that the assessment of the importance of G_{max} on the stress strain behaviour should consider all the relevant factors which control the non linearity of soil's response, in particular the recent stress history of the soil and the geometry of the boundary value problem.

LIST OF SYMBOLS

A	a constant in a power law relationship between G_{max} and p' for normally consolidated soil
A(T)	empirical material constant in Equation 2.16
A_s	a constant in a power law relationship between G and p' for normally consolidated soil at any particular strain
A_0	initial area of a triaxial sample
A_c	current area of a triaxial sample
B	Skempton's pore pressure multiplier
B_t	total breakage
B_p	breakage potential
B_r	relative breakage
C	empirical material constant in Equation 2.22
D_0	initial diameter of a triaxial sample
E	Young's modulus
E_{max}	Young's modulus at very small strains
E_v	Young's modulus in vertical direction for a cross anisotropic soil
E_h	Young's modulus in horizontal direction for a cross anisotropic soil
E^*	equivalent Young's modulus for a cross anisotropic soil
F(e)	void ratio function
F	deviatoric force measured by the load cell in the triaxial apparatus
F_A	foundation load calculated for a characteristic material A
G	tangent shear modulus
G_{max}	shear modulus at very small strains
G^{ij}_{max}, G_{ij}	shear modulus at very small strain for a cross anisotropic material measured by bender element method (i direction of wave propagation, j- direction of polarisation)
G_{hh}	shear modulus in horizontal plane for a cross anisotropic soil
G_{vh}, G_{hv}	shear moduli in either vertical plane for a cross anisotropic soil
G_u	shear modulus for undrained loading
G_s	specific gravity
H_0	initial height of a triaxial sample
I_v	void index
K	bulk modulus
K_u	bulk modulus for undrained loading
K_0	coefficient of earth pressure at rest
K^*	equivalent bulk modulus for a cross anisotropic soil

L_a, d	length of travel path for the shear wave
M_w	mass of water in a triaxial sample
M_s	mass of solids in a triaxial sample
OCR	overconsolidation ratio in terms of vertical effective stress
R_0	overconsolidation ratio defined as p'_p/p'
R_d	ratio between the shear wave travel distance and the wavelength
S, S_{ij}	empirical material constant in Equations 2.18 and 2.19, respectively
T, t	time
T_p	period of oscillation
T_a	travel time of a shear wave
TT	ratio of the size of the yield surface in the 3-SKH model
TS	ratio of the size of the history surface in the 3-SKH model
U	transverse motion of a point
V_0	initial volume of a triaxial sample
V_s	volume of solids in a triaxial sample
W_s	dry wight of solids in a triaxial sample

e	voids ratio
e^*_{100}	voids ratio at a vertical effective stress of 100kPa for a reconstituted soil on normal compression line
e^*_{1000}	voids ratio at a vertical effective stress of 1000kPa for a reconstituted soil on normal compression line
f	frequency
i	the distance from the centre line of a tunnel to the point of inflection of the Gaussian curve
k	empirical material constant in Equation 2.17
m	a coefficient in a power law relationship between R_0 and G_{max} for overconsolidated soil
n	a coefficient in a power law relationship between G_{max} and p' for normally consolidated soil
n_p	porosity
n_s	a coefficient in a power law relationship between G and p' for normally consolidated soil at any particular strain
p'	mean effective stress
p_a	atmospheric pressure
p_r	reference pressure (1kPa)
$2p'_o$	mean effective pressure at the intersection of the current swelling line with the normal compression line
p'_p	mean effective stress used in the calculation of R_0 as shown in Fig. 1.2
p'_e	equivalent mean effective stress
q	deviatoric stress
u	displacement

v	specific volume
v_λ	specific volume of overconsolidated soil projected to p' 1kPa
v_{cs}	specific volume at critical state
v_p	velocity of the compressive wave
v_s	velocity of the shear wave
v^{ij}_s	velocity of shear wave for a cross anisotropic material measured by bender element method (i- direction of wave propagation, j- direction of polarisation)
w	water content
x, y, z	cartesian coordinate axis
Γ	specific volume of soil on the critical state line at p' 1kPa
Γ_a	analytical solution for the propagation of body waves
Δ, δ	increment of
M	slope of critical state line projected to q:p' plane
N	specific volume of normally consolidated soil at p' 1kPa
α	degree of anisotropy of a cross-anisotropic soil
ε	strain
ε_a	axial strain
ε_r	radial strain
ε_s	shear strain
ε_v	volumetric strain
η	q/p'
κ	slope of the swelling and recompression line in the v:lnp' plane
λ	slope of the normal compression line and the critical state line in the v:lnp' plane
λ_w	wave length
ν	Poisson's ratio
ν^*	equivalent Poisson's ratio for a cross anisotropic soil
ν_{hh}	Poisson's ratio in horizontal plane of a cross anisotropic soil
ν_{vh}	Poisson's ratio in vertical plane of a cross anisotropic soil
ρ	mass density
ρ_s	mass density of solids
ρ_a	coefficient of added mass density to account for the fluid inertia
ρ_f	mass density of pore fluid
ρ_T	total mass density
σ'	normal effective stress

σ'_a	axial effective stress
σ'_r	radial effective stress
σ'_i	normal effective stress acting in the i direction
τ	shear stress
τ_{ij}	shear stress acting in the i:j plane
θ	angle of the stress path rotation
τ_s	tortuosity
ψ_i	state parameter for sands
ψ	exponent in the hardening modulus for the 3 SKH model
ω	angular velocity
ω_i	component of rotation around the axis i

1.1 BACKGROUND TO THE PROJECT

The research described in this thesis investigated the stiffness of soils at very small and small strains. Assessing the characteristic stress strain behaviour of soils for monotonic loading Atkinson & Sallfors (1991) distinguished three ranges of shear strain (Fig. 1.1). At very small strains which are generally less than a yield strain ε_c of 0.001% the shear modulus G is nearly constant with strain. For small strains which are generally less than an arbitrary limit of around 1% the tangent shear modulus G is a non-linear function of strain. The large strain zone exceeds 1% and the shear stiffness is very small as the soil approaches failure.

Very small strains are typically associated with the soil response to dynamic loading, but it is now well established that small strain behaviour also plays an important role in soil response to static loading. Simpson (1992), Burland (1989) and others showed that the strain level around engineering structures is in the range of very small to small strains (up to around 0.2%) emphasising the importance of evaluating the decay of stiffness with strain. The benchmark parameter of this characteristic stiffness-strain curve for any soil which is not currently yielding is the very small strain shear modulus or G_{max} which is sometimes also referred to as G_0.

Values of G_{max} can be measured in the laboratory using resonant column tests or other dynamic tests based on wave propagation methods. In this research G_{max} was determined from the results of bender element tests which measured the propagation time of a shear wave passing through the soil sample. An attempt was made to improve the design of bender element configuration in the triaxial apparatus and theoretical and numerical studies were carried out (Section 3.4) to remove the subjectivity in measuring the propagation time. Bender elements were also incorporated into high pressure triaxial cells. Stiffnesses were also determined from continuous loading tests in which the measurement of very small strains was carried out using local axial displacement transducers attached directly to the sample following techniques developed by Cuccovillo & Coop (1997).

The topic on which most effort in the research has been focused is the investigation and interpretation of the small strain stiffness behaviour for coarse grained soils (Chapter 4). Previous research work on sands indicated that G_{max} varies with the current stress and stress history of the soil (Hardin & Richart, 1963; Hardin & Blandford, 1989). However, it is important to note that the majority of these tests were carried out at moderate stresses which prevented researchers relating their findings

with fundamental material parameters which can only be identified at significantly higher pressures as will be shown later. In consequence, a general framework for the stiffness behaviour of sands has not, so far, been established. This research was, therefore, designed to test sands at considerably higher pressures than before with the aim of relating the stiffnesses not only to the confining stress but also to the current volumetric state of the soil. Three reconstituted sands with very different geological origins were tested and an attempt has been made to establish a new general framework for the stiffness of sands. The influence of bonding on G_{max} of a cemented sand has been also investigated within the framework.

Using polarised seismic body waves under biaxial confinement, Roesler (1979) and Stokoe et al., (1985) showed that G_{max} is a directional property so when related to the current stress state it depends only on the principal stresses which act in the plane of deformation. In Chapter 5 this stress induced effect on G_{max} anisotropy has been investigated for reconstituted clays under anisotropic axi-symmetric stress states. Some aspects of structural anisotropy were also assessed and contrasted with the stress induced anisotropy. By testing reconstituted clays using bender elements incorporated in stress-path triaxial cells, Viggiani & Atkinson (1995b) established a framework for G_{max} in fine grained soils relating the stiffness to the state and nature of the soil. They showed that G_{max} is related to the current mean effective stress and overconsolidation ratio and assessed the influence of the plasticity of soil on these relationships. The influence of high overconsolidation ratio on G_{max} has also been examined in Chapter 5.

The very small and small strain stiffness is thought to be particularly relevant for the prediction of soil behaviour at small strains and is required for most non-linear soil models. Although the work in this thesis was focused on the measurement and interpretation of the small strain stiffness behaviour of soils a limited attempt has been made to assess the importance of G_{max} on calculated ground movements (Chapter 6). For this purpose a series of finite element analyses in the form of parametric studies were carried out using a kinematic hardening model, (3-SKH), developed by Stallebrass (1990b). The soil model used in the analyses was evaluated only for small strain behaviour of overconsolidated clays (Stallebrass & Taylor, 1997) so no attempt was made to model the behaviour of sands.

In summary, the main objectives of the research were:

(i) The improve the design of the bender element configuration in the triaxial apparatus and to install it into high pressure cells

(ii) To develop objective criteria for the determination of propagation time from the bender element method

(iii) To evaluate variations of G_{max} with stress, overconsolidation and specific volume for three different sands

(iv) To extend the work in (iii) above to develop a general framework for G_{max} in coarse grained soils

(v) To investigate the influence of anisotropic axi symmetric stress state and anisotropic soil fabric on G_{max} for clays

(vi) To examine the influence of G_{max} on calculated ground movements by parametric studies using finite element method and the 3-SKH model

1.2 THEORETICAL FRAMEWORK

The general stress parameters which are independent of the choice of coordinate axis are called stress invariants. When expressed using principal effective stresses confined to the triaxial plane where σ'_1 σ'_a and $\sigma'_2=\sigma'_3=\sigma'_r$ these are given as the mean effective stress:

$$p' = \frac{1}{3}(\sigma'_a + 2\sigma'_r) \qquad 1.1$$

and the deviator stress:

$$q = (\sigma'_a - \sigma'_r) \qquad 1.2$$

where σ'_a and σ'_r are the axial and radial effective stress respectively. The strain invariants which correspond to the stress invariants defined above are given as the volumetric strain:

$$\varepsilon_v = \varepsilon_a + 2\varepsilon_r \qquad 1.3$$

and the shear strain:

$$\varepsilon_s = \frac{2}{3}(\varepsilon_a - \varepsilon_r) \qquad 1.4$$

where ε_a and ε_r are the axial and radial strains respectively. For axi symmetric stress conditions acting on a triaxial sample, the state of the soil will be described by the stress invariants p', q and the specific volume v (Schofield & Wroth, 1968) where v is the volume in space occupied by a unit volume of soil grains. It can be shown that:

$$\delta\varepsilon_v = -\frac{\delta v}{v} \qquad 1.5$$

where $\delta\varepsilon_v$ and δv are increments of volumetric strain and specific volume respectively. For isotropic and elastic materials confined to the triaxial plane the general constitutive equations are given by:

$$\begin{bmatrix}\delta\varepsilon_v \\ \delta\varepsilon_s\end{bmatrix} = \begin{bmatrix}\frac{1}{K} & 0 \\ 0 & \frac{1}{3G}\end{bmatrix}\begin{bmatrix}\delta p' \\ \delta q\end{bmatrix} \qquad 1.6$$

where K and G are the bulk modulus and shear modulus, respectively, both defined for effective stresses. If undrained, the elastic deformation is then considered as:

$$\begin{bmatrix}\delta\varepsilon_v \\ \delta\varepsilon_s\end{bmatrix} = \begin{bmatrix}\frac{1}{K_u} & 0 \\ 0 & \frac{1}{3G_u}\end{bmatrix}\begin{bmatrix}\delta p \\ \delta q\end{bmatrix} \qquad 1.7$$

Since there is no change in volume in undrained conditions for a saturated soil:

$$\delta\varepsilon_v = \frac{\delta p}{K_u} = 0 \qquad 1.8$$

so the undrained bulk modulus K_u is infinite. The deviator stress is independent of pore pressure and so is the deviatoric strain $\delta\varepsilon_s$ so that the undrained shear modulus G_u equals G. For soils deforming plastically the matrix of constitutive equations (Equation 1.6) will have non zero off-diagonal elements which implies coupling between the deviatoric and volumetric behaviour.

The experimental results in this thesis will be presented on the basis of the framework of critical state soil mechanics (Schofield & Wroth, 1968). It is understood that this framework describes a model of soil behaviour which it is possible to modify and extrapolate so that the constitutive relations used conform better with the behaviour of the real soil. The change of volume of normally consolidated soils during isotropic compression is assumed to be caused by the rearrangement of the particles. It is also assumed by the model that the change is linear in v:lnp' space (Fig. 1.2) so that the isotropic normal compression line is given by:

$$v = N - \lambda \ln p' \qquad 1.9$$

The change of volume during a cycle of unloading and reloading is also idealised by a straight swelling line in v:lnp' space so that:

$$v = v_k - \kappa \ln p \qquad 1.10$$

In the equations above N and v_k are the values of v for the normally consolidated and overconsolidated soil respectively at p' 1kPa. The values of λ and κ are the gradients of the isotropic normal compression line and the swelling lines, respectively.

The overconsolidation ratio describes the state of the soil by its distance from the isotropic normal compression line so that it is defined as:

$$R_o = \frac{p'_p}{p'} \qquad 1.11$$

where p'_p is the past maximum value of p'. For normally consolidated soil R_0 equals 1. The value of p' is often normalised with respect to an equivalent effective stress on the isotropic normal compression line p'_e (Fig. 1.2) where:

$$p'_e = \exp\left(\frac{N - v}{\lambda}\right) \qquad 1.12$$

The value of p'/p'_e is analogous to R_0 and can also be used as a state variable.

An additional assumption of the framework is that all possible soil states in p':q':v space are bounded by the state boundary surface. It is also assumed that soil when sheared will ultimately reach continuous plastic deformation where would be no further change of its state. This is defined as the critical state by Schofield & Wroth (1968). For a given soil, the critical state line is a unique line in p':q':v space and is defined by its projections in the v:lnp' plane and p':q' planes so that:

$$v = \Gamma - \lambda \ln p' \qquad 1.13$$

$$q = Mp' \qquad 1.14$$

where M is the gradient of the critical state line and Γ is the value of specific volume on the critical state line taken at p' 1kPa. The values of N, Γ, λ, κ and M are considered as material parameters for a given soil. An example of a state boundary surface in the p':q' plane is given in Fig. 1.3 which shows the ellipse defined by the Modified Cam Clay model (Roscoe & Burland, 1968).

Although originally developed for clays the framework of critical state soil mechanics was applied as a useful tool within which the behaviour of sands was examined (e.g. Coop 1990, Coop & Lee 1993) as will be discussed in greater detail in Chapter 2. Even though particle breakage was recognised as the principal mechanism for plastic deformation which

is a different process than that for clays, Coop & Lee (1993) identified critical state parameters for three different sands. Been & Jefferies (1985) emphasised the importance of the state of a sand relative to the critical state line in the v:lnp' plane showing that as for clays this is a principal factor determining the strength of the soil. A second principal difference between sands and clays is that clays reach a given state only through preconsolidation while for sands a change of state may be reached also through compaction. Coop (1990) showed that a sand sample which had been truly overconsolidated had a different stress strain behaviour from a sample which had reached the same state through compaction and first loading. This distinction between compacted and overconsolidated samples will be followed in interpreting the experimental results for sands in this thesis.

CHAPTER 2 LITERATURE REVIEW

2.1 INTRODUCTION

This literature review examines the research work in two main areas. These are the development of experimental techniques for the measurement of soil stiffness in the laboratory and the current knowledge of the dependence of soil stiffness on the stress-volume state and structure of a soil. Additionally, the mechanics of granular materials and numerical modelling of soil behaviour are reviewed to the extent to which they are relevant to the present project.

The review of experimental techniques in the laboratory (Section 2.2) focuses on the determination of stiffness from the local measurement of strains during continuous loading. In addition, emphasis is given to dynamic loading tests for the evaluation of stiffness. The theoretical background of pulse propagation methods through saturated porous media is also examined because of its relevance to the measurement technique used in the research.

The experimental evidence for the dependence of soil stiffness on the current stress-volume state and corresponding theories are examined and discussed in Section 2.3. These theories and some relevant elements of the theory of the mechanics of granular materials presented in Section 2.5 will be used as a framework for the interpretation of experimental results from tests on coarse grained soils given in Chapter 4. In Section 2.4 recently established knowledge of the influence of structure on the small strain stiffness has been reviewed and considered in order to avoid repetition of research work. In addition, the current understanding of the influence of the anisotropic fabric on stiffness is presented for comparison with the experimental findings of this research given in Chapter 5. Finally kinematic hardening models developed for the prediction of soil stress-strain response have been reviewed in Section 2.6. This type of model was considered as suitable for the assessment of the importance of very small strain stiffness on calculated ground movements, the research work presented in Chapter 6 of this thesis.

2.2 MEASUREMENT OF SOIL STIFFNESS IN THE LABORATORY

2.2.1 Evaluation of stiffness from measurements of strain

Accurate determination of soil stiffness at small strains is rarely achieved in routine laboratory testing. Conventionally, the determination of the stiffness of a triaxial sample is based on external measurements of displacement between the axial loading ram and the triaxial cell. The

sources of error involved in the external measurement of axial displacement are shown in Fig. 2.1. The principal errors are; seating errors due to the closing of gaps between the internal load cell and platen and the porous stones and platens, errors which result from the misalignment of the axial loading system and specimen, bedding errors caused by irregular or disturbed sample ends and compliance errors which may occur in the internal load cell, as shown in the diagram, but also in the loading system.

Misalignment arises from the improper positioning of the specimen or its ends not being perpendicular to its axis. Atkinson & Evans (1985) suggested that forcing the specimen into alignment using a rubber suction-cap to connect the top platen to the internal load cell at an early stage of consolidation reduces substantially the misalignment errors during shearing. Using this method and an accurate calibration of the compliance of the system the authors reached an accuracy of the external measurement of axial strain of ±0.01%.

Even when measured locally the axial strains are still prone to an error due to misalignment leading to non-uniform stresses within the sample. In the testing of rock samples the importance of such errors has long been recognised (Vogler & Kovari, 1978) so that there are specifications for the flatness and parallelism of the sample ends in sample preparation. For the stiffest soils and soft rocks the samples are usually so stiff at low stress levels that the deformation of the soil can be similar to that of the apparatus so that the local measurement of axial strains becomes essential, as emphasised by Cuccovillo & Coop (1997). In this case even when the data are corrected for compliance the external measurements are meaningless, as shown in Fig. 2.2. Differences between the external and local measurements of axial strain can also be caused by the effect of restraint of the sample ends and consequent barrelling of the sample at larger strains. Ideally the measurement of local axial strain should be made over the central third of the specimen so that end restraint effects are minimised (Kirkpatrick & Younger, 1970).

Errors due to seating, bedding and compliance of the system can be eliminated by measuring the axial displacement inside the cell. There has been a large number of techniques developed in the last two decades. These include imaging techniques such as X ray radiography (Balasubramanian, 1976) and optical methods (Atkinson, 1973). In general, however, the local measurements of axial strains can be divided into non contacting methods such as use of proximity transducers (Hird & Yung, 1987) and contacting methods such as linear variable differential transformers or LVDTs (Brown & Snaith, 1974; Costa Filho, 1985; Cuccovillo & Coop, 1997), inclinometers of the electrolevel or pendulum designs (Burland & Symes, 1982; Jardine et al., 1984; Ackerley et al., 1987), Hall effect transducers (Clayton & Khathrush, 1986) and strain

gauged local deformation transducers (LDTs) (Goto et al., 1991). Typically, these transducers gave a smallest measurable strain of around 0.001% except in the cases of Goto et al., (1991) and Cuccovillo & Coop (1997) where an accuracy about an order of magnitude better was achieved. Scholey et al., (1995) made a comprehensive review of the techniques used for the measurement of axial strains inside the cell (Table 2.1). They compared the advantages and disadvantages of the various transducers used in contacting techniques. Some had the inconvenience of a non-linear calibration (LDTs, inclinometers), a limited working range (Hall effect transducers, LDTs), were difficult to set-up (proximity transducers) or in the case of the inclinometers were sensitive not only to axial strains but also to rigid body rotation.

At City University Hall effect transducers developed by Clayton & Khathrush (1986) have commonly been used to measure axial strains locally. As will be discussed later the smallest strain which can be accurately measured by this transducer is about ±0.002% which is not satisfactory for the measurement of very small strains. Recent work by Cuccovillo & Coop (1997) at City University highlighted the use of LVDTs for the local measurement of axial strains as a transducer which is more accurate than current devices. In a comparative study Scholey et al., (1995) showed that LVDTs were less affected by temperature fluctuations, electrical noise and drift than the other contact transducers. LVDTs also benefit from linear calibration and virtually infinite resolution. The use of both Hall effect transducers and LVDTs is explained in more detail in Section 3.2.1.

Stiffness is derived from both strain and stress measurements so adequate accuracy of stress measurements is also required to resolve the stiffness at small strains. In the case of an internal load cell which is in direct contact with the sample high quality signal conditioning is therefore required. In the calculation of derived quantities from triaxial tests such as the shear strains during drained shearing a consistent set of axial and radial strains is needed, i.e. these strains should be measured both either locally or externally. In the latter case the radial strain is often simply calculated from the measurements of axial and volumetric strain by assuming that the sample preserves its cylindrical shape during deformation.

Radial strains are usually measured locally at the mid-height of the specimen. Transducers for the local measurement of radial strain have long been available. LVDTs (Brown & Snaith, 1974) and Hall effect transducers (Clayton et al., 1988) have been used on radial strain belts or callipers while proximity transducers (Hird & Yung, 1989) have been used to measure the radial displacement directly. They are however in less frequent use than local axial devices. This may be attributed to the fact that they are often difficult to set-up and often cannot resolve the smallest strains accurately because of the membrane compression.

2.2.2 Dynamic methods for the determination of soil stiffness

In engineering practice the results of dynamic tests performed both in the laboratory and in the field have been traditionally used only for the design of dynamically loaded structures. Dynamic methods for determination of soil stiffness established in the laboratory in the 1960s are now being re-evaluated and used for the measurement of design parameters also for statically loaded soil structures. The methods currently available in the laboratory may be divided into harmonic and wave propagation methods. In both methods the soil sample is subject to dynamic excitation and from its response the soil properties are evaluated.

The most common test based on a harmonic method is the resonant column test. In the resonant column apparatus the cylindrical sample is made to oscillate at a frequency corresponding to the first mode of its natural frequency thereby experiencing resonance (Richart et al., 1970). It is assumed that the strains imposed on the sample are very small so that soil response is elastic. The soil sample is excited either longitudinally or torsionally and the wave velocity is determined from the resonant frequency and the dimensions of the specimen. From the resonant frequency for the longitudinal and torsional propagation the Young's modulus, E_{max} and shear modulus, G_{max} are determined, respectively. From the amplitude of the motion the corresponding strains can also be calculated. Starting from a resonant condition the excitation can be switched off and the free vibration of the sample monitored to determine the damping characteristics.

The difficulty with the resonant column test is that both the driving apparatus used for the excitation of the specimen and the motion monitoring instruments must be attached to the specimen. This alters the specimen boundary conditions so that the interpretation of the test is based on the assumption that the attachments are lumped into a mass which oscillates with the specimen. There is a variety of designs of resonant column apparatus which differ in the type of boundary conditions imposed on the sample. The most common design shown in Fig. 2.3 is with the sample base fixed while the top is free to vibrate in torsion.

Drnevich (1972) developed a resonant column apparatus to test a specimen of hollow cylindrical shape so that the sample could be exposed to stress states out of the triaxial plane. Isenhower (1979) added a torsional shear device to the resonant column apparatus. In the torsional shear test the sample is subjected to a given number of low frequency cycles of torsional load and the soil stiffness is obtained directly from the torque-twist relationship.

Resonant column tests can be used to evaluate soil stiffness at shear strain amplitudes as low as 10^{-5}%. When the strain amplitude exceeds the strain level within which the soil behaviour is elastic the interpretation of the tests is necessarily based on additional assumptions of non-linear soil response (Drnevich, 1978; Papa et al., 1989). Results from resonant column tests have been found to be generally consistent with results from other tests based on wave propagation methods (Dyvik & Madshus, 1985). Georgiannou et al., (1991) showed a good agreement between undrained monotonic shearing tests in the triaxial apparatus and resonant column tests carried out on the same soil, as shown in Fig. 2.4.

Wave propagation methods are based on the theory of propagation of waves through an infinite isotropic elastic medium. The equilibrium of forces acting on an infinitesimal element in motion (Fig. 2.5) is given by the set of Navier's equations :

$$\begin{aligned} &\frac{\partial \sigma_i}{\partial x_i}+\frac{\partial \tau_{ji}}{\partial x_j}+\frac{\partial \tau_{ki}}{\partial x_k}=\rho\frac{\partial^2 u_i}{\partial t^2} \\ &\frac{\partial \sigma_j}{\partial x_j}+\frac{\partial \tau_{ij}}{\partial x_i}+\frac{\partial \tau_{kj}}{\partial x_k}=\rho\frac{\partial^2 u_j}{\partial t^2} \\ &\frac{\partial \sigma_k}{\partial x_k}+\frac{\partial \tau_{ik}}{\partial x_i}+\frac{\partial \tau_{jk}}{\partial x_j}=\rho\frac{\partial^2 u_k}{\partial t^2} \end{aligned} \qquad 2.1$$

where σ and τ are the normal and the shear components of the stress tensor, u_i, u_j and u_k are the components of the displacement, x_i, x_j and x_k are the coordinates in i,j, and k directions, t is the time coordinate and ρ is the mass density of the material. There are the two solutions for the equations of motion of an element for an elastic and isotropic material (Timoshenko & Goodier, 1951). The first solution is given for the component of deformation taking place in the direction of wave propagation (i.e. the compression wave):

$$\frac{\partial^2 \epsilon_v}{\partial t^2}=v_p^2\nabla^2\epsilon_v \qquad 2.2$$

where:

$$\nabla^2=\frac{\partial^2}{\partial x_i^2}+\frac{\partial^2}{\partial x_j^2}+\frac{\partial^2}{\partial x_k^2} \qquad 2.3$$

$$v_p=\sqrt{\left(\frac{L+G}{\rho}\right)} \qquad 2.4$$

and where v_p is the velocity of the compression waves and ϵ_v is the total volumetric strain:

$$\epsilon_v=\epsilon_i+\epsilon_j+\epsilon_k \qquad 2.5$$

The material elastic constant L is given by:

$$L=\frac{\nu E}{(1+\nu)(1-2\nu)} \qquad 2.6$$

where ν, E and G are the Poisson's ratio, Young's modulus and shear modulus, respectively for an elastic material.

The second solution of Equation 2.1 is given for the component of deformation taking place in the direction perpendicular to the direction of the wave propagation (i.e. the shear wave):

$$\frac{\partial^2 \omega_i}{\partial t^2}=v_s^2 \nabla^2 \omega_i \qquad 2.7$$

where:

$$\omega_i=\frac{1}{2}\left(\frac{\partial u_j}{\partial x_k}-\frac{\partial u_k}{\partial x_j}\right) \qquad 2.8$$

and where ω_i is the component of rotation around axis i and v_s is the velocity of the shear wave given by:

$$v_s=\sqrt{\frac{G}{\rho}} \qquad 2.9$$

The solution given in Equation 2.8 is valid for each of the three axes. It should be noted that for an isotropic elastic material the velocity of the shear wave is therefore directly related to the shear modulus:

$$G=\rho v_s^2 \qquad 2.10$$

Wave propagation through saturated soils is more complex than through an elastic medium. In this case the propagation of the wave involves two phases: the soil skeleton and the water in the pore spaces. The theoretical study by Biot (1956) showed that as a result of the multi phase nature of saturated soil there are two compressional waves, one which travels through the water and one which travels through the soil skeleton. There is only one shear wave which travels through the soil skeleton since water has no shear resistance.

The interaction between the solid and fluid phases of saturated porous media result from inertial, viscous and mechanical coupling. Gajo (1995,1996) gave a detailed analysis of the propagation of simple shaped driving pulses (a square wave and a single sine pulse) through saturated porous media considering the consequences of viscous coupling. For the condition of infinite viscous coupling the behaviour of the saturated porous media corresponds to a single phase medium. This behaviour is typical of a low permeability soil (coefficient of permeability, $k<10^{-4}$cm/sec), a low frequency driving pulse (frequency, f<100kHz) and long

propagation distances (length, x>10cm). In this case the velocity of propagation is calculated from:

$$v_s = \sqrt{\frac{G}{(1-n_p)\rho_s + n_p\rho_f}} \qquad 2.11$$

where n_p is porosity, ρ_s mass density of solid grains and ρ_f is mass density of the fluid, so that:

$$v_s = \sqrt{\frac{G}{\rho_T}} \qquad 2.12$$

where ρ_T is the total mass density of saturated soil.

The second characteristic case is associated with low viscous coupling where the porous medium behaves as a two phase medium so that the inertial acceleration of one phase relative to the other cannot be neglected. This inertial coupling is expressed as:

$$\rho_a = (\tau_s - 1) n_p \rho_f \qquad 2.13$$

where ρ_a is a coefficient which represents the added mass of the porous solid to account for the fluid inertia. The added mass is related to the geometry of the pore space which is described by the parameter τ_s, the tortuosity. The velocity of propagation is then calculated from:

$$v_s = \sqrt{\frac{G}{(1-n_p)\rho_s + \frac{\tau_s - 1}{\tau_s} n_p \rho_f}} \qquad 2.14$$

According to Gajo (1996) this behaviour is typical for permeable soil ($k>10^{-4}$cm/sec), high frequency driving pulse (f>100kHz) and short propagation distances (x<10cm). Between these two extremes of behaviour there is a fairly rapid transition over a quite narrow range of the parameters involved.

Traditionally all wave propagation tests carried out on saturated soils have been interpreted using Equation 2.12 so that stiffness has been calculated from:

$$G = \rho_T v_s^2 \qquad 2.15$$

Summarising the work of Gajo (1996), for wave propagation tests on high permeability soils ($k>10^{-4}$cm/sec) both ways of calculating v_s (i.e determining G) given by Equations 2.11 and 2.14 should be considered, determining which is relevant. According to Gajo (1996), at appropriate conditions, the value of G calculated using the traditional interpretation (Equation 2.12) may overestimate by up to around 15% the real value of G.

The main difficulty in applying Gajo's interpretations is the assessment of the key parameter, tortuosity. The measurement of tortuosity requires tests on the electrical conductivity of the soil (Brown, 1980) but this may not be reliable for angular or platy particles. The results of different experimental studies suggest that the porosity is related to tortuosity but the clear trend is only seen for the spherical particles (Gajo, 1996). An additional difficulty may occur if the soil is exposed to higher pressures during the test so that particle breakage occurs, as this will certainly affect the tortuosity. It is not known how this effect would be quantified.

Wave propagation methods are based on the direct measurement of the velocities of shear or compressive waves as they travel trough the soil in the form of seismic disturbance. The distance between source and monitoring point is known so that the measurement consists of detection of the arrival time at the monitoring point as the wave passes. A comprehensive description of wave propagation methods for in situ tests is given by Abbiss (1981).

In the laboratory Knox et al., (1982) used geophones as sources and either accelerometers or other geophones as receivers for 2m wide cubic samples. Nakagawa et al., (1996) mounted a set of compressive and shear piezoceramic transducers in the top platen and pedestal of a triaxial apparatus. Testing saturated sand by using very sensitive compressive wave transducers, they claimed detection of both fast compression waves which travel through pore water and slow compression waves which travel through soil skeleton.

Shear plates made of piezoceramic were used by Lawrence (1963) (as reported by Brignoli & Gotti, 1992) both to generate and receive shear waves. Piezoceramic not only generates movement when subjected to a voltage, but when it is deformed, it generates a voltage. When an voltage is applied, the shear plate is deforming in the manner shown in Fig. 2.6. If one of the faces in the plate is in contact with the soil sample a shear wave will be propagated in a direction perpendicular to the face of the plate. Located on the opposite end of the sample the other piezoelectric shear plate is also used to detect the arrival of the shear wave. The difficulty with the shear plates is that they are considerably stiffer than most soils and they do not protrude into the sample so the transfer of energy between the transducer and the soil is poor.

This problem has been overcome with bender elements which are thin piezoceramic plates which achieve better coupling by protruding into the soil sample. When placed so as to protrude with the free end in the soil (Fig. 2.7) and excited with an external voltage the transmitter bender element will move and send a shear disturbance through the soil. The arrival of the disturbance can be detected by the receiver element located on the opposite end of the sample. Bender elements were

originally developed by Shirley & Hampton (1977) for testing soft marine sediments. Schulteiss (1982) described the use of bender elements in the oedometer. Dyvik & Madshus (1985) gave a comprehensive description of the bender element configuration for a standard triaxial apparatus while Gohl & Finn (1991) reported a successful use of bender elements in the centrifuge. The technique is now gaining acceptance because it is versatile, less expensive and easier to use than other dynamic techniques in the laboratory. The bender element method is described in greater detail in Section 3.4.

2.3 DEPENDENCE OF STIFFNESS ON THE CURRENT STRESS-VOLUME STATE OF THE SOIL

2.3.1 Introduction

As discussed in Section 1.1, for the majority of soils yielding occurs at strains which are very small i.e. less then 0.001% (Atkinson and Sallfors, 1991) and at subsequent small strains the stress strain behaviour becomes highly non-linear (see Fig. 1.1). Using resonant column and torsional shear tests Georgiannou et al., (1991) made the observation that the yield strain which defined the end of initial elastic plateau, i.e very small strains, was dependant on the plasticity of the soil and that it was of the order of 0.01% for a plastic clay and about 0.001% for sands. This review will focus on the factors which influence the stiffness of soil at very small and small strains. In the domain of very small strains these factors, as summarised by Atkinson & Sallfors (1991), are the current stress-volume state of soil, the loading rate and periods of rest at constant stress. In subsequent sections the experimental evidence which examines the influence of the current stress volume state of the soil on stiffness will be presented.

In Section 1.2 the state of the soil was defined as a point in p':q':v space whose position was defined relative to the state boundary surface While the behaviour of a reconstituted soil depends predominantly on its current state (i.e. stress state and specific volume) structured soils have a more complex pattern of behaviour. As outlined by Mitchell (1976) the principal components of structure are fabric and bonding or cementing. Fabric may include particle orientation, inhomogeneities, layering and fissuring. Leroueil & Vaughan (1990) and Burland (1990) summarised the principal features of the behaviour of structured soils They showed that the presence of structure generally increases the strength and stiffness and allows soils to exist at states outside the state boundary surface of the corresponding destructured soil The influence of the principal components of structure on stiffness will be reviewed separately (Section 2.4), and this section will concentrate on

other factors controlling stiffness.

There is plenty of experimental evidence which shows that the stiffness of soils at very small strains is independent of the loading rate (i.e. the frequency of propagating waves) suggesting that at these strains soils do not exhibit viscous behaviour. Bolton & Wilson (1989) compared the stress-strain behaviour of dry Leighton Buzzard sand using resonant column tests and low frequency cyclic tests on the same sample. Their results which are shown in Fig. 2.8 and correspond to a range of frequencies from 0.001Hz to 120Hz show that the soil behaviour does not depend on the frequency of loading at very small strains. Similar results were obtained among others by Hardin & Drnevich (1972), Iwasaki et al., (1978), Pane & Burghignoli (1988) and others.

In the region of small to moderate strains experimental evidence shows an increase of the stiffness of around 5% per one logarithmic cycle of the strain rate increase (Isenhower & Stokoe, 1981; Dobry & Vucetic, 1987; Tatsuoka & Shibuya, 1992). As summarised by Lo Presti (1995) the change in stiffness with the strain rate increases with plasticity index so that for coarse grained soils very small effects are expected.

The processes of creep and aging are associated with periods of rest at constant stresses. Richardson (1988) showed that periods of rest generally increase the stiffness of soil. Anderson & Stokoe (1978) found that the very small strain stiffness of sands and clays increased following extended periods of confinement (Fig. 2.9). They found that for sands the effect was around 2% per logarithmic cycle of time but it was more pronounced for overconsolidated clays and very pronounced for normally consolidated clays. The change of soil state due to the decrease in voids ratio caused by the creep may explain at least some of the observed increase of stiffness. The increase determined by the change of state could be used to correct the stiffness possibly isolating the aging effect (Schmertman, 1991) but this was not done by Anderson & Stokoe (1978).

2.3.2 Micro-mechanical parameters of stiffness at very small strains

Using the theory of elasticity the deformation of elastic bodies in contact can be calculated in terms of contact pressures and elastic material parameters. The early theoretical work by Hertz (as reported by Richart et al., 1970) showed that the stiffness of an assembly of elastic spheres depends upon the cube root of the normal stress which acts between them and elastic properties of the spheres themselves. Hertz's theory considered a simple cubic packing of equal spheres where only normal forces acted between them, so did not take into account shearing forces which will necessarily develop on particle contacts in real soils. Mindlin et al., (1951) concluded that the tangential stiffness of the contacts contributed to the overall stiffness of the assembly of spheres but the dependency of stiffness upon the cube root of the normal stress was found to be the same. Experimental evidence suggests, however, that this power coefficient is generally around 0.5, a difference which is usually attributed to the variety of different particle sizes within a real soil, together with their shape and angularity and the random nature of the particle contacts.

Mindlin's work also considered the nature of the deformation on the contacts between spheres. As shown in Fig. 2.10 Mindlin distinguished two conditions of shear stress acting on the contacts. The first condition which allows slippage between particles produced a distribution of shear stress which had finite values. The second condition of no slip between the particles leads to an infinite shear stress at the periphery of the contact areas. This indicates that slippage must occur even for the smallest tangential force so that simultaneous elastic and plastic strains will be produced. Mindlin's solution for the nature of elastic stiffness for a single contact can be extrapolated to the behaviour of an assembly of particles in contact so that, as pointed out by Hardin (1978), the elastic behaviour for a particulate material is restricted exclusively to infinitesimal increments of loading. Evaluation of the elastic properties of soils is therefore most conventionally achieved by dynamic methods, as the small wave amplitude imposes a cyclic loading on the sample which causes only very small strains which may be regarded as elastic.

The most important conclusion to be learned from the results of the Hertzian-Mindlin theory is that the elastic properties of the soil particles and the number of contacts per single particle are the two micro-mechanical parameters which govern the value of small strain stiffness. It is expected that the number of contacts per soil particle is closely related to compressibility of the soil, and as will be shown later, there is strong evidence to support this assumption. This was also indicated by the results of numerical studies of inter particle

interaction between spherical elastic particles in an assembly (Dobry et al., 1989; Rothenburg & Bathurst, 1989). Although particulate modelling gives an insight into the behaviour of granular materials it has still to achieve a realistic reproduction of all the shapes, orientations and locations of individual particles which are all relevant to particle interaction and so is not reviewed here in detail.

2.3.3 Experimental evidence for the dependence of stiffness at very small strains on current stresses

In the early 1960s Hardin & Richart (1963) performed an extensive set of resonant column tests on different sands. Their results, some of which are presented in Fig. 2.11, showed that the velocity of shear waves varied linearly with void ratio and with confining pressure raised to the power of 0.5. For clays a set of resonant column tests was used by Hardin & Black (1968) to propose that the elastic stiffness of soils G_{max} can be written in the following form which shows both its dependence on void ratio and confining pressure:

$$G_{max}=A(T)\,F(e)\,p'^{n} \qquad 2.16$$

where A(T) is a dimensionless number which characterizes a particular material, F(e) is a function of void ratio which reflects the influence of material density and n is a power coefficient which was found to be equal 0.5 for the majority of the materials tested. This semi-empirical relationship has also appeared in other forms, such as:

$$G_{max}=1230\,\frac{(2.973-e)}{(1+e)}\,(OCR)^{k}p'^{(1/2)} \qquad 2.17$$

which was proposed for clays by Hardin & Black (1969) where OCR is the overconsolidation ratio in terms of vertical stress and k is the corresponding power coefficient which was shown later by Hardin & Drnevich (1972) to depend on the plasticity index. Both equations lack dimensional coherency and the values of G_{max} and p' are given in PSI. Based on Rowe's (1971) study of the behaviour of an assembly of elastic spheres in contact Hardin (1978) suggested a refined version of a similar type:

$$G_{max}=S\,F(e)\,OCR^{k}p_a^{1-n}p'^{n} \qquad 2.18$$

where S is now a dimensionless modulus which represents the influence of soil structure, mineralogy and fabric and p_a is atmospheric pressure needed for dimensional coherency of the equation.

An important step in the research into the nature of small strain stiffness was made by Roesler (1979). Later work carried out by Stokoe et al., (1985) confirmed his findings that the elastic shear stiffness of soil does not depend on the stress which is normal to the plane of

shearing. The test results are shown in Fig. 2.12 where the symbols σ'_i, σ'_j, and σ'_k denote the three effective principal stresses. The stresses σ'_i and σ'_j are in the plane of shearing with σ'_i acting in the direction of shear wave propagation and σ'_j acting in the direction of polarisation. According to Roesler the shear wave velocity increases either when σ'_i or σ'_j increases but is essentially independent of changes in σ'_k. This finding leads to the conclusion that an anisotropic stress state which acts on a soil will necessarily result in G_{max} becoming an anisotropic parameter. It also contradicts all previous findings since, according to Roesler, G_{max} does not depend solely on the mean effective stress p'. For constant values of σ'_i and σ'_j the value of σ'_k may vary as would p' but G_{max} would stay the same. It is important to note that all the experimental evidence which supports this finding follows from the results of tests on sands which were exposed to moderate changes of stress of several hundred kPa and so correspondingly small changes in volume. The extrapolation of this conclusion to fine grained materials requires caution as being generally more compressible than sands, clays may undergo significant volume change even for moderate increases of normal stresses (including σ'_k), which would then necessarily affect G_{max}.

Following the findings of Roesler and also taking the structure of soil into account, Hardin & Blandford (1989) finally redefined their empirical expression as:

$$G_{ij} = \frac{OCR^k}{f(e)} \frac{S_{ij}}{2(1+\nu)} p_a^{1-n} (\sigma'_i \sigma'_j)^{n/2} \qquad 2.19$$

$$f(e) = 0.3 + 0.7e^2$$

Hardin considered the role of the different parts of Equation 2.19. He proposed that G_{ij} was the elastic shear modulus in the plane of principal effective stresses σ'_i and σ'_j, while the term $2(1+\nu)$ defines the effect of Poisson's ratio. The parameter S_{ij} is a dimensionless coefficient associated with the fabric of the material and includes the elastic properties of individual particles. The voids ratio function f(e) is a measure of soil density which depends both on the fabric at the time of the soil's deposition and subsequent changes due to stress history. The term $(\sigma'_i \sigma'_j)^{n/2}$ accounts for the current state of stress including changes in fabric associated with the application of that stress while the overconsolidation ratio OCR is now defined in terms of p'. However, even for an isotropic soil Equation 2.19 treats stiffness as a vector since it is correlated with the product of the principal effective stresses of biaxial compression σ'_i and σ'_j. It is not clear exactly how G_{ij} is related to the soil stress state since soil cannot exist in a condition solely of biaxial compression.

Equation 2.19 has been shown by various authors to fit the test data for

both sands and clays (eg. Bellotti et al., 1996; Jamiolkowski et al., 1995) but this does not, however, help in understanding which parameters control the value of G_{ij} since the equation takes into account all possible influences, not distinguishing possible correlations between them. For example if we restrict this discussion to reconstituted clay under isotropic stress then Equation 2.19 takes form of Equation 2.18. In that case we should consider that the current voids ratio depends uniquely on the stress history and the current stress state. As demonstrated by Rampello et al., (1995b) at a given value of current stress the overconsolidation ratio and voids ratio are related so, in Equation 2.19 one of the parameters, OCR or f(e), is redundant.

With the formulation given in Equation 2.19 a complexity also arises since, as discussed above, the current stress state is not fully defined so it is not possible to correlate the stress history with the current stress state. It is interesting to assess the influence of the principal stress normal to the plane of shearing, σ'_k, on the value of G_{ij} given in the equation. An increase in σ'_k would cause reduction in the void ratio (i.e compression of the soil) and consequently an increase in G_{ij}. This contradicts the finding of Roesler (1979) that G_{ij} does not depend on σ'_k.

The theoretical work of Hertz and Mindlin at a particulate level showed that G_{max} is a function of the properties of soil particles and the stress state on the contacts. It seems logical, therefore, to assume that G_{max} will be closely related to the parameters which control the compressibility of the soil since compression will increase the number of inter-particle contacts. As pointed out by Hryciw & Thomann (1993) it does not seem possible for a single function of void ratio f(e) (Equation 2.19) to be valid for all soils. A single function would imply for example that for an identical decrease in void ratio well graded and poorly graded sands would develop the same number of new contacts which seems unlikely. For this reason among others Jamiolkowski et al. (1995) used different expressions for f(e) which were more suited to describe the results obtained from tests on different soils.

Wroth & Houlsby (1985) suggested that the elastic shear modulus for sands can be expressed as a dimensionally coherent power function of the confining stress:

$$\frac{G_{max}}{p_r} = A\left(\frac{p'}{p_r}\right)^n \qquad 2.20$$

where p_r is a reference atmospheric pressure and A and n are non dimensional material parameters. Zytinski et al., (1978) demonstrated that the shear modulus of a purely elastic material could not be simply a function of p' since in that case a cycle of deviator stress q would result in work being done. It is more likely therefore that the shear

modulus depends both on p' and q as proposed by Lade & Nelson (1987) which would allow there to be no energy loss during the cycle. Experimental evidence indicates that the effect of deviatoric stress on elastic shear modulus exists but also that is not very pronounced (Tatsuoka et al., 1979; Viggiani, 1992; Bellotti et al., 1996) at least when the soil is far from failure. This question will be elaborated further in Section 5.3.2.

2.3.4 The dependence of stiffness at very small strains on the current stress-volume state of soil

Analyses by Wroth (1971) of tests carried out by Webb (1967) on London clay suggested that the elastic shear modulus G when normalised by the current value of the mean effective stress p' is linearly dependant on the parameter v_λ (see Fig. 2.35) where:

$$v_\lambda = v + \lambda \ln p' \qquad 2.21$$

Taking into account that v_λ is linearly related to overconsolidation ratio R_0 (Schofield & Wroth, 1968) Wroth assumed that the ratio G/p' for overconsolidated soil obeys the following relationship:

$$\frac{G}{p'} = \left(\frac{G}{p'}\right)_{nc}(1 + C\ln(R_o)) \qquad 2.22$$

where $(G/p')_{nc}$ is the normalised value of G with respect to p' for normally consolidated soil. This relationship was later approximated by Houlsby & Wroth (1991) to:

$$\frac{G}{p'} = \left(\frac{G}{p'}\right)_{nc} R_o^{\,m} \qquad 2.23$$

where C and m are material constants. From undrained triaxial test on glacial till Little & Atkinson (1988) also found that at larger strains the value of G/p' for tangent stiffnesses at any particular strain level increased linearly with the logarithm of overconsolidation ratio as shown in Fig. 2.13.

As a result of an extensive set of bender element tests on reconstituted fine grained materials Viggiani & Atkinson (1995b) showed that the relationship between G_{max} and p' for normally consolidated clays can be expressed in a similar form to Equation 2.20:

$$\left(\frac{G_{max}}{p_r}\right)_{nc} = A\left(\frac{p'}{p_r}\right)^n \qquad 2.24$$

where p_r is the reference pressure of 1kPa and the pressure multiplier, A, and the pressure exponent, n, are soil parameters. It is important to

note that in this case the parameters A and n are related to the state of the soil on the normal compression line. For overconsolidated soils Viggiani & Atkinson took into account the influence of the state of the sample relative to the normal compression line using overconsolidation ratio as suggested by Wroth & Houlsby (Equation 2.23). The full expression which relates the state of the soil to G_{max} then became:

$$\frac{G_{max}}{p_r} = \left(\frac{G'_{max}}{p_r}\right)_{nc} R_o^m = A\left(\frac{p'}{p_r}\right)^n R_o^m \qquad 2.25$$

The variation of G_{max} (denoted as G_0) with stresses and overconsolidation ratios for reconstituted Speswhite kaolin is presented in Fig. 2.14.

As previously discussed, the strong link between the compressibility of the soil and number of contacts per soil particle would justify the assumption of A, n and m being material parameters. As pointed out by Rampello et al., (1995b) the stiffness parameters A, n and m are akin to the compression parameters N, λ and κ respectively. The parameter A controls the magnitude of G_{max} of normally consolidated soil at a reference pressure just as N does the specific volume, while the variations of G_{max} and v with p' are given by the indexes n and λ for normally consolidated states and by m and κ for overconsolidated states.

Viggiani & Atkinson (1995b) examined whether there is a correlation between the parameters A, n and m and the plasticity index PI which was used to characterise the nature of the soil. In addition to the data from Viggiani (1992) also shown in Fig. 2.15 are points representing tests on various other fine-grained soils reported by Pane & Burghignoli (1988) and Weiler (1988). The scatter in the data is high but the trend shows that A decreases with PI while the coefficients n and m both increase.

2.3.5 The dependence of stiffness at small strains on the current stress-volume state of the soil

It was originally assumed by Wroth (1971) that the ratio G/p' is constant for normally consolidated clays while Little & Atkinson (1988) showed that the ratio is constant for normally consolidated till for stiffnesses at strains greater than 0.1%. This linear increase of G with p' may be expected if the soil is idealised as an assembly of rigid frictional particles. As will be shown later this assumption becomes valid only at larger strains when the stiffness of the assembly is negligible relative to the stiffness of the particles. As could be seen from Hertzian-Mindlin theory, at small strains where the stiffness of the assembly is high, the deformability of soil particles imposes that the variation of G_{max} with p' is not linear but a power function.

Viggiani & Atkinson (1995b) studied the variation of stiffness with strain at intermediate strain levels (i.e. between 0.005% and 0.1%) for monotonic stress paths. The results from constant p' drained triaxial compression tests carried out on normally consolidated samples of Speswhite kaolin are shown in Fig. 2.16. Values of stiffness at particular strain levels are plotted against mean effective stress, both normalised with respect to the reference pressure p_r. The authors found that at each strain level the variation of stiffness with mean effective stress is also represented by power function as in Equation 2.24 but both A and n vary with strain as shown in Fig. 2.17. The value of A decreases rapidly a result of pronounced non-linearity in the stress-strain response over this range of strain. The parameter n rises from n=0.65 for very small strains up to around 1.0 at larger strains. Similar results were reported by Lo Presti (1995) for Toyoura sand for strain levels between 0.01% and 1%.

Tatsuoka & Kohata (1995) measured the stiffness of Toyoura sand both at very small and at small strains (Fig. 2.18). However, the authors were not able to correlate the observed differences in stiffnesses for two samples with different stress histories with their volumetric states since the position of the reference state (e.g. normal compression line) was not known.

Atkinson at al. (1990) used the term recent stress history to describe the previous stress path relative to the current stress state by means of the angle of rotation required to follow the new stress path. They showed that the stiffness for any given stress path is initially highly dependant on the recent stress history so that the increase in stiffness is greater for sharper changes in the direction of the stress path. Viggiani & Atkinson (1995b) performed constant p' shearing stages after isotropic compression and swelling so the angle of rotation was either $+90^0$ or -90^0. It is important to note that the values of A and n at larger strains that they determined are valid only for these two rotations of the stress path which were found to give almost identical answers but other rotations and other stress paths would give different values of A and n. The recent stress history effect is described in more detail in Section 2.6.1.

2.3.6 Summary

The experimental evidence presented in this section showed that the stiffness at very small strains does not depend on the rate of loading. An increase of very small strain stiffness with time of confinement is observed for both clays and sands but it is unclear whether this can be attributed solely to the change of the volumetric state of the soil caused by creep.

The theoretical work of Hertz and Mindlin on a particulate level showed that the G_{max} of an assembly of the particles is a function of the elastic properties of the soil particles, the stress state on the contacts and the number of contacts per single particle. There is substantial experimental evidence which correlates the parameters describing soil compressibility and parameters which control the stiffness of soil at small strains.

Semi-empirical and empirical correlations used to describe the dependence of soil stiffness on current stress and stress history without taking into account the current volumetric state of the soil generally fail to identify the key factors which control the value of G_{max}. For reconstituted fine grained soils under isotropic stress states a framework has been established by Viggiani & Atkinson (1995b) which correlates the state of the soil and the stiffness at very small and small strains. For anisotropic stress states, experimental results from tests on coarse grained soils showed that G_{max} is a directional property, i.e. it does not depend on the stress which is normal to the plane of shearing. For anisotropic axi-symmetric stress states there are indications that this stress induced effect is small, at least when the soil is far from failure.

2.4 DEPENDENCE OF STIFFNESS ON THE STRUCTURE OF A SOIL

2.4.1 Introduction

The origin of structure in natural clays was examined by Tavenas & Leroueil (1987). Void ratio e plotted against the logarithm of vertical stress in the ground was used (Fig. 2.19) to represent the idealised compressive behaviour of structured natural clays. States I to A represent primary and secondary compression while states A to P represent the loading path followed by the soil which has undergone strengthening of the particle contacts due to thixotropic hardening and cementation. The influence of the cementing on compressibility gradually reduces when the soil is compressed to stresses higher than σ'_{vc} (states P to C) so that the normal compression line of the intact soil converges with the normal compression line of the destructured soil (annotated as α-α). Graham & Li (1985) showed that the normal compression lines of intact and destructured soils may remain parallel even at high compressive stresses.

Highlighting uncertainties related to the term destructured Burland (1990) suggested that the reconstituted soil should be a reference material to which the behaviour of intact soils is to be compared. In the case of clays a reconstituted soil is defined as one that has been

thoroughly mixed to a water content equal to or greater than the liquid limit and then recompressed. In order to compare the in situ states of a large number of normally consolidated clays with the corresponding normal compression lines of the clays in a reconstituted state Burland introduced the void index I_v:

$$I_v = \frac{e - e^*_{100}}{e^*_{100} - e^*_{1000}} \qquad 2.26$$

where e^*_{100} and e^*_{1000} denote the voids ratio of the reconstituted soil at values of vertical effective stress of 100kPa and 1000kPa, respectively. The void index plotted against the logarithm of the vertical stress σ'_v in Fig. 2.20 identified, by definition, a unique intrinsic compression line for normally consolidated reconstituted clays and a narrow band for the in situ states of normally consolidated natural clays represented by a single line named the sedimentation compression line. This line was seen to be parallel to and above the intrinsic compression line which was attributed to the presence of structure in the natural clay deposits. Coop & Cotecchia (1995) pointed out that I_v normalisation would not be appropriate for sands, many of which would not reach their normal compression lines at only 100kPa as will be discussed in Section 2.5.

Tavenas & Leroueil (1987) showed that the state boundary surfaces of the intact soils lie above those of the equivalent reconstituted soils allowing the intact samples to exist in states not permitted to the reconstituted samples (Fig. 2.21). It was demonstrated by Graham et al., (1983) that, similarly to reconstituted clays, the shear behaviour of natural clays is controlled by their state relative to the state boundary surface. Due to the means of their preparation the principal components of soil structure, bonding and natural fabric, are not present in reconstituted samples. Therefore the effects of structure on soil behaviour may be examined by comparing the results of tests carried out on intact samples with those from reconstituted samples. As pointed out by among others Coop et al., (1995), since the behaviour of soil depends on the current state in order to isolate the influence of structure it is necessary to test intact and reconstituted samples at the same state. Alternatively the test data may be normalised with respect to the state of the sample so that any differences in the states of the samples are taken into account.

2.4.2 Influence of structure on stiffness

Cuccovillo (1995) investigated the shear behaviour of cemented sands. Intact and reconstituted samples of a calcarenite were isotropically compressed and then sheared either in drained constant p' or undrained conditions. During isotropic compression (Fig. 2.22) the initially stiff

and linear response of the intact samples was marked by an abrupt change in compressibility which was attributed to the onset of bond degradation. As bonding degraded the post-yield compression line converged towards the normal compression line of reconstituted soil.

The dependence of G_{max} on p' was investigated through shearing probes carried out from different initial values of p'. The strains were measured using local LVDTs directly attached to the sample (Cuccovillo & Coop, 1997). The variation of the tangent shear moduli with deviator stress for cyclic undrained probes on intact samples is shown in Fig. 2.23. The reduction of G_{max} seen in cycles 2 and 3 is associated with the mechanism of bond degradation which occurred during the first cycle.

For both the calcarenite and a silica sandstone the value of G_{max} prior to yielding did not vary with changes in the mean effective stress. This is shown in Fig. 2.24 where G_{max} values for the intact and reconstituted calcarenite are plotted against p'/p'_{IB} where p'_{IB} is the corresponding equivalent mean effective stress on either the intact or reconstituted normal compression line as appropriate (see Fig. 2.22). The values of G_{max} were normalised by the reference pressure of p_r=1MPa. While the reconstituted soil showed a linear increase of G_{max} with the normalised state variable p'/p'_{IB} the G_{max} of the intact soil prior to yielding (points A1,B1,C1 and D1) is independent of the state. After the yielding the bonds degraded either due to isotropic compression (point E1) or due to cyclic loading (point D3)(see Fig. 2.33). The state then became a dominant factor influencing G_{max}. It can be seen that the G_{max} values of destructured calcarenite (points E1 and D3) are around 20% higher than those of reconstituted calcarenite at the same state but the gradient of increase with p'/p'_{IB} is the same for both soils.

Cuccovillo found that for a silica sandstone prior to yielding the value of G_{max} again did not vary with changes in p'. After yielding G_{max} increased so that the values of the shear stiffness were very much higher than those of reconstituted soils at comparable states. This difference in the behaviour by comparison with the calcarenite is attributed to their different structural features. In calcarenite the structure consists predominantly of strong bonding so that the transition to frictional behaviour after de-bonding resulted in the collapse of the stiffness. Conversely, in the silica sandstone the structure consists of a dense natural fabric and weak cementing so that stiffness remains high after bond degradation and even increases with the mean effective stress after yield.

For clays the influence of structure is perhaps more complex. Comparing results of tests on intact and reconstituted samples of Vallericca clay Rampello et al., (1993) showed that the isotropic normal compression and critical state lines of the intact samples were parallel to and placed

to the right of the isotropic normal compression and critical state line of the reconstituted samples (Fig. 2.25). Rampello et al., (1995a) used the resonant column and bender element methods to examine the stiffness of the same clay. The state paths are shown in Fig. 2.26a for both intact and reconstituted samples. The dots in the graph refer to the points of measurement of very small strain stiffness using either of the two dynamic methods as indicated in the figure. Values of G_{max}, denoted in the figure as G_0, plotted against p' show higher stiffnesses of the intact samples than the reconstituted even though they have the same specific volume and mean effective stress (Fig. 2.26b). Rampello et al., attributed the observed difference in stiffness between samples to their different positions relative to their corresponding normal compression lines. When this is taken into account no difference in stiffness between the intact and reconstituted soil is observed. This is seen in Fig. 2.27 where G_{max} for overconsolidated states has been normalised with respect to G_{max} on the normal compression line and plotted against corresponding values of the state variable p'/p'_e.

Vallericca clay showed behaviour typical of the influence of natural fabric as opposed to cementing so that the state of the intact sample did not approach the intrinsic behaviour of reconstituted sample during normal consolidation even at high stresses. Similar compressional behaviour was observed for natural Boom clay by Coop et al., (1995) who also evaluated the soil stiffness in the triaxial apparatus using shearing probes and local measurement of very small and small strains. It was shown for both clays that the state boundary surfaces of the intact samples lie above those of the equivalent reconstituted samples which highlights the influence of structure on the strength of both soils. The stiffnesses were measured both at very small and small strains for both clays and there was no evidence that the structure affected stiffness provided that the stiffnesses were normalised to take into account of the current state of the sample relative to the appropriate normal compression line.

2.4.3 Influence of anisotropic fabric on stiffness

If the particles of a soil are platy or elongated some particular forms of their orientation and arrangement may give rise to anisotropy of the soil (Mitchell, 1976). This structural anisotropy should be distinguished from the component of soil anisotropy caused by the current anisotropic stress state which is called stress induced anisotropy (Stokoe et al., 1995) or stress-system induced anisotropy (Tatsuoka & Kohata, 1995) (see Section 2.3.3). It is important to note that in order to separate out structural and stress induced anisotropy the soil sample must be tested at an isotropic stress state.

Structural anisotropy may be formed by the type of a soil's geological deposition but it can be also either created or altered by large straining (Mitchell, 1976). The latter effect is called strain induced anisotropy. Structural anisotropy is sometimes called inherent anisotropy although care must be taken using this term to describe the anisotropy of clays or sands. For sands the inherent anisotropy is defined as that which results from the depositional fabric (Arthur & Menzies, 1972). As the strains between deposition and testing of sand soils would be generally small the strain induced effect which will be superimposed on the initial inherent anisotropy will be also small. For a natural clay, however, the strains between deposition and testing are generally very large so that the inherent anisotropy, if it existed immediately after deposition, will be largely if not completely transformed by straining. Therefore, in contrast to sands the term inherent anisotropy for clays is likely also to be associated with the strain history. The eventual development of some form of natural structure after deposition such as bonding, could additionally alter the inherent anisotropy of either clays or sands.

Many soils were deposited over areas of large lateral extent. Symmetry with respect to the vertical axis dictated the direction of subsequent deformations since lateral movements were suppressed. This type of anisotropy where a soil responds differently if compressed in the vertical direction or in the horizontal direction but responds in the same way if compressed in either of the two horizontal directions is called cross-anisotropy. In the literature the following seven constants are usually associated with cross-anisotropy: E_v, the Young's modulus in vertical direction; E_h, the Young's modulus in horizontal direction; υ_{hv}, the Poisson's ratio in the vertical direction associated to strain in the horizontal direction; υ_{vh}, the Poisson's ratio in the horizontal direction associated to strain in the vertical direction; υ_{hh}, the Poisson's ratio in the horizontal direction associated to strain in the horizontal direction normal to the former; G_{hv} or G_{vh}, the shear moduli in either of the vertical planes and G_{hh}, the shear modulus in the horizontal plane. Two of the constants are redundant since the symmetry of the compliance matrix requires that:

$$\frac{\nu_{vh}}{E_v} = \frac{\nu_{hv}}{E_h} \qquad 2.27$$

and the isotropy of horizontal plane leads to:

$$G_{hh} = \frac{E_h}{2(1+\nu_{hh})} \qquad 2.28$$

Due to symmetry around the vertical axis G_{vh} must be equal to G_{hv} for either of the two horizontal directions, so only five elastic constants need to be specified (Love, 1927) for an elastic cross-anisotropic

material. The compliance matrix is then given by:

$$\begin{bmatrix} \delta\varepsilon_x \\ \delta\varepsilon_y \\ \delta\varepsilon_z \\ \delta\varepsilon_{yz} \\ \delta\varepsilon_{zx} \\ \delta\varepsilon_{xy} \end{bmatrix} = \begin{bmatrix} \frac{1}{E_v} & -\frac{\nu_{vh}}{E_v} & -\frac{\nu_{vh}}{E_v} & 0 & 0 & 0 \\ -\frac{\nu_{vh}}{E_v} & \frac{1}{E_h} & -\frac{\nu_{hh}}{E_h} & 0 & 0 & 0 \\ -\frac{\nu_{vh}}{E_v} & -\frac{\nu_{hh}}{E_h} & \frac{1}{E_h} & 0 & 0 & 0 \\ 0 & 0 & 0 & \frac{1+\nu_{hh}}{E_{hh}} & 0 & 0 \\ 0 & 0 & 0 & 0 & \frac{1}{2G_{vh}} & 0 \\ 0 & 0 & 0 & 0 & 0 & \frac{1}{2G_{vh}} \end{bmatrix} \begin{bmatrix} \delta\sigma'_x \\ \delta\sigma'_y \\ \delta\sigma'_z \\ \delta\tau_{yz} \\ \delta\tau_{zx} \\ \delta\tau_{xy} \end{bmatrix} \qquad 2.29$$

where x denotes the vertical axis and y and z denote the horizontal axes. As can be seen from Equation 2.29, anisotropy involves coupling between shear and volumetric strains so it should be regarded as an important characteristic of soil behaviour. In undrained shearing, as pointed out by Graham & Houlsby (1983), cross-coupling between volumetric and distortional behaviour determines the initial excess pore pressure response within the soil. The consequence of this is that the direction of the stress path will be affected and so will the corresponding mobilized stiffness. There is substantial experimental evidence that anisotropy affects both strength (Arthur & Menzies, 1972; Arthur et al., 1977; Oda, 1981) and the stiffness of soil (Arthur et al., 1977, Atkinson, 1973; Park & Tatsuoka, 1994).

The evaluation of anisotropy in terms of G_{max} is usually performed using dynamic methods. It is important that the soil specimen used to determine the influence of an anisotropic fabric on stiffness is placed and tested with its principal axes coincident to that of the fabric. Additionally, the stresses imposed by the propagating waves, i.e. the direction of propagation and direction of polarisation (particle movement) should coincide with the principal axes of the fabric. This assumes that the principal axes of fabric are known so the common approach is to assume some form of anisotropy within the material, such as, for example, cross-anisotropy. Otherwise the interpretation of dynamic tests becomes difficult since waves propagating at an angle through anisotropic material are neither purely shear nor compressive (Love, 1927).

Bellotti et al., (1996) studied the anisotropy of small strain stiffness of dry Ticino sand using a calibration chamber which held a 1.2m diameter cylindrical specimen which was 1.5m high. The measurements of small strain stiffness were performed using a multi-directional arrangement of geophones which were used both as sources and receivers of shear and compressive waves. The samples were formed by dry pluviation at different initial densities. Under isotropic stress conditions the velocity of horizontally polarized body waves exceeded by 10% that of vertically polarized body waves reflecting the inherent cross-anisotropy of the sand

tested. As reported by Bellotti et al. (1996), similar results from tests on dry pluviated sands were obtained by Lee & Stokoe (1986). Bellotti et al. also examined stress-induced anisotropy where the sample was put under an axi-symmetric stress state with $\eta(=q/p')$ constant. Their results, shown in Fig. 2.28, have been re-plotted in terms of G_{vh} and G_{hh} against p'. For the majority of tests at most values of η the initial inherent anisotropy was not altered by the stress induced effect. A small effect is seen only for $\eta=0.5$ but the gradient of increase of either G_{vh} or G_{hh} with p' was the same as for the other tests.

Jamiolkowski et al., (1995) investigated anisotropy in terms of very small strain stiffness of six different natural clays. The tests were performed using an oedometer which allowed the measurement of horizontal stresses and was fitted with bender elements. It is important to note that the authors were unable to evaluate separately structural anisotropy since the oedometer sample was subjected exclusively to anisotropic stress states. All of the clays tested show the characteristic features of a cross-anisotropic material where the degree of anisotropy expressed as the ratio G_{hh}/G_{vh} varied between 1.2 and 2. The data from tests on the Pisa and Panagaglia clays are shown in Fig. 2.29. The authors used Equation 2.19 to present their data so the value G_{ij} normalised with respect to the void ratio function f(e) has been plotted against $\sigma'_i\sigma'_j$. It can be seen in the same figure that the degree of anisotropy G_{hh}/G_{vh} can be expressed as a power function of $K_0(=\sigma'_h/\sigma'_v)$. Proposing that the ratio G_{hh}/G_{vh} is solely a function of K_0 the authors implicitly assumed that there were no strain induced changes in the structural anisotropy due to further one dimensional compression of the clays in the laboratory.

2.4.4 Summary

The literature review has examined the influence of the principal components of soil structure, bonding and natural fabric, on the stiffness of the soil. The experimental evidence confirms that the presence of the structure generally increases the strength and stiffness and allows the soil to exist at states outside the state boundary surface of the corresponding reconstituted soil.

Results from the tests on cemented sands suggest that during isotropic compression the value of G_{max} does not vary with mean effective stress which is the type of the behaviour typical for cohesive material. After bonding degradation the transition of the material to frictional behaviour is either followed by the collapse in stiffness for strongly cemented sands or by a continuous rise in stiffness for sands where the

dense natural fabric is the dominant structural component.

The experimental evidence confirms that the presence of natural fabric increases the strength of natural clays. It is also established that the natural fabric does not affect the very small and small strain stiffness provided that the stiffness is normalised to correctly take into account the current state of the soil relative to its own normal compression line, i.e. the normal compression line for the reconstituted or natural soil, as appropriate.

The most common form of anisotropic fabric in soil is cross-anisotropy which assumes symmetry, typically about the vertical axis. Cross-anisotropy is a consequence of either the type of the deposition (i.e. inherent anisotropy) or due to one-dimensional compression, when it is strain induced. The current understanding is that an anisotropic fabric influences both the strength and stiffness of the soil but little is known about how it affects the value of G_{max}.

2.5 THE MECHANICS OF GRANULAR SOILS

2.5.1 Introduction

As demonstrated by Schofield & Wroth (1968) and Atkinson & Bransby (1978) the framework of critical state soil mechanics can be used to interpret the important features of the behaviour of sands. However a simple analogy between the behaviour of clays for which the critical state theory was originally developed and the behaviour of sands cannot exist. That is, while clays develop plastic strains during compression by rearrangement of the particles sands develop plastic strains predominantly by means of particle breakage (Hardin 1985, Coop 1990).

Coop & Lee (1993) identified unique and straight isotropic normal compression lines and critical state lines for three different sands (Fig. 2.30) at high stresses, where the principal mechanism for plastic volumetric compression is governed by the breakage of particles. The material parameters for the calcareous Dogs Bay sand, a decomposed granite and the Ham River quartz sand are presented in Table 2.2.

Hardin (1985) suggested that the amount of particle breakage could be quantified by comparing the grading curves of soil samples before and after the test. He used the term total breakage, B_t, (Fig. 2.31) for the area between the curves and a vertical at the 74μm sieve size. It was assumed that the contribution of fines to the overall particle breakage could be neglected. Hardin recognized that the potential of a soil's

particles for breakage increases with their size and so is dependant on the initial grading of the soil. As indicated in the figure, breakage potential, B_p, was defined as the area between the original grading curve of the soil and a vertical at 74μm. Normalizing total breakage with respect to breakage potential Hardin introduced relative breakage:

$$B_r = \frac{B_t}{B_p} \qquad 2.30$$

which is independent of particle size distribution and therefore can be used for comparison between different soils.

Coop & Lee (1993) plotted values of B_r against the logarithm of p' for Dog's Bay sand (Fig. 2.32). The values of p' were taken during isotropic compression and at critical states after shearing. As for the normal compression and critical state lines when plotted against specific volume, it can be seen at higher stresses that the relationship between B_r and the logarithm of p' is unique and linear for both compression and shearing. This result introduces particle breakage as a major mechanism of plastic straining of sands.

Coop (1990) and Coop & Lee (1993) demonstrated that particle breakage gives rise to some unusual features of shear behaviour for sands. The stress paths from standard drained triaxial tests were normalised with respect to the current preconsolidation pressure p'_p and identified a state boundary surface, denoted as the Roscoe surface, with a peak on the right side of the critical state (Fig. 2.33a). This is a consequence of a non-associated flow at the critical state which was a feature predicted analytically by Chandler (1985) for soils with deformable grains. Additionally, normalized stress paths from constant p' tests apparently gave a boundary surface inside that from standard drained tests. Similarly, the normalized stress paths of the undrained tests on normally consolidated samples were located well inside the state boundary surface and so could not be used to identify it (Fig 2.33b).

Coop (1990) emphasised the importance of the stress history and associated particle breakage which preceded arrival at the current state of the soil. He distinguished between truly overconsolidated samples which had been compressed to the normal compression line and then unloaded to reach a given state and 'compacted' samples which had been compacted mechanically before loading and had arrived at the same given stress-volume state under first loading. The comparison between the undrained shear behaviour of an overconsolidated and a compacted sample at the same initial state is shown in Fig. 2.34. The stiffer behaviour of the overconsolidated sample was attributed to less particle crushing being experienced during shearing since some breakage of the grains had already occurred during preconsolidation.

2.5.2 State variables for sands

In contrast to the fundamental material properties of soils the state of a soil is a description solely of its current conditions. State is a significant parameter for describing soil behaviour since the most important soil properties such as strength and stiffness generally vary as a direct function of state. State is defined in terms of the void ratio and stress but it must also be measured against a reference condition. This reference condition must represent a state which is not influenced by the initial density of the sample, so that all samples of the soil can reach a state which is then used as a reference. The reference state is uniquely related to the fundamental material properties such as those which define the position of the critical state line or isotropic normal compression line in the v:lnp' plane. For example, the overconsolidation ratio (Equation 1.11) is a traditional state variable for clays which is defined relative to the isotropic normal compression line.

In contrast to clays, for sands, in general, there are often experimental difficulties in identifying the critical state and isotropic normal compression lines so the definition of a reference state and state variable is not straightforward. Because sand samples normally exist at states on the dry side of the critical state line there are considerable experimental difficulties in achieving the uniform stress and strain conditions at large deformations that are required to bring the specimens to a critical state. For this reason it is still a subject of research whether the critical state line for sands at low stresses is curved in the v:lnp' plane (Jefferies, 1993) or continues straight. As suggested by Coop (1990) the apparent curvature of the critical state line which is often observed may often be caused by inadequate testing procedures.

Atkinson & Bransby (1978) suggested the use of v_λ as a state variable for sand where:

$$v_\lambda = v + \lambda \ln p' \qquad 2.31$$

as shown in Fig. 2.35. Been & Jefferies (1985) introduced a state variable which they called 'the state parameter' ψ_i (also Fig. 2.35) where the reference condition is the critical state line as:

$$\psi_i = v_\lambda - \Gamma \qquad 2.32$$

They showed that ψ_i is a principal factor determining the stress strain behaviour of large number of sands. As opposed to Atkinson & Bransby (1978) who treated v_λ as a variable of current state Been & Jeffries (1985) attempted to extrapolate the concept of state variable and treated ψ_i as an initial index parameter which was independent of material type.

As pointed out by Wood (1990) the use of initial values of ψ_i is not satisfactory since the different volumetric changes associated with different stress paths will lead to continuous and significant variations in v_λ and hence ψ_i. As for v_λ, ψ_i should therefore only be used as a current state variable (Jeffries, 1993). Alternatively Wood (1990) proposed $v-v_{cs}$ as a state variable where v_{cs} is defined as the specific volume on the critical state line for the current value of p', as also shown on Fig. 2.35.

The yielding of sands during compression requires much higher stresses than for clays. However, when they are achieved in the laboratory the identification of a normal compression line is straightforward, as demonstrated by Coop & Lee (1993). The isotropic normal compression line is then a much more convenient choice for the reference condition upon which the state variable is to be defined. A state variable for sands can then be defined in the same way as the overconsolidation ratio for clays or by normalising the current p' with respect to an equivalent effective stress on the isotropic normal compression line p'_e (Fig. 2.35) where:

$$p'_e = \exp\left(\frac{N-v}{\lambda}\right) \qquad 2.33$$

and where λ is the gradient of the normal compression line and N its intercept at a p' of 1kPa. It is important to observe that when the isotropic normal compression line is used for the reference condition a distinction between overconsolidated and compacted states must be made. This is due to the different stress histories and corresponding amounts of particle breakage experienced by the sample in reaching a given state.

2.6 NUMERICAL MODELLING OF SOIL BEHAVIOUR

2.6.1 Introduction

Models describing soil behaviour are used both for collapse calculations where stability criteria are assessed and for deformation analyses where serviceability criteria are investigated. This review will focus on a certain group of soil models developed to be used for deformation analyses. In particular the modelling of the behaviour of overconsolidated clays using kinematic hardening models will be described. The use of kinematic hardening is highlighted as a reasonable approach to model the soil's response to non-monotonic loading for which the stiffness at very small strains becomes very important. For this reason this type of model was considered as suitable for the assessment of the importance of very small strain stiffness on calculated ground movements, which is one of the topics of this research project.

In engineering practice predictions of ground movements caused by construction have generally been carried out assuming linear elastic soil behaviour at working conditions and perfectly plastic behaviour under failure conditions. A typical example is the Mohr-Coulomb soil model where a frictional failure criterion distinguishes between an elastic and a perfectly plastic response. Experimental evidence suggests, however, that the available angle of shearing resistance is dependant on the mode of deformation which makes the Mohr-Coulomb model inappropriate for collapse calculations. Also for deformation analyses the model ignores the general observation that pre-failure soil behaviour is non-linear.

Elastic-plastic hardening models were a significant step forward in the development of soil models. They are often based on the framework of Critical State soil mechanics (Schofield & Wroth, 1968) which was presented briefly in Section 1.2, and the Modified Cam Clay model (Roscoe & Burland, 1968) is a typical example. As previously mentioned, in the Modified Cam Clay model the boundary surface (Fig. 1.3) bounds the region of possible stress states of the soil. Within the model the strains for stress paths below this surface are elastic so that the boundary surface coincides with the yield surface. The Modified Cam Clay model has the merit of having only five physically based parameters (G, κ, λ, N, M - see Section 1.2) while covering many of the essential features of soil behaviour. The applicability of the model is much greater than for the Mohr-Coulomb model but due to the unrealistic assumption of linear elastic behaviour within the boundary surface it is restricted to predictions of large deformations associated with collapse calculations.

Among others, it was the work of StJohn (1975) which highlighted the necessity of modelling the non-linearity of soil behaviour inside the boundary surface. Back-analysing ground movements around retaining walls in London clay Simpson et al., (1979) carried out non-linear analyses using a simple kinematic hardening model. In that way the predicted profiles of ground movements were found to be closer to the field observations.

In an attempt to model the non-linearity of soil behaviour Duncan & Chang (1970) proposed a model which assumes a hyperbolic stress strain curve in which the stiffness varies with the current deviatoric stress, confining pressure and axial strain. A similar approach was adopted by Jardine et al., (1986) and more recently by Gunn (1993). All these models imply non-linear elasticity for any monotonic stress path, within which would be considered all stress and strain paths where there is no significant change of direction such as, for example, the standard triaxial compression path. If all that is required is to model the soil response during monotonic loading then non-linear elastic models such as these can be adequate (Jardine et al., 1991; Hight & Higgins, 1995) to refine the prediction of ground movements. However, it is rare that a calculation of ground movements is associated only with monotonic stress

paths in the soil surrounding a geotechnical structure. More realistic applications of soil modelling should consider all possible stress paths which may be traversed during loading and the corresponding response of the soil to them.

In order to asses the influence of non-monotonic loading on the stiffness behaviour of a soil, Richardson (1988) performed a series of tests on natural and reconstituted clay samples. Following the approach of Richardson, Atkinson et al., (1990) used the term recent stress history to name the angle of rotation θ between the current and previous stress paths (Fig. 2.36). From the results on tests on London clay shown in the figure it can be observed that the stiffness is initially highly dependant on the recent stress history so that the increase in stiffness is greater for sharper changes in the direction of the stress path. The recent stress history effect decreases as loading is continued in the same direction up to the point where soil loses its memory of the previous stress path. From an examination of the strains from the same tests it was found that the recent stress history also determines whether the initial volumetric response of soil is dilatant or compressive. Additionally the authors showed that the volumetric and shear strains measured in these tests are coupled and irrecoverable which implies elastic-plastic deformation.

The observation that the stiffness of soils increases when the stress or strain changes direction has been also made, as reported by Wood (1995), by Wood (1975) for Spestone kaolin and Alawaji et al., (1990) for Leighton Buzzard sand. Similar behaviour was also observed by Bolton et al., (1995) for Gault clay. Taking into consideration the magnitude of the recent stress history effect based on this experimental evidence it is necessary that a constitutive model should reflect the increase of stiffness when stress or strain paths change direction (Wood, 1995). Models based on non-linear elasticity fail to predict the increase of the stiffness due to unloading. Some modifications of the original Duncan & Chang model have been attempted to include this effect (Duncan & Chang, 1972) but these changes have been, however, inadequate to cover all the important consequences of the recent stress history effect.

Using a different experimental approach, Jardine et al., (1986, 1991) and Smith et al., 1992) assessed the recent stress history effect considering the yielding behaviour of natural clays. The framework outlined from the tests on various soils (Fig. 2.37) comprised of an outer yield surface Y3 defined in stress space and two inner sub-yield surfaces, Y1 and Y2, which surround the current effective stress state. The authors proposed that these zones defined regions in which the stress-strain response is linearly elastic (Y1) or recoverable (Y2). The surfaces Y1 and Y2 are kinematic i.e. they follow the current stress state. It was also observed that the surfaces change shape and size as the soil is subjected to different stress histories. From the material published so far it is

unclear whether this framework has been used to model soil behaviour.

2.6.2 Kinematic hardening models

Models which use kinematic hardening allow plastic straining inside the boundary surface and have one or more inner yield surfaces which enclose zones of higher stiffness and which are "dragged" by the current stress state. In the case of non-monotonic loading the reversal of the stress path will traverse the inner yield surfaces so that the response of soil will be modelled as being stiffer.

Mroz et al., (1979) described a kinematic hardening model which enclosed a single yield surface inside the boundary surface. The model was refined by Mroz et al., (1981) and Mroz & Norris (1982) where the single yield surface was replaced by multiple nested yield surfaces so that the stiffness response became inversely related to the number of surfaces dragged by the current stress state.

Hashiguchi (1985) combined the bounding surface theory (Dafalias & Popov 1977) with features of kinematic hardening and formulated a three-surface model with a translation rule of the movement of the surfaces which prevents intersection between them. This concept was further developed by Al-Tabbaa (1987) and Al-Tabbaa & Wood (1989) who incorporated a single yield surface (bubble) within the Modified Cam Clay boundary surface (Fig. 2.38). A stress reversal from the overconsolidated state A will initially traverse the bubble and mobilise a high stiffness. Continuing the stress path in the previous direction will only translate the bubble mobilising a lower stiffness which is then proportional to the distance from the boundary surface. Like the other models of kinematic hardening outlined above this model is able to distinguish between loading and unloading events producing patterns of behaviour similar to those observed in the laboratory tests. However no attempt has been made to use this model to assess the complexity of the recent stress history effect.

The three-surface kinematic hardening model (3-SKH) developed by Stallebrass (1990b) is an extension of Al-Tabbaa & Wood's 'bubble' model. The model incorporates an additional kinematic surface (Fig 2.39) which is essential if the effects of stress history and yield at small strains are to be modelled (Atkinson & Stallebrass, 1991). Again the Modified Cam Clay boundary surface is used as the bounding surface. The yield surface bounds the purely elastic region and a history surface determines the region within which the soil has a memory of the direction of the previous stress path. The inner surfaces are both of the same shape as the bounding surface but scaled down by the factors TT and TS, respectively, which are regarded as model parameters. The translation laws controlling the magnitude and direction of movement of the kinematic

surfaces are of the same form as other similar models (Hashiguchi, 1985) so that the centre of the inner surface moves along a vector joining the current stress state to its conjugate point on the next surface as shown in Fig 2.40. In this way the surfaces are dragged by the current stress state but never intersect and gradually align along the current stress path direction.

For stress states within the yield surface the deformations are governed by isotropic elastic constitutive equations. Otherwise the stress-strain behaviour is elastic-plastic with an associated flow on all three surfaces. The hardening rule links the expansion or contraction of all three surfaces to changes in plastic volumetric strain and employs an additional parameter Ψ which determines the decay of stiffness as the stress state approaches the bounding surface. For a stress state at the bounding surface the hardening rule degenerates into the standard Modified Cam Clay hardening rule.

Five out of eight parameters used in the 3-SKH model have the same origin as the corresponding parameters of the Modified Cam Clay model (see Section 2.6.1) which in common with two of the other parameters, TT and TS, (i.e. the sizes of the inner surfaces) can be evaluated from stress path triaxial tests. The elastic parameters are determined from either dynamic tests such as bender element tests or from continuous loading tests performed with sufficient accuracy. Only the hardening rule parameter Ψ is derived from parametric studies.

A comparison between experimental stiffness data from tests on Speswhite kaolin and model predictions is given in Figure 2.41. The experimental data show that the stiffness which is initially dependent on the recent stress history (i.e. the angle θ) decreases as loading continues until the soil loses its memory of the previous loading, a pattern which was also well reproduced by the model. As reported by Stallebrass & Taylor (1997), it can be observed that the model tends to overestimate the reduction in stiffness at larger strains and to some extent overestimates the dilatant component of volumetric straining.

The 3-SKH model was developed to simulate the principal features of behaviour of overconsolidated clays at small strains and to be used primarily for deformation analyses. Stallebrass & Taylor (1997) showed good agreement between model predictions and data from centrifuge tests performed modelling of a rigid circular foundation. In Figure 2.42 the test data are presented with the results from analysis Run1 where the 3-SKH model was used contrasting with the poorer agreement from the analysis Run2 where the Modified Cam Clay model was used. The model was also used to study the deformation around a tunnel in London clay (Stallebrass et al., 1995a). The stress history of the soil at a particular location was modelled followed by the excavation of the

tunnel. The results of field measurements are presented together with the model predictions in Fig. 2.43. There is good agreement between the observed data and the predictions extending from the surface to a depth just above the tunnel crown proving that the model was capable of simulating well the whole deformation pattern around a tunnel in stiff clay.

The majority of constitutive models developed for soils are defined in stress space with strain increments deduced in response to increments of stress. Recently a 'brick and string' model has been developed by Simpson (1992) as a plane strain model defined in strain space. In this case the recent stress history effect was modelled by the disposition of memory points of the previous strain history. The model is described in the terms of an analogy with a man walking with bricks attached to his legs. The current strain (the man) is allowed to be at certain distances (the strings) from several memory points (the bricks). As the current strain changes one or more of the memory points will be dragged along too. The similarity with the multiple surface kinematic hardening models mentioned above is obvious since the stiffness response is inversely related to the number of memory points dragged. The important difference between these two type of models is in the disposition of the memory points which in the Simpson model is based in strain space. Brick model parameters were chosen to fit the stiffness-strain curve for the stress path DOX obtained from the experimental data of Richardson (1988) (Fig. 2.44). Model predictions of the stiffness response for other stress paths were then found to simulate well the experimental data, as can be seen in the figure.

2.6.3 Summary

The stress-strain response of soil to non-monotonic loading is described by the recent stress history effect which is based on experimental evidence. The ability of kinematic hardening models to predict that the very small strain stiffness will be fully mobilised whenever the stress path traverses the inner yield surface make them suitable for the assessment of the importance of the G_{max} and related parameters on calculated ground movements. Although all kinematic hardening models have the ability to take into account the increase of stiffness due to changes of the direction of the stress path, only the 3-SKH model proposed by Stallebrass (1990b) has been evaluated for all the important aspects of the recent stress history effect.

CHAPTER 3 LABORATORY EQUIPMENT AND EXPERIMENTAL TECHNIQUES

3.1 INTRODUCTION

The experimental work consisted predominantly of tests conducted using controlled stress path triaxial cells equipped with conventional instrumentation. The cells were also fitted with instrumentation for bender element tests which measured the propagation time of shear waves passed through the soil sample. The dynamic tests were non-destructive and were performed during triaxial tests. The tests on fine grained materials were carried out mostly in Bishop & Wesley (1975) apparatus which had a capacity of 700kPa and were designed to test a 38mm diameter sample. The triaxial tests on coarse grained materials were carried out mostly in a stress path apparatus with a capacity of 5MPa (Taylor & Coop, 1990) and some of the tests were carried out in an apparatus with the capacity of 70MPa (Cuccovillo, 1995). The high pressure cells were designed for testing 50mm diameter samples.

The computer controlled systems for triaxial stress path testing at moderate and at high pressures used in this research have been developed at City University during the last decade. The specifications and details of the systems are given by other authors (Atkinson et al., 1985; Richardson, 1988; Taylor & Coop, 1990; Viggiani, 1992). The description of the laboratory equipment and experimental techniques given in this Chapter will be focused on the important aspects that are particularly relevant to the present project. Emphasis will be given to dynamic aspects of testing and the techniques which have been used in the interpretation of test results.

The development of the equipment included some improvements in the control of the test. Software routines were added to the original computer program which was also transferred from GW Basic to the more versatile Quick Basic. To improve the accuracy of measurements during the tests the software was altered to perform autoranging of the logging channels during analogue to digital conversion of the signal. For the same purpose an entirely new data logging system was built with a greater attention given to the quality of signal conditioning and the overall stability of the electrical signals.

At City University piezoelectric bender elements were incorporated into the Bishop & Wesley cell by Viggiani (1992) following an original design from the Norwegian Geotechnical Institute (Dyvik & Madshus, 1985). The existing configuration was further developed during the project in an attempt to reduce the electronic noise and thus improve the clarity of the signal. This improvement proved to be a very important step in the development of more objective criteria for the determination of G_{max} from bender element tests which followed, also, as a result of theoretical and numerical studies. Finally, bender elements were successfully

incorporated into the high pressure triaxial cells enabling an insight to be made into the stiffnesses of granular materials at considerably higher pressures than before.

3.2 TRIAXIAL TESTING

3.2.1 Bishop & Wesley triaxial cell and instrumentation

The triaxial testing systems were located in temperature controlled rooms to improve the signal quality coming from the electrical measuring devices. For some of the specialised testing requiring a particularly high accuracy of the measurement of very small strains even a stabilised temperature regime with a fluctuation of $\pm 1^{o}$ caused problems for the readings. As will be discussed further in Section (3.3.3) further measures were, therefore, taken to isolate the system from changes in the ambient temperature.

A standard hydraulic triaxial cell (Bishop & Wesley, 1975) with dynamic instrumentation added is presented schematically in Fig. 3.1. The pressure unit comprised three pressure controllers which delivered cell pressure, back pressure to the volume gauge system and axial pressure to the loading ram. The controllers used were analogue pressure converters. The air was supplied from an air compressor which maintained the pressure in the range of 800-900kPa. From each of the controllers the air pressure passed trough air-water interfaces giving hydraulic pressure to the apparatus. When control of the axial strain rate was required the axial load was applied by a Bishop ram which was powered by a stepper motor and controlled by a timed relay.

The instrumentation provided in the Bishop & Wesley cell consisted of standard triaxial instruments to measure the deviatoric force, cell pressure, back or pore pressure, axial displacement and volume change. The deviatoric force was measured using an internal submersible load cell of the Surrey University type with a capacity of 5kN. The sample was attached to the load cell using a rubber suction cap (Atkinson & Evans, 1985). The cell water pressure and the back or pore pressure were measured by Druck pressure transducers with a range of 0-1000kPa. The axial displacement was measured externally by a linear variable differential transformer (LVDT) which was attached to the top of the cell and measured the movement of the pedestal. Volumetric strains were measured using a standard 50cc volume gauge of the Imperial College type. The gauge was fitted with a LVDT of the same type as that used for the external measurement of the axial displacement.

In a number of the tests the axial strain was measured internally using

submersible Hall effect transducers presented in Fig. 3.2 (Clayton & Khathrush, 1986). The development of an electrical field in a current carrying conductor placed within a magnetic field (the Hall effect) is used to measure the relative displacement between two points on the sample along the central gauge length (Fig. 3.2). The pendulum which holds the magnet is suspended from a top mount which is fixed to the specimen while the Hall effect chip is fixed in the bottom mount.

In one of the cells small water-submersible LVDTs (Cuccovillo & Coop, 1997) were used for the local measurement of axial strains. As pointed out in Section 2.2.1, the LVDTs were chosen to try to achieve measurements of stiffness at strain levels comparable to those caused by the dynamic loading of the bender element. A pair of RDP D5/200 LVDTs was used (Fig. 3.3) with a through bobbin bore and a right cable entry which allows free passage of the armature through the transducer at large strains. For the AC to DC signal conditioning a pair of RDP S7AC amplifiers was used.

The instruments were carefully calibrated before each series of tests in a particular cell and the linear range was recorded. The calibration constants were then checked routinely between the tests or at least within three to four months intervals. The standard procedures for calibration in use at City University are described by Lau (1988), Richardson (1988) and Stallebrass (1990a).

3.2.2 High pressure triaxial cells

The high pressure triaxial systems of 5MPa and 70MPa capacities were equipped with the standard triaxial instrumentation for the external measurement of axial and volume strain and more specialised transducers which would allow measurements of the high pressures. Both cells were also equipped with the bender element configurations which were redesigned to allow their incorporation into each apparatus.

A schematic diagram of the 5MPa triaxial system is given in Fig. 3.4. The triaxial cell with the capacity of 70MPa was of very similar design to the 5MPa cell but more heavily constructed to sustain the very high operating pressures. Details of the latter system are given by Cuccovillo (1995). The axial load in the 5MPa high pressure cell was applied by an axial load ram passing through the top of the cell. Stress controlled axial loading was achieved by means of a hydraulic cylinder located on top of the ram. Constant strain axial loading was applied by the motorised 5 tonne loading frame.

Analogue pressure converters for the axial stress, cell pressure and back pressure were again supplied with compressed air from the main

compressor. The air pressures for the axial loading and for the cell pressure acted through pressure multipliers which delivered oil at about ten times the input pressure for the 5MPa system, or one hundred times the input pressure for the 70MPa system. A pair of accumulators acted as the absorbers of spikes in the pressures which occurred during the function of the multipliers. For convenience the 5MPa cell was filled with water and the pressure from the multiplier passed through an oil-water interface while the 70MPa apparatus was oil filled. The 5MPa cell was also equipped with a separate hydraulic system to work within the low pressure range. This has been omitted from the schematic in Fig. 3.4 for clarity. The back pressure system was operated exclusively in the low pressure range, i.e. 0-0.7MPa, in which the volume gauge acted also as an air-water interface.

The axial load in the 5MPa cell was measured by an internal load cell with a capacity of 25kN of the Surrey University type. Cell and pore pressures were measured by Druck pressure transducers with a range of 6MPa. The axial displacement relative to the top of the cell was measured by an LVDT fixed to the ram. The volume changes were measured by standard 50cc volume gauge of the Imperial College type. The cell was also provided with a pair of Hall effect transducers (Clayton & Khathrush, 1986) for the local measurement of axial strain.

The axial load in the 70MPa cell was measured by an internal load cell with a capacity of 200kN while pore and cell pressures were measured by Maywood transducers with a range of 70MPa. The cell was provided with an LVDT transducer for external measurement of axial strains and a pair of oil-submersible LVDTs for local measurement of axial strains.

3.2.3 Control and data logging system

The control systems for each cell typically consisted of a single IBM compatible personal computer which ran a control program during the test. A computer program written in Quick Basic converted the readings into engineering units and made corrections for the apparatus compliance where necessary. During controlled stages the program calculated the differences between the actual stresses and these required and applied incremental changes accordingly to the analogue outputs which controlled the pressure converters. The program also allowed storage of the test data, providing both a soft and a hard copy of them.

In the standard configuration the transducer signals were logged by a CIL Electronics data logging card placed within the computer casing. The card was provided with eight channels for analogue to digital (A/D) conversion and four channels for digital to analogue (D/A) conversion. The A/D conversion was on a 16 bit basis and gave a resolution of 2^{15} of the full

scale input voltage. The gain could be selected from either a ±10V, ±1V or ±100mV range. A new subroutine was added to the program which performed autoranging of the channels giving the maximum resolution for any particular voltage input.

Based on experience in the measurement of very small strains developed at City University (Cuccovillo, 1995; Cuccovillo & Coop, 1997) a completely new data logging system was built for one of the Bishop & Wesley cells. The purpose of the new design was to achieve a high accuracy in the measurement of local axial strain so that stiffnesses determined during continuous loading tests could be directly compared with stiffnesses determined for the same soil specimen using bender elements.

The new data logging system consisted of Data Translation (DT) logging cards which were chosen because of their high input specifications. Two DT cards were employed each with eight differential input channels and sixteen bit resolution. One of the cards with better specifications had a working range of 20 mV at the highest gain and was used exclusively for logging the most critical input signals coming from the local axial transducers and the load cell.

The level of electrical noise during A/D conversion is critical to the accuracy of the measurement of very small strains. In order to minimise the electrical noise all of the transducer cables were carefully shielded and the shields were correctly grounded. All the connections were gold plated and twisted pair wires were used wherever possible. A new 10V power supply to the transducers was purposely built so as to be stable to $\pm 10^{-3}$V since any noise from the power supply would be seen in the output from the instruments. Finally, the autoranging software utility was employed with an integration of each reading over a relatively long period of 0.8 sec in an attempt to further reduce the effects of electrical noise.

3.2.4 Accuracy of the measurements

The characteristics of the transducers used are given in Table 3.1. The figures given for the resolution of the transducers correspond to a minimum gain and 16 bit A/D conversion. It should be noted that autoranging of the A/D channels was performed so as to get the data-logger to use the smallest possible input range for each transducer, thereby giving the smallest possible resolution and generally increasing the accuracy. The resolution is given as a value of the measured physical quantity and corresponds to a 38mm diameter and 76mm high sample for the Bishop & Wesley cell and a 50 mm diameter and 100m high sample for the

high pressure cells. The error of the measurement is given in two separate columns. The error determined predominantly by the electrical noise of the A/D conversion, is given as a value of the measured quantity so that for the strain transducers % refers to percentage strain. The relative error is given as a percentage of the current transducer reading so that for a strain transducer if the relative error is 0.3% and the current strain is 1% then the absolute error would be ±0.003% strain. The overall error is the sum of the two components, noise and relative error. The relative error is caused by the hysteresis, the non-linearity or by the drift of the transducer. The drift often originates from the changes in the supply voltage to the transducers and, more importantly, from the effect of the temperature fluctuations in the laboratory. The data for relative error given in the table are calculated for a monitoring period of 24 hours assuming a change of the stresses of around 500kPa and a change of the strains of about 1%.

If the measurement of the quantity is indirect such as an external measurement of axial strain or the measurement of volume change, the error of the measurement does not necessarily correspond to the accuracy of the instruments. As previously discussed in Section 2.2.1, other errors in the external measurement of axial strains (Baldi et al., 1988) may be caused by different sources such as tilting and misalignment of the sample, bedding and seating errors and the compliance in both load cell and loading system (see Fig. 2.1). Similarly, the volume of water in the volume gauge is temperature sensitive causing other inaccuracies in the measurement. However, the temperature fluctuation in the laboratory is time dependant so quick tests lasting only several hours will be less affected.

For the apparatus configuration and types of sample tested here, it was found that if the test was carried out with particular care and the sources of the errors were taken into account the external measurement of the axial strain was accurate to about ±0.005%. Generally, the volumetric strains were measured to about ±0.01% but for quick tests this was improved to about ±0.005%. If the measurement of the physical quantity is direct, as in the case for the axial load, the pore and cell pressures and the axial strain when measured locally then the accuracy of the measurement corresponds to the total error, as given in Table 3.1.

The importance of the temperature fluctuation in the laboratory is greatly amplified if the accurate measurement of very small strains is attempted. Water located in closed systems such as the hoses which lead to the axial loading chamber from motorised Bishop ram, tends to change its volume and accordingly pressure due to changes in ambient temperature. Additionally the state of the sample itself may be affected by temperature fluctuations thus making the total temperature effect very difficult to quantify. The isolation of the test from the environment and

the stabilisation of the temperature field surrounding the apparatus were, therefore, the remaining problems to be solved once the electrical noise had been reduced to the acceptable level.

In the apparatus for which the new A/D conversion system was specially built to reduce electrical noise, a pair of LVDTs was used for the local measurement of the axial strain (see Fig. 3.3). Applying the design measures given in the previous section the accuracy of the local measurement of axial strains was increased to be ± 0.00005% for a 76mm long sample. It should be emphasised that this figure is valid only for the most sensitive range of the data logger (±0.02V) which would be employed during a shearing probe up to about 0.01% axial strain which typically lasted for about the first 10 minutes of the test. It is considered that in that period of time there would be no drift and that the temperature fluctuation would be negligible since the cell and the hoses were covered by insulating materials and thus isolated from the rest of the laboratory. For the determination of the stiffness the deviatoric stress readings had to be made to an accuracy which was compatible with the strains. In this case the best achieved accuracy was determined by the noise on the load cell readings which was less than ±0.05kPa.

3.3 EXPERIMENTAL PROCEDURES

3.3.1 Preparation and setting up of the samples

The research programme consisted of testing a wide variety of soils which resulted in an extensive set of preparation techniques. The two fine grained soils (Speswhite kaolin and London clay) were reconstituted in the laboratory from a slurry while some natural samples of London clay were prepared from undisturbed tube samples. The coarse grained materials (Dogs Bay sand, decomposed granite and Ham River sand) were tested at a variety of initial densities, so that they have been prepared by water-pluviation, wet-compaction and dry-compaction. Finally cemented sand samples of Lower Greensand were prepared from cut blocks.

In all cases, care has been taken that the bender elements protruded undamaged and correctly aligned into the samples. It was necessary to make up a firm contact between the elements and soil sample to ensure a good transfer of energy between them. This requirement was not easy to achieve in stiff soils since bender elements are delicate and can be easily damaged if simply pushed in. Also it was necessary to ensure that the positioning of the elements did not cause disturbance to the sample. To satisfy these conditions a new techniques were developed for the

positioning of the elements in the materials which were being tested for the first time. A summary of all the techniques used for placing the bender elements into contact with the material is given in Table 3.2 and a description of each technique is given in this section.

(i) reconstituted samples

The samples of Speswhite kaolin were reconstituted from dry powder. The soil was mixed by hand with de-aired water in the ratio of 1:1.3 to form a slurry which was then de-aired in the vacuum chamber. The length of the de-airing process depended on the amount of slurry and lasted as long as was necessary for the trapped air to be evacuated and no less than 30 minutes. The slurry was then poured into a perspex consolidometer tube with the bottom piston, porous stone, filter paper and removable ring extension assembled, as shown in Fig. 3.5. The inner wall of the tube was previously lubricated with silicon oil to reduce the development of the friction between the soil and the perspex. The filter papers were slightly oversized to prevent the slurry from escaping through the gaps between the porous stones and the tube walls. After the slurry was poured in, the top of the consolidometer was cleaned leaving 2cm to 2.5cm clearance for the placement of the top piston, porous stone and filter paper. The sample was then loaded carefully along the vertical axis, initially only by the weight of the load hanger (approximately 1kg) and left to consolidate for several hours. All samples were then loaded further with discrete increments up to the total load of 8kg which corresponded to a total vertical stress of around 70kPa. The base extension ring was removed after the first loading step so that from that point onwards the consolidometer tube was floating.

Before the sample was taken from the consolidometer the triaxial cell was prepared for the test. The cell body was filled with water and while open to the atmosphere all the stresses were zeroed. The water in the drainage system (i.e. pore pressure leads, volume gauge and volume gauge leads) was replaced by fresh de-aired water using a Bishop ram. The base pedestal was then greased with silicon grease around its perimeter to ensure a good seal between the membrane and the metal once the sample was mounted. The filter papers to be placed on the top and bottom of the sample were cut with a slot in the middle to allow the bender elements to pass through. The porous stone was de-aired for 45 minutes in a vacuum chamber.

At the end of the consolidation the sample was extruded onto a brass cradle which was slightly greased with silicon oil to prevent the sample sticking. While resting in the cradle the sample ends were carefully trimmed using a wire saw. The weights of the trimmed material and the sample were then measured on a precision balance. The trimmed material was immediately placed in the oven for 24 hours to dry so that initial water content could be determined. The height of the sample and its

diameter were then measured using a vernier calliper. The initial dimensions were determined from the mean values of the five measurements taken across the sample.

At this stage the porous stone was placed on the pedestal with a previously dampened filter paper on the top of it. The filter paper was wiped off swiftly to remove excess water. While rotating the cradle through 90^0 with one hand the second hand gently maintained the sample in a vertical position. The sample was then placed with careful alignment directly onto the base pedestal. The sample was in relatively soft state so that bender element easily penetrated the soil. A previously dampened filter paper for the radial drainage was then placed on the sample with its slot positioned so as to allow the top bender element to be aligned with the bottom one. The membrane was first placed over the sample and then the top platen was inserted. Finally the membrane was released from the stretcher to grip the pedestal, the top cap and the sample. The O-rings were next positioned, two on the top and two on the base pedestal, ensuring a seal. The rubber suction cap was then placed on the top platen.

If it was required at this stage a pair of Hall effect transducers was mounted (Fig. 3.2b) on the opposite sides of the sample. The transducers were held by the two mounts with the distance of around 50mm between them. The bottom mount was simply glued directly to the membrane in a previously marked position. The top mount with the pendulum holding the magnet was then carefully aligned with the bottom one and again glued to the membrane. Jardine et al. (1985) showed that it was not necessary to hold local axial strain transducers to the sample with pins as there was no slippage between the membrane and soil until very large strains. The semiconductor chip was finally inserted into the slides of the bottom mount, positioned so as to deliver the required initial output voltage and fixed using two miniature screws. Finally the distance between the mounts was determined from the average of two measurements.

For some tests a pair of miniature submersible LVDTs was used for the measurement of the local axial strain. They were also attached directly to the sample diametrically opposite to each other as shown in Fig. 3.3b. The mounts were vertically aligned and glued directly to the membrane again using a cyanoacrylate instant cement. The stiffness of the transducer cables hindered the vertical positioning of the transducers. For this reason the cables were reinforced by a copper wire shown in the figure which was coiled around them, allowing the cables to be bent to the required shape. The transducers were then vertically positioned so that the position of the armature gave the required initial output voltage. Finally, the transducer was fixed in place with a miniature screw and the distance between the mounts was carefully measured using a vernier calliper.

The preparation of the reconstituted sample of London clay differed from that of the kaolin only in that it was done starting from its natural water content and not a dried powder. To create the slurry the material from the sampling tube was, therefore, first left submerged in distilled water for a couple of days and then thoroughly mixed. The estimated water content of the slurry was calculated as 50% greater than the liquid limit of the soil following the recommendation of Burland (1990).

(ii) natural samples

The preparation of the natural samples was performed in a room in which a relative humidity of 80% was controlled. Material was extracted from rotary cored tubes and cut to the required height using a wire saw. To prepare a 38mm diameter sample the soil was firstly trimmed with a sharp knife or saw to the approximate dimensions of 50X50X100mm following the original orientation of the sample in the tube. Care was taken that the ends were perpendicular to the axis of the sample. The sample was then mounted in a hand lathe. Trimming was done using a wire saw cutting thin slices from the perimeter of the sample down to the required size. At different stages during trimming the discarded material was used for the determination of the water content.

After being trimmed to the correct diameter the sample was placed in the cradle and further trimmed at the ends to the required height of 76mm. Again care was taken to ensure that the ends were plane and perpendicular to the axis of the sample. The initial dimensions were again determined from the average of five measurements taken across the sample. The slots for bender elements were marked at the ends of the sample and then carefully excavated using a miniature tool, ensuring their correct alignment. The slots were cut slightly undersized so that bender elements protrude into fresh soil once the sample was mounted in the cell.

The setting up procedure for the natural samples was otherwise the same as previously described for reconstituted samples.

(iii) pluviated samples

Wet-compaction and water-pluviation (Bishop & Henkel, 1962) were chosen as the principal preparation methods used to produce sand samples in as loose a state as possible. All the samples had a known initial grading which was controlled so the preparation of the samples started by weighing the various particle size fractions to create a specimen of the required weight and grading for the particular test. The various gradings of the sample were then thoroughly mixed, submerged and left to de-air in the vacuum chamber for 45 minutes.

The triaxial cell was prepared for the test as described earlier. A split mould with a suction tube was used for the preparation of the samples.

The mould was firstly greased at the contact edges to ensure the air-tightness and then assembled. A de-aired porous stone was placed on the pedestal and the membrane was passed over it and fixed to it with an O-ring. The mould was then passed over the membrane and positioned vertically resting on the pedestal o-ring. The membrane was stretched over the top of the mould. A small vacuum pump was then attached to the mould's suction tube creating the vacuum which held the membrane in full contact with the mould.

The drainage lead to the bottom pedestal was connected to a burette by a hose which was water filled. The burette was placed on the floor so that when a valve to the burette was opened a negative pressure of around 10kPa would be developed within the water in the mould. Care was taken that the mould was always full of water while the sand was poured in with a small spoon. The process of pouring was stopped when the clearance between the top of the specimen and the top of the mould was about 2mm. The top of the specimen was then made flat and the top cap carefully positioned on the top of the sample so that the bender elements were aligned. The cap was then gently pushed in taking care of its vertical alignment. The membrane and top O-ring were then placed on the top platen and the burette valve opened. The initial dimensions were determined from an average of several measurements taken across the sample. The initial diameter was calculated deducting the thickness of the membrane.

(iv) wet-compacted samples

The preparation of samples by wet-compaction (Lee, 1991) was used mainly for the decomposed granite. This soil could not be pluviated because its well graded nature would have caused segregation. Decomposed granite was difficult to saturate so that the wet-compaction was followed by the flushing of the sample with a carbon dioxide. Carbon dioxide is more soluble in water than air so by replacing the air in the pore space full saturation is made possible. The same carbon dioxide treatment was also applied to the dry-compacted samples.

Preparation of the sample started by weighing the air-dried particle size fractions in the proportions to create the correct initial grading. The specimen was then thoroughly mixed in a dry condition and then further mixed with water in the proportion of 10% of its dry weight, after which it was covered with cling film and left for an hour.

The preparation of the cell, the sample mould, the membrane and the burette was as already described for the pluviated samples. The material was placed in the mould in 10-12 layers with a small spoon. Each layer was lightly compacted with a wooden tamping rod. For samples intended to be very loose the tamping was done with minimum energy while ensuring the homogeneity of the sample. For samples intended to be denser the tamping was more energetic while not allowing any breakage of the particles. The

process of pouring and compacting was stopped when the clearance between the top of the sample and the mould was about 2mm. At this stage carbon dioxide under a light pressure (1-2kPa) was introduced into the sample through the bottom drainage lead. The gas was evacuated from the top of the sample through a special temporary drainage lead. The flow of carbon dioxide was detected by passing the gas drainage through a calcium hydrodioxide solution. It usually took a couple of minutes to detect the gas flow but the supply was left for another 20 minutes. After that, the gas supply was removed and de-aired water was introduced into the sample through the bottom drainage lead. The water was allowed to seep slowly in from a small reservoir located above the sample giving a pressure of 1-2kPa. The process was stopped when it was seen that there were no more gas bubbles coming out of the sample. The sample was then completed by removing the temporary top cap and placing the bender element top platen on the top of the sample. The suction to the pore fluid was then applied via the burette, as previously described. The initial dimensions were measured as for the pluviated samples.

Decomposed granite has very sharp particles and the first few high pressure tests were lost due to punctures of the membrane. In subsequent tests a total of three or four standard thickness membranes were used. Additionally particular care was taken that there were no particles trapped between the base pedestal or top platen and the membrane. As was understood from the examination of the punctured membranes, particles trapped between the membrane and the rigid boundaries at the base or top of the sample had caused the punctures.

(v) dry compacted samples

The soil sample was assembled from the particle size fractions following the required grading and then thoroughly mixed. The sample was then placed in the prepared mould in 10 to 12 layers. Each layer was compacted by a vibration which was caused by gently tapping the mould with the metal rod. The procedure was otherwise the same as for the wet-compacted samples.

(vi) cemented sand samples

The samples were cut from the blocks of known orientation using an electric saw to the rough dimensions of 70X70X130mm. Care was taken to ensure the verticality of the sample axis and that the ends were flat and perpendicular to it. The sample was then mounted in a 50mm trimming lathe and then trimmed around its perimeter with a specially designed knife with quick and energetic movements. After trimming the perimeter the sample was moved to the cradle where the ends were further trimmed giving the sample the required height of 100mm. It was very important to ensure that the sample had a precise flatness at its ends since any irregularities could have endangered the operation of the bender elements

during the test. The sample was then submerged in de-aired water and left in the vacuum chamber for several hours.

The slots for the bender elements were marked and then excavated by hand. The slots were made slightly larger than elements leaving the gap of 1mm at the sides which was then filled to ensure a firm contact between the elements and the soil. A quick setting epoxy mixed with the soil particles in a ratio of approximately 1:1 by weight was chosen for the filling material so that the acoustic impedances of the soil and filler were similar. This enabled the exchange of the energy between the element and the material to be made with minimal losses. The bender elements were greased with silicon grease, pushed into the slots which already contained the filler and left in position for the epoxy to set (Fig. 3.6). The thin film of grease isolated the elements from the epoxy so that the test could be dismantled without damage to them.

Reconstituted samples of Lower Greensand were made by breaking the bonding between the particles. An attempt was made to do that by hand but this was found to be impossible. A technique which allowed the bonds to be broken without damaging the particles was to place two pieces of the rock together and gently scrape them. The force used was minimal so it is believed that no particle breakage was caused.

3.3.2 Saturation and stress controlled stages

Once the sample had been placed in the triaxial apparatus the cell body was fixed in place and the cell was filled with water. The positions of the externally mounted strain transducers were adjusted to be within their linear range. After zeroing the strain transducer readings the test proceeded with the saturation stage.

(i) clays

Using the computer control the cell pressure was increased up to a value which caused the pore pressure in the sample to be the same as the preferred back pressure to be used throughout the subsequent drained stages of the test. During this initial undrained stage the rate of loading was typically 10kPa per hour. After reaching its final value the cell pressure was kept constant and the test was left overnight for the pore pressure to stabilize.

The saturation of the sample was monitored by measuring Skempton's (1954) 'B' value. Ideally a 'B' value of 1.0 should be obtained indicating full saturation of the sample. It was considered that a 'B' value greater than 0.98 was satisfactory enough for the test to proceed. The 'B' value was only occasionally higher than 0.98 at the first attempt even for

reconstituted samples. This may be attributed to the fact that there was some air trapped in the gap between the bender element and the porous stone. In order to eliminate trapped air in the drainage system flushing of the drainage leads was carried out. The flushing was done slowly, not allowing the pore pressure in the sample to drop more than 2-3kPa. After flushing the 'B' value was checked again and if still under the limit of 0.98 the sample was then left to saturate as long as necessary. After saturation the suction cap was connected to the load cell following the procedure described by Lau (1988).

The majority of the tests consisted of drained isotropic compression stages. Each stage was typically carried out using the computer control of the stresses which varied at constant rate. The rate of loading was chosen so as not to allow any significant excess pore pressure to develop during the stage, following the recommendation of Cherrill (1990). When the required stresses were reached the sample was left under constant stresses as long as was necessary for any small remaining excess pore pressure to dissipate, giving stable volume strain readings. At this point the measurement of the small strain stiffness using bender elements was carried out. For the two soils tested (Speswhite kaolin and London clay) no noticeable influence of creep was seen on the value of G_{max}.

The test was ended by detaching the suction cap, closing the drainage and releasing the cell pressure. The sample was then dismantled from the cell quickly and final dimensions were measured. The sample was then cut into three pieces horizontally and the final water content measured for each.

(ii) sands

Typically the sand samples manufactured were not fully saturated so that they had to be further saturated in the triaxial cell. The cell pressure and the back pressure were adjusted so as to give a 20kPa effective stress once the drainage was open. The drainage leads were then flushed through. A controlled increase of the cell pressure and the back pressure was started so as to maintain a constant effective stress. The back pressure was increased up to the preferred value which was to be used during the drained isotropic compression stages. When the stresses reached their final values they were kept constant and the sample was left to saturate as long as necessary. In some cases the acceptable level for 'B' value was reduced to 0.95 as a compromise between the length of saturation and the expected error in the readings of the volume change due to a slight partial saturation.

After the attachment of the suction cap the isotropic compression stage was carried out drained by varying the stresses using the computer control. Generally, the loading was applied at constant rate of 20kPa per hour at stresses up to 2000kPa and 50kPa per hour at higher pressures. These rates of loading will be discussed in detail in Section 4.3 where

the influence of the creep and aging on G_{max} is also analyzed. Bender element measurements of the soil stiffness were taken during the loading stages together with a record of the current state of the soil.

At the end of the test the suction cap was detached from the load cell and the drainage valve was closed. When the pressures were released the sample was carefully removed from the pedestal and quickly placed into a beaker and the water content measured. The membrane was weighed before and after it was thoroughly cleaned so that the material left on it could be taken into account when the determination of the final sample weight was carried out.

3.3.3 Shearing stages

With the purpose of comparing static and dynamic measurements of soil stiffness at very small strains, a series of shearing probes was carried out on one of the sands under undrained conditions. The tests were performed using a Bishop & Wesley cell and data logging system which was especially built for this purpose, as previously described in Section 3.2.3.

In order to resolve the required stiffnesses it was necessary to ensure that there was a smooth increase of the axial load. This was done using a strain controlled loading rather than stress controlled and was achieved by means of a stepper motor attached to the Bishop ram. It was considered that stress control loading was not capable of delivering a sufficiently smooth increase of stresses. Even in its most stable condition the tolerance of stress control is of the order of 0.5-1.0kPa which is much greater than the accuracy of deviatoric stress required to resolve the stiffnesses at very small strains.

For the same reason the cell pressure was also not controlled by computer throughout the shearing stage. Because a hydraulic triaxial cell was used, a small change in cell pressure would have affected the deviatoric stress on the sample. The cell chamber was therefore isolated from the pressure control system by closing the air valve placed in front of the air-water interface. The flexibility of the static cell pressure system thus created was ensured by including the interface. In that way the cell pressure was not sensitive to the change of the volume of the cell water due to a temperature fluctuation or the penetration of the axial ram into the cell.

As previously discussed, the temperature stability of the room and the electrical performance of the logging system were critical for the high accuracy of the small strain measurement. Before each stage of shearing the cell body and all the hydraulic hoses were covered with insulating

materials isolating the cell from the rest of the air in the laboratory. The air-conditioning was temporarily switched off to prevent any air temperature fluctuation in the room during the stage. A slow increase of temperature was found to be less problematic than rapid changes due to the air-conditioning switching on and off.

Finally, to resolve the very small strains at the start of the shearing stage the local LVDTs were set at their electrical zero. This was done by adjusting the zero potentiometer on the amplifier. The small output from the transducer thus allowed the data logger to work in its most sensitive range (±20mV) since the logging was controlled by the new autoranging software routine. Before the shearing stage was started the system, including the stepper motor of the Bishop ram, was left to warm up for at least 30 minutes to achieve a constant temperature.

3.3.4 Calculation procedures

The calculation of the specific volume of the sample during the test was based on the initial specific volume, the measured volume change during the test and also the final specific volume at the end of the test. In the case of the clays the initial specific volume could be calculated from the initial water content of the trimmed material. The water content, w, was determined by weighing a sample of the soil and then drying the sample for 24 hours in an oven at a temperature of 105-110^{o}C and re-weighing it. The water content can then be calculated from:

$$w = \frac{M_w}{M_s} \qquad 3.1$$

where M_w is mass of water and M_s is mass of solids. The specific volume was then calculated from:

$$v = 1 + wG_s \qquad 3.2$$

where G_s is the specific gravity of the solid particles taken from published material for the particular soil.

In the case of the coarse grained materials the initial specific volume, v, was calculated from the dry weight and initial dimensions of the sample assuming full saturation. In that case:

$$v = \frac{V}{V_s} \qquad 3.3$$

where V is the volume of the sample and V_s is the volume of the solids calculated from:

$$V_s = \frac{W_s}{\gamma_s} \qquad 3.4$$

where W_s is the dry weight and γ_s is the unit weight of solids.

It was not always possible to achieve a perfect agreement between the values of the final specific volumes (v_f) calculated from the final water content measurements and those ($\underline{v}_f$) calculated from the initial specific volume. Examples of the comparison are given for each type of soil in the relevant chapters (Tables 4.1a and 5.1). For the clays some of the error seen may be accounted for by an unrecorded change in water content caused by the pressure relief at the end of the test which unloads the sample, making it swell and sucking some water in from the drainage leads. To avoid this error in the determination of the final water content the clay samples were cut into three pieces horizontally and the water contents of the pieces were measured separately. It was always the case that the bottom piece, being the nearest to the drainage leads, had the highest water content. In the calculation of the final water content of the clay samples this measurement was usually ignored. The specific volumes during each test were determined as the average of values calculated from the initial and final values.

In the case of the sands small discrepancies between the initial and final water content were again seen. The average variation between the specific volumes calculated from the initial and final values was, however, only 0.3%, as can be seen in Table 4.1a for the samples of Dogs Bay sand. In comparison with data published by other authors who tested the same materials (Lee, 1991; Coop, 1990) it was found that the specific volumes calculated from the initial state were more consistent with the published data and these have, therefore, been used in the processing of the results.

The standard set of formulae for the calculation of stresses and strains in the triaxial test is based on the assumption that the sample deforms preserving its original cylindrical shape. In this case the current cross sectional area, A_c, of the specimen is calculated from:

$$A_c = A_0 \frac{(1-\varepsilon_v)}{(1-\varepsilon_a)} \qquad 3.5$$

where A_0 is initial cross sectional area of the sample and ε_v is the volume strain:

$$\varepsilon_v = -\left(\frac{\Delta V}{V_0}\right) \qquad 3.6$$

where V_0 is the initial volume of the specimen and ΔV is the change of the volume. The axial strain ε_a is determined from:

$$\varepsilon_a = -\left(\frac{\Delta H}{H_0}\right) \qquad 3.7$$

where H_0 is the initial length of the specimen and ΔH is the change of the length. The radial strain is then calculated from:

$$\varepsilon_r = -\frac{\sqrt{\frac{4A_c}{\pi}} - D_0}{D_0} \qquad 3.8$$

where D_0 is initial diameter of the specimen. Finally the axial stress is calculated from:

$$\sigma_a = \frac{F}{A_c} + \sigma_r \qquad 3.9$$

where F is the deviatoric force measured by the load cell and σ_r is the radial stress measured by the cell pressure transducer.

Out of the three sands tested only the decomposed granite had the grading sufficiently coarse to necessitate a correction of the volume strain data for membrane penetration. The dependence of the volume correction per unit area of the membrane surface (i.e. unit membrane penetration) on the radial stress was taken from the experimental results of Lee (1991) who tested the same soil with the same initial grading. When more than one membrane was used on the same sample the correction has taken into account that the amount of penetration is inversely proportional to the third root of the membrane thickness. No corrections for the membrane restraint have been made on any of the test data for the shearing probes. It was considered that the effect was sufficiently small at the pressures used to be neglected, particularly as the shearing probes reached only 0.1% axial strain.

The value of undrained tangent stiffness was defined as:

$$G = \frac{1}{3}\frac{\delta q}{\delta \varepsilon_a} \qquad 3.10$$

where δq is the change in deviatoric stress and $\delta\varepsilon_a$ is the change in axial strain. Numerically, the stiffness was calculated as one third of the gradient of a regression line for a certain number of points from the graph of the deviator stress plotted against the axial strain. The regression line was determined using the least square method. The number of points for the regression was chosen ensuring that the interval did not exceed 15% of a logarithmic cycle of strain. This procedure is explained further in Section 4.6.1.

3.4 BENDER ELEMENT MEASUREMENT TECHNIQUE

3.4.1 Instrumentation

Piezoelectricity is an electrical polarisation produced by mechanical strain in certain crystals. The piezoelectric polarisation is proportional to the amount of straining and changes sign with its direction. Conversely the electrical polarisation of a piezoelectric crystal will induce a mechanical strain proportional to the input and corresponding in sign to it. Piezoelectric properties occur naturally in some crystals but can be induced in other polycrystalline materials by the process of poling in which the crystal is exposed to an intense electrical field at elevated temperatures. Poled piezoceramic materials have found a broad use in industry as electromechanical transducers. The polarity of poled piezoceramic elements may be altered if they are exposed either to high pressures or a high temperature regime.

A bender element is a piezoceramic element made of two transversely poled plates bonded together with surface electrodes coating it (Fig. 3.7). A voltage applied to the electrodes causes the plates to deform in opposite directions, i.e one expands and the other one contracts. When one end of the element is fixed the excitation by the external voltage will make the opposite end move and the element will bend in the direction normal to the face of the plates, as illustrated in the figure. Conversely, the movement of the element will generate a small voltage which is detected at the electrodes. The bender bimorph element used in the project was made of piezoelectric ceramic (lead zirconate titanate), PZT-5B. It was manufactured and cut to a size of 13X10X0.5mm by Vernitron Ltd.

The element with the series connection (see Fig. 3.7) of the electrodes will produce twice as much voltage as the parallel connected one and is therefore preferred to receive the energy from the soil. This response occurs because the voltage is equal to the sum of the potentials available to the electrodes of each of the polarised plates. An element with parallel connected electrodes will provide twice as displacement as one with a series connection and is therefore preferred to transmit the energy of movement to the soil. With a parallel connection the available voltage is applied to each ceramic plate and is not divided between them as in the series connection.

The output of the transmitter can be also detected since, as in the case of the receiver, the small voltage is generated by its movement. This is done by isolating a part of both piezoceramic plates from the rest of the element and attaching a separate wiring to them which is independent of the driving voltage. This self-monitoring element, described in detail

by Schulteiss (1982), was found to be a useful tool in the interpretation of the bender element test.

When placed so as to protrude with the free end into a soil sample and excited with an external voltage the transmitter element will move and send a shear disturbance through the soil. The arrival of the disturbance can be detected by the receiver located at the opposite end of the sample and aligned in the same direction as the transmitter. The time between the transfer of the motion from the transducer to the soil and the motion of the receiver represents the travel time of the shear disturbance through the sample. Bender elements can be set up in most laboratory apparatus such as the oedometer (Schulteiss, 1982), the triaxial (Dyvik & Madshus, 1985) and the true triaxial (Agarwal & Ishibashi, 1991) apparatus but has also been used in the centrifuge (Gohl & Finn, 1991).

The apparatus configuration fitted into the triaxial apparatus used in this research is presented in Fig. 3.1. The transmitter and the receiver both protruded about three millimetres into the sample. The elements were isolated from the pore water by an epoxy casing and were connected with the instruments via submersible cables. The pulse generator (Thandor TG105) and the function generator (Thandor TG501) both had a range of 5Hz to 5MHz and were used to supply the transmitter with a waveform driving voltage of typically 20 volts amplitude. The transmitted and received signals were logged by the two channels of a Tektronix 2211 (50MHz) digital oscilloscope. The high sampling rate of this oscilloscope ($20x10^6$ samples per second per channel) was required to enable sufficiently accurate measurements to be made of the time distance between the characteristic points of the signals which varied between 0.1ms to 0.5ms. The measurement was taken directly from the screen image which is shown in Fig. 3.8. The data were then usually dumped via an RS232 interface to the hard disk of a PC-IBM compatible for further processing.

During the course of this project a departure from the original design of the bender element configuration was needed in order to improve the quality of the received signal which was found to be severely corrupted by the electrical noise. For the purpose of reducing the electrical noise an aluminium foil shielded cable (Belden miniature 9452) replaced the existing coaxial cable in connecting the elements to the electrical instruments. All soldered connections were also more carefully shielded than had previously been the case. The shields, triaxial cell and electrical instruments were also properly grounded making sure that no ground loops occurred. A more complex design of the top cap and the bottom pedestal, shown in Fig. 3.9, was needed to accommodate the new shielded cables and prevent any leaks of cell water into the cables.

These modifications resulted in a substantial reduction of the electrical noise so that no external amplification of the signals prior to the oscilloscope was needed, nor any filtering or averaging the data. The

high quality of the received signal was of critical importance in developing new objective criteria for the determination of the arrival time, as it will be explained in Section 3.4.4.

Before use, the system was checked for the time delay between the excitation of the transmitter and the response of the receiver caused by sources which were not related to the propagation time through the sample. The traces from the self-monitoring element shown in Fig. 3.10b show that no time-lag was observed between the excitation of the element and its response. In order to check if there was any time delay in the response of the receiver a special clamp was designed to put the receiver and the transmitter into stationery and full contact. Under these conditions, for some configurations a time delay was seen between the driving and received signals due to inertia of receiver but it was always less than 1.5μsec (Fig. 3.10a). As will be discussed in Section 3.4.4, the total error of the measurement of the arrival time was around $\pm$1% which for the arrival times typically measured, exceeds this inertia offset by a ratio of five to ten.

During the three years of the research the performances of the systems were generally stable and no depolarisation of the elements was seen even though the elements were exposed on some occasions to high pressures of up to 70MPa during the tests. Initially there were some leakage related problems when the water from the cell entered the cable which leads to the element so that electrical shorts occurred. Once these had been solved the bender elements were used without further difficulties.

3.4.2 Theoretical background to the method

The theoretical background related to all wave propagation methods has been summarised in Section 2.2.2. Here, theoretical and numerical studies have been carried out to examine specific aspects of the bender element measurement technique in the triaxial apparatus. The work of Gajo (1996) on the propagation of pulses through saturated porous media, which is relevant to the bender element technique was also given in Section 2.2.2 and will not be repeated here.

The bender element configuration in the triaxial apparatus is used to measure the time of the propagation of a shear wave through the soil sample. Excited by the external voltage the transducer element moves and acts as a source releasing energy into the soil so that shear stresses propagate away through soil sample. The waves are captured by the receiver which is aligned so as to detect the transverse motion which travels with the shear stresses. The travel time T_a is measured as a time distance between the characteristic points on the screen of the

oscilloscope, as shown in Fig. 3.8. Point 1 corresponds to the start of the transmitter motion which is in this case a single sine pulse. This represents the moment of energy transfer from the source to the soil. Point 1' corresponds to the start of the receiver motion and represents the moment of the energy transfer from the soil to the element. Assuming that the strains induced by the bender elements to the soil are elastic and knowing the current tip to tip distance L_a between the elements the velocity of shear waves is calculated by:

$$v_s = \frac{L_a}{T_a} \qquad 3.11$$

so that the very small strain (i.e. elastic) shear modulus G_{max} is determined from:

$$G_{max} = \rho v_s^2 \qquad 3.12$$

where ρ is the mass density of a dry sample or total mass density of a saturated sample.

The bender element method is based on the following simplifying assumptions which underlay all wave propagation methods:

(i) the strains induced in the soil by the transmitter are very small, i.e. the soil response to the dynamic loading is elastic

(ii) the travel distance of the shear wave corresponds to the tip to tip distance between the elements

(iii) the body wave imposed by the transmitter to the soil is a plane shear wave, i.e. only transverse motion travels with the velocity of the shear wave

(iv) the soil sample acts as an infinite medium for the given source-receiver configuration, i.e. all the waves reflected from the boundaries of the sample arrive later at the receiver than the direct wave originating from the transmitter

There is a very little evidence to support directly assumption (i) since it is virtually impossible to measure the actual strain which occurs at the contact between the soil and the element. The guidance given by Dyvik & Madshus (1985) that the level of strain does not exceed 0.001% is probably just an estimate. For free-air (i.e. unrestrained) conditions the transmitter movement can be calculated from the piezoelectric constants of the material and the amount of input voltage applied but these do not correspond for an epoxy coated element which is in the contact with the soil. However, the hypothesis that the soil response is genuinely elastic for the strain level imposed at the contact could be

regarded as experimentally sound. In the course of this testing programme the stiffnesses of some samples were low but no accumulation of the strain was ever observed in the sample due to the dynamic loading. That is, when bender element tests were performed on drained samples no extra volume change was observed or when they were performed on undrained samples no build up of excess pore pressures was found. Taking into account that the dynamic loading was essentially cyclic this fact suggests that the soil developed recoverable strains only. It should be also noted that the level of the strain is not constant in the sample but is expected to reduce further from the source due to geometric damping, as will be demonstrated from the results of numerical analyses given in the next section.

Viggiani (1992) established the validity of assumption (ii). Three sets of reconstituted samples of Speswhite kaolin were tested each under the same stress-strain state but having different lengths. The length of the sample plotted against the arrival time should lie on straight line since the velocity of shear wave is the same (Equation 3.11). For each set of tests the straight lines met at the same intercept which was found to be equal to the sum of the protrusions of the elements into the sample. This proved that the distance between the tips of the elements is the actual travel distance of the shear wave. Dyvik & Madshus (1985) calibrated measurements from bender element tests based on the same assumption. The calibration took place in a resonant column apparatus and the same conclusion has been reached.

Assumption (iii) is generally not valid. For the range of distances and frequencies typically used in the bender element test in the triaxial apparatus the waves generated by the point source represented by the transmitter cannot be considered plane but are spherical, so that it is not the case that only transverse motion travels with the velocity of the shear wave. Spherical front waves exhibit a far more complex propagation and polarisation pattern than plane waves and, theoretically, the absolute separation of the body wave into shear and compression components is not possible.

The most comprehensive analytical solution to the problem of the body wave propagation through the soil is given by Sanches-Salinero, Roeset & Stokoe (1986). The subject of the study was the propagation of a wave front originating from a point source through an infinite and isotropic elastic medium. The analytical solution for the time record of the point located at a certain distance from the source is given in the Appendix. The source point is subjected to motion of the shape of a sine pulse which is transversely polarised relative to the position of the receiver. The resulting wave was far from being a simple transversely polarised shear wave propagating in a longitudinal direction as is assumed by the bender element method. It was found to have three coupled components, corresponding to the three terms of the solution given by Equations A3.2

and A3.3. The same equation is presented in simplified form in Equation A3.4 as a sum of three terms Γ1,Γ2 and Γ3 which all represent transverse motion but which travel with different velocities. The first two (Γ1 and Γ2) travel with the velocity of a shear wave, and the third (Γ3) travels with the velocity of a compression wave.

Geometric damping results from the fact that the same amount of energy reaches more material as the wave propagates through the sample. For the three components the attenuation arising from geometric damping occurs at different rates, the second and third terms (Γ2 and Γ3) attenuate one order of magnitude faster than term Γ1. Terms Γ2 and Γ3 are known as a near field waves since they are detected only near the source. Term Γ1 is a pure shear wave and is the only one detected in the far field.

Far from the source the near field waves attenuate to the point where they become negligible. Geometric damping therefore separates the near field coupled compression and shear waves from the far field, pure shear waves. Sanches-Salinero et al., (1986) expressed their results in terms of a ratio denoted here as R_d. They recognized that this will control the shape of the receiver trace at the point of monitoring through the degree of attenuation due to geometric damping. The value of R_d is defined as the ratio between the source-receiver distance d and the wavelength of the source wave λ_w:

$$R_d = \frac{d}{\lambda_w}, \lambda_w = \frac{v_s}{f} \qquad 3.13$$

so that:

$$R_d = f\frac{d}{v_s} \qquad 3.14$$

and f is the frequency of the source wave. Two traces for different values of R_d are shown in Fig. 3.11. Whereas the solution given in the Appendix includes material damping through its complex part the results plotted in Fig. 3.11 are for the case with no material damping which is compatible with the assumption of linear elasticity made by the bender element method. The traces plotted then correspond to the real part of Equation A3.3. The time axis is normalized with respect to the theoretical value of shear wave arrival time so that value of 1.0 on the axis should be seen as the sharp reversal on the receiver trace if it does represent the arrival of the shear wave. According to solution this feature is clearly observed only for values of R_d higher than 2.0. For low values of R_d there is an initial downward deflection of the trace before the shear wave arrives, representing the near field effect given

by the third component (Γ3). At high values of R_d the near field effect is almost absent.

In conclusion, assumption (iii) is valid only in the absence of the near field waves. This is achieved, as seen in Fig. 3.11, by increasing the frequency of the transmitted wave, following Equation 3.14, since d and v_s are constant for any particular measurement. Being of predominantly one frequency, a single sine pulse is the most convenient choice for the shape of the transmitted wave. The practical aspects of this conclusion on the interpretation of the bender element test will be discussed in Section 3.4.4.

Finally, assumption (iv) was not possible to check analytically since the complex boundary conditions of the bender element configuration in the triaxial apparatus prevent any closed form solution. Instead, finite element analyses, described in detail in the next section, were used to examine the independence of the method from the source-receiver configuration.

3.4.3 Numerical solution

The analytical solution by Sanches-Salinero et al., (1986) is based on an idealised geometry where the source and receiver are regarded as points with an unbounded medium between them. In the bender element configuration the elements act as the source and as the receiver while the soil sample acts as the medium. In this case the geometry is thus defined in finite dimensions where the elements are in certain proportions to the sample and the conditions on the boundaries are dictated by the overall design. As a consequence, while the analytical solution is based on the assumption that there is no influence of the source-receiver configuration on the propagation of the waves through the medium this point has yet to be proved for the bender element configuration in the triaxial apparatus. Since no closed form analytical solution is possible due to the complex geometry involved, the only way to prove the point is to check the applicability of the analytical solution using numerical analyses. This is to be clarified further by analysing not only the dynamic aspects of the numerical solution but also the state of strain in the sample during wave propagation.

A set of numerical analyses was done using the program package Solvia 90 provided by the University of Bristol. The program is written to perform stress-strain analyses of structures undergoing dynamic loading using the finite element method. Solvia 90 was chosen as it is a program which is able to perform analyses for which the geometry of the model is defined in three dimensional space (3D analyses) allowing the complex geometry of the prototype to be accurately modelled. For the frequencies of

interest the analyses required a fine mesh and a very short time step. As a consequence, 3D analyses proved to be extremely expensive in terms of computation time and required memory. For this reason plane strain "probe" analyses were carried out first (2D analyses). The "probe" analyses were based on the assumption that the movements out of the plane defined by the propagation and polarisation directions of the shear disturbance are very small. As will be shown later, a subsequent set of 3D analyses, in which the geometry of the problem was more strictly modelled, gave qualitatively the same result but because of the expense did not have the high resolution achieved in the 2D analyses.

In both analyses an isotropic and elastic numerical material was used to model the soil response to dynamic loading. The material properties corresponded to the results of a bender element test in the triaxial apparatus on saturated Speswhite kaolin under an isotropic confining pressure of 200kPa. The value for Young's modulus E of 118MPa was back calculated from the results of a bender element test which measured the small strain shear modulus G_{max}, assuming a Poisson's ratio of 0.5. To avoid numerical instability in the finite element analyses the value of Poisson's ratio was assumed to be 0.4999. By choosing the value of 0.5 for Poisson's ratio it is anticipated that the seismic loading is essentially undrained so that no volume change occurs during the soil response. The total mass density of the soil ρ was 2000kg/m^3.

The mesh for the 2D analyses which is shown in Fig. 3.12a followed the geometry of the soil sample in the plane defined by the propagation-polarisation directions of the loading wave. It consisted of 1600 nodes and 2500 elements. The density of the mesh was initially determined following the criterion that the size of the largest element did not exceed one tenth of the wavelength of the loading wave. For the highest frequency of the loading wave the size of the mesh and the value of the time step were varied to establish the independence of the solution of those two parameters. Satisfying this convergence criterion, the uniqueness of the solution with regard to these parameters was ensured (Simić, 1996). The transmitter and receiver were modelled as source and monitoring points represented as the nodes located at the sample ends and lying on its vertical axis. All nodes in the mesh were declared as nodes with no restrictions of movements, including the nodes on the perimeter.

The loading was applied as a movement of the transmitter tip point which was perpendicular to the sample vertical axis and in the shape of a sine pulse. The response of the soil to the seismic disturbance imposed by the transmitter tip was investigated for two different frequencies of the source: 1.8kHz and 15kHz. The results which represent the movements of the monitoring point against time are presented in Fig. 3.13. The time scale on the horizontal axis is normalised by the value of the supposed arrival time of the shear wave which has been calculated from the input

values of L_a, ρ, E and ν from Equations 3.11 and 3.12 and the relationship:

$$G = \frac{E}{2(1+\nu)} \qquad 3.15$$

which is valid for isotropic elastic materials. As for the analytical solution, at a low value of R_d (R_d=1.1) the near field effect is again clearly present and is represented by the initial downward movement of the trace before the true shear wave arrives at a value of T/T_a of 1.0. The precise shape of the near field effect is a little different to that of the analytical solution given in Fig. 3.11. This probably results from the simplified geometry of the 2D analyses, and the full 3D analyses was found to model this aspect more accurately. As predicted by the analytical solution and seen here, for high values of R_d (R_d=8.1) the near field effect is not discernible. It should be noted that the finite mesh size tends to smooth slightly the sharpness of the rise in the received trace.

The mesh for the 3D analyses, shown in Fig. 3.12b, represented the cylindrical shape of the soil sample. It consisted of 1300 nodes and 2000 elements where eight noded cubic elements were used to make up the model of the soil sample. The bender elements were modelled by two noded beam elements. The nodes of the beam elements at the ends of the sample were the only nodes with restricted movement. Again, the loading was applied as a movement of the free node of the beam element which modelled the tip edge of the transmitter. The motion was again perpendicular to the vertical axis of the sample. This time the shape of the movement was not only modelled as a sine pulse but also as a square wave.

The results of the 3D analyses are presented in Fig. 3.14. These are solutions for the identical sine pulses of the source as were used for the 2D analyses given in Fig. 3.13. Here again, the consistency between the analytical and numerical solutions can be seen.

The differences between the results from the 2D and 3D analyses arise from the greater fidelity of the model to the geometry of the prototype for the latter. However, the 3D analyses had a poorer resolution so that for the high frequency solution the sharpness of the rising point at the receiver trace is more severely smoothed by the larger mesh size. By extrapolating the smoothed curves with straight lines it can be seen that the lines would cross at a value of T/T_a of 1.0. Apart from confirming assumption (iii) the results of 3D analyses also confirmed the validity of assumption (ii) as the tip to tip distance between the elements was found to be the true travel distance.

For the measurement of the arrival time Dyvik & Madshus (1985) initially used a square wave at the source. Its complexity arises from the fact that a square wave is composed of a spectrum of different frequencies.

It is therefore impossible to associate a single R_d value for the square wave at the source and for the corresponding length of travel. Part of the square wave spectra is within the low frequency range so that the near field effect is necessarily expected to be seen in the receiver trace. The results of the 3D analyses confirm this, as is presented in Fig. 3.15. The near field effect is presented as the part of the trace between points 0 and 1. As will be shown in next section this is in a good agreement with the test data.

For the highest frequency of the dynamic loading at the source which ensures that no near field waves reach the receiver, the stress-strain state of the sample has been analyzed. The first set of results is given in Fig. 3.16 and presents the contours of strain level on the cross-section of the sample in the plane of motion. The contours of strain are in direct proportion to the contours of stresses since the material is modelled as elastic and for the same reason the values of strains are determined arbitrarily. The strain contours are given for three distinct time instants: immediately after the excitation, in the middle of the travel and at the moment of the arrival of the shear wave at the node which represents the tip of the receiver. It can be seen that in all three instants the wave front propagates along the sample axis and is parallel to the sample base. The shear disturbance becomes more widely spread along the sample with the time and the strain level declines due to geometric damping by about one order of magnitude by the time the wave reaches the monitoring point. There are no reflections from the sides of the mesh and the direct wave reaches the receiver first.

In Fig. 3.17 the strain contours for the three characteristic time instants are given in the plane perpendicular to the plane of the motion. Ideally there should be no straining in this plane. Strains are however present and were caused by the wave front which propagated in the opposite direction from the main wave front (Fig. 3.16) and then reflects from the base of the sample gaining its shape from the three-dimensional nature of the waves and the boundaries. The reflected wave front follows the main wave but is delayed in time and does not interfere with it. The direct wave front critical to the validity of the measurement is therefore unaffected by the source-receiver configuration.

The finite element analyses were used to examine the validity of the assumptions associated with the bender element method. Treating the soil as elastic the analyses confirmed the validity of the assumptions of the tip to tip length being the true travel distance and that the wave propagation is independent of the source-receiver configuration. Finally the analyses highlighted the importance of the near field effect on the method of measurement. As was found for analytical solution the propagation-polarisation pattern required by assumption (iii) was found only to be possible for high R_d values where the near field waves are absent.

3.4.4 Interpretation procedure

The basic Equation 3.12 for the calculation of G_{max} from the bender element test may be reformulated to contain all the variables measured during the test as:

$$G_{max} = \rho \frac{L_a^2}{T_a^2} \qquad 3.16$$

The total error in the determination of the G_{max}, as already discussed by Viggiani & Atkinson (1995a), is given as a percentage of the true value as:

$$\Delta G_{max}(\%) = \Delta \rho(\%) + 2\Delta L_a(\%) + 2\Delta T_a(\%) \qquad 3.17$$

The potential error in the determination of the total mass density is very small for a sample of cylindrical shape. It contains the error of the measurement of volumetric strain during the test and the largest error is from the calculation of the initial specific volume. This can be calculated both from the final water content of the sample and the initial water content of the trimmings so that overall reliability is around 0.05%.

If it is accepted that the value of L_a is the distance between the tips of the elements (see Sections 3.4.1 and 3.4.3) then the potential error in the determination of L_a corresponds to the sum of the error in the determination of the initial length of the sample and the error of measurement of the axial strain during the triaxial test. As discussed in Section 3.2.4, the latter error should not exceed 0.01% but the initial length is measured accurately at about 0.05% thus dominating the sum error.

The accuracy of the method is most dependant by far on the accuracy of the determination of the arrival time since, as will be explained later, the arrival time cannot be judged to better than ±1% of its true value. This error is about twenty times greater than the error in the measurement of ρ and the error in the measurement of L_a. Following Equation 3.17 it can be calculated that the total error in the determination of G_{max} should not exceed around 2.2%.

The principal problem with the method has always been the subjectivity of the determination of the arrival time T_a. Typically a square wave at the source is used and Fig. 3.18. gives an example of the received trace. As mentioned before its complexity arises from the fact that a square wave is comprised of a spectrum of different frequencies. The time scale has been normalised with respect to the true arrival time of the shear

wave (T_a) as determined by other means which will be discussed later. From the received trace of the square wave alone, it is uncertain whether the shear wave arrival is at the point of first deflection (0), the first reversal point (1), or some other point.

Viggiani & Atkinson (1995a) attempted to reduce the degree of subjectivity in the interpretation and to avoid the difficulty in interpreting the square wave response they suggested using a sine pulse as the input signal. Being mainly of one frequency the output wave was generally of a similar shape, which allowed them to apply cross-correlation and cross-power spectrum numerical techniques to reduce the uncertainty in the arrival time down to around ±7%. Viggiani & Atkinson tested predominantly clay soils but the research in this project was orientated towards making measurements in stiffer materials for which the potential error in stiffness through incorrect identification of the arrival time is greatly magnified. This section describes the methods that have been developed in response to this problem, but which may be used for any soil.

The results of the two bender element tests given in Fig. 3.19 are for a sample of Speswhite kaolin normally consolidated to an isotropic effective stress of 200kPa as had been modelled in the finite element analyses. The two traces are also for the same R_d values of 1.1 and 8.1 which for the 76 mm long sample correspond to frequencies of 1.8kHz and 15kHz. Again the time scale is normalised with respect to T_a, the shear wave arrival time, which was 0.44ms in this case. The experimental data in Fig. 3.19. confirm the results of the numerical analysis in Figs. 3.13 and 3.14 and the analytical solution of Sanches-Salinero et al., (1986) in Fig. 3.11. The trace for the lower R_d value has a pronounced near field effect prior to the shear wave arrival at a value of T/T_a equal to 1.0. As expected the trace for the higher R_d value is unaffected and the arrival of the far field shear wave is clearly seen.

These data show that the simplest way to obtain a bender element trace which may be interpreted objectively is to use a sinusoidal wave rather than the more usual square wave and to select a frequency which is high enough so that a high R_d ratio is obtained for the particular measurement. Unfortunately, this cannot always be achieved as at the high frequencies which are required for stiffer materials overshooting of the transmitting element can occur. Two traces given in Fig. 3.20 were obtained from a self-monitoring element performing a test in a cemented sand. At 2.96kHz the element follows perfectly the input wave, but at 29.6kHz it does not and overshooting occurs. This is seen as discontinuities in the trace of the self-monitoring element.

The limiting frequency at which overshooting starts depends on the relative impedances of the soil and the element and so becomes a more

severe problem in stiffer materials for which the bender element becomes relatively flexible. The problem is also more pronounced for square waves because the rise time of the wave which is ideally zero corresponds to an infinite frequency. The trace of a receiver element shown in Fig. 3.21 is for a test conducted on the same soft rock using a square wave. The correct arrival time indicated by the broken line A-A is lost within the noise resulting from the overshooting.

Because of overshooting, there are therefore circumstances in which measurements will need to be made at lower frequencies in the presence of a near field effect. Two methods have been devised to overcome this problem. The first is to distort the shape of the input wave using the function generator, as illustrated in Fig. 3.22. The amplitude of the first upward cycle of the wave may be reduced so as to cancel out the near field effect, giving a distinct arrival of the shear wave at a T/T_a of 1.0.

The test data shown in Fig. 3.18 and Fig. 3.19 are from the same kaolin sample at the same stresses as those in Fig. 3.22. By comparison of the various sine wave methods, each of which gave a value for T_a of 0.44 ms, it can be seen that for the square wave in Fig. 3.18. the first reversal point (1) is close to the correct arrival time of the shear wave (T/T_a = 1.0), as had been proposed by Dyvik & Madshus (1985). The part of the trace between points 0 and 1 therefore represents a near field effect, as previously discussed.

Finally an attempt was made to force the oscillation of the receiver at one of its natural frequencies in which case resonance occurs. This has been done by adjusting the frequency of the input wave which is in this case five connected sine pulses. In ideal circumstances the lowest resonant frequency is found to enhance the response of the receiver so that the energy of its movement is much higher than that which originates from the near field waves. In this case the arrival time may be simply taken from one of the peaks or troughs of the input wave and the corresponding point on the output. In the example shown in Fig. 3.23. the time is taken for the fourth peak which on the normalised time scale is 1.0. This resonant oscillation may be treated as a forced oscillation of a single-degree of freedom system which is in this case the receiver element. It is important to note that the resonant system is not completely free of damping due to the restriction of the movement of the receiver which is in contact with the soil. It is observed that for lower stiffnesses of the soil sample the damping in the resonant system was very high so that the resonant frequency was not easily found, if at all, as should be expected from the theory. Additionally, for frequencies higher than the natural frequency of the element it may happen that the forced oscillation changes polarity which further complicates this method. Generally the resonance criterion method was used only to compare with the other methods and only when the damping level was considered

very small.

The techniques outlined in this section show that G_{max} can be determined simply and objectively by direct measurement from the oscilloscope trace and with no need for complex numerical analyses. For any measurement of G_{max}, and particularly if a new soil was being tested, several of the methods were tried and the results compared, improving confidence in the data. By these means, measurements of the arrival time T_a have been routinely made to an accuracy of ±1%.

3.4.5 Summary

The changes in the original design of bender element set-up were needed in order to improve quality of the received signal which was partially corrupted by electrical noise. Cables connecting the elements to the electrical instruments were shielded and shields and instruments were correctly grounded. The modification in design resulted in a high quality of received signal so that measurement of the arrival time could be taken directly from the screen of the oscilloscope and with no need for complex numerical analyses.

Theoretical studies focused on the assumptions underlying the bender element technique have been carried out with an aim of developing objective criteria for determining the arrival time. It was found that for the range of frequencies and distances for the propagation of the waves in the technique as typically used, the near field waves can corrupt the arrival of the true shear wave. The criterion for reducing the near field effect has been highlighted and typical traces relevant to the problem have been discussed.

The analytical solution assumed an idealised geometry so that dynamic finite element analyses were carried out to examine the possible effects of the geometry of the source-receiver configuration on the applicability of the method. The analyses showed that the direct waves generated by the transmitter element propagate with no interference from the boundaries of the sample and also highlighted the importance of the near field waves on the method of the measurement.

Finally, techniques for the measurement of the arrival time have been suggested which provide objective means for determining the arrival time to an accuracy of ±1% by direct measurement from the oscilloscope. These are based on an understanding and recognition of the main features of the received trace. To obtain consistency in the data different techniques may be used for measurement of the arrival time particularly when new soil is tested.

CHAPTER 4 THE STIFFNESS OF COARSE GRAINED SOILS AT VERY SMALL AND SMALL STRAINS

4.1. INTRODUCTION

The description of the variation of G_{max} in sands so far has been largely empirical. In the 1960s Hardin & Black (1966) identified that both the voids ratio and stress history of soils influence G_{max} but no attempt was made to relate the stiffness to the soil state relative to some reference condition (e.g. the normal compression line or critical state line). Since then the influence of state on G_{max} of sands has received little attention. In consequence, the numerous empirical descriptions for G_{max} (see Section 2.3.3) emphasise the fact that a general framework for the stiffness behaviour of sands has, so far, not been established.

It is very likely that the main reason for the absence of the framework which will relate G_{max} with the volumetric state of the soil lies in the fact that the large strain mechanics of coarse grained soils is still not fully understood. Been & Jeffries (1985) showed that the strength of sands is controlled by their current volumetric state and Coop (1990) and Coop & Lee (1993) demonstrated that many important aspects of the mechanics of sands can be explained using the framework of critical state soil mechanics. However, the identification of a reference condition for a particular soil is still hampered by considerable testing difficulties and more research of the behaviour of sands is needed, especially at low stresses. As pointed out in Section 2.5.1 the reference condition represents a state which can be reached by all samples of the same soil regardless of their initial density. The reference condition is also uniquely related to fundamental material properties of soil such as the position, inclination or possible curvature of both the critical state line and the isotropic normal compression line in the v:lnp' plane.

This research attempts to identify a framework which will relate G_{max} to the volumetric state of a coarse grained soil. For this purpose the state of isotropic normal compression was chosen as the reference condition i.e. the stiffnesses acquired at normally consolidated states will be compared with the stiffnesses at other states. The general characteristics of the mechanics of coarse grained soils identified by Coop & Lee (1993) have been used here to interpret the main features of the framework.

As already outlined in Section 2.5.1, Coop & Lee (1993) showed that compression of coarse grained soils at high stresses resulted in each soil reaching a unique isotropic normal compression line which was independent of the initial densities. Critical states were found to lie on a unique critical state line which was parallel to the isotropic normal compression line (see Fig. 2.30). They showed that particle crushing was associated with the large plastic volumetric strains which

occurred both during isotropic compression or during shearing to a critical state. The points on the critical state line and the isotropic normal compression line were found to be uniquely related to a corresponding degree of breakage using Hardin's (1985) concept of relative breakage. The terminology used in their paper, and also here, is different to that used by some other authors. Jefferies (1993), for example, used the term "normal compression line" to refer to the first loading compression curves before they reach the unique line so that there is an infinity of "normal compression lines" for samples of different initial densities. Also Been et al., (1991) have suggested that the critical state line is curved as its gradient increases due to particle breakage at higher stresses. However, for the three soils they tested Coop & Lee (1993) showed that the critical state lines were straight and parallel to the normal compression lines on a v:lnp' graph within the range of densities tested. Since the initial densities were very similar to those used in this research the normal compression and critical state lines are here too assumed to be straight.

The work of Viggiani & Atkinson (1995b) established a framework for G_{max} for fine grained soils by relating the stiffness to the state and nature of the soil. The corresponding framework for coarse grained materials should take into account the important differences between clays and sands, in particular, in the means by which these two kinds of soils reach their current states. Clays in their loosest possible state, at low stress levels, lie on the normal compression line. Sands, in contrast, even in their loosest state at low stresses, demonstrate a gradual yield during first loading as the soil approaches the unique normal compression line. In contrast to the first loading behaviour, the unloading and reloading of sands is rigid and followed by a well defined yield point as the particle crushing only restarts when the preconsolidation pressure has been reached. Additionally, unlike the clays, sands can reach a given state by either compaction followed by a first loading or through true overconsolidation. As discussed in Section 2.5.1, Coop (1990) showed that samples which had undergone compaction and first loading to reach a given state had a substantially different stress-strain behaviour during shearing from those which reached the same state by overconsolidation.

Due to the differences between clays and sands outlined above, the straightforward application of the framework for clays of Viggiani & Atkinson (1995b) to the stiffness behaviour of sands was not possible. This is also reflected in the fact that they used the plasticity index (PI) to relate stiffness to the nature of the soil, which is a parameter with no meaning for sands.

The research was, therefore, aimed at the development of a general framework for G_{max} in coarse grained materials which would take into account the state of the soil, including the means how that state was reached. Three reconstituted sands with very different geological origins

were tested over a wide range of stresses in an attempt to gain an objective representation of the general behaviour of sands in the region of very small and small strains. Additionally, a cemented Lower Greensand was tested in order to assess the influence of cementing on G_{max} in sands.

Recently, local axial strain transducers have become sufficiently accurate to give the possibility of making a direct comparison between dynamic and continuous loading stiffnesses in the triaxial apparatus (Goto et al., 1991; Cuccovillo & Coop, 1997). So far, comparisons between dynamic and continuous loading stiffnesses have generally been made between resonant and torsional shear tests carried out in the resonant column apparatus (Iwasaki et al., 1978; Bolton & Wilson, 1989). A good agreement between stiffnesses has been observed thus demonstrating that the stiffness of soils at very small strains is independent of the loading rate.

Using instrumentation attached to the triaxial sample Viggiani & Atkinson (1995b) made comparisons between the dynamic and continuous loading stiffnesses. At that time the stiffnesses obtained from continuous loading shearing probes could only be measured accurately down to 0.01% strain which was inadequate to match dynamic stiffnesses at much lower strain levels. Here, dynamic stiffnesses from bender element tests are compared with very small strain stiffnesses obtained from continuous loading shearing probes using local LVDT-s for the measurement of axial strain. An attempt has also been made to correlate the stiffnesses at larger strain levels with the volumetric state for one of the sands.

4.2 SOILS TESTED

For consistency with the previous work on the mechanics of sands (Coop, 1990; Lee, 1991; Coop & Lee, 1993) the same three sands were used in this research. Dogs Bay sand, decomposed granite and Ham River sand had been originally chosen for their diversity of origins and characteristics. Grading curves for all three sands are given in Fig. 4.1. Lower Greensand was used by Cuccovillo (1995) to examine the stiffness at small strains of structured sands. Here, the same material has been used to examine the influence of cementing on G_{max}. The grading curve of the destructured Greensand is also given in Fig. 4.1.

Dogs Bay sand, from the west of the Republic of Ireland, is a biogenic carbonate sand consisting largely of foraminifera and mollusc shells. The sand is poorly graded with a high calcium carbonate content (Houlsby et al., 1988). The soil was identified and gathered by Evans (1987) from a dune environment. The sand particles are relatively unbroken (Fig. 4.2a) and their open and angular nature gives rise to the soil's high voids ratios. The large strain behaviour of Dogs Bay sand was investigated by

Golightly & Hyde (1988) and in more detail by Coop (1990).

The Korean decomposed granite is a residual soil classified by a weathering grade V on the scale of the Geological Society (1990). It occurs naturally with a complex structure so in order to form a reconstituted soil the material was mechanically destructured by breaking the inter-particle bonds. In the process, the particles greater than 5mm were discarded. Since the soil has not been transported it is well graded with angular and sub-angular particles (Fig. 4.2b). Decomposed granite is a product of chemical weathering so each particle is formed of an amalgam of different minerals. Quartz and feldspars were inherited from the parent rock while kaolin, mica and smectite are the results of the weathering process. The decomposed granite was tested extensively by Lee (1991) and Lee & Coop (1995).

The Ham River sand is a quartz sand gathered from a Thames gravel quarry near Chertsey, England. Being typical of a river transported soil the sand is poorly graded with sub-angular to rounded particles (Fig. 4.2c). The Ham River sand was extensively researched at Imperial college (Skinner, 1975; Porovic, 1995).

The material chosen to investigate the effects of cementing was a silica sandstone from the Lower Greensand series in Kent, England, which was used in an extensive research programme by Cuccovillo (1995). The soil was deposited in a shallow water marine environment and cementing developed during diagenesis. Prior to the cement deposition the high overburden pressure caused an increase in density followed by the development of a fabric characterised by a large area of inter-particle contacts (Fig. 4.2d). The iron-oxide cement coating which is coloured white in the micrograph thin section provides only a weak bonding. The dense packing of the grains can also be seen.

4.3 TESTING PROGRAMME

Detailed descriptions of the sample preparation techniques, triaxial apparatus, instrumentation used and bender element measurement techniques were given in Chapter 3. Typically the samples were created using wet compaction but some of the samples were dry compacted or pluviated in order to achieve the desired density. For the cemented silica sand, a detailed description of the preparation of the slots for the bender elements was also given in Section 3.3.1.

Test programmes for the Dogs Bay sand, decomposed granite and Ham River sand are given in Table 4.1 while the test programme for the Greensand is given in Table 4.2. Generally the samples were isotropically loaded and unloaded within a stress range from 0.05 to 70MPa. The bender element

measurements of stiffness were made while the compression stages continued. Long periods of rest were avoided thus minimising the influence of creep. The soil most affected by creep was Dogs Bay sand so a preliminary series of tests was carried out in order to quantify and control this effect. The increase in G_{max} caused by creep relative to the initial value of stiffness at zero time is shown in Fig. 4.3a. Prior to the rest period started at a p' of 500kPa, a stress rate of 20kPa per hour had been used. An increase in G_{max} of up to 15% was recorded over a period of three days. It was found that for the same stress rate during the approach path the increase was proportionally worse at low stress levels and better for higher stress levels, as indicated in Fig. 4.3b. The effect is the most pronounced for samples undergoing first loading but there was also a measurable increase in stiffness for samples undergoing either unloading or reloading (Fig. 4.3a). In the latter cases the volumetric creep was in the opposite sense, so the increase in stiffness cannot be attributed to it and is probably caused by aging (Schmertman, 1991). However, this effect was found to be small and did not exceed more than 4% during three days of rest at a p' of 500kPa. In order to minimise the effect of creep a loading rate of around 0.5% of the current isotropic stress per hour was chosen so as to give an expected rise in G_{max} of only 2% during the first day of a delay occurring in the test. Delays did not usually exceed the overnight hours and the tests typically lasted a few weeks so that the measured stiffnesses were largely unaffected by the creep.

As pointed out in Section 2.2.2, Gajo (1996) identified that for sands the standard method of calculation of G_{max} from the propagation of shear waves in saturated soils (Equation 2.15) can give rise to an error of 10-15% as a result of the inertial coupling of the solid and the fluid phase of the material. It was not possible to quantify this correction due to the experimental difficulty in evaluating the key parameter tortuosity (see Equation 2.14). However, the majority of measurements were taken at frequencies which were substantially lower than the frequency identified by Gajo (1996), below which the effect would be small for the wave travel distances used here. If the correction were needed it would have affected only the absolute values of the stiffnesses but not the relationship between them since the error should be similar at all stress levels for each of the sands tested. Therefore the normalisation techniques used to develop an understanding of the variation of G_{max} with stress and volumetric state in the sands should not be affected.

In order to examine the stiffness behaviour for continuous loading, specimens of Dogs Bay sand were subjected to multi-stage tests of isotropic compression followed by undrained shearing probes. The probes were stopped at an axial strain of only 0.1% so that the straining during the successive isotropic compression stage would erase the effect of the previous shearing probe. The shearing stages of this series of tests are

summarised in Table 4.3. These tests were carried out in an attempt to measure very small strains which would be used to calculate stiffnesses at strain levels comparable to those imposed by bender elements. Details of the testing procedures for the use of the local axial transducers during the shearing probes were given in Section 3.3.3.

4.4 THE STIFFNESS OF RECONSTITUTED SANDS AT VERY SMALL STRAINS

4.4.1 Tests on Dogs Bay sand

The samples of Dogs Bay sand were prepared in as wide a range of initial densities as possible by using a variety of techniques (see Section 3.3.1). The initial specific volumes varied from 2.429 for the densest sample prepared by dry compaction to 2.740 for the loosest sample prepared by wet compaction. The test programme for all samples is summarised in Table 4.1a.

The volumetric paths during isotropic compression are given in the v:lnp' plane in Fig. 4.4. Regardless of their initial densities all the samples tend towards a unique isotropic normal compression line (NCL). The approaching path is one of gradual yield, and being closer to the normal compression line, the loose samples reach the reference state at lower stresses than the dense ones. For example the loosest sample 9db reached a normally compressed state at 700kPa while the most dense sample 8db would have required around 3MPa to reach the normal compression line.

During unload-reload cycles the behaviour of all samples tested was very rigid with a well defined yield point on reloading when the preconsolidation pressure was reached. This typical recompression behaviour is the result of particle breakage which restarts at pressures higher than the preconsolidation pressure, as already discussed. Testing the same material Coop (1990) identified approximately the same position of the isotropic normal compression line in the v:lnp' plane as presented here (see Table 2.2).

Bender element measurements during the first loading of isotropic compression are given in Fig. 4.5. Each bender element reading is shown on the graph as a data point. By direct comparison of the results from Fig. 4.4 and Fig. 4.5 it can be seen that initial density of the samples has a significant influence on the corresponding G_{max} values. For a difference in specific volumes between the loosest sample 9db and the densest 8db of 17% a difference in G_{max} of about 70% is observed. The decrease in initial density is followed consistently by a corresponding increase in the initial value of G_{max} for all the samples tested.

It can be observed from Fig. 4.5. that on first loading the values of G_{max} for all initial densities tend towards a unique line indicated on the figure which corresponds to the isotropic normal compression line in the v:lnp' plane. This result demonstrates that the state of normal compression is not only a reference state for the volumetric change of the soil but it is also a reference state for the very small strain stiffness. This unique line on Fig. 4.5 appears to be straight in the log-log plot so it can be fitted by a power function of the form:

$$\left(\frac{G_{max}}{p_r}\right)_{nc} = A\left(\frac{p'}{p_r}\right)^n \qquad 4.1$$

where $(G_{max})_{nc}$ corresponds to the measured values of G_{max} at the states of normal compression and p_r is the reference pressure of 1kPa needed for the dimensional coherence of the equation. The same equation was used by Viggiani & Atkinson (1995b) for the variation of G_{max} with p' for normally consolidated clays.

Equation 4.1. should not be confused with the empirical Equation 2.18 of Hardin (1978) and similar empirical correlations suggested by others of the same power function type. In these equations the power coefficients involved do not correspond to the reference state of the soil but to the portion of the curved approach path to the $(G_{max})_{nc}$ line. Since that portion of the curved line in the log:log plot was typically small a linear fit could be used. As can be seen in Fig. 4.5 the gradients of the first loading stiffness data prior to reaching the $(G_{max})_{nc}$ line vary due to the curvature and are in the range of 0.5-0.6. The gradient of the $(G_{max})_{nc}$ line n of 0.686 is unique, as is the intercept A of 3100, so that both parameters should be regarded as fundamental material properties since they are associated with the reference state of normal compression.

The stiffnesses vary from 70MPa for the loosest sample at low stresses up to around 1GPa at the maximum pressure reached of 5MPa at reference state. Fiorovante et al., (1995) tested Quiou sand, a material of similar mineralogy as Dogs Bay sand but which is well graded. At a p' of 1MPa, for the denser Quiou sand approximately 30% higher values of G_{max} were recorded than for Dogs Bay sand at the same pressure.

The stiffnesses to which Equation 4.1 is applied were obtained during isotropic compression only. As already discussed in Section 2.3.3, the work of Roesler (1979), who also used wave propagation methods for the measurement of stiffness, showed that the value of the principal stress which acts out of the plane of the motion does not affect the stiffness measured. Consequently, Hardin & Blandford (1989) omitted this stress from the function relating G_{max} to the confining stress (Equation 2.19). Here, in the case where the stresses are equal in all directions, it is immaterial whether or not the stress which acts out of the plane of the motion appears in the stress invariant, so that Hardin & Blandford's

Equation (2.19) reduces to the form of Equation 4.1.

By direct comparison of Fig. 4.4 and Fig. 4.5 it can be observed that sample 8db had not reached the normal compression line so that, correspondingly, the $(G_{max})_{nc}$ line had not been reached. However, the tendency towards it is clear, as indicated by an arrow in Fig. 4.5. It is important to note that the curvature of the approaching path of G_{max} to the $(G_{max})_{nc}$ line is much less pronounced than the curvature of the corresponding volumetric path in the approach to the normal compression line. In consequence there is a tendency to reach the reference state in terms of stiffness (i.e. the $(G_{max})_{nc}$ line) before reaching the reference state of normal compression in terms of volume. For example the loosest sample 9db reaches the reference state in terms of stiffness at about 300kPa but does not reach the reference state in terms of volume until about 700kPa.

The stiffnesses measured during isotropic unload-reload loops in which all the samples were unloaded from the normal compression line are shown also in the $\log G_{max}$:logp' plane in Fig. 4.6. These data plot on curved lines above the reference $(G_{max})_{nc}$ line also presented in the figure. Each line corresponds to a swelling line of the particular sample (see Fig. 4.4) so that the location of the line is determined by the value of the corresponding preconsolidation pressure. A small amount of hysteresis is observed in the volumetric variation during the same unload-reload cycle but the stiffnesses measured during reloading are indistinguishable from those measured during unloading.

At the start of unloading there is often a small section where the stiffness does not change much even though the stress is reduced. This is a result of creep which gave continued volumetric compression during the initial part of unloading thus counteracting the decrease in stiffness due to unloading. This is seen in detail in Fig. 4.7 where the effect of creep was to keep G_{max} almost unchanged during the reduction in the stresses from 600 to 350kPa. It is interesting to note that reloading resulted in stiffnesses following exactly the values measured during unloading including those values affected by the creep. This result implies that the particle contacts are unaffected by the stress and volume changes during an unload-reload cycle so that the material holds these in its "memory" until new particle crushing causes changes.

4.4.2 Tests on decomposed granite

In the preparation of the samples of the well graded decomposed granite pluviation was abandoned since it would have caused a segregation of particles resulting in inhomogeneous specimens. Instead the samples were

prepared by wet or dry compaction after which carbon dioxide was circulated through the sample prior to flooding it so as to improve the subsequent saturation. In total five samples of decomposed granite were tested (Table 4.1b) with a range of initial specific volumes varying between 1.490 and 1.605.

The gradual yield of the samples is seen in Fig. 4.8 as they tend towards a unique normal compression line. The position of the latter in the v:lnp' plane was also identified by Lee (1991). The gradient of normal compression line is almost four times lower than that for Dogs Bay sand (see Table 2.2) resulting from a very low compressibility of this well graded soil. Similar features of unload-reload behaviour are seen as were observed for the Dogs Bay sand indicating a similarity in the mechanical behaviour caused by the particle breakage.

Bender element measurements of G_{max} for the first loading of isotropic compression are given in Fig. 4.9. The influence of initial density on the initial value of G_{max} is also observed for this sand, the maximum difference in specific volumes of 8% resulting in about 50% difference in stiffness. As was observed previously for Dogs Bay sand, during the first loading of the samples of decomposed granite the values of G_{max} tend towards a unique $(G_{max})_{nc}$ line regardless of the samples' initial densities. This line is again straight in the $\log G_{max}$:logp' plane so that the material parameters (see Equation 4.1) can be identified as A=760 and n=0.884. By direct comparison of Fig. 4.8 and Fig. 4.9 it can be observed that samples 1dg, 2dg and 4dg had not reached the normal compression line. Correspondingly the $(G_{max})_{nc}$ line had not been reached, but the tendency towards it is clear, as indicated by arrows in Fig. 4.9.

Unload-reload stiffness data for the samples which were unloaded from the normal compression line are given in Fig. 4.10. Here again no hysteresis is observed in terms of stiffness during the cycle and the locations of the lines are determined by the corresponding preconsolidation pressures. In contrast to the curved lines observed for Dogs Bay sand, the stiffness lines in this case appear straight in the log:log plot. However, the lines are in both cases parallel thus indicating that there is a relationship between the volumetric states and the corresponding values of G_{max}.

4.4.3 Tests on Ham River sand

The samples of Ham River sand were prepared by wet compaction which was considered a consistent means of producing homogeneous samples with a variety of initial densities. A total of four samples was tested as summarised in Table 4.1c.

Volumetric paths in the v:lnp' plane are presented in Fig. 4.11. The tests on the loose sample 1hr and the dense sample 2hr were carried out in the high pressure apparatus in which the maximum capacity allowed during isotropic compression was only 5MPa. This pressure caused only a small change in volume of about 1.5%. In order to reach the reference state of normal compression a substantially higher pressure was needed and the two loose samples 4hr and 5hr were tested in the high pressure apparatus with a capacity of 70MPa. The gradual yield of the samples increased at around 10MPa which is a yield pressure one logarithmic cycle higher than observed for the two sands previously tested. However in the same manner as observed for the other two soils the samples reached a unique normal compression line, the position of which was also identified by Coop & Lee (1993). The gradient of the normal compression line of Ham River sand is about half that of Dogs Bay sand and about twice that of the decomposed granite (Table 2.2).

The variation of G_{max} on first loading of isotropic compression is given in Fig. 4.12. As was observed for the other two materials, the initial density controls the initial value of G_{max}. This time the effect was much smaller so that the maximum difference in specific volumes of around 7% gave a difference in G_{max} of about 25% which is about a third of the effect observed for Dogs Bay sand and about a half that observed for decomposed granite. This feature of Ham River sand that the volumetric state does not affect greatly G_{max} is in contrast with the behaviour of the two other sands tested. It will be shown later that this characteristic behaviour of the silica sand persists at all stress levels.

As can be seen from the stiffness data in Fig. 4.12 the curvature of the approaching paths to the unique $(G_{max})_{nc}$ line for the samples with different densities is very small. A close inspection is needed to distinguish the straight portion of the line which corresponds to the reference state from the curved approaching paths. This again indicates that the mean effective stress is the dominant parameter which controls G_{max} for this sand. The parameters which characterise the $(G_{max})_{nc}$ line of Ham River sand have been identified as A=3900 and n=0.593, as indicated in the figure.

The portion of the curved approach path to $(G_{max})_{nc}$ line between 100kPa and 700kPa has a lower gradient of around 0.5 which is in good agreement with data from Porovic & Jardine (1995) who tested the same soil using resonant column tests. The absolute difference in the G_{max} values for loose samples between their measurements and those presented here is only about 5%. The difference may result from differences in specific volumes which were not reported by the authors.

The stiffnesses measured during isotropic unload-reload loops are shown

in Fig. 4.13. Again these data lie on straight lines above the $(G_{max})_{nc}$ line and each line corresponds to a swelling line in the v:lnp' space so that both are controlled by the corresponding preconsolidation pressure. A close inspection shows that the stiffness lines remain parallel at all pressures thus indicating again that there is a relationship between the volumetric state and the stiffness, even though the effect is small.

4.4.4 Discussion

Three sands with different minerologies and different geological origins showed a remarkable similarity in their behaviour. The question arises as to whether there is a unique framework which would be applicable to the stiffnesses of all three sands and, very likely, for *reconstituted* sands in general. Here, an attempt is made to develop such a framework by introducing the influence of volumetric state on stiffness using a similar approach to that previously found to apply to reconstituted clays by Viggiani & Atkinson (1995b).

During the first loading of each sand it was observed that the values of G_{max} for all samples at all initial densities eventually reach a unique line which corresponds to the isotropic normal compression line in the volumetric plane. This unique line of very small strain stiffness of a normally consolidated sand (i.e. the $(G_{max})_{nc}$ line) can be characterised by Equation 4.1 using the gradient of the line n and its intercept A in the $\log G_{max}$:logp' plot. As already indicated the values of A and n should not be confused with other similar parameters given in the literature since, unlike the others, they characterise the reference condition of soil in terms of G_{max} and should be regarded as material properties. Even though the parameters A and n vary significantly between the three materials (Table 4.4) the general positions of the $(G_{max})_{nc}$ lines are fairly similar as illustrated in Fig. 4.14. This result demonstrates that three very different normally consolidated sands have similar stiffnesses, a feature which could be of interest for the evaluation of design parameters for reconstituted sands in general.

For the three sands tested it was observed that on first loading the stiffnesses on the approach paths to the $(G_{max})_{nc}$ line depend on the samples' initial densities. As already mentioned, the gradients of the curved approaching paths are approximately in the range of 0.5 to 0.7 which is close to the values given in the literature. The values of n given in Table 4.4 are somewhat greater, the value of 0.884 for decomposed granite being about three times greater then the value of 1/3 derived from Hertzian theory by Duffy & Mindlin (1957). It is important to note that the work of Duffy & Mindlin did not take into account particle breakage and treated the deformation of the particles in contact

as purely elastic. Although they also did not include particle breakage in their theoretical work, Ko and Scott (1967) accounted for the increased number of contacts between particles during compression and showed that this resulted in higher volumetric stiffnesses than those predicted by Hertzian theory. As already discussed in Section 2.3.2, by using a numerical simulation of the behaviour of a random system of spheres Dobry et al., (1989) also highlighted the importance of the number of contacts per particle on the soil stiffness. The very high value of n for decomposed granite seen here is therefore probably the result of the high ability of this well graded material with angular particles to develop a large increase in the number of contacts per particle as the crushing of particles progresses during compression.

Viggiani & Atkinson (1995b) related the values of A and n for normally consolidated clays to their nature which was characterised by the plasticity of the soil. It is very likely that there is a relationship between the nature of sands and these parameters but the characterisation of the nature will probably have to take into account micro-mechanical parameters which control the interaction between particles. It was considered too early to determine these controlling parameters from the data available for only three materials.

The stiffnesses at both overconsolidated and compacted states were found, for all three soils, to be greater than at normally consolidated states for the same mean effective stress. An attempt has then been made to examine whether there is a unique relationship between the volumetric state and stiffness, taking into account both ways of how a given state may be reached, i.e. by overconsolidation or by compaction and first loading. In this context the term overconsolidated will be reserved for those samples which are currently at stresses which are below the preconsolidation pressure that they have experienced in a state of isotropic normal compression. The term compacted will be used to define those samples which are undergoing first loading prior to reaching the isotropic normal compression line whatever their initial density. It is important to note that samples unloaded before reaching the state of normal compression are neither truly overconsolidated nor compacted by this terminology.

The normalisation procedure for defining the volumetric state of the samples was chosen to be one which would not depend on the means of how the volumetric state is reached. The current volumetric state has been determined by normalising the current mean effective stress p' with respect to the equivalent pressure p'_e taken at the same specific volume on the normal compression line (see Fig. 2.35) where:

$$p'_e = \exp\left(\frac{N-v}{\lambda}\right) \qquad 4.2$$

and where λ is the gradient of the normal compression line and N its

projected intercept at a p' of 1kPa. The use of the state variable p'/p'_e is analogous to using overconsolidation ratio for clays. Here, it was preferred not to use the usual definition of overconsolidation ratio (Equation 1.11) since it has a physical meaning only for truly overconsolidated samples and not for the compacted ones. The volumetric state defined relative to the critical state line (see Section 2.5.2), for example a state parameter (Jefferies, 1993), could also not be used here since the reference state in terms of stiffness was measured at the state of isotropic normal compression. The choice of the critical state line for a reference state in terms of volume is not appropriate since the tangent stiffnesses at critical states are zero by definition.

The values of G_{max} for the overconsolidated and compacted samples have also been normalised relative to the reference state in terms of stiffness, i.e. the $(G_{max})_{nc}$ line representing the values of G_{max} for normally consolidated states at the current value of mean effective stress. The values of $(G_{max})_{nc}$ have been calculated from Equation 4.1 so that:

$$(G_{max})_{nc} = p_r A \left(\frac{p'}{p_r}\right)^n \qquad 4.3$$

In the same way that for p'_e a projection to the normal compression line at the current volume is made, for $(G_{max})_{nc}$ the projection is made to the $(G_{max})_{nc}$ line at the current value of mean effective stress.

By plotting normalised stiffnesses, $G_{max}/(G_{max})_{nc}$, versus normalised volumetric states, p'/p'_e, all of the stiffnesses of samples lying on the normal compression line plot as a single point at 1:1. This is shown in Fig. 4.15 where normalised plots are given in the form of semi-logarithmic graphs for the three sands. The same pattern of behaviour can be recognised for each material. All the compacted samples at all volumes define one unique relationship for normalised stiffness with volumetric state. Similarly all the overconsolidated samples define different but also unique lines for all samples at all volumes. It is observed that for both overconsolidated and compacted samples there is a general increase of normalised stiffness with decreasing state variable p'/p'_e, i.e. with increasing distance from the normal compression line for compacted samples or with increasing overconsolidation for overconsolidated samples.

The basis of the framework is the uniqueness of the lines which are the graphical representations of unique mathematical descriptions of the relationships which hold between G_{max} and stress-volume state for the three sands. That is, the value of n (Equation 4.1) does not vary with volumetric state (i.e. p'/p'_e) so that for a given state the $\log G_{max}$:$\log p'$ relationship for either compacted or overconsolidated samples would plot

as a straight line parallel to and above the $(G_{max})_{nc}$ lines which are given in Fig. 4.14.

For the loosest samples the normalisation presented above involves a short extrapolation of the straight normal compression line beyond the experimental data (see Figs. 4.4, 4.8 and 4.11). This hypothesis, which is also consistent with the procedure of the identification of unique boundary surfaces for same materials adopted by Coop & Lee (1993), is based on the fact that the critical state line remains straight within the same rage of specific volumes, as shown in Fig. 2.30. Similarly, the normalisation involves an extrapolation of the $(G_{max})_{nc}$ line to lower pressures beyond the experimental data. The fact that the result of this normalisation gives the unique relationships between normalised stiffnesses improves confidence in the correctness of the procedure.

The stiffness data for Dogs Bay sand (Fig. 4.15a) demonstrate that there is a significant influence of state on stiffness for this poorly graded sand with angular particles which are prone to crushing. At the lowest stresses at which the tests were conducted this influence gives rise to 70% higher stiffnesses of overconsolidated samples relative to corresponding compacted samples. The approach path of the compacted samples to the reference state at a p'/p'_e of 1 (i.e. the normal compression line) is fairly flat when p'/p'_e is greater than about 0.3. This was also seen in the appearance of reaching the $(G_{max})_{nc}$ line (Fig. 4.5) prior to reaching the normal compression line in the v:lnp' plane (Fig. 4.4), a feature already discussed in the previous section. This result can be interpreted as there being almost no influence of volumetric state on G_{max} for a range of values of p'/p'_e between 0.3 and 1 for compacted samples. As will be discussed later, this may be one of the reasons why much previous research has failed to highlight the importance of volumetric state on the stiffness of sands.

There is a substantial difference between the influence that volumetric state has on stiffness for the various sands tested. While the normalised stiffness of overconsolidated samples of Dogs Bay sand is nearly linear when plotted against normalised state with semi-logarithmic scales, for the decomposed granite it is distinctively curved (Fig. 4.15b). However the magnitude of the increase of stiffness with increasing distance from the normal compression line is similar for both materials as can be observed by comparing Fig. 4.15a and Fig. 4.15b. This similarity may arise from the fact that both sands have angular particles which are prone to crushing.

The influence of the state on stiffness for Ham River sand is the least pronounced of the three sands (Fig. 4.15c). The maximum measured difference in stiffness between the most heavily overconsolidated samples (i.e. with the lowest p'/p'_e values) and the corresponding compacted

samples is only about 25% which is about one third that observed for the two other soils. It should also be noted that this effect is seen at an order of magnitude lower value of the state variable p'/p'_e than for the two other sands, thus emphasising the difference in the behaviour. This may be explained by the fact that silica sand has rounded and solid particles, unlike the carbonate sand and decomposed granite, which is perhaps the cause of a less pronounced tendency in this material to develop new contacts between particles during compression.

The effect of state on the stiffness of compacted samples of Ham River sand is also smaller (Fig. 4.15c) as it can be seen that the gradient of the normalised stiffness for compacted samples is about half that of the overconsolidated samples. From the survey of the literature (see Section 2.3.3) it can be noted that in most of the research to date, compacted samples, usually of silica sands, have been tested typically over a very limited range of stresses which will correspond only to a small portion of the line of normalised stiffness given in Fig. 4.15c. As already discussed, this is probably the reason why the influence of stress state had received more attention than the influence of volumetric state on stiffness of sands.

The framework presented above is associated with compacted and truly overconsolidated samples only. As previously indicated, samples which were unloaded prior to reaching the normal compression line are neither truly compacted nor overconsolidated. The stiffnesses of these samples, which will be defined here as "overconsolidated-compacted", are interpreted within the framework in Fig. 4.16 for Dogs Bay sand. Similar results were obtained for the other two sands.

As previously discussed, during first loading the stiffnesses again follow the unique line in approaching the reference state. The data tend towards that state (i.e. the point 1:1 in the graph) but never reach it since the sample was unloaded before reaching the normal compression line. During unloading, the state variable p'/p'_e reduces and the stiffnesses along that path, as presented in the figure, are greater than those of the compacted samples but lower than those of truly overconsolidated samples. The exact position of the data depend on the maximum value of the p'/p'_e value reached, i.e. how closely the sample approached the normal compression line prior to being unloaded. Sample 1db which reached a p'/p'_e of 0.8 has a greater normalised stiffness during unloading than sample 8db which reached a maximum p'/p'_e of only 0.4. It can be seen in this figure that the normalised stiffnesses of overconsolidated-compacted samples do not plot on a unique line as the samples never reached the reference state either in terms of volume or G_{max}. However, their position is determined by the maximum value of state variable p'/p'_e reached and is always above the unique line for compacted samples and below the unique line for truly overconsolidated samples. It

can be concluded now that the lines for the normalised stiffness identified for compacted and overconsolidated samples (Fig. 4.15a) define a domain of possible stiffnesses that result from different combinations of compaction and overconsolidation for the particular soil.

As can be observed by the direct comparison of the graphs in Fig. 4.15 the size of the stiffness domain varies considerably between the three sands. The size of the domain is most prominent for the carbonate sand which is the most prone to particle breakage and could, therefore, result in there being a greater effect of crushing on the nature of the particle contacts. In the case of the decomposed granite the stiffness domain is small perhaps indicating that for this well graded soil made of angular particles, the breakage adds little to the nature of the particle contacts and to the already high potential for developing new contacts between particles during compression. Ham River sand has the least prominent size of the stiffness domain perhaps showing that the nature of contacts between solid and rounded particles was less affected by particle breakage.

4.5 THE STIFFNESS OF CEMENTED SANDS AT VERY SMALL STRAINS

4.5.1 Tests on Lower Greensand

Two intact samples of Greensand were tested along with a single sample of the same material after it had been destructured. The technique used to de-bond the soil grains without damage to them was described in Section 3.3.1. The tests carried out on the samples of Greensand are summarised in Table 4.2.

The reconstituted sample was manufactured by wet compaction in an attempt to produce as loose a sample as possible. The natural samples were precisely trimmed from blocks to the required size and small slots were cut into each end by hand to accommodate the bender elements. The technique adopted to seal the bender elements into the slots so that they effectively transmitted and received shear waves is also explained in detail in Section 3.3.1.

At an early stage of the research a preliminary test was carried out on a natural sample in a standard triaxial cell in an attempt to examine whether the bender element technique could be used in a stiff material such as Greensand. It was found that there was no difficulty in carrying out a bender element test providing that the seal ensured good contact between the elements and the material. The sample was isotropically compressed up to 600kPa and then unloaded, during which no change in the recorded value of G_{max} of 2.7GPa was observed.

Cycles of isotropic compression and swelling were later carried out at high pressures on both natural and reconstituted samples during which bender element measurements were taken. The influence of creep was minimised by choosing an appropriate rate of loading during isotropic compression, as previously explained in Section 4.3. The volumetric paths for both samples are presented in Fig. 4.17. As can be seen, up to about 25MPa, the volume change of the natural sample was very small, with almost no hysteresis upon unloading. In contrast, the reconstituted sample gradually yielded before the reference state of normal compression was reached at a p' of approximately 10MPa. Its unload-reload behaviour was also characterised by little hysteresis and by a pronounced yield point after the preconsolidation pressure was reached. As already discussed in Section 2.5.1, these features of the volumetric compression of the reconstituted sample are characteristic of particle breakage.

The variations of G_{max} with p' for both the reconstituted and natural samples are presented in Fig. 4.18 using log:log axes. The stiffness of the reconstituted sample varies in a similar manner as was observed for Ham River sand. This similarity reflects the grading and mineralogy of two materials which is common to both materials (see Section 4.4). The reference state in terms of stiffness for the Greensand (i.e. the $(G_{max})_{nc}$ line) is again reached before the corresponding reference state is reached in terms of volume (i.e. the normal compression line), which is similar to the behaviour of Ham River sand. The approach path to the $(G_{max})_{nc}$ line is again only slightly curved and close inspection is needed to distinguish the straight portion of the line from the curved approach path. The values of the material parameters, A=4000 and n=0.587, are also almost identical to those of Ham River sand (see Table 4.4). The influence of volumetric state on stiffness is also seen in the fact that the sample in an overconsolidated state has higher stiffnesses than when it was in compacted states at the same value of p'.

The values of G_{max} measured during isotropic compression and swelling of the natural sample are also shown in Fig. 4.18. As can be seen, the stiffness is constant about 2.8GPa up to a p' of about 9MPa, thus demonstrating that the stiffness in this stress range is controlled by bonding. A slightly higher value of G_{max} of 3GPa was obtained by Cuccovillo (1995) who tested the same material but used local measurement of strains to determine the stiffness. At effective stresses higher than about 9MPa it can be seen from the figure that there is a gradual increase in the values G_{max} with p'. However, this increase is slow and is probably the result of the gradual destructuring of the natural material caused by the high effective stress.

4.5.2 Discussion

The results from tests on both reconstituted and natural samples of Greensand may be interpreted within the framework for very small strain stiffness for sands presented in Section 4.4.4. This is shown in Fig. 4.19 where the normalised stiffness $G_{max}/(G_{max})_{nc}$ is plotted against the state variable p'/p'_e. As previously discussed, the value of the state variable p'/p'_e describes the distance of the current volumetric state from the normal compression line in the v:lnp' plane. The normal compression line identified for the reconstituted sample has also been used here to normalise the states and stiffnesses of the natural sample. The natural sample is very dense (see Section 4.2) so that very high pressures, well above the capacity of the apparatus, would have been needed to bring the sample to a state of normal compression. Using this normalisation, the stiffnesses of the reconstituted sample at normally consolidated states plot as a single point at 1:1. The natural sample approaches this point but, as can be seen in the figure, it is not known whether it would eventually reach it, i.e. it is not known whether the reconstituted and natural samples would have the same normal compression line. Work from Cuccovillo (1995) on the same material highlighted the differences in the fabric of the natural and reconstituted materials and it is likely that these lines may not be the same.

The results given in Fig. 4.19 show that the stiffnesses of the natural sample are considerably greater than the stiffnesses of the destructured sample which can be attributed to bonding. The graph represents the variations of the differences between stiffnesses with state so that the reduction of $G_{max}/(G_{max})_{nc}$ for the natural sample is caused predominantly by the increase of $(G_{max})_{nc}$ with pressure, as the variation of G_{max} of the natural sample is small. The increase in G_{max} observed for the natural sample after yield at about 9MPa (Fig. 4.18) is in agreement with the results of Cuccovillo (1995) who attributed this feature to the fact that the transition from cohesive to frictional behaviour during destructuring is dominated by the high density of the natural fabric, as discussed in Section 2.4.2, so that there is no sudden volumetric collapse or reduction in stiffness.

The stiffnesses of the reconstituted sample resemble the familiar pattern of behaviour within the framework which was observed for the three sands in Section 4.4.4. As can be seen from Fig. 4.19 the influence of volumetric state on stiffness is not very pronounced. The gradients of normalised stiffness with state variable for both compacted and overconsolidated samples are low and comparable to those observed for Ham River sand. The normalised stiffnesses for the sample in overconsolidated states plot a little higher than those for the sample in compacted states

defining a relatively small zone of possible stiffnesses for various combinations of compaction and overconsolidation.

The interpretation of the results for a cemented sand given in Fig. 4.19 demonstrates that features of very small strain stiffness of natural samples can be explained by adding to the framework based on the behaviour of reconstituted soils. In this context, the relationships between volumetric state, stress and G_{max} previously established for reconstituted sands are found to be a useful tool in explaining the influence of structure on the very small strain stiffness of a cemented sand.

4.6 THE STIFFNESS OF RECONSTITUTED SANDS UNDER CONTINUOUS LOADING

4.6.1 Tests on Dogs Bay sand

The samples of Dogs Bay sand were used to examine the stiffness behaviour of the soil in the region of very small and small strains under continuous loading. The samples were manufactured in as loose a state as possible using the wet compaction method. Prior to being flooded with water the samples were flushed through with carbon dioxide, thus ensuring full saturation when the back pressure was subsequently applied (see Section 3.3.1).

Two tests on 38mm diameter samples were conducted in a standard Bishop & Wesley triaxial cell. The data logging facilities of the cell were built especially for the purpose of these tests. The cell was equipped with both bender elements and a pair of miniature LVDTs (see Figs. 3.1 and 3.3) so that a comparison between stiffnesses obtained using dynamic and continuous loading could be made for the same sample. The system of miniature LVDTs (Cuccovillo & Coop, 1997) allows the stiffnesses to be established at strains down to about 0.0001%, which was regarded as being comparable to the strains imposed in the soil by bender elements. The description of the improvements made to the instrumentation of the cell in order to reach the required accuracy is given in detail in Section 3.2.3.

One of the tests was carried out in the high pressure cell with a capacity of 5MPa. A 50mm diameter sample was tested and a pair of Hall effect transducers was used for the local measurement of axial strain. Using this system the smallest reliable strain was 0.005% so that the direct comparison between the dynamic and continuous loading stiffnesses was not possible.

The test programme for each sample consisted of successive stages of

isotropic compression and undrained shearing. Between the stages of isotropic compression and swelling, undrained shearing probes were carried out using a constant rate of strain of about 0.1% per hour. Prior to starting the probes it was ensured that the rate of strain of the sample following isotropic compression was small relative to the subsequent rate of shearing. The probes were stopped at only 0.1% axial strain in order to avoid significant deformation of the sample during shearing. It was believed that the strains of around 2 to 3% that the sample underwent during isotropic compression between the probes were sufficient to erase the influence on the stiffnesses measured of the memory of the previous probe. The procedure and techniques used to perform the shearing probes so as to give the required accuracy of measurements are described in detail in Section 3.3.3. The test programme which consisted of 15 probes during three multi-stage tests is summarised in Table 4.3.

A typical stress-strain curve for a probe is given in Fig. 4.20 where an average strain for the two transducers is plotted against deviator stress at two different scales. For each transducer about 500 data points were logged not of all which are shown in the figure. The difference between the two transducer readings was typically less than 5% of the current reading and an average value was used for the calculation of the tangent stiffness. Some typical stiffness-strain curves obtained at different initial mean effective stresses, p'_i are given in Fig. 4.21. The tangent stiffness has been defined as:

$$G = \frac{1}{3}\frac{\delta q}{\delta \varepsilon_a} \qquad 4.4$$

and has been calculated using a linear regression typically through 15 points of the stress-strain curve (Fig. 4.20). Fewer points were used (typically 7-9) at the beginning of the curve where the data were more scarce. The resulting tangent stiffness then corresponded to the middle point of the strain interval. At very small strains (i.e. below 0.0001%) the random noise dominates, giving a wide variation in the stiffnesses calculated which does not represent the soil behaviour. The values of stiffness below 0.0001% have therefore been omitted from the graphs.

In many cases stick-slip behaviour also restricted the minimum strain at which the stiffness could be defined. Out of total of 15 shearing probes carried out, only two probes gave the possibility of calculating the stiffness at 0.0001% strain. The stick-slip effect was worse at higher pressures as the flexibility of the loading system increased relative to the stiffness of the sample and was particularly bad for samples which had been unloaded prior to shearing.

Typical stiffness-strain curves for overconsolidated samples are given in Fig. 4.22 where because of the stick-slip behaviour the stiffness data

have generally being omitted at strains lower than 0.001% except for the probe sh8 where p_i' was relatively low (150kPa). It should be noted that these samples were not truly overconsolidated since the capacity of the cell was not sufficient to bring the samples to the reference state of normal compression. As previously mentioned, these samples will be referred as overconsolidated-compacted.

4.6.2 Comparison between G_{max} measured using dynamic and continuous loading

As indicated in the previous section, the instrumentation of the apparatus allowed a direct comparison to be made between stiffnesses obtained during dynamic and continuous loading of a single sample. These comparisons are also presented in Fig. 4.21 in which the bender element measurements are given along with the stiffness-strain curves for the samples during first loading (i.e compacted samples). A good agreement is seen between the dynamic and continuous loading stiffnesses at a strain of 0.0001%. In contrast, for overconsolidated-compacted samples the first reliable stiffnesses from the continuous loading measurements were obtained at about 0.001% so that direct comparisons were not possible (Fig. 4.22).

In order to overcome the problem that only a few data are available at the smallest strain of 0.0001% an attempt has been made to find an objective way of comparing the stiffness-strain curves obtained at different stress levels. This has been done by normalising the current stiffness with respect to G_{max} so that curves from different stress levels can be superimposed.

An inspection of the stiffness-strain curves given in Fig. 4.21 will show that at different stress levels the stiffness reduces at different rates. In order to superimpose curves taking this into account the final stiffness from the probe at 0.1% strain ($G_{0.1}$) was deducted both from G_{max} and the current value of tangent stiffness, G, so that the value of $G-G_{0.1}$ can then be normalised with respect to the value of $G_{max}-G_{0.1}$. In this way the normalised stiffness curves are all fixed to pass through zero at 0.1% and at 1.0 at 0.0001% if there is an agreement between the dynamic stiffnesses and the continuous loading stiffnesses at the latter strain level. This normalisation is presented in Fig. 4.23 where it is perhaps more clear that there is an agreement between bender element stiffnesses (i.e. G_{max}) and the LVDT tangent stiffnesses at the smallest strain level achievable of 0.0001%. The stiffness curves which have a deficiency in the measurement caused by stick-slip behaviour follow the trend, as it appears that if the curves were extrapolated, that would bring them to a normalised stiffness of 1.0 at 0.0001% strain. These data, in contrast

to previously published data on various soils (e.g. Georgiannou et al., 1991; Porovic & Jardine, 1995), show no evidence of a plateau of constant stiffness and it is not therefore known whether the trend of increasing stiffness from the continuous loading tests would have continued at strains smaller than 0.0001%.

The same normalisation procedure has been used for the data from the overconsolidated-compacted samples and the resulting plot is given in Fig. 4.24. Here, there is some indication of an elastic plateau extending to around 0.001% which is then followed by a rapid reduction in stiffness which, subsequently, decreases more moderately with strain. Similar data were obtained by Tatsuoka & Kohata (1995) (see Section 2.3.5. and Fig. 2.18) for overconsolidated-compacted samples. It is interesting to note that the 3-SKH model (See Section 2.6.2) developed by Stallebrass (1990b) predicts this type of stiffness behaviour for overconsolidated clays.

It should be noted that for compacted samples the angle between the stress path of isotropic compression and the stress path of the undrained shearing probe was $+90^{o}$ while for the overconsolidated-compacted samples both angles of $+90^{o}$ and -90^{o} were used. Other stress path rotations would give different stiffnesses because of the recent stress history effect (Atkinson et al., 1990), as discussed in Section 2.6.1.

As previously mentioned in Section 3.4.2., Dyvik & Madshus (1985) estimated that the strains imposed in the soil by the transmitter bender element were around 0.001%. Here, and also from the comparison of dynamic and continuous loading stiffnesses from tests on Speswhite kaolin (see Section 5.6), a good agreement is seen at a lower strain level of 0.0001%. The results of dynamic finite element studies of shear wave propagation through the soil sample given in Section 3.4.3 showed that the strain level imposed by the bender element decayed due to geometric damping by one order of magnitude by the time the shear wave reached the receiver. The results of tests presented here show that the strain of 0.0001% is very likely to be an average strain imposed by the bender element to the soil which leads to the conclusion that Dyvik and Madshus's (1985) proposal is probably a slightly overestimated figure.

The good agreement in the comparison between dynamic and continuous loading stiffnesses indicate that the differences in the interpretation of bender element tests which might arise from the influence of the inertial coupling (Gajo, 1996) (see Section 2.2.2) should not be large for the tests presented here, as discussed in Section 4.3. There is also a possibility that there is, to some extent, an inherent anisotropy in the soil arising from the preparation methods which would give rise to a difference in the stiffnesses measured by the two means. Although it cannot be ruled out that the two effects cancel each other out giving the good agreement, it is the opinion of the author that both effects are small and do not substantially affect the interpretation of the tests.

4.6.3 Discussion

The stiffness at very small strains is usually presented as a power function of p' and extensive experimental evidence suggests that the power coefficient is greater than the value of 1/3 as predicted by Hertzian theory but also less than 1 (see Sections 2.3.2 and 4.4.4). Viggiani & Atkinson (1995b) showed that at small strains the stiffnesses at different strain levels for reconstituted Speswhite kaolin in a normally consolidated state depends on the mean effective stress. They used an equation of the form:

$$\left(\frac{G}{p_r}\right)_{nc} = A_s \left(\frac{p'}{p_r}\right)^{n_s} \qquad 4.5$$

where nc denotes the normally consolidated state. The parameters A_s and n_s are associated with a particular strain level and were determined from a continuous loading path in which p' was held constant. At that time the stiffnesses from continuous loading could only be measured accurately at about 0.01% strain leaving a considerable gap between these stiffnesses and those obtained using dynamic methods. Coop et al., (1995) showed that a relationship of the type of Equation 4.5 holds in a slightly different form for stiffnesses at very small and small strains for a natural Boom clay and Lo Presti (1995) showed that the stiffness data from tests on Toyura sand could be interpreted using the same equation.

Here, the stiffnesses obtained during the undrained shearing probes at larger strain levels for the compacted samples of Dogs Bay sand are compared with the G_{max} values obtained from bender element tests. This is shown in Fig. 4.25 in which the variation of stiffness is presented at different strain levels along with the $(G_{max})_{nc}$ line from Fig. 4.5. The data from the two continuous loading tests in which the stiffness was obtained at 0.0001% strain can be seen to plot on the $(G_{max})_{nc}$ line along with the bender element data. It should be noted that the samples did not reach the state of normal compression in terms of volume so these results are related to the similar features of stiffness behaviour observed from dynamic measurement of stiffness. That is, the reference state in terms of stiffness (i.e. the $(G_{max})_{nc}$ line) was reached before the comparative state in terms of volume (i.e. the normal compression line), as discussed in detail in Section 4.4.4.

A set of lines sub-parallel to the $(G_{max})_{nc}$ line is seen for the larger strains in the same figure. These lines converge towards higher stresses indicating that the stiffness reduces at a higher rate with increasing stress level and which can be also seen from the individual stiffness-strain curves given in Fig. 4.21. The same behaviour was observed by Viggiani & Atkinson (1995b) for clays, so Equation 4.5 is also used here

to fit the stiffness lines at any particular strain level, as indicated in the figure.

The convergence of the stiffnesses with increasing p' is described graphically in Fig. 4.26 where the values of the parameters A_s and n_s are plotted against the corresponding strain level. It can be seen that the value of the parameter A_s decreases towards zero while the power coefficient n_s increases with the strain level. It was not possible to examine whether the power coefficient would reach a value of 1 at larger strains since the probes could not be continued to such high strains.

The variation of parameters A_s and n_s starts at 0.0001% strain with the values of the parameters A and n, respectively, which were used to describe the $(G_{max})_{nc}$ line and were obtained from bender element tests, as indicated in the figure. It is important to emphasize that the parameters A and n are fundamental soil properties since they describe the elastic stiffness of Dogs Bay sand at the reference state of normal compression. In contrast, the values of the parameters A_s and n_s at any particular strains depend both on the loading path and recent stress history and so are not fundamental soil properties.

The tangent stiffnesses of the overconsolidated-compacted samples obtained for different strain levels are presented in Fig. 4.27 within the framework given in Section 4.4.4. Here a logarithmic $G/(G_{max})_{nc}$ scale has been used for convenience to plot the larger strain data. The G_{max} line for truly overconsolidated states (Fig. 4.15a) has been re-plotted here and lies above the G_{max} values. As previously discussed, the bender element measurements were taken during unloading but since the samples never reached the state of normal compression their normalised stiffnesses plot within the stiffness zone defined for overconsolidated-compacted samples. The normalised stiffness data for different strain levels show a clear pattern of unique lines in which the stiffness increases with the distance from the normal compression line (i.e. as p'/p'_e reduces) with approximately the same gradient for all strain levels. This result demonstrates that the stiffnesses at small strains, as was shown for the stiffnesses at very small strains, can be described within this framework, again illustrating the influence of volumetric state on stiffness.

4.7 SUMMARY

Tests on three sands with different mineralogies and geological origins have been carried out in order to examine the influence of volumetric state on stiffness at very small strains. High pressures were used to bring the soil samples of various densities to the state of isotropic normal compression. This state was used as the reference state for the stiffness at very small strains, the latter being measured using bender elements. The stiffnesses at other states have been compared with the stiffnesses at this reference state and, by means of correct normalisation of the data, a new framework was proposed which emphasises not only the influence of the confining stress on stiffness but also that of volumetric state.

A particular feature of the framework is the distinction between truly overconsolidated sands and those which have only undergone first loading, as it was found that they have significantly different stiffnesses at the same volumetric state. Between these benchmarks a zone of possible stiffnesses has then been identified in which stiffnesses for all combinations of compaction and overconsolidation would be found. Since the initial compaction of a soil deposit would be controlled by the means of deposition, the framework highlights the influence that the geological history of the soil and its subsequent loading history would have on stiffness.

The framework is based on the behaviour of three sands originally chosen for the diversity of their properties, so it is likely that it is generally applicable. In order to obtain a complete understanding it was necessary to use high pressure testing, but it should be emphasised that the framework is applicable for all stress levels. The understanding upon which the framework is based gives an explanation why the influence of volumetric state on stiffness has, so far, received little attention.

At the start of the work creep was identified as having a significant effect on the measured stiffness. It was beyond the scope of this work to investigate the influence of creep but while it may affect the absolute value of stiffness it is unlikely that it has a great effect on the framework proposed. The same comment is also valid for the effects of aging which was also detected, but since it is not related to volume change was not included within the framework.

Measurements of G_{max} have been made successfully on samples of a cemented sand using bender elements. The stiffness of the natural sand during isotropic compression was found to be larger than that of destructured soil even after correct normalisation of the data for the volumetric state, a feature which can be attributed to bonding in the natural

sample. The framework previously established for reconstituted sands was also used to explain differences in stiffnesses observed between the natural and reconstituted samples tested.

A new system of local axial measurement of strain has been used in the triaxial apparatus which was sufficiently accurate to allow comparison of continuous loading and dynamic stiffnesses. It was found that the bender element stiffnesses corresponded to the tangent stiffnesses measured under continuous loading at about 0.0001% strain and no evidence of an elastic plateau was identified for samples undergoing isotropic first loading. The system was also used to examine the stiffness behaviour of a sand on first loading in the region of small strains. The stiffnesses obtained at larger strains during continuous undrained shearing probes were compared with those obtained at very small strains. A set of sub-parallel strain contours has been identified for which the stiffnesses converge towards higher stresses in the same manner as was previously observed for clays. The tangent stiffnesses of overconsolidated-compacted samples have also been presented within the new framework, highlighting the influence that volumetric state has on stiffness not only for very small strains but also in the region of small strains.

CHAPTER 5 THE INFLUENCE OF STRESS STATE AND FABRIC ON G_{max} ANISOTROPY OF FINE GRAINED SOILS

5.1 INTRODUCTION

The stiffness of fine grained soils at very small strains has been the subject of much detailed research in recent years. Viggiani & Atkinson (1995b) established a framework for reconstituted clays by relating the small strain stiffness to soil state. Rampello et al., (1995a) examined the stiffness of natural clays and by taking into account the soil state showed that there is no influence of structure on G_{max}. In order to avoid any repetition of previous work, this research focused on the anisotropy of G_{max} of both reconstituted and natural clays. The work also examined the influence of very high overconsolidation ratios on G_{max} and included a comparison of statically and dynamically measured stiffnesses.

As already discussed in Section 2.4.3. the factors which lead to anisotropic behaviour of soil are stress induced anisotropy and inherent anisotropy. Stress induced anisotropy results from the anisotropy of the current stress condition, whereas inherent or structural anisotropy is that which results from the anisotropic fabric of soils. For clays, inherent anisotropy may be caused by continued straining in one direction in which case it may be referred to as being strain induced. As summarised in the literature review much of the previous work on the anisotropy of clays was focused on large strain behaviour while here the current work examines the influence of anisotropic fabric on G_{max}.

The anisotropy of the stiffness at very small strains of sands has been the subject of past research (Roesler, 1979; Knox et al., 1982; Stokoe et al., 1995). In contrast, there is little experimental evidence of anisotropy of G_{max} in clays and while the presence of anisotropic fabrics in clays has been long recognised, little is known how this affects G_{max} and what is the relative magnitude of the inherent to the stress induced components of anisotropy. As discussed previously in Section 2.4.3 the inherent and strain induced components of anisotropy can only be separated from the stress induced component under an isotropic stress state. Jamiolkowski et al., (1995) identified G_{max} anisotropy in a number of natural clays but the relative importance of these components was not distinguished as the tests were conducted in an oedometer apparatus in which the stress state is generally anisotropic. The stress path triaxial apparatus, however, allows the application of both isotropic and anisotropic stress states and being fitted with bender elements was used in this research to separate out and contrast the different components of soil anisotropy in terms of G_{max}.

The set-up of the triaxial apparatus used (Fig. 3.1) consisted of a single pair of bender elements which were located along the vertical axis of the sample. Consequently, the axial effective stress was always the

stress in the direction of the wave propagation and the radial stress was always the stress in the direction of the wave polarisation (i.e. the direction of the particle movement) as shown in Fig. 5.1. Due to the axial symmetry in the triaxial apparatus the radial effective stress acts also in the direction out of the plane of vibration so it is not possible to vary independently the stress which acts perpendicularly to the plane of vibration and the stress which acts in the plane of vibration.

Following the notation in Fig. 5.1 the suffix a (axial) denotes the direction of the propagation and the suffix r (radial) denotes the direction of polarisation. The limitation of this standard configuration is that the bender element method can measure only G_{ar}, that is, G_{13} in compression or G_{31} in extension. More complex arrangements of elements in the triaxial cell have been used by Pennington (1996) on a 100mm diameter sample so that waves can be propagated and received both axially and diametrically across the sample. However, this set-up would not be practical on the much smaller 38mm diameter samples used here and the test times would be much longer if 100mm diameter samples were used. In any case, only a true triaxial apparatus fitted with pairs of bender elements on opposite sides of the cube sample will allow independent variation of the three principal stresses and corresponding measurement of variations in G_{max} in different directions.

This disadvantage of the standard configuration is unimportant if the soil tested is isotropic. If not, then the standard configuration can measure only one out of twenty-one parameters which are necessary to characterize the fully anisotropic elastic material. If the soil has at least one axis of symmetry (e.g. a cross-anisotropic soil) then it must be ensured that the direction of propagation and the direction of polarisation coincide with the principal axis of the fabric. Otherwise, as previously indicated in Section 2.2.2, the interpretation of the bender element test is very difficult, since waves propagating at an angle through an anisotropic medium are neither purely shear nor compressive (Love, 1927).

In order to interpret the bender element test correctly it is, therefore, necessary to know the principal axis of the fabric of the material. The common approach is to make the preliminary assumption of some particular form of anisotropy, for example cross-anisotropy (see Section 2.4.3). In this case the value of G_{max} is calculated as:

$$G_{max}^{ij} = \rho \, v_s^{ij} \qquad 5.1$$

where v_s^{ij} is the directional velocity of the shear wave, ρ is the total mass density of the soil, i is the direction of propagation and j is the direction of the wave polarisation, these directions coinciding with the principal axes of the soil fabric. In the case of cross-anisotropy the horizontal plane is isotropic so any horizontal axis is a principal axis

of the fabric. From the test results the assumption of the type of anisotropy, upon which the test has been interpreted, can be examined.

Using the standard configuration given in Fig. 5.1 it is possible to measure stiffness in the three different propagation-polarisation patterns of a cross-anisotropic soil. By cutting the samples horizontally or vertically and orientating the slots of the bender elements horizontally or vertically it is possible to measure the three different stiffnesses: G_{vh}, G_{hv}, and G_{hh} (see Equations 2.28 and 2.29). This is shown in Fig. 5.2 where the suffixes v (vertical) and h (horizontal) refer to the original orientation of the sample in the ground for a natural sample or in the consolidometer for a reconstituted sample and which are assumed to be the principal axes of the fabric.

5.2 TESTING PROGRAMME

In order to examine anisotropy of very small strain stiffness in clays four series of tests were performed. Tests on reconstituted Speswhite kaolin were carried out to identify the magnitude of the stress induced component of anisotropy on G_{max}. These were performed in such a way as to separate out the effects of stress and strain induced anisotropy so that their magnitudes could be compared. A further series of tests used natural samples of London clay to identify the inherent anisotropy of the soil. This was followed by a final set of tests on the reconstituted London clay which was aimed at reproducing the inherent anisotropy observed in the natural samples so that the role of the structure of the clay could be evaluated. Details of the apparatus used, sample preparation methods, triaxial test procedures and bender element test methods are given in Chapter 3.

In the first group of tests a series of measurements of G_{max} was made on a single sample of reconstituted Speswhite kaolin. The test followed a series of constant p' stress paths at successively higher pressures. At selected values of stress ratio η =q/p' bender element tests were carried out. Although these stress paths imposed anisotropic stress states on the sample due to the alternating directions of the probes, the net strains were approximately isotropic. A series of three tests was then conducted in which the sample was compressed along paths of constant stress ratio η allowing anisotropic strains to develop. For the tests with a negative η the sample was cut horizontally from the consolidometer cake so as to give polarisation in what had been the direction of the major principal stress in the consolidometer i.e. vertical . By this procedure the sample would continue to experience the major principal stress in the direction of polarisation once the sample was tested in the triaxial cell. The test programme for the influence of anisotropic stress

states on G_{max} and initial and final specific volumes of all samples tested are given in Table 5.1.

The loading conditions imposed by the triaxial apparatus are axi-symmetric so that the anisotropic straining of the reconstituted soil could give rise to cross-anisotropy. Since the vertical axis is the axis of symmetry the evolving anisotropy is only measured by shear waves both propagating and polarised in the horizontal direction which measure G_{33} (see Fig. 5.2). This was not possible to achieve with the standard configuration where shear wave propagates along the line of symmetry and therefore, in these tests on kaolin, only the stress induced effect could be measured.

Since it was not possible to measure directly the strain induced effect on anisotropy it was necessary to investigate the magnitude of the effect using oriented samples. Reconstituted samples of Speswhite kaolin were consolidated in a 100mm consolidometer and then cut in either the vertical or horizontal directions. The samples were oriented in the triaxial apparatus so that bender element would give a shear wave polarised either in the original horizontal or vertical direction, as shown in Fig. 5.2. The samples were consolidated to different vertical stresses in the consolidometer and after transferral to the triaxial cell an isotropic stress equal to the vertical consolidation pressure was applied. The use of isotropic stresses ensured that no stress induced effect on anisotropy was present so that only the effect of strain induced anisotropy developed during one-dimensional compression in the consolidometer was measured. For each test only one measurement of stiffness was carried out. A total of ten tests on oriented samples of reconstituted Speswhite kaolin were carried out, as summarised in Table 5.2. Some of the tests were carried out by Arnold (1996) under the supervision of the author, as indicated in the table.

The same methodology was used to investigate the inherent anisotropy of natural London clay. The soil had been sampled from a site in West London by means of rotary coring using a polymer flush. Four sets of three tests were carried out for each depth as summarised in Table 5.3. The samples were cut horizontally and vertically and the slots of the bender elements were oriented so as to measure the different stiffnesses. After being transferred to the triaxial cell the samples were subjected to isotropic stresses equivalent to the estimated values of the in-situ mean effective stress before a single bender element test was carried out.

In an attempt to reproduce the inherent anisotropy of the natural clay in the laboratory a set of five tests was carried out on reconstituted London clay. Remoulded natural material was mixed into a slurry and one-dimensionally consolidated to either 400kPa or 1500kPa in a 100mm diameter consolidometer. The two samples which were compressed to 1500kPa were subsequently unloaded within the consolidometer to a vertical

effective stress of 400kPa so as to better reproduce the geological stress history of the London clay deposit (Jardine, 1985) which is heavily overconsolidated. Again, the samples were cut horizontally or vertically and the bender element slots were oriented relative to the principal axis of soil fabric as indicated in Fig. 5.2. After being transferred to the triaxial cell the samples were consolidated under an isotropic stress of 400kPa. The two samples which had been compressed to 1500kPa in consolidometer were then subsequently isotropically compressed in stages up to 3MPa. At each stage the sample was allowed to fully consolidate before the bender element test was performed. The test programme for the reconstituted London clay is summarised in Table 5.4.

Finally the influence of high overconsolidation ratios on G_{max} was investigated by using reconstituted Speswhite kaolin and Boom clay. The test on Boom clay was carried out by Agah (1996) under the supervision of the author. In each case the soil samples were isotropically compressed up to 600kPa in the triaxial apparatus and then unloaded in stages down to low stresses of around 10kPa. Again at each stage the sample was allowed to consolidate fully before the bender element measurement was performed.

There were no specific tests carried out to compare the very small strain stiffnesses obtained from the bender element tests with those from monotonic loading tests. Instead, the test results of G_{max} on isotropically normally consolidated Speswhite kaolin were compared with the results of tests carried out by Coop (1996) in which very small strain stiffnesses were obtained using local triaxial instrumentation. The technique of using the LVDTs (Cuccovillo & Coop, 1997) for the local measurement of axial strain is described in detail in Chapter 3. The samples of Speswhite kaolin had been isotropically compressed and successive undrained shearing probes were carried out at increasing values of mean effective stress (Coop, 1996). The probes were stopped at an axial strain of only 0.1% so that the strain during the isotropic compression which followed was sufficient to erase any influence on the stiffness measured from the memory of the previous probe. The undrained probes had been started when the rate of strain continuing from the previous isotropic compression stage was insignificant relative to the strain rate of about 0.01%-0.02% per hour which was used during the probes.

5.3 STRESS INDUCED ANISOTROPY OF G_{max}

5.3.1 Tests results

The stress induced anisotropy of G_{max} was examined using samples of reconstituted kaolin (see Table 5.1). Figure 5.3a illustrates a test programme carried out on a single sample which followed a series of constant p' stress paths at successively higher pressures. Bender element tests were carried out at selected values of the stress ratio as indicated in the figure.

The sample was first reconstituted into a slurry and then one-dimensionally compressed to 70kPa vertical effective stress in the consolidometer. As will be shown later, this consolidation already caused an anisotropic fabric to be developed within the material. Therefore the bender element tests measured the values of G^{ij}_{max}, that is, G^{13}_{max} in compression or G^{31}_{max} in extension. It is important to note that the test did not measure the value of G^{33}_{max} and that the test results that follow are therefore restricted to G^{ij}_{max}.

The results presented in Fig. 5.3b show that the influence of stress anisotropy is small. This is seen in the figure by comparing the values of G^{ij}_{max} at the same p' but at different stress ratios η. The differences between the values of G^{ij}_{max} do not exceed 5% and they appear random. These data do not take into account the volume changes of the sample because the soil was normally and in some cases very slightly overconsolidated throughout the test. It should be noted that the proximity of successive constant p' probes caused the expansion of boundary surface which was such that the soil was slightly overconsolidated at the start of the next probe. The influence of this slight overconsolidation contributes to the scatter in the data but does not affect the measured stiffnesses by more than about 3-4%.

The alternating direction of the probes during the test resulted in the net strains being approximately isotropic. In order to allow anisotropic strains to develop a series of three tests was then carried out in which the sample was compressed along paths of constant stress ratio (Table 5.1 and Fig. 5.4a). As previously mentioned the sample which followed the negative stress ratio path was reconstituted in a 100m diameter consolidometer so that it could be cut horizontally, thus ensuring that the direction of straining within the sample in the consolidometer was preserved in the triaxial test. The measured values of G^{ij}_{max} are plotted against p' in Fig. 5.4b. At stresses lower than 200kPa no difference in the G^{ij}_{max} values is observed for any of the stress paths. At higher

stresses the stiffnesses diverge slightly so that the η=0.75 path gives lower values of G^{ij}_{max} than the isotropic path (η=0) which in turn gives lower values of G^{ij}_{max} than the path η=-0.6. These differences in stiffness within range of stresses used are small and only at higher stresses the differences become significant (i.e. about 7%.).

This result confirms the conclusion from the previous test that there is a relatively small influence of anisotropic stress state on the value of G^{ij}_{max}. As previously mentioned, due to limitations of the standard bender element configuration it was not possible to follow changes in G^{33}_{max} during the test so this conclusion is restricted to values of G^{ij}_{max}. Although all the samples were normally consolidated throughout the test their normal compression lines were different in the v:lnp' plane since their anisotropic stress paths were different. When compared to the state of isotropic normal compression the volumetric states of the samples which followed the anisotropic stress paths appear slightly overconsolidated. This apparent "overconsolidation" of the samples has not been considered here, but it would not affect the measured stiffness as by more than about 5%.

5.3.2 Discussion

From the test results on Speswhite kaolin described in this section it can be concluded that the effect of an anisotropic stress state on G^{ij}_{max} is small. As outlined in Section 2.4.3 similar results have been presented by other authors. Here an attempt has then been made to correlate these findings with the results of other theoretical and empirical studies of stress induced anisotropy.

As discussed in Section 2.3.3, Zytinski et al., (1978) demonstrated that the shear modulus of an elastic material could not be simply a function of p' since a cycle of deviator stress q would result in dissipation of energy. This implies that the shear modulus is more likely to depend both on p' and q in such a way as to prevent any energy loss or gain during the cycle. This was proposed by Lade & Nelson (1987) who used an analytical expression in which the Young's modulus of an elastic material depends on the first two generalised invariants of the stress tensor:

$$E = Cp_a\left[\frac{I_1^2}{p_a^2} + R\frac{J_2}{p_a^2}\right]^{n/2} \qquad 5.2$$

where C is a constant, p_a is atmospheric pressure, n is a power coefficient which is a material parameter and where:

$$R=6\frac{1+\nu}{1-2\nu} \qquad 5.3$$

where ν is the Poisson's ratio. For an axi-symmetric stress state in the triaxial apparatus:

$$I_1=3p',\ J_2=\frac{q^2}{3} \qquad 5.4$$

Rewriting this in terms of q and p' gives:

$$G_{max}=\frac{C3^n}{2(1+\nu)}p_a^{(1-n)}(p')^n\beta^{n/2} \qquad 5.5$$

where:

$$\beta=(1+R\frac{\eta^2}{27}) \qquad 5.6$$

Using a completely different approach Hardin & Blandford (1989) proposed an empirical relationship between G_{max} and the current stress state, (see Equation 2.19) based on the work of Roesler (1979). This equation was discussed in detail in Section 2.3.3 and here it is rewritten for the axi-symmetric stress state of triaxial compression:

$$G_{max}=Sf(e)\,OCR^k p_a^{1-n}(\sigma_1')^{n/2}(\sigma_3')^{n/2} \qquad 5.7$$

where S is a coefficient associated with the fabric of the isotropic material, f(e) is a function of void ratio, OCR is the overconsolidation ratio in terms of p' and k is the corresponding coefficient. This form of equation can be readily related to the expression derived by Lade & Nelson (1987) which is known to be theoretically sound. This is clearer if it is written in terms of the stress invariants for the axi-symmetric stress state of the triaxial test, so that:

$$G_{max}=Sf(e)\,OCR^k p_a^{1-n}(p')^n\beta^{n/2} \qquad 5.8$$

where β is given by:

$$\beta=(1+\frac{\eta}{3}-\frac{2\eta^2}{9}) \qquad 5.9$$

It is remarkable that Equations 5.5 and 5.8 relate G_{max} to the current stress state in terms of stress invariants using a very similar mathematical description despite the fact that one has a purely theoretical origin while the other has a purely empirical origin. It is important to note that the stress induced anisotropy is determined by the parameter $\beta^{n/2}$ which is a function of the stress ratio η for both equations. This means that the difference of G_{max} with respect to that

measured under an isotropic stress at the same p' should be a function of only $\beta^{n/2}$.

The stress induced effect on anisotropy is, therefore, theoretically and experimentally based on remarkably similar mathematical expressions. Further research then focused on the evaluation of the magnitude of this effect. This has been examined by calculating values of $\beta^{n/2}$ using Equations 5.6 and 5.9. for the typical range of power coefficients n for different materials and different values of the stress ratio η. From the data presented in the literature it was seen that the coefficient n generally varies between 0.4 and 0.8. It is important to note that here n relates to G_{max} only and should be, therefore, regarded as a unique parameter for each soil. Other authors (e.g. Viggiani & Atkinson, 1995b) used n to denote the power coefficient relating tangent stiffness and p' at a particular strain level in which case n is a stress path dependant variable and should not be confused with the coefficient used here.

The results of the calculations are presented in Fig. 5.5. As can be observed, for the Hardin & Blandford proposal (Equation 5.9) the effect of the stress induced anisotropy is very small as for typical values of stress ratio η, even when the soil is near to failure, the value of $\beta^{n/2}$ will be usually less than 1.05. For example for the value of n of 0.65 for kaolin (Viggiani & Atkinson, 1995b) at the stress ratio η=0.75 used in the tests the value of $\beta^{n/2}$ is equal to 1.04. This means that the increase of G_{max}, with respect to that measured under an isotropic stress at the same p', should only be about 4%. This result is in good agreement with the test data presented in Fig. 5.3b where such a small difference in stiffness would be lost within the scatter of the data arising from the slight overconsolidation of some of the samples. As previously discussed, the stress path with a positive value of η gives around 7% lower stiffnesses at higher stresses from the isotropically loaded sample (Fig. 5.4) which is not in agreement with the predictions from Fig. 5.5.

The theoretical proposal from Lade and Nelson (Equation 5.6) is given in the same figure as a family of dotted curves for the same range of values of n and for a single value of Poisons ratio of 0.25. For the value of n=0.65 for Speswhite kaolin, the increase of G_{max} predicted to result from the anisotropic stress state of η=0.75 is only about 9%.

The test results demonstrate that the stress induced effect on the anisotropy of G_{max} is small which confirms the theory but the differences in the values of G_{max} for the same p' appear random and do not follow exactly the predictions given in Fig. 5.5. As already indicated the test results did not consider the slight overconsolidation of the samples, and taking into account the fact that the effect which it was attempted to measure was small, the differences which would arise from the theoretical

predictions have not been seen.

Both the experimental results and theoretical studies predict that the stress induced effect for the axi-symmetric stress state should be expected to be small. Additionally, the theoretical and empirical studies showed that this should hold for the majority of soils. As will be demonstrated later the magnitude of the stress induced component of anisotropy is about an order of magnitude smaller than the magnitude of the inherent component of anisotropy for natural clays which have been one-dimensionally compressed during their geological history.

5.4 INHERENT ANISOTROPY OF G_{max}

5.4.1 Tests on Speswhite kaolin

This series of tests was designed to measure strain induced anisotropy of Speswhite kaolin, the soil which had previously been used to examine the stress induced anisotropy. Reconstituted samples were consolidated in the consolidometer from a slurry which, since it had a consistency of a liquid would initially have been essentially isotropic. There was no attempt to model a depositional process by sedimentation of the slurry. In this way any inherent anisotropy of the reconstituted samples would be solely strain induced and unrelated to any depositional fabric. The samples were consolidated to four different vertical stresses (see Table 5.2) and then cut in the required directions. After being transferred into the triaxial apparatus an isotropic stress equal to the vertical consolidation pressure was applied to the sample. A single bender element test was then carried out after the end of consolidation. The use of isotropic stresses ensured that any differences in the measured stiffnesses resulted only from strain induced anisotropy which developed within the soil during one-dimensional consolidation.

The results from the tests are presented in Fig. 5.6 as a variation of stiffness with p'. In contrast with the notation used for G_{max} measured under anisotropic stress states, here the suffixes v and h are used, referring to the original vertical and horizontal directions of the sample in the consolidometer. As discussed in the literature review (Section 2.4.3) a cross-anisotropic soil has the feature that the values of G_{vh} and G_{hv} are the same. Confusion should be avoided here as the values of G_{vh} and G_{hv} are not necessarily defined for a single plane, as it might be thought from the notation, but may be for different planes which are determined by the same vertical axis but different horizontal axes.

The results of the test show that the values of G_{vh} and G_{hv} are almost the same, thus suggesting that in the consolidometer the axi-symmetric stress state dictated that the strain induced anisotropy had taken the form of cross-anisotropy. The values of G_{hh} are about 70% higher than either G_{vh} or G_{hv}. As will be discussed in Section 6.1.1 the degree of anisotropy can be represented by the ratio of stiffnesses, $\alpha(=G_{hh}/G_{vh})$ (Graham & Houlsby, 1983), which in this case equals 1.7. It is important to note that the degree of anisotropy does not increase for the samples compressed to higher stresses in the consolidometer. This feature of strain induced anisotropy will be also discussed later.

It should be noted that there has been an increase of p' that the samples experienced in the triaxial cell relative to that which was applied to them in the consolidometer where the stress state was anisotropic. This increase caused moderate isotropic volumetric strain of around 4-5% which might have reduced the degree of anisotropy. As will be shown later this reduction in the degree of anisotropy should be expected to be small since very large isotropic volumetric strains are needed to change substantially the degree of anisotropy.

In Fig. 5.7 a composite graph from Fig. 5.4 and Fig. 5.6 is formed in order to compare the stress induced and strain induced components of anisotropy. The values of G_{vh} and G_{hv} are in broad agreement with the results from the constant η tests (Section 5.3.1) as they represent the results of bender element tests with the same propagation-polarisation pattern. It can be observed that the values of G_{vh} and G_{hv} are slightly higher than those of G_{13} and G_{31} as a result of the slight overconsolidation arising from the disturbance in transferring the oriented samples to the triaxial cell. While the stress induced effect appears to be lost due to the effect of overconsolidation, the strain induced effect dominates the anisotropy of the soil throughout the stress range used.

5.4.2 Tests on undisturbed samples of London clay

As previously discussed, with the standard configuration of bender elements in the triaxial apparatus the strain induced or inherent anisotropy can only be investigated by a "single shot" bender element test under an isotropic stress state. Following the same methodology used for the oriented samples of reconstituted Speswhite kaolin a series of tests was then conducted on natural London clay in order to examine the inherent anisotropy of G_{max} in the soil (see Table 5.3).

In Section 2.4.3 of the literature review the inherent or structural anisotropy was defined as that which results from the anisotropic fabric

of soils. Here an attempt has been made to measure the degree of inherent anisotropy of the natural samples of London clay and the undisturbed samples were subjected to isotropic effective stresses in the triaxial apparatus which were approximately equal to those in situ. It was believed that the stresses in situ were also isotropic. The soil was heavily overconsolidated so the application of the stresses during the test caused only very small volumetric strains. For this reason and due to the fact that the clay was fissured and difficult to trim into high quality samples only one horizontally cut sample was used for both tests with horizontally propagated waves. After the measurement of G_{hh} the sample was rotated through 90^0 with respect to the direction of bender elements (see Fig. 5.2) and repositioned on the pedestal allowing the test for G_{vh} to be performed. In the process, new slots were excavated (see Section 3.3.1) and the sample ends were trimmed slightly so that elements protruded into fresh soil.

The results of the tests are shown in Fig. 5.8 again as the variation of stiffness with mean effective stress. The suffixes for G_{max} now refer to the original orientations of the samples in the ground. The test results are very consistent in indicating an inherent anisotropy, as at any particular depth G_{hh} was about 50% greater than G_{vh} and G_{hv} which were equal. As discussed before, the cross-anisotropy is also confirmed by the consistency of G_{vh} and G_{hv} values for different depths despite the fact that the horizontal orientation of the samples as retrieved from the borehole was not known and so was random. Butcher & Powell, (1995) reported values of G_{max} which are in good agreement with the ones presented here although they used geophysical in-situ testing at a different site in London clay to that here. The only significant difference between the two sets of data is in the fact that in-situ G_{hv} values were about 20% higher than the in-situ G_{vh} values while here the cross-anisotropy was identified. It is not explained by the authors what would be the possible reason that this occurred.

From the results presented in Fig. 5.8 it can be seen that the degree of anisotropy α is constant at all stress levels, a feature which had also been observed for the strain induced anisotropy of the reconstituted Speswhite kaolin. In this case the degree of anisotropy was 1.5 which is about 30% lower than that observed for the kaolin.

5.4.3 Tests on reconstituted London clay

In an attempt to reproduce the inherent anisotropy observed in natural samples three specimens were normally compressed from a slurry in the consolidometer up to 400kPa vertical effective stress. The samples were then cut, oriented and transferred to the triaxial cell where they were subjected to isotropic compression under an effective stress of 400kPa. The stiffnesses measured and shown as the NC samples on Fig. 5.9a indicated a strain induced anisotropy which developed within the soil during one-dimensional compression in the consolidometer. The degree of anisotropy was found to be about 1.25 which was significantly less than the degree of inherent anisotropy of the natural samples which was 1.5.

A second series of tests was then carried out to better reproduce the history of London clay, as already discussed before. The samples were one-dimensionally compressed in the consolidometer up to 1500kPa which was an estimate of a preconsolidation pressure and then unloaded to 400kPa. They were then cut from the consolidometer cake in the chosen orientation and transferred into the high pressure triaxial cell. Two horizontally cut samples were used to measure G_{hh} and G_{hv} only. It was considered unnecessary to measure G_{vh} since the cross-anisotropy of one-dimensionally compressed reconstituted samples was considered well established. The creation of the sample for the measurement of G_{vh} would also have required an excessively long consolidation time for the thicker reconstituted sample, which was found to be impractical.

The samples which are denoted OC in Fig. 5.9 were isotropically compressed to 3000kPa in a series of steps (Fig. 5.9b) and the results of bender element tests are presented in the form of the variation of stiffness with p' in Fig. 5.9a. Initially an isotropic effective stress of 400kPa was applied which was approximately equal to the final p' in the consolidometer. The degree of anisotropy was found to be 1.5 which was in agreement to that observed for the natural soil. The tests were designed to examine the change of inherent anisotropy of the soil resulting from continued isotropic straining. In Fig. 5.10a are presented the variation of the degree of anisotropy with p' along with the strain increment ratio of radial to axial strain. The radial strains were calculated from the measurement of axial and volumetric strains by assuming that the sample preserves a cylindrical shape during deformation. Up to the preconsolidation pressure both ratios remain constant and almost equal at about 1.5. After yield the strain increment ratio immediately becomes isotropic having a value of about 1.0. In contrast, the degree of anisotropy of G_{max} decreases very gradually so that the strain induced anisotropy of G_{max} persists long after the strain increments have become isotropic. At the maximum pressure reached the

degree of anisotropy was still high at about 1.4.

The degree of anisotropy of G_{max} is plotted against volumetric strain in Fig. 5.10b. From the data presented it can be concluded that very large strains would be required to obtain the isotropy of G_{max} appropriate to the new stress regime. In the same figure are presented data from the set of tests on the normally consolidated samples. Before the isotropic consolidation in the triaxial cell results from bender element tests indicated a degree of anisotropy of 1.33. These measurements were made under a total stress which was isotropic but with the drainage shut so that no consolidation took place. This degree of anisotropy was then reduced to about 1.25 as a result of the isotropic compression which followed. The effect observed here is similar to that observed with the overconsolidated samples again indicating that very large straining is needed to change the degree of inherent anisotropy.

5.4.4 Discussion

It was observed from the tests carried out on reconstituted samples of both Speswhite kaolin and London clay that cross-anisotropy of G_{max} had developed within the soils during one-dimensional compression from a slurry. This result demonstrates that anisotropic plastic straining is one means by which anisotropic stiffnesses are developed in clays. Kirkpatrick & Renie (1972) studied the fabric of reconstituted kaolin using electro-micrographs of vertically and horizontally cut cross-sections of the specimens. They observed that the samples which were one-dimensionally consolidated from slurry developed an anisotropic fabric seen, to the certain extent, as the characteristic arrangement of platy particles along the horizontal planes.

It is very likely that the anisotropy of G_{max} measured here is the result of the presence of an anisotropic fabric which was imparted to the soil during one-dimensional compression. In micro-mechanical terms this might mean that the waves with horizontal polarisation-propagation pattern (i.e. v_{hh} waves) are more likely to cause a sliding between the platy clay particles while the waves with vertical polarisation or vertical propagation (i.e. v_{hv} or v_{vh} waves) are more likely to cause bending of particles as they propagate through the soil. These different modes of deformation (i.e sliding and bending) could perhaps explain the differences in stiffness observed in the corresponding directions. In terms of very small strain stiffness this is seen as the difference between G_{hh} and G_{vh} or G_{hv}, the latter two being equal for a cross-anisotropic soil. The degree of anisotropy was found in both soils tested to be greater than one, a feature also characteristic of many natural clays, as reported by Graham & Houlsby (1983).

Anandarajah & Kuganenthira (1995) investigated the strain induced anisotropy of one-dimensionally compressed kaolin by means of electrical conductivity. They observed that an initially isotropic slurry gradually developed anisotropy during straining. The increasing degree of anisotropy eventually reached a saturation level at about 100kPa vertical effective stress after which it did not change. This is in good agreement with the results of the tests on reconstituted kaolin (Fig. 5.6) where it was observed that the degree of anisotropy was constant for the range of stresses applied in the consolidometer, which varied from 150 to 600kPa.

In terms of anisotropic fabric caused by one-dimensional compression it appears that there is a limit to the extent to which the alignment of particles influences the material properties of the soil so that continued straining in one particular sense might create a maximum or full degree of anisotropy appropriate to that anisotropic state. This means that there is a possibility that the degree of anisotropy of the natural sample can be reproduced in the laboratory even if precisely the correct preconsolidation stress is not used.

From the tests on reconstituted London clay it was shown that the influence of the plastic straining can reverse the development of an anisotropic fabric, i.e. continued isotropic straining may reduce the degree of anisotropy. This is seen after the yield of the sample at the preconsolidation pressure of 1500kPa when the value of G_{hh} starts to converge with G_{hv} (Fig. 5.9). The imposition of the strains associated with the new isotropic loading regime tended to erase the existing inherent anisotropy as the soil reverted towards isotropy on what was the new horizontal plane. However, this process was very slow and from Fig. 5.10a it can be seen that the inherent anisotropy of G_{max} persists long after the strain increments reached a ratio appropriate to isotropy. Therefore, inherent anisotropy in clays can be regarded as a variable factor which is related to the plastic strain history of the soil up to its current state. As a consequence, only if there have been very large continuous strains in one sense will the degree of anisotropy take a unique value.

From the tests on undisturbed samples of London clay it can be concluded that the soil is cross-anisotropic with relatively high degree of anisotropy of 1.5. It was shown that the normally consolidated samples of reconstituted London clay had a much lower degree of anisotropy than the undisturbed samples. In contrast, the overconsolidated samples which had been subjected to a preconsolidation pressure of 1500kPa had the same degree of anisotropy as the undisturbed samples. Although this may be a coincidence it may also suggest the possibility that 1.5 is the maximum degree of anisotropy for this soil. One possible explanation of the fact that the normally consolidated samples had a lower degree of anisotropy is that at 400kPa London clay, unlike the kaolin, had not yet reached the

saturation in terms of anisotropy of G_{max}.

The values of G_{max} of the overconsolidated reconstituted samples of London clay are about 60% lower then those of the undisturbed samples at the same mean effective stress (see Figs. 5.8 and 5.9). This is not an unexpected result since the specific volume of the overconsolidated reconstituted samples are about 10% percent higher than those of undisturbed samples at the same p', indicating that the natural soil was more heavily overconsolidated (Tables 5.3 and 5.4) and that the estimate of the preconsolidation stress had not been correct. It is not likely that this difference in specific volumes arises from the difference in fabric since the degree of anisotropy was found to be the same for both materials. This is also in agreement with the work of Viggiani (1992) who showed that the structure of natural London clay does not influence the value of G_{max}. Here it is observed that the natural structure and the sedimentation history of London clay have also not significantly influenced the degree of anisotropy in terms of G_{max}. Therefore the inherent or structural anisotropy of London clay is very likely to be equivalent to the strain induced anisotropy, and appears not to be related to the fabric of the soil at deposition.

5.5 THE INFLUENCE OF HIGH OVERCONSOLIDATION RATIO ON G_{max}

5.5.1 Introduction

As discussed in detail in Section 2.3.4, on the basis of the tests on reconstituted clays, Viggiani & Atkinson (1995b) correlated the state of the soil with G_{max} using an empirical relationship of the form:

$$\left(\frac{G_{max}}{p_r}\right)_{oc} = \left(\frac{G_{max}}{p_r}\right)_{nc} R_o^{\,m} \qquad 5.10$$

where the suffixes oc and nc correspond to overconsolidated states and normally consolidated states respectively and where:

$$\left(\frac{G_{max}}{p_r}\right)_{nc} = A\left(\frac{p'}{p_r}\right)^{n} \qquad 5.11$$

while R_0 is the overconsolidation ratio and p_r is the reference pressure of 1kPa. The pressure multiplier, A, and the pressure exponents, n and m, are regarded as material parameters which are related to the nature of the soil. Rampello et al., (1995b) showed that this relationship is valid for a variety of reconstituted clays.

The tests performed by Viggiani & Atkinson (1995) and Rampello et al., (1995b) were carried out only up to relatively low values of overconsolidation ratio, which usually did not exceed a value of 8. The set of tests presented here was, therefore, aimed at examining the variation of G_{max} of reconstituted clays at higher overconsolidation ratios. Reconstituted Speswhite kaolin was used as this material was also tested by Viggiani & Atkinson. Tests on Boom clay from Mol, Belgium carried out by Agah (1996) are also presented here.

5.5.2 Tests results and discussion

The samples of reconstituted Speswhite kaolin were isotropically compressed to 600kPa and then unloaded in stages down to 7kPa so that a maximum overconsolidation ratio of about 90 was achieved. Bender element tests were carried out at the end of the consolidation stages when no further change in G_{max} was observed due to un-dissipated pore pressures. Speswhite kaolin has a low creep characteristic and no influence of creep on G_{max} was observed.

The test on Boom clay was carried out with a suction cap used to attach the sample to the internal load cell. The drift of the load cell during the very long test caused the malfunctioning of the control of the test so that the sample failed and the test had to be terminated at the relatively low overconsolidation ratio of about 30. Possible drift of the load cell becomes critical to the control of the tests at low pressures so, in order to prevent any complications, the isotropic compression of the Speswhite kaolin was carried out with no attachment of the sample to the internal load cell. The axial strain was therefore measured using local instrumentation.

The variation of G_{max} with p' and the volumetric path for the test on reconstituted kaolin are given in Fig. 5.11. For the normally consolidated states a linear variation of $\log G_{max}$ with $\log p'$ is found from which the parameters A=1840 and n=0.670 for Equation 5.11 have been identified as shown in the figure. Similar values for A and n for Speswhite kaolin were reported by Viggiani & Atkinson (1995b).

The influence of state on G_{max} is presented in Fig. 5.12 where the value of $(G_{max})_{oc}$ is normalised with respect $(G_{max})_{nc}$ (see equations 5.10 and 5.11). This is plotted on a logarithmic scale against the logarithm of the overconsolidation ratio R_0 so that all normalised stiffnesses of normally consolidated states plot at the origin. According to Equation 5.10 the dependence of normalised stiffness with overconsolidation ratio should be linear on a log-log plot so that the gradient of the line given in Fig. 5.12 is used to determine the parameter m. From the test data

presented a straight line is seen only for low values of overconsolidation ratio. The data almost overlap with the line for Speswhite kaolin proposed by Viggiani & Atkinson (1995b) given in the same figure. At values of R_0 higher then 10 a well defined curvature is apparent and at values of R_0 greater than 20 little further influence of overconsolidation ratio on G_{max} is seen. This result indicates that for Speswhite kaolin Equation 5.10 holds only for low values of overconsolidation ratio and that in general m is not a material parameter but a variable which is also dependant on the stress history of the soil.

Test results for Boom clay are presented in the same manner as the data for kaolin in Fig. 5.13. In this case values of the parameters A=185 and n=1.04 for the normally consolidated soil were determined by Agah (1996) which were then used to normalise the values of G_{max} at overconsolidated states. In contrast to the data for kaolin the linearity of the dependence of stiffness on overconsolidation ratio is seen also at reasonably high values of overconsolidation ratio. The differences in the behaviour of two different soil tested may be caused by their different nature. Speswhite kaolin is a low plasticity clay with a plasticity index of 24 while Boom clay is a plastic clay with a PI of 47.

From these tests on only two clays it is still inconclusive how G_{max} varies with high overconsolidation ratios. For a more complete understanding a comprehensive test programme is needed which would cover a number of soils of different plasticities. These tests indicate that Equation 5.10 should be used with care as for some clays it may significantly overestimate G_{max} at high overconsolidation ratios.

5.6 COMPARISONS BETWEEN G_{max} VALUES MEASURED USING DYNAMIC AND CONTINUOUS LOADING TESTS

The data obtained from the bender element tests will be compared with continuous loading tests on two samples of Speswhite kaolin. In both cases the samples were reconstituted into slurries and then one-dimensionally compressed in the consolidometer to a vertical stress of around 50kPa. After being transferred to the triaxial apparatus the samples were isotropically compressed in stages to 600kPa.

The continuous loading tests, carried out by Coop (1996), consisted of successive undrained shearing probes at increasing initial isotropic stress states. Measurements of very small strains were made using LVDT-s directly attached to the samples (Cuccovillo & Coop, 1997) as described in detail in Chapter 3. The first reliable stiffness data are obtained at about 0.0001% strain. Typically around 500 readings were recorded during the probe. The stiffnesses were calculated using a linear

regression through approximately 15 successive data points on the stresses-strain curve, the strains being averaged from the readings of the two transducers. Fewer points were used in the regression at the start of shearing where the data were sparser. The tangent stiffness was defined as:

$$G = \frac{1}{3}\frac{\delta q}{\delta \varepsilon_a} \qquad 5.12$$

In Fig. 5.14, stiffness-strain data from one of the continuous loading tests are presented along with the stiffness from a bender element test, conducted by the author, at the same value of mean effective stress. A good agreement is seen between the bender element stiffness and the value of the LVDT measured tangent stiffness at the smallest strain level achievable of 0.0001%. From this typical stiffness-strain curve there is no evidence of a region of linear elastic behaviour as the stiffness continuously reduces from the start. It should be noted that this feature of the stress-strain behaviour of normally consolidated Speswhite kaolin was observed in most of the shearing probes. Similar behaviour has been observed for Dogs Bay sand, as already discussed in Section 4.6.2.

The good agreements between the bender element stiffnesses and LVDT tangent stiffnesses at 0.0001% strain are seen at all stress levels in Fig. 5.15, where the variation of G_{max} with p' for normally consolidated states is shown. A similar agreement was also obtained between dynamic and continuous loading tests on a sample of Dogs bay sand as was also shown in Section 4.6.2. As previously discussed, the good agreement of stiffnesses at a strain level of 0.0001% might imply that this is the average strain induced in the soil by the propagating wave originating from the bender elements. A good agreement between the bender element and continuous loading stiffnesses suggests that the inherent anisotropy which was imparted to the soil during the preparation of the sample from slurry was to some extent modified by the isotropic compression so that the resulting anisotropy, up to the points when the probes were conducted, was small.

5.7 SUMMARY

The research on fine grained materials was focused on the anisotropy of G_{max} for both reconstituted and natural clays. The anisotropy of G_{max} was measured using the standard configuration of bender elements fitted into a triaxial apparatus. It was demonstrated that cross-anisotropy of very small strain stiffness can be comprehensively examined in the conventional apparatus using the techniques presented.

From the tests on reconstituted kaolin it was found that the stress induced component of anisotropy is very small for axi-symmetric stress conditions. An examination of empirical correlations and theoretical studies presented in the literature showed that this conclusion should hold for most soils.

The inherent or structural component of anisotropy was found to be much more significant than the stress induced component. It was demonstrated that anisotropic plastic straining is one means by which anisotropy of G_{max} is developed in both Speswhite kaolin and London clay. It is probable that such anisotropy is associated with the development of an anisotropic fabric within the soil. The inherent anisotropy in this case is therefore strain induced.

The degree of anisotropy measured in undisturbed samples of London clay has been reproduced in reconstituted samples. This suggests that the depositional structure is likely to be less influential on the final in situ degree of anisotropy than the strain history of the soil. It was found that continued straining in one particular sense will create a maximum degree of anisotropy appropriate to that anisotropic stress state. It was also found that the strain induced anisotropy is reversible but the rate of change is very slow so that when a new stress regime is imposed the anisotropy of G_{max} persists long after the plastic strain increments of the soil had become appropriate to the new stresses.

Tests on kaolin showed that the variation of G_{max} with state cannot be simply described with a power function of stiffness with overconsolidation ratio as proposed by Viggiani & Atkinson (1995b). The initial increase of G_{max} with overconsolidation ratio does follow a power function description but at higher values of overconsolidation ratio the increase in G_{max} reduces and eventually levels off. In contrast it was found that for the more plastic Boom clay a steady increase in G_{max} with overconsolidation ratio was seen which can be described using a power function regardless of the value of overconsolidation ratio.

From the tests on reconstituted Speswhite kaolin it was found that the dynamic and continuous loading stiffnesses are in good agreement at 0.0001% strain. This was the lowest strain at which stiffness could be determined for continuous loading and implies that the average strain imposed by the bender elements to the soil sample must be equal to, or less than, this value.

CHAPTER 6 THE INFLUENCE OF VERY SMALL STRAIN STIFFNESS ON CALCULATED GROUND MOVEMENTS

6.1 INTRODUCTION

The very small strain shear modulus G_{max} is required for most non-linear soil models. It is generally defined as a member of the isotropic elastic stiffness matrix which relates increments of elastic shear strain to deviatoric stress. For elastically attainable states of stress bounded by a yield surface this stiffness matrix is used for the calculation of elastic strains. As will be explained in detail in the next section, there is no difficulty in incorporating an anisotropic elastic description of the soil response within the yield surface. Changes of stress for states outside the yield surface are accompanied by both plastic and elastic strains. In that case the total strain is calculated as the sum of elastic and plastic strain components where the elastic shear strain is again determined using G_{max}.

Although G_{max} can be measured relatively easily in dynamic laboratory and in situ tests, few attempts (Jardine et al., 1991; Hight & Higgins, 1995) have been made so far to study the importance of this parameter for calculated ground movements. As outlined in Chapter 2 there are few models which describe the most important features of the non-linearity of the stress-strain behaviour of soils. Even though some of the available non-linear models include G_{max} as an input parameter they fail to take into account some other important aspects of the problem so they are not generally appropriate for this study.

The purpose of the research work described in this chapter was to examine the importance of G_{max} and related parameters of elastic soil response in the prediction of ground movements using the 3-SKH model (Stallebrass, 1990b). Numerical analyses were carried out using the finite element program CRISP (Britto & Gunn, 1987). The non-linear soil behaviour was approximated using an incremental method so that the final solution of the boundary value problem represented an integral of the corresponding linear solutions.

The importance of G_{max} for the stiffness response of soil is closely related to the current state of soil in terms of yielding and the stress path mobilised by the current loading conditions. For a stress path that starts inside the yield surface the value of G_{max} fixes the starting point of the stiffness-strain curve and in that way characterises the subsequent mobilisation of the stiffness over the whole range of strain. When a stress path starts away from the yield surface the influence of G_{max} on the deformation behaviour of soil is less pronounced due to the predominance of plastic straining. In this case, as will be shown later, for a particular type of deformation the mobilisation of the elastic stiffness may be also very important.

The dependence of the mobilisation of G_{max} on the stress path direction and the state of the soil in terms of yielding is a concept that is only easily understood for a single element of a soil domain. In real engineering situations the soil surrounding a structure (i.e. the soil domain) is subjected to variety of stress paths which are determined by the loading and boundary conditions. If the response of the soil domain for a particular boundary value problem can be characterised by the response of a single soil element to a single stress path, that stress path will be named the representative stress path. It is possible that for a particular boundary value problem and the deformation pattern of interest the stress path which is representative cannot be found.

The research work on the importance of very small strain stiffness for calculated ground movements was divided into three parametric studies. The first study examined the influence of G_{max} on the mobilisation of soil stiffness in a single soil element for different recent stress histories. This analysis modelled a soil sample under undrained triaxial compression. The other two studies examined the undrained deformation behaviour of a soil domain loaded by a foundation and the deformation caused by the undrained excavation of a tunnel.

The model parameters used throughout the studies were based on the parameters for the 3-SKH model established for London clay by Viggiani & Stallebrass (1994). To perform the parametric studies two parameters used for description of the soil's isotropic elastic response were varied: the absolute value of G_{max} and the size of the yield surface. Additionally the isotropic elastic response was replaced with cross-anisotropic elasticity. This modification of the 3-SKH model which required only one additional parameter is described in detail in the next Section.

Table 6.1 identifies the different sets of parameters used in the analyses. The original set of parameters identified by Viggiani & Stallebrass for London clay assumes an isotropic elastic response and is annotated as material type G45. To create material type G90 the value of G_{max} was doubled while the other parameters remained the same as for G45. Similarly, the size of the innermost yield surface (i.e. parameter TT) was doubled to create artificial material type T08 while the other parameters were kept constant. Finally material A15 was created by using a cross-anisotropic description of elasticity while leaving all the other parameters the same as for the reference material type G45. The parameter α represents the degree of the soil's elastic anisotropy and is set to the value of 1.5 for the cross-anisotropic soil and 1.0 for the isotropic soil. The nature and the magnitude of the parameter α is also discussed in the next section.

6.1.1 Modelling of the cross-anisotropic elastic response of soil

As pointed out by Wood (1995), in modelling soils it is necessary to include both the anisotropy controlled by the history of the soil and an evolving anisotropy which is dependant on the stress and strain changes that the soil subsequently experiences. Like the other kinematic hardening models the 3-SKH model is able to describe the generation of evolving anisotropy. The recent stress history effect upon which the model has been developed and evaluated (Stallebrass & Taylor, 1997) can be interpreted as an effect of evolving anisotropy within the material caused by the plastic straining which occurred during the previous stress path.

As already pointed out in Chapter 4 the anisotropy in terms of very small strain stiffness is an important aspect of soil deformability. There is substantial experimental evidence of its presence (Jamiolkowski et al., 1995) in many natural clays including London Clay (see Section 5.4.2). However, the knowledge of how this aspect of anisotropy affects soil deformability is far from complete. An attempt has, therefore, been made to include an elastic anisotropic response into the 3-SKH model so that both the evolving anisotropy (i.e. the recent stress history effect) and the anisotropy caused by the geological history of the soil (i.e. the inherent anisotropy) are covered. This change of the 3-SKH model relied on the findings presented in Section 5.4.3. It was shown that the rate of change of the degree of G_{max} anisotropy with strain is very slow so that when a new regime of stresses is applied the degree of anisotropy persists long after the total strain increments have become appropriate to the new stress regime. No attempt was made to include the stress induced component of anisotropy since the experimental evidence presented in Section 5.3.2 suggested that this component is very small.

In order to include the inherent anisotropy the model was modified by replacing the isotropic elastic stiffness matrix by a cross-anisotropic stiffness matrix (Equation 2.29). In this way, for the stress states inside the yield surface the soil behaviour is controlled by the inherent anisotropy and is modelled as elastic cross-anisotropic. For the stress states outside the yield surface the soil behaviour is controlled by plastic straining where the evolving anisotropy dominates but the elastic strains are again calculated as cross-anisotropic.

Describing the general features of a cross-anisotropic elastic material Graham & Houlsby (1983) introduced the factor α^2 the ratio of direct stiffnesses in the horizontal and vertical directions as a measure of anisotropy. Using this approach the five parameters commonly used to describe a cross-anisotropic material can be reduced to only three

parameters E^*, ν^* and α by assuming:

$$E_v=E^*, E_h=\alpha^2E^*, \nu_{vh}=\frac{\nu^*}{\alpha}, \nu_{hh}=\nu^*, 2G_{vh}=\frac{\alpha E^*}{(1+\nu^*)} \qquad 6.1$$

which leads to the compliance matrix:

$$\begin{bmatrix}\delta\varepsilon_x\\ \delta\varepsilon_y\\ \delta\varepsilon_z\\ \delta\varepsilon_{yz}\\ \delta\varepsilon_{zx}\\ \delta\varepsilon_{xy}\end{bmatrix} = \begin{bmatrix} \frac{1}{E^*} & -\frac{\nu^*}{\alpha E^*} & -\frac{\nu^*}{\alpha E^*} & 0 & 0 & 0\\ -\frac{\nu^*}{\alpha E^*} & \frac{1}{\alpha^2 E^*} & -\frac{\nu^*}{\alpha^2 E^*} & 0 & 0 & 0\\ -\frac{\nu^*}{\alpha E^*} & -\frac{\nu^*}{\alpha^2 E^*} & \frac{1}{\alpha^2 E^*} & 0 & 0 & 0\\ 0 & 0 & 0 & \frac{1+\nu^*}{\alpha^2 E^*} & 0 & 0\\ 0 & 0 & 0 & 0 & \frac{1+\nu^*}{\alpha E^*} & 0\\ 0 & 0 & 0 & 0 & 0 & \frac{1+\nu^*}{\alpha E^*} \end{bmatrix} \begin{bmatrix}\delta\sigma'_x\\ \delta\sigma'_y\\ \delta\sigma'_z\\ \delta\tau_{yz}\\ \delta\tau_{zx}\\ \delta\tau_{xy}\end{bmatrix} \qquad 6.2$$

where x represents the vertical and y and z the horizontal axes. Directly comparing Equation 2.29 and Equation 6.2 it can be observed that the parameter α corresponds to the ratio of G_{hh}/G_{vh}. Both values of very small strain stiffness, G_{hh} and G_{vh}, can be determined from bender element tests as described in detail in Chapter 5. As mentioned before, in the tests under an isotropic stress state on natural London clay and on reconstituted samples that had previously been one-dimensionally compressed, the value of α was found to be 1.5. This value of α was therefore used throughout these parametric studies (see Table 6.1).

Apart from the degree of anisotropy α, to assemble the stiffness matrix of a cross-anisotropic elastic material it is necessary to determine the two other parameters E^* and ν^*. Graham & Houlsby (1983) showed that the bulk modulus can be expressed in the form:

$$K^*=\frac{E^*}{9(1+\nu^*)(1-2\nu^*)}(1-\nu^*+4\alpha\nu^*+2\alpha^2) \qquad 6.3$$

The bulk modulus defined by the 3-SKH model (Stallebrass, 1990b) is given by:

$$K'=\frac{p'}{\kappa} \qquad 6.4$$

where κ is determined from stress path triaxial tests as the gradient of *the swelling line in the lnv:lnp' plane immediately following a stress* path reversal. Combining equations 6.1, 6.3 and 6.4 it can be shown that:

$$\nu^* = \frac{2(1+2\alpha^2)G_{vh}\kappa - 9\alpha p'}{2(1-4\alpha)G_{vh}\kappa - 18\alpha p'} \qquad 6.5$$

Finally the value of the modified Young modulus E^* is calculated from:

$$E^* = \frac{2G_{vh}(1+\nu^*)}{\alpha} \qquad 6.6$$

In this way by replacing K' with K^*, G with G_{vh} and adding the parameter α, the 3-SKH model was modified to cover cross-anisotropic elastic behaviour. If α is specified as 1.0 the model is reduced to original description of isotropic elasticity. The changes described above have been incorporated into the finite element program. The modification of the model was validated by comparing the results of elastic analyses with the analytical solution provided by Graham & Houlsby (1983).

6.2 PARAMETRIC STUDIES OF SOIL RESPONSE TO UNDRAINED SHEARING

6.2.1 Boundary value problem and method of analyses

Finite element analyses were carried out to investigate the response of a triaxial sample under standard undrained triaxial compression. The geometry of the triaxial sample was modelled as a cylinder 76mm in height and 38mm in diameter. Due to symmetry in both the horizontal and vertical directions only a quarter of the sample has been represented by the axi-symmetric finite element mesh which consisted of cubic strain triangles (Fig. 6.1). No restriction of the boundary of the sample was required so the boundary conditions of the mesh were dictated only by the symmetry of deformation, as presented in the same figure.

The numerical analysis was aimed at investigating the stiffness response during undrained shearing of an overconsolidated soil sample which was previously subjected to two characteristic recent stress histories. Typical stress paths for an overconsolidated soil deposit are shown in Fig. 6.2. The soil was first compressed one-dimensionally and then swelled during erosion (History 1, path 1-2) as illustrated in Fig. 6.2a. The initial direction of the stress path during subsequent undrained compression is indicated by an arrow. The figure also shows the approximate positions of the kinematic surfaces of the 3-SKH model at the end of the swelling stage. In some cases after the swelling stage the soil deposit is re-compressed due to either the deposition of alluvial deposits or underdrainage. The stress paths associated with recompression (History 2, path 1-2-3) and the corresponding position of the kinematic surfaces are illustrated in Fig. 6.2b. The stages of the analyses which

modelled the recent stress histories were carried out drained and under one-dimensional conditions. The maximum vertical effective stress reached was 1050kPa, the soil was then swelled to σ'_v=100kPa and, in the case of History 2 recompressed to σ'_v=200kPa.

For the four characteristic material types G45, G90, T08 and A15 (see Table 6.1) the final stress state at the end of the drained stage was the same so the differences in the mobilised stiffnesses during subsequent undrained shearing were exclusively due to differences in their parameters. Analyses of undrained triaxial compression of a soil sample were carried out by increasing the total axial stress while the radial stress remained unchanged.

6.2.2 Computed mobilised stiffness

The purpose of the parametric study was to compare the computed mobilised stiffnesses for the four characteristic materials which experienced the same recent stress history, either History 1 or History 2. In the case of History 1 the stress path for undrained compression (Fig. 6.2a) will initially traverse the yield surface mobilising an elastic response from the material. In the contrasting case of History 2 (Fig. 6.2b) the undrained compression stress path is always out of the yield surface and the deformation of the material is predominantly plastic. Since only the elastic parameters were varied a greater effect of the change in the parameters on the model behaviour is therefore expected during the initial response which follows History 1.

The results of the analyses of undrained shearing following History 1 are given in Fig. 6.3a. where undrained tangent stiffness is plotted against axial strain. The value of undrained tangent stiffness was defined as:

$$G = \frac{1}{3}\frac{\delta q}{\delta \varepsilon_a} \qquad 6.7$$

where δq is the change in deviatoric stress and $\delta\varepsilon_a$ the change in axial strain. Numerically, the stiffness was calculated as one third of the gradient of a regression line for at least two points of the deviatoric stress plotted against the axial strain. As can be seen on the figure material G90 has the highest initial stiffness of 90MPa while G45 and T08 have initial stiffnesses of 45MPa as was specified as an input to the analyses. Material A15 has a slightly lower initial value of tangent stiffness due to the anisotropic nature of straining. After the stress paths passed the yield surface the computed stiffnesses dropped, the highest change of 100% is seen for T08. Material T08 had an enlarged yield surface so it maintained the elastic stiffness up to a greater threshold strain of ε_a=0.005% while in the case of the other three

materials the threshold strain was 0.002%. After the initial drop, the stiffness decayed slowly with strain for all the materials as the stress path traversed the history surface. The decay of stiffness with strain then increased between 0.01% and 0.1% axial strain as the stress path approached the bounding surface. At 0.1% axial strain all the materials mobilised the same stiffness which indicated the dominance of plastic straining so that the elastic parameters had little influence on the observed behaviour.

Comparing the computed stiffnesses of material G90 with the stiffnesses of reference material G45 it can be observed that the initial difference in stiffness of 100% is reduced to 60% after the initial drop but continues to be significant (around 50%) up to 0.01% mobilised axial strain. As can be seen in Fig. 6.4a, *there is no difference in the* mobilised stress paths between the two materials since the relative positions of the kinematic surfaces are unrelated to the elastic shear modulus.

The difference between the calculated stiffnesses of material T08 when compared to that of reference material G45 can be explained by comparing the corresponding stress paths. In the detailed portion of the graph in Fig. 6.4a it can be seen that material T08 has a prolonged vertical stress path relative to that of G45. This coincides with the wider plateau of elastic stiffness for T08 as shown in Fig. 6.3a. Compared to G45 the subsequent change of the direction of the stress path is more pronounced for T08 due to the proximity of the stress path to the boundary surface. This is seen in the stiffness curve (Fig. 6.3a) as a significantly larger drop in stiffness for material T08 relative to the others. Although this behaviour is reasonably explained in terms of mobilised stress paths it appears that for material T08 the model predicts lower stiffnesses than might be expected. This unusual feature of the model may or may not correspond to the behaviour of real soils, as will be discussed in the next section.

Finally, the mobilised stiffness calculated for the anisotropic material A15 is compared with that of the reference material G45. As shown by Graham & Houlsby (1983), for a cross-anisotropic elastic material with $\alpha>1.0$ the undrained stress path diverges to the left from verticality. This is a result of a coupling between the shear and volumetric strains during undrained shearing and can be seen in detailed portion of Fig. 6.4a. Different stress paths for A15 and G45 cause a different positioning of the surfaces and a lower value of mobilised p' so as can be seen in Fig. 6.3a material A15 consistently mobilised a stiffness about a 20% lower than that of G45. This was evident up to a strain level of 0.1% where the stiffnesses became equal due to the dominance of plastic strain.

In all the analyses of undrained shearing following History 2 a very

small influence of the elastic parameters on the mobilised stiffness was found. This result was anticipated since the mobilised stress path does not traverse the yield surface (Fig. 6.2b) so there is no full mobilisation of the elastic stiffness. The mobilised stress paths are presented in Fig. 6.4b in the same manner as for Fig. 6.4a. From the stiffness data (Fig. 6.3b) it can be observed that all the materials have similar initial values of stiffness ranging between 17MPa and 22MPa. Materials G45 and T08 have identical stiffnesses while G90 remains stiffer by about 5% up to 0.01% axial strain. It is apparent that in the case of material A15 the observed difference in the mobilised stress path had a marginal influence on stiffness.

6.2.3 Discussion

Characteristic stiffness-strain curves predicted by the model take the form presented in Fig. 6.3a whenever the current stress path initially traverses the yield surface. The curves have distinctive features such as the presence of a plateau up to the certain level of the elastic threshold strain and a subsequent abrupt drop in stiffness. For real soils however the elastic plateau is not always observed even though the values of dynamically and statically measured stiffnesses coincide at very small strains. This is seen in the stiffness-strain behaviour of both the Dogs bay sand (Fig. 4.21) and Speswhite kaolin (Fig. 5.14), as already discussed in Chapter 4 and Chapter 5. Both materials have been sheared after isotropic normal compression when, using the terms of the 3-SKH model, the current stress path would not traverse the yield surface and consequently the elastic stiffness should not be mobilised. A possible explanation for this departure of the model from the observed behaviour is that even the small amount of creep which preceded the shearing probes resulted in plastic straining and caused isotropic hardening of the soil. In this way all the kinematic surfaces might have enlarged so that the current stress state ended up inside the yield surface.

The pronounced drop in the stiffness which is seen in the calculated stiffness-strain curves as soon as the yield surface has been traversed (Fig. 6.3a) is a feature of the model which has not been observed in the behaviour of clays. Results from Richardson (1988) shown in Fig. 2.36 and Coop (1996) shown in Fig. 5.14 indicate only smooth stiffness stress-strain curves from shearing probes on London Clay and Speswhite kaolin, respectively. However this feature has been observed for overconsolidated sands, for example in Toyoura sand (Fig. 2.18) or there is an indication of this type of behaviour in the shearing probes on overconsolidated Dogs bay sand (Fig. 4.22).

The parametric study showed that the material with an enlarged yield

surface (i.e. material T08) produced a drop in stiffness of almost 100% percent after the stress path traversed the yield surface and thus mobilised the lowest stiffness of all the characteristic materials. It is unlikely that this unusual feature of the model corresponds to the behaviour of a real soil. This result may also indicate that the choice of an overconsolidated clay with an enlarged yield surface as a characteristic material is unrealistic. A more realistic approach may be to assume that the elastic plateau of the characteristic stiffness-strain backbone curve is very small.

6.2.4 Summary

From the results of the parametric studies of undrained shearing it can be seen that when the stress path traverses the yield surface an increased value of shear modulus produces a stiffer response from the soil model over two logarithmic cycles beyond the threshold elastic strain. An enlarged yield surface initially prolongs the elastic response but the subsequent stiffness after yield is predicted by the model to be relatively low. The effect of elastic anisotropy is reflected in the difference in the undrained stress paths along which a consistently lower stiffness is mobilised when compared with the material with isotropic elasticity. In the case when the undrained stress path is always outside the yield surface there is only a small influence of the elastic parameters on the calculated stiffness.

From the parametric study described above it can be concluded that the influence of the elastic parameters on the calculated soil deformation is critically dependant on the previous stress path. Therefore the influence on soil deformation of the value of elastic shear modulus, the size of the innermost yield surface and elastic anisotropy should be examined relative to the recent stress history of loading of the particular soil.

The parametric study showed that there are some features of the model which are not in the full agreement with the most recent research into the stiffness behaviour of the soils at very small strains. It should be noted that the model has only ever been evaluated for the behaviour of soil at small strains but not the very small strains. However, the recent stress history effect which is the main feature of the model is experimentally based and gives a comprehensive framework for the behaviour of overconsolidated clays.

6.3 PARAMETRIC STUDIES OF THE BEHAVIOUR OF A LOADED FOUNDATION

6.3.1 Boundary value problem and the method of analyses

The parametric study described in this section investigates the influence of the elastic parameters on the modelled behaviour of a rigid foundation. The geometry and ground conditions of the shallow strip footing placed on a deposit of overconsolidated clay are given in Fig. 6.5a. This is not any specific foundation or geological profile but may be regarded as an example of a shallow foundation on a layer of London clay.

The finite element analyses were carried out under the assumption of plane strain deformation. The finite element mesh consisted of 324 linear strain triangles with elements concentrated below the edge of the foundation (Fig. 6.5b). The mesh extended 10m in depth and 20m to one side of the centre line of the foundation. It was restrained horizontally at the sides and fixed at the base to comply with the symmetry of the problem and the geometry of the profile.

All the parametric studies of the vertical loading of the foundation were carried out undrained using the same geometry. The foundation was assumed to be absolutely rigid so the vertical displacement was applied across the footing in stages and the corresponding loading forces were back-calculated. The material parameters were the only variables so that analyses were performed for the four characteristic materials G45, G90, T08 and A15 (see Table 6.1) as described in Section 6.1. The conclusion from the previous study that the influence of the elastic parameters needs to be examined relative to the recent stress history of the loading (see Section 6.2.3) was taken into account, so the analyses of the foundation behaviour were carried out for three different recent stress histories.

The first stage of each analysis was carried out under drained conditions and followed one of three stress histories that might occur to an overconsolidated layer of London clay. The stress paths corresponding to an element at 5m depth for the different stress histories are given in Fig. 6.6a while the corresponding positions of the kinematic surfaces of the 3-SKH model are given in Fig. 6.6b, Fig. 6.6c and Fig. 6.6d. In the case of History E (Fig. 6.6b) after one-dimensional compression, the soil was assumed to have been eroded to a final thickness of 10m with the water table falling during erosion to a depth of 5m below the current ground level. In the two other cases it was assumed that the water table was at ground level after the erosion. History B then consisted of a further fall of the water table after erosion to a depth of 5m causing

recompression of the soil while during History D the water table fell to a depth of 10m and then rose 5m causing recompression followed by swelling. It was also assumed that the soil could develop negative pore pressures which varied linearly with depth. It is important to note that the stress states E, B and D (Fig. 6.6a) have the same vertical effective stress but the stress states in terms of q and p' are different because the values of K_0 are different. The stress histories were chosen such that Histories B and D resulted in a similar distribution of K_0 with depth while Histories E and D lead to similar initial positions of the kinematic surfaces relative to the future loading path i.e. similar recent stress histories.

An investigation of the consequences of modelling the effect of recent stress history on the behaviour of the rigid foundation of the same geometry and ground conditions as used in this study has been completed by Stallebrass et al., (1995b) and will not be repeated here. In this Section are presented parametric studies for the four characteristic materials (see Table 6.1) for each recent stress history. Any difference in their deformation behaviour for a given stress history should be attributed only to the difference in their parameters.

6.3.2 Load-settlement response

The characteristic load-settlement behaviour of a foundation was compared for all four characteristic materials. In all the analyses a similar pattern of deformation of the settlement trough was observed so the comparison was focused on the mobilisation of foundation load for a wide range of settlements. The characteristic load-settlement curves had all similar hyperbolic shapes such as those seen in Fig. 6.10b. The direct comparison between the behaviour of materials G90 and G45 for histories E,B and D is shown in Fig. 6.7 where the ratio of mobilised foundation loads F_{G90}/F_{G45} is plotted against the settlement. The dependence of the ratio on the settlement is of the same shape for all histories. It can be seen that the influence of the higher elastic shear modulus is most pronounced at low values of settlement. In order to mobilise a settlement of 0.1mm (around 0.001% strain) material G90 has to be loaded with a 40-60% larger force than G45. As the settlement progresses the difference in the foundation loads for a given settlement reduces. It levels off at larger settlements taking a final value of about 20% at a settlement of 10mm which corresponds to around 1% strain.

The effect of increased elastic stiffness on the load-settlement behaviour is very pronounced only at small values of settlement where it is directly related to the particular recent stress history. The initial loading force mobilised at small settlements after Histories E and D (Fig. 6.6) which were similar to History 1 for the undrained

triaxial test (Fig. 6.2a) are 50% higher than the loading force after History B which was similar to History 2 (Fig. 6.2a). This corresponds to the response in terms of mobilised stiffness of the triaxial sample under undrained triaxial compression which followed either Histories 1 and 2 (see Section 6.2.2). The undrained stress paths following History E for the element 1 (Fig. 6.5) are given in Fig. 6.8. These stress paths are of almost identical shape to the stress paths computed for a triaxial sample under undrained shearing following History 1 (Fig. 6.4a). Their similarity is a product of similar recent stress histories and as a consequence there is also similarity in the stiffness response of the two boundary value problems. This leads to the conclusion that undrained compression may be regarded as a representative stress path for the boundary value problem of a loaded foundation.

The comparison between the behaviour of materials T08 and G45 is again presented as the ratio of foundation loads plotted against settlement (Fig. 6.9). It can be observed that for all stress histories the enlarged yield surface contributes positively to the mobilised load ($F_{T08}/F_{G45}>1$) only at very small settlements i.e. up to about 0.2mm. As the settlement progresses the model predicts a low stiffness for material T08 so that the ratio F_{T08}/F_{G45} reduces to less than 1 at small displacements and remains below 1 until larger settlements. Again, similar results have been obtained from the parametric study of the behaviour of the triaxial sample under undrained triaxial compression (see Fig. 6.3a), which were discussed in Section 6.2.3.

The results of the comparative study of the behaviour of the anisotropic material A15 and reference material G45 are given only for History E. The results for the other two stress Histories B and D gave similar results but the effect of elastic anisotropy was less pronounced. The ratio between the loads F_{A15}/F_{G45} is plotted against settlement in Fig. 6.10a. It can be observed that the initial mobilised load for material A15 was only 60% of that for G45. As the settlement increased the contribution of plastic straining to the total strain became dominant so that the difference between the loads decreased and finally levelled off at about 80% at a settlement of 10mm. The shape of the stress path for element 1 (Fig. 6.8) which is regarded as representative for the boundary value problem indicates that the anisotropic material failed to mobilise the elastic stiffness since the stress path diverted from the vertical so that the yield surface was not traversed. Again this significant difference in the response of the two materials can be explained only in terms of coupling between shear and volumetric strains and its influence on mobilised stiffness.

The different responses of the materials with isotropic and anisotropic descriptions of elasticity are examined here in more detail. In Fig. 6.10b the foundation loads F_{A15} and F_{G45} are plotted separately against

settlement. The difference in settlement for the same value of foundation load ranges from 80% at small strains to 30% at large strains. For the example of a foundation load of 200KN it can be observed that material A15 mobilised a maximum settlement of 3.7mm while G45 mobilised a maximum settlement of 2.2mm.

The settlement profiles for the same mobilised force of 200KN are given in Fig. 6.11a while the settlement profiles for the same mobilised settlement of 10mm are given in Fig. 6.11b. It can be seen that the shape of the settlement profile at the same settlement appears to be almost unaffected by elastic cross-anisotropy. This can be explained by the fact that the vertical axis is the axis of symmetry of the cross-anisotropic material and that plane strain deformation is assumed. This means that there is no straining in the plane normal to the plane of the boundary value problem which is the plane of higher stiffness for the anisotropic material. As a consequence the whole effect of elastic cross-anisotropy is seen in a decrease in the overall stiffness but not in changes in the pattern of deformation.

The analyses predict the increased settlement for an anisotropic material due to a relatively small change in the stress path direction which is probably a result of the model being very sensitive to the stress path changes. The change of the direction of the stress path seen in the analysis conforms to the current theoretical and experimental evidence but although the overall effect of anisotropy is reasonably predicted by the model, it is the opinion of the author that the effect is probably less pronounced in the behaviour of real soils.

6.3.3 Summary

From the analyses of the undrained load-settlement behaviour of the shallow foundation it can be concluded that the representative stress path is similar to the stress path of a triaxial sample under standard undrained triaxial compression. At very small strains the recent stress history effect dominates the stiffness response of the material and consequently dominates the effect of the elastic stiffness on the deformation behaviour.

The results of the parametric study suggest that the value of the elastic shear modulus has a significant influence on the settlement of the foundation. For an increase in the value of the elastic shear modulus by a factor of two the mobilised loading force is around 50% higher for a given settlement in the range of small strains. The same effect is observed at larger settlements but is less pronounced levelling off at about a 20% difference. An enlarged size of the yield surface contributes to the stiffer response only at very small strains while at larger

strains the model tends to predict a lower stiffness response. A cross-anisotropic description of elastic stiffness leads to a lower mobilised loading force which at small strains reached a minimum of 60% of the mobilised loading force of the isotopic material. For this boundary value problem the effect of elastic cross-anisotropy was seen only in the mobilisation of stiffness but not in the pattern of deformation.

6.4 PARAMETRIC STUDIES OF GROUND MOVEMENTS AROUND A TUNNEL

6.4.1 Boundary value problem and method of analysis

The ground conditions and tunnel geometry used in the analysis correspond to the geometry of a typical tunnel in London Clay (Fig. 6.12a). The tunnel was 4m in diameter with its axis 34m below ground level while the water table was at a depth of 11m. Due to the effect of underdrainage which exists in London Clay the distribution of pore pressure was modelled as sub-hydrostatic, the pore pressure increased linearly up to 190kPa at 30m and then stayed constant with depth. It was also assumed that the soil could develop negative pore pressures which varied linearly with depth having a value of -110kPa at the surface.

The analyses were carried out assuming plane strain deformation and symmetry about the vertical axis of the tunnel. The finite element mesh (Fig. 6.12b) consisted of approximately 350 linear strain triangles extending 60m in depth and 120m to one side of the tunnel centre line. The mesh was restrained at the sides and fixed on the base, thus simulating the interface between the clay layer and a rigid strata. The mesh was sufficiently wide for the movements in the far field to be negligible.

The soil stratum in which the excavation of the tunnel was modelled had the properties of each of the four characteristic materials (see Table 6.1). The in situ stress state of the soil layer was modelled as that which resulted from the overconsolidation caused by the erosion of overlying deposits. In these analyses it was assumed that maximum effective vertical stress had been 1000kPa while erosion resulted in a reduction of the effective vertical stress of either 670kPa (History DTI1), 710kPa (History DTI2) or 780kPa (History DTI4). While for History DTI1 this point represented the in situ state for DTI2 and DTI4 the recent stress history consisted of subsequent re-deposition of a stratum such as Brickearth or a change in the water table. This was modelled as an increase in the vertical stress by 40kPa and 110kPa for histories DTI2 and DTI4, respectively. All histories resulted in the same final vertical effective stress σ'_v but with different horizontal effective stresses σ'_h. The difference in K_0 was however less then 5% at the excavation level and

was considered negligible. The difference between the histories was seen, in terms of the 3-SKH model, only in the different initial positioning of yield surfaces. History DTI1 was very similar to History 1 (Fig. 6.2a) while Histories DTI2 and DTI4 were very similar to History 2 (Fig. 6.2b).

The first stages of the analyses were carried out as drained one-dimensional compression and swelling. The excavation of the tunnel was carried out undrained and was simulated by replacing the elements in the tunnel by an equivalent overburden pressure which was then reduced in stages up to a total of 40% (Simpson el al., 1996).

The influence of the recent stress history on the ground movements around the tunnel of the same geometry and boundary condition was examined in detail by Stallebrass et al., (1995a). In this parametric study the response of four characteristic materials G45, G90, T08 and A15 was analyzed for the same particular recent stress history. Therefore the difference in the response for a given stress history should be attributed exclusively to the difference in the material parameters.

6.4.2 Computed surface settlement profiles

The calculated volume loss developed by the reduction of the overburden pressure has been compared for all four characteristic materials and all recent stress histories. This approach in presenting the results is analogous to the observation of the load-deflection behaviour of a loaded foundation presented in previous Section. In Fig. 6.13 where the volume loss is plotted against the percentage reduction in overburden pressure it can be seen that there is almost no difference between the results even though the recent stress histories were different. This feature contrasts with the results of the parametric study of a loaded foundation (see Section 6.3.2). For all recent stress histories material G90 gives around a 20% stiffer response than material G45, a difference that also remained constant with the reduction of overburden pressure i.e. with the level of mobilised strain. As was observed in the other studies the stiffness of material T08 is predicted by the model to be low so it gives around a 30% higher volume loss than material G45 for the same reduced overburden pressure. For the material with an anisotropic elastic response, A15, almost no difference could be observed from the behaviour of material G45. This feature is also in contrast to the result of the parametric study of a loaded foundation.

The contrast in the results of the analyses of the boundary value problem of a tunnel with that of a foundation can be explained in terms of the influence of the different recent stress histories on the mobilised stiffness and using the concept of a representative stress path. In the case of the foundation there is a representative stress path which is

similar to the stress paths relevant to the load-deflection behaviour and which are developed within soil domain. In that case the initial position of the surfaces (i.e. the recent stress history effect) determines whether the very small strain stiffness is fully mobilised or not which is then the behaviour that is predominant for the whole domain. In the case of the tunnel the relationship between volume loss and reduction in overburden pressure is dependant on the stress path response of all elements around the tunnel which are all different and therefore regardless of the recent stress history the same proportion of the soil will mobilise similar stiffnesses. Consequently a representative stress path cannot be distinguished for the boundary value problem of a tunnel due to the nature of the loading.

Settlement profiles for all histories and for all four characteristic materials are given in Fig. 6.14. It was shown by Stallebrass et al., (1995a) that the calculated settlement profiles are highly dependant on the recent stress history effect and this feature may also be seen by comparing Figures 6.14a,b and c. For histories DTI2 and DTI4 the variation of settlement with distance from the centre line is fairly similar for all four materials. Only for History DTI1 do the values of settlement above the crown differ substantially but this results from the arching effect predicted by the model and the absolute values of displacement are very small. Generally, material G90 gives a stiffer response, T08 gives a weaker response and A15 gives an almost identical response to the reference material G45.

Although large differences cannot be seen in terms of absolute values of the settlements an important difference is observed in their distribution along the surface profile. When the settlements for materials G90 and G45 for the recent stress history DTI4 are compared (Fig. 6.14c) it can be seen that material G90 produced maximum settlement which is 15% higher than that of G45 even though the volume loss for material G90 was 20% less than that of G45. This result shows that the absolute value of G_{max} can give rise to subtle but important deformation features within the domain which are relevant to the particular boundary value problem.

A common method of analyses of settlement induced by tunnelling is to fit a Gaussian distribution curve to the field surface settlement measurements (Peck, 1969). The Gaussian curve has a general form of:

$$S = S_{max} \exp\left(-\frac{x^2}{2i^2}\right) \qquad 6.8$$

where S_{max} is the maximum settlement at the centre line of the tunnel, S is the settlement at a horizontal distance x from the tunnel centre line and i is the value of x at the point of inflection of the curve. In Figure 6.15 the normalised surface settlement profiles for materials G90 and G45 are compared to a normalised Gaussian distribution. For the

Gaussian curve a value of i has been chosen to be equal to half the depth of the tunnel axis (i.e. i=0.5z), as suggested by O'Reilly & New (1982) for London Clay. It can be seen that both curves resemble the Gaussian distribution but have more distant points of inflection. The best fit of Gaussian curve for material G90 gives i=0.75z while for material G45 i=1.15z which is about 65% higher. This result indicates that under-estimation of G_{max} might produce a serious under-estimation of differential settlements calculated for the structures above the tunnel during the excavation.

6.4.3 Summary

The parametric study showed that mobilisation of the small strain stiffness is unrelated to the recent stress history effect for the volume loss caused by the excavation of a tunnel in stiff clay. This is attributed to the fact that the representative stress path cannot be distinguished for this particular boundary value problem since all the relevant stress paths of the elements surrounding a tunnel cavity are different. From the relationship between volume loss and the reduction of overburden pressure it was found that the material with the value of G_{max} which was twice that the reference material gave around a 20% stiffer response while the material with an enlarged yield surface gave around a 30% weaker response. The material with an anisotropic elastic response showed almost no difference in behaviour to that observed for the isotropic reference material.

It was found that for the particular stress history DTI4 the accurate evaluation of G_{max} is important since it controls the shape of the settlement trough. The material with the higher value of G_{max} gives rise to a 65% percent greater inclination of the settlement trough, a difference which may be critical for the differential settlements calculated for the structures above the tunnel.

6.5 DISCUSSION

The attempt to examine the influence of the very small strain shear modulus on calculated ground movements had a limited scope. It consisted of finite element predictions made using the 3-SKH model (Stallebrass, 1990b). The parametric studies were based on model parameters determined for London Clay and a more detailed approach should consider a variety of modelled soils. The limitation of modelling the behaviour of an overconsolidated clay resulted from the fact that the 3-SKH model had only been evaluated for this type of soil. Further limitation is that the

model was evaluated for the small strain behaviour and not for the very small strains. The conclusions which follow are, therefore, constrained by the limitations of the study listed above. However, they are based on the predictions of the model which has a comprehensive description of a soil behaviour so their validity to the behaviour of real soils should be judged accordingly for both the limitations and assets of the model itself.

Parametric studies were carried out for undrained soil conditions where the tendency of the soil to dilate or compress is seen through the generation of excess pore pressures which then determine the shape of the effective stress path. Undrained analyses were therefore chosen since the effects are easier to visualize in terms of mobilised stress paths. A more complete study should also include drained behaviour. However the conclusions drawn from these parametric studies are based on soil behaviour in terms of effective stresses and they give an indication of soil deformation behaviour regardless of drainage conditions.

The analysis of a deformation behaviour of a triaxial sample under undrained triaxial compression showed that for a single element of soil the value of G_{max} determines the magnitude of the recent stress history effect. It was found that the same was true for the other related parameters of soil stiffness at very small strains which were the size of the of the yield surface and the anisotropy of the elastic response. For all currently non-yielding soils the value of G_{max} was found to be critical for the whole range of mobilised strain. In contrast, for soils which are yielding the mobilised stiffness was almost unrelated to the value of G_{max}.

The parametric study showed that the conclusions drawn above for a triaxial test were also valid for the understanding of the influence of small strain stiffness on the load-deflection behaviour of a loaded foundation. In this case the boundary and loading conditions were such that a stress path which is similar to the majority of the mobilised stress paths in the soil can be distinguished and in this case this was similar to that for the undrained triaxial test. This stress path is then representative for the load deflection behaviour of a foundation and is easily associated with the recent stress history of the soil. The latter determines the influence of G_{max} on the soil deformation so that the very small strain stiffness has a large influence on the observed behaviour. This conclusion is likely to be valid for any boundary value problem where the loading and boundary conditions are not symmetric, such as *foundations*, retaining walls or embankments.

Analyses of the ground movements around the tunnel showed that when there is no representative stress path the effect of G_{max} on the overall deformation behaviour cannot be related to the recent stress history

effect and the variation of the very small strain stiffness properties of the soil are then less important for the overall behaviour. It is likely that the same conclusion can be extrapolated to similar boundary value problems which involve excavation with some form of symmetry of loading conditions relative to the soil domain. In contrast to this conclusion, the effect of the stiffness at very small strains can be very important for the pattern of deformation which is of interest. It was demonstrated for a deep tunnel that the absolute value of G_{max} was particularly relevant to the shape of calculated settlement trough.

The analyses showed that the importance of G_{max} for the deformation behaviour of soil should be assessed only allowing for its interaction with other factors relevant to the non-linearity of the soil stress-strain response. In particular, the practical significance of G_{max} should be related to the recent stress history effect. The importance of G_{max} for overall deformation will also closely depend on the geometry of the boundary value problem which dictates the directions of the mobilised stress paths and thus affects the deformation behaviour of the soil.

CHAPTER 7 SUMMARY AND CONCLUSIONS

7.1 EXPERIMENTAL TECHNIQUES

The measurement of stiffness at very small strains, G_{max}, was carried out using the bender element measurement technique (Section 3.4). The original design of the bender element system in the triaxial apparatus of the Norwegian Geotechnical Institute was improved to reduce the electrical noise which hampered the measurement of the arrival time of the shear wave. The shielding of the cables leading from the elements to the instrumentation resulted in a significant improvement of the quality of the received signal.

Theoretical and numerical studies have been carried out to develop objective criteria for the determination of G_{max} using the bender element method (Sections 3.4.2. and 3.4.3). The corruptive interference of near field waves on the true shear wave has been identified and several techniques of measurement have been suggested to overcome the problem (Section 3.4.4). These techniques, which are based on an understanding and recognition of the main features of the received trace allow a direct measurement of the arrival time from the oscilloscope to be made routinely to an accuracy of ±1%.

The determination of soil stiffness was also carried out using continuous loading of the sample in the triaxial apparatus covering the range of very small to small strains. The continuous loading tests were carried out in a Bishop & Wesley stress path cell equipped with LVDT-s for the local measurement of axial strains (Section 3.2.1) and state of the art equipment for signal conditioning. It was shown that, when correctly used, LVDT-s allow a sufficiently accurate measurement of axial strains as to give the possibility of making a direct comparison between bender element and continuous loading stiffnesses. A good agreement in the comparison between the stiffnesses obtained by the two means was found at 0.0001% strain for both Dogs Bay sand and Speswhite kaolin (Sections 4.6.2 and 5.5.2)

7.2 THE STIFFNESS OF COARSE GRAINED SOILS AT VERY SMALL AND SMALL STRAINS

Three sands with very different geological origins (Section 4.2) were tested over a range of stresses of 0.5 to 70MPa to investigate the influence that confining stress and volumetric state have on stiffness at very small strains, G_{max}. High pressures were used in the triaxial apparatus (Section 3.2.2) to bring the samples to the reference state of isotropic normal compression at which the measurements of G_{max} were

carried out using bender elements. By means of correct normalisation of the data (Section 4.4.4) the stiffnesses at other states were compared to those at the reference state and a new general framework for stiffness has been established. Within the framework unique relationships have been derived for each soil which demonstrate that the confining stress and volumetric state relative to the normal compression line are principal controlling factors for G_{max} (Fig. 4.15).

The framework also demonstrates the importance of the means by which sands arrive at their current stress-volume state for the values of G_{max}, i.e. whether the means is by geological overconsolidation or compaction during the depositional process. Between these benchmarks a zone of possible stiffnesses for all combinations of overconsolidation and compaction has been identified. Within the framework the stiffness of a cemented sand has been compared to that of the destructured material (Section 4.5.2) and effects of the bonding have been highlighted. A limitation of the framework is that it does not include the influence of creep and aging (Section 4.3) on stiffness, topics which have been beyond the scope of the research.

By using LVDTs for the local measurement of axial strains the stiffness response of Dogs Bay sand under continuous loading was investigated. Tangent stiffnesses at 0.0001% strain agreed well with bender element stiffnesses and little evidence of an elastic plateau on the stiffness backbone curve has been found for undrained shearing. When plotted against the mean effective stress, the tangent stiffnesses for first loaded samples at any particular strain level are found to form sub-parallel lines which converge towards higher stresses in the same manner as was found for clays by Viggiani & Atkinson (1995b). The framework was also used to interpret the tangent stiffnesses of samples which were unloaded prior to reaching the normal compression line. The capacity of the apparatus did not allow the true overconsolidation of the samples but the influence that volumetric state has on stiffness has been again highlighted as the stiffnesses at any particular strain level increased with the distance of the volumetric state from the normal compression line.

7.3 ANISOTROPY OF G_{max} IN FINE GRAINED SOIL

Both natural and reconstituted clays were tested up to high stresses using a standard configuration of bender elements in the triaxial apparatus (Fig. 3.1). The tests were designed to examine the stress induced and inherent components of anisotropy in terms of G_{max} (Sections 5.3.2 and 5.4.4) which are associated with axi-symmetric stress states and a cross-anisotropic soil fabric, respectively.

The stress induced anisotropy of Speswhite kaolin for axi-symmetric loading conditions has been found to be very small and an examination of theoretical and empirical studies in the literature showed that this should hold for most soils. From the tests on both reconstituted kaolin and reconstituted London clay it was demonstrated that anisotropic plastic straining can give rise to an inherent anisotropy of G_{max}, which therefore can be said to be strain induced in these two cases.

Natural London clay has been shown to be cross-anisotropic with a relatively high degree of G_{max} anisotropy. The same degree of anisotropy was reproduced in the reconstituted samples of London clay by anisotropic straining thus suggesting that the degree of inherent anisotropy of the natural soil results predominantly from the strain history. In consequence, it appears that the structure of London clay at deposition is likely to be less influential on the degree of anisotropy than the strain history of the soil. The development of the inherent anisotropy was found to be a reversible process, but the rate of change was very slow. That is, when an isotropic stress regime was applied the degree of G_{max} anisotropy persisted long after the plastic strain increments became isotropic.

7.4 THE INFLUENCE OF G_{max} ON CALCULATED GROUND MOVEMENTS

Finite element analyses have been carried out using the 3-SKH model (Stallebrass, 1990b) (Section 2.6.2) to examine the influence of G_{max} and related parameters on calculated ground movements. Parametric studies of the stress-strain behaviour of a triaxial sample under undrained triaxial compression, the load-deflection behaviour of a foundation and the ground movements around a tunnel were carried out for different recent stress histories and different elastic parameters of the modelled material. The anisotropy of G_{max} was also included in the studies and the necessary changes were incorporated in both the model and computer program.

The limitations of the analyses (Section 6.5) are reflected in the fact that only one model has been used which is, in addition, validated only for the small strain behaviour of overconsolidated clays and not for very small strains. However, the predictions of the model highlighted some aspects of the importance of G_{max} on ground movements which are likely to be relevant for the behaviour of real soils. It was found that the influence of G_{max} on deformation behaviour can be significant but this conclusion depends also on the interaction of other factors which control the non-linear response of the soil, in particular its recent stress history and the geometry of the boundary value problem.

7.5 IMPLICATIONS OF THE RESEARCH

The modifications of the design of the bender elements which took place in the early stage of the project improving the quality of the received signal (Section 3.4.1) have already been copied by various laboratories both in this country and abroad. In addition, the incorporation of bender elements into high pressure cells, the successful use of bender elements to test cemented sands and the development of techniques for the interpretation of bender element tests should all contribute to the usefulness of the method. In particular, the objectivity of the criteria established for the determination of G_{max} and the increased simplicity of the measurement technique will make bender elements more attractive for wider use in industry.

The new framework developed for the stiffness of reconstituted sands (Section 4.4.4) emphasises both the influence of the confining stress and that of volumetric state on the small strain behaviour. The framework is based on the behaviour of three sands with very different geological origins, mineralogies, gradings and nature of particles and so is likely to be generally applicable. High pressure testing was necessary to develop a complete understanding but it should be emphasised that the framework is appropriate for all stress levels and covers all combinations of overconsolidation and compaction which can bring the soil to its current stress-volume state. In the light of the above the framework offers a basis for future improvements in the constitutive modelling of sands. Although the work on the stiffness response to continuous loading (Section 4.6) covers only some combinations of recent stress path rotations it gives valuable data with which non-linear constitutive models for sand could be validated. A particular feature of the framework is that it highlights the importance of the means of arriving at the initial stress-volume state. Therefore, the evaluation of design parameters for sands should distinguish between soils which have undergone either geological overconsolidation or have achieved the current density only by means of compaction during the depositional process. The framework also highlights the importance of micro-mechanical parameters for the characterization of the nature of sands and it has been discussed which of those parameters are likely to be relevant to G_{max}.

The work on fine grained materials highlights some aspects of the influence of anisotropic stress states and anisotropic fabric on G_{max}. The axi-symmetric stress state, which is common to both triaxial tests and the in situ stresses of many natural deposits was found to cause little stress induced anisotropy of G_{max} in the vertical plane. The inherent component of anisotropy was found to be a variable factor associated predominantly with the strain history of the deposit. The rate of change

of the degree of anisotropy with strain was found, however, to be very small. The fact that G_{max} anisotropy persists, when a new regime of stresses is applied, long after the plastic strain increments in the soil have become appropriate to the new stress regime is also of interest to constitutive modelling of the behaviour of clays. This finding initiated changes of the 3-SKH model to accommodate an anisotropic elastic stiffness matrix in its elastic-plastic description of soil behaviour (Section 6.1.1).

The implications of the research related to the finite element analyses are limited by the fact that only one model has been used which is, in addition, validated only for the small strain and not very small strain behaviour of overconsolidated clays. However, the results of the parametric studies gave an insight into importance that G_{max} might have on the calculated ground movements which is likely to be valid for the understanding of the behaviour of real soils.

7.6 LIMITATIONS OF THE RESEARCH AND RECOMMENDATIONS FOR FUTURE WORK

As previously discussed, no attempt has been made to investigate the influence of creep and aging on G_{max} in sands (Section 4.3). The research programme was designed to avoid these effects and the new framework includes only the influence of confining stress and volumetric state on stiffness. For a complete understanding of all the effects which influence G_{max} in sands a new research programme is needed which will focus on the effects of creep and aging and their relationships to the framework proposed. The instrumentation for such a programme could be the same as described here and, for the sake of consistency, the same sands could be used.

The tests which examined the stress-strain behaviour during continuous loading (Section 4.6.1) were carried out in a Bishop & Wesley cell which had instrumentation built for the purpose of accurate measurements of stresses and very small strains. Due to the low capacity of the cell of 700kPa even the loosest samples of Dogs Bay sand could not reach the normal compression line at the maximum pressure. In consequence, the stress-strain behaviour examined corresponded to the first loading of compacted samples in their loosest state possible and not strictly to normally consolidated sand. For the same reason the behaviour of the unloaded samples did not correspond strictly to the behaviour of a truly overconsolidated sample. In order to bring samples of Dogs Bay sand to the reference state of normal compression, high pressures are needed, so the state of the art instrumentation for the accurate measurement of very small and small strains should in future be fitted in the 5MPa cell in which the bender elements are already in place. Using the improved 5MPa

triaxial apparatus the small strain behaviour of sand under continuous loading could then be examined in more detail covering both normally consolidated and truly overconsolidated samples.

It is important to emphasise that the research related to the stress-strain behaviour of sands was carried out only for certain stress path rotations (Section 4.4.4). For a more complete understanding, the response for a range of stress paths rotations should be examined so that the effect of the recent stress history can be evaluated as has previously been done for clays. The Bishop & Wesley cell with the instrumentation built during this research, along with a high pressure cell of similar capabilities would be appropriate equipment for the research.

The importance of a less descriptive and more objective characterization of the nature of coarse grained materials also arose from the research work on sands. The micro-mechanical considerations of inter-particle contacts which are very important in the variation of G_{max} with the stress and volumetric state have, so far, only been based on very simple theoretical and numerical simulations of the complex mechanics which appear at a different scale from that in which we can measure and quantify soil behaviour. Numerical simulations will look more promising only when the computational power of current machines enters a new generation.

The work on the anisotropy of G_{max} was limited by the standard configuration of only one pair of bender elements (Section 5.1) which was fitted into the triaxial cell. A true triaxial cell with the pairs of bender elements at each side of the cube would be the most effective apparatus in examining different aspects of this topic. In terms of materials tested the work was restricted to only two clays. More detailed research would require the incorporation of bender elements into a true triaxial apparatus and use of several different reconstituted and natural clays covering a wide range of plasticities.

The limitations of the finite element analyses which examined the influence of G_{max} on calculated ground movements (Section 6.5) were numerous since they used only the 3-SKH model (Stallebrass, 1990b) which was, in addition, validated only for the small strain behaviour of overconsolidated clays. Future work should include the validation of the 3-SKH model in the region of very small strains which would require a combination of laboratory and numerical work. In general, more detailed research of the influence of G_{max} on calculated ground movements should include different constitutive models and different modelled soils.

APPENDIX

A solution for the three-dimensional transmission of spherical waves through an infinite isotropic elastic medium was obtained by Sanches-Salinero et al. (1986). The notation in a Cartesian coordinate system is illustrated in Fig. A3.1. The excitation motion of the source point located at the origin is in the X direction and is given in an exponentional form of a complex number $e^{i\omega t}$ where t is the time and ω the angular velocity. The monitoring point of transverse (shear) motion is located at a distance *d* from the source in the Y direction.

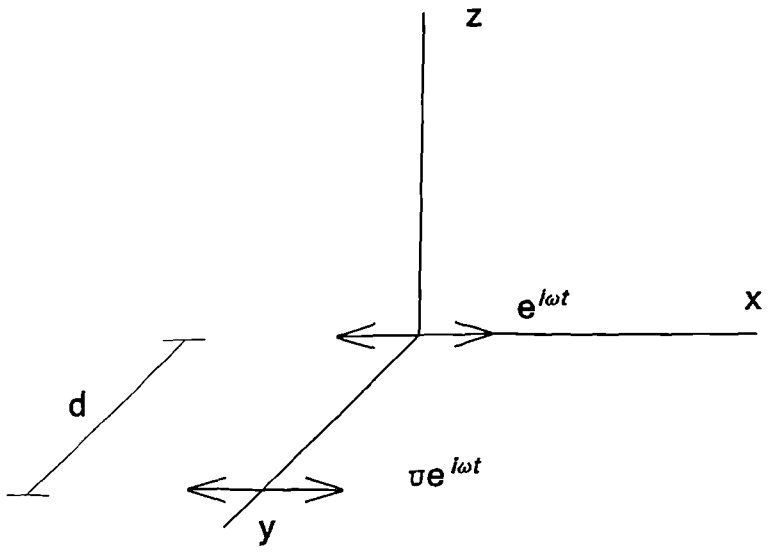

Fig. A3.1 Notation for three-dimensional motion of points

The set of formulae which define the motion is given in Equations A3.1 where λ_w is the wavelength, f is the frequency and T_p is the period.

$$\lambda_w = \frac{V_s}{f}, \quad f = \frac{\omega}{2\pi} = \frac{1}{T_p} \qquad \text{A3.1}$$

The fundamental solution for the transverse motion U caused by a unit concentrated harmonic force (Sanches-Salinero at al., 1986) is given in the form:

$$U = \frac{1}{4\pi\rho V_s^2}\Gamma_a \qquad \text{A3.2}$$

where v_s is the velocity of shear wave, v_p is the velocity of the compression waves, ρ is the density of the medium and the function Γ_a is given as:

$$\Gamma_a = \frac{1}{d} e^{-i\frac{\omega d}{v_s}} + \left(\frac{1}{i\frac{\omega d^2}{v_p}} - \frac{1}{\frac{\omega^2 d^3}{v_p^2}}\right) e^{-i\frac{\omega d}{v_s}} - \left(\frac{v_s}{v_p}\right)^2 \left(\frac{1}{i\frac{\omega d^2}{v_p}} - \frac{1}{\frac{\omega^2 d^3}{v_p^2}}\right) e^{-i\frac{\omega d}{v_p}} \qquad \text{A3.3}$$

The motion U is given per unit force while the velocities v_s and v_p are defined as complex variables which include a hysteretic damping ratio. The function Γ_a can be broken into three parts Γ_1, Γ_2 and Γ_3 shown in Equation A3.4, as discussed in the text.

$$\Gamma_a = \overbrace{\Gamma_1}^{\text{shear wave}} + \overbrace{\Gamma_2 - \Gamma_3}^{\text{compression wave}} \qquad \text{A3.4}$$

Γ_1: far field term; $\Gamma_2 - \Gamma_3$: near field term

REFERENCES

Abbiss, C.P., (1981). Shear wave measurements of the elasticity of the ground, Geotechnique, Vol. 31, No. 1, pp. 91.104.

Ackerly, S.K., Helling, J.E., Jardine, R.J., (1987). Discussion on: A new device for measuring local axial strain on triaxial specimens by Clayton, C.R.I and Khathrush, S.A., Geotechnique, Vol. 33, No. 4, pp. 445-451.

Agah S. (1996). Personal communication

Agarwal, T.K., and Ishibashi, I. (1991). Multi-directional wave velocity by piezoelectric crystals. Proc. Recent advances in instrumentation, data acquisition and testing in soil dynamics. ASCE, Orlando, Florida, pp. 102-117.

Alawaji, H., Alawi, M., Ko, H.Y., Sture, S., Peters, J.F. and Wood, D.M. (1990). Experimental observations of anisotropy in some stress-controlled tests on dry sand. Proc. Yielding, damage and failure of anisotropic solids. London: Mech. Eng. Public., pp. 251-264.

Al-Tabbaa, A. (1987). Permeability and stress-strain response of Speswhite kaolin. PhD Thesis, University of Cambridge.

Al-Tabbaa, A., and Wood, D.M., (1989). An experimentally based "bubble" model for clay. Proc. NUMOG III, Elsevier Applied Sci., pp. 91-99.

Anandarajah, A. and Kuganenthira, N., (1995). Some aspects of fabric anisotropy of soil. Geotechnique., Vol. 45, No. 1, pp. 69-81.

Anderson, D.G., Stokoe, K.H., (1978). Shear modulus: a time dependant soil property. Dynamic Geotech. Testing, ASTM STP 654, pp. 66-90.

Arnold, M. (1996). Personal communication

Arthur, J.R.F. and Menzies B.K., (1972). Inherent anisotropy in a sand. Geotechnique, Vol. 22, No. 1, pp. 115-128.

Arthur, J.R.F., Chua, K.S., Dunstan, T. (1977). Induced anisotropy in a sand. Geotechnique, Vol. 27, No. 1, pp. 13-30.

Atkinson, J.H., (1973). The deformation of undisturbed London Clay. PhD Thesis, University of London.

Atkinson, J.H. and Bransby, P.L. (1978). The Mechanics of Soils. McGraw-Hill, London.

Atkinson, J.H. , Evans, J.S., Scott, C.R., (1985). Developments in stress path equipment for measurements of soil parameters. Ground Engineering, Vol. 18, No. 1, 15-22.

Atkinson, J.H. and Evans, J.S. (1985). Discussion on: The measurement of soils stiffness in the triaxial apparatus by Jardine, R.J, Symes, N.J. and Burland, J.B. Geotechnique, Vol. 35, No. 3, pp. 378-382.

Atkinson, J.H., Richardson, D. and Stallebrass S.E., (1990). Effect of recent stress history on the stiffness of overconsolidated soil. Geotechnique, Vol. 40, No. 4, pp. 531-540.

Atkinson, J.H and Sallfors, G. (1991). Experimental determination of soil properties. Proc. X ECSMFE, Florence, Vol. 3, pp. 915-956.

Atkinson, J.H and Stallebrass, S.E., (1991). A model for recent history and non-linearity in the stress-strain behaviour. Proc. Computer methods and advances in Geomechanics. Cairns, pp. 555-560.

Balasubramanian, A.S. (1976). Local strains and displacement patterns in triaxial specimens of a saturated clay. Soils and Foundations, Vol. 16, No. 1, pp. 101-114.

Baldi, G., Hight, D.W. and Tomas, G.E. (1988). A reevaluation of conventional triaxial test methods. Advanced triaxial testing of soil and soft rock (eds R.T. Donaghe, R.C. Chaney and M.L. Silver) ASTM, STP 977, pp. 219-263.

Been, K. and Jefferies, M.G (1985). A state parameter for sands. Geotechnique, Vol. 35, No. 1, pp. 99-112.

Been, K., Jefferies, M.G. and Hachey, J. (1991). The critical state of sands. Geotechnique, Vol. 41, No. 3, pp. 365-381.

Bellotti, R., Jamiolkowski, M., Lo Presti, D.C.F., and O'Neil, D.A. (1996). Anisotropy of small strain stiffness in Ticino sand. Geotechnique, Vol. 46, No. 1, pp. 115-131.

Bishop, A.W., and Henkel, D.J. (1962). The measurement of soil properties in the triaxial test. Edward Arnold (2nd edition), London.

Bishop, A.W., Wesley, L.D., (1975). A hydraulic triaxial apparatus for controlled stress path testing. Geotechnique, Vol. 25, No. 4, pp. 657-670.

Biot, M.A., (1956). Theory of propagation of elastic waves in a fluid saturated porous solid. I and II. Journ. of the Acoustical Soc. of America, Vol. 28. No. 2.

Bolton, M.D. and Wilson, J.M.R. (1989). An experimental and theoretical comparison between static and dynamic torsional shear tests. Geotechnique, Vol. 39, No. 4, pp. 585-599.

Bolton, M.D., Desari, G.R. and Ng. C.W.W. (1995). Discussion. Inter. Symp. on Pre-Failure deformation characteristics of geomaterials, IS-Hokkaido, Saporo. Vol. 2, pp. 1108-1111.

Brignoli, E., and Gotti, M. (1992). Misure della velocita di onde elastichi di taglio in laboratorio con l'impiego di traduttori piezoeletrici. Riv. Ital Geotec., Vol. 26, No. 1, pp. 5-16.

Brignoli, E., Gotti, M. and Stokoe, K.H. (1997). Measurement of shear waves in laboratory specimens by means of piezoelectric transducers. Geotech. Testing Journ. ASTM. To be published.

Britto, A.M. and Gunn, M.J. (1987). Critical state soil mechanics via finite elements. Ellis Horwood Ltd., Chichester, UK

Brown, R.J.S. (1980). Connection between formation factor for electrical resistivity and fluid-solid coupling factor in Biot's equations for acoustic waves in fluid-filled porous media. Geophysics 45, pp. 1269-1289.

Brown. S.F and Snaith, M.S (1974). The measurement of recoverable and irrecoverable deformation in the repeated load triaxial test. Geotechnique, Vol. 24, No. 2, pp. 255-259.

Burland, J.B. and Symes, M.J.R.P. (1982). A simple displacement gauge for use in the triaxial apparatus. Geotechnique, Vol. 32, No. 1, pp. 62-64.

Burland, J.B. (1989). The Ninth Bjerrum Mem. Lecture: Small is beautiful - the stiffness of soils at small strains. Can. Geotech. Journ., Vol. 26, pp. 499-516.

Burland, J.B. (1990). On the compressibility and shear strength of natural clays. 30th Rankine Lecture, Geotechnique, Vol. 40. No. 3., pp. 329-378.

Butcher, A.P, and Powell, J.M.M (1995). The effects of geological history on the dynamic stiffness in soils. Proc. XI ECSMFE. Copenhagen, Vol. 1 , pp. 27-36.

Chandler. H.W.(1985). A plasticity theory without Drucker's postulate suitable for granular materials. Journ. of Mech. Phys. of Solids, Vol. 33, pp. 215-226.

Cherrill, H.E., (1990). Rates of loading in the triaxial test. PhD Thesis. The City University.

Clayton, C.R.I., and Khathrush, S.A., (1986). A new device for measuring local axial strains on triaxial specimens. Geotechnique, Vol. 36., No. 4., pp. 593-597.

Clayton, C.R.I., Khathrush, S.A., Bica, A.V.D., Siddique, A., (1988). The use of Hall effect semiconductors in geotechnical instrumentation. Geotechnical Testing Journ., Vol. 12, No. 1, pp. 69-76.

Coop, M.R. (1990). The mechanics of uncemented carbonate sands. Geotechnique, Vol. 40, No. 4, pp. 607-626.

Coop, M.R. and Lee, I.K. (1993). The behaviour of granular soils at elevated stresses. Proc. Wroth memorial Symposium: Predictive soil mechanics, Thomas Telford, London, pp. 186-198.

Coop, M.R. and Lee, I.K. (1995). The influence of pore water on the mechanics of granular soils. Proc. XI ECSMFE. Copenhagen, Vol. 1, pp. 63-73.

Coop, M.R., Atkinson, J.H. and Taylor, R.N. (1995). Strength and stiffness of structured and unstructured soils. Proc. XI ECSMFE. Copenhagen, Vol. 1. pp. 54-63.

Coop, M.R. & Cotecchia, F. (1995). The compression of sediments at the archaeological site of Siberi. Proc. XI ECSMFE. Copenhagen, Vol. 8. pp. 19-27.

Coop, M.R. (1996). Personal communication

Costa Filho, L.M. and Vaughan, P.R. (1980). Discussion on: A computer model for the behaviour of London clay by Simpson, B., O'Riordan, N.J. and Croft, D.D. Geotechnique, Vol. 30, No. 3, pp. 336-339.

Costa Filho. L.M., (1985). Measurement of axial strains in triaxial tests on London Clay. ASTM, Geotechnical testing Journ., Vol. 8, No. 1, pp. 3-13.

Cuccovillo, T. (1995). Shear behaviour and stiffness of naturally cemented sands. PhD Thesis, The City University.

Cuccovillo, T. and Coop, M.R. (1997). The measurement of local axial strains in triaxial tests using LVDT's. Geotechnique. To be published.

Dafalias, Y.F., and Popov, E.P. (1977). Cyclic loading for materials with a vanishing elastic region. Nuclear Eng. and Design., Vol. 41, No. 2, pp. 293-302.

Dobry, R., and Vucetic, M. (1987). State-of-the-art report: Dynamic properties and response of soft clay deposits. Proc. Int. Symp. on Geotech. Eng. of Soft Soils, Vol. 2, pp. 51-87.

Dobry, R., Ng, T.T. and Petrakis, E. (1989). Deformation characteristics of granular soils in the light of particulate mechanics. Atti delle conferenze di geotecniche di Torino, Politecnico di Torino, Vol. 3, pp. 1-34.

Drnevich, V.P. (1972). Undrained cyclic shear of saturated sand. Journ. of Soil Mech. and Found. Div., ASCE, Vol. 98, No. SM8, pp. 807-825.

Drnevich, V.P. (1978). Resonant column. - problems and solutions. Proc. Dynamic Geotech. Testing. ASTM., STP 654, pp. 384-398.

Duffy, J. and Mindlin, R.D. (1957). Stress-strain relations and vibrations of a granular medium. Journ. of Appl. Mech. Trans., ASME, Vol. 24, pp. 585-593.

Duncan, J.M. and Chang, C.Y (1970). Non-linear analyses of stress and strain in soils. ASCE. Journ. of the Soil Mech. and Found. Eng. Div., Vol. 96, SM5, pp. 1629-1653.

Duncan, J.M. and Chang, C.Y (1972). Discussion on : Non-linear analyses of stress and strain in soils by Duncan and Chang ASCE. Journ. of the Soil Mech. amd Found. Eng. Div., Vol. 98., SM5, pp. 867-871.

Dyvik, R. and Madshus, C., (1985). Laboratory measurements of G_{max} using bender elements. Proc. ASCE Annual convention: Advances in the art of testing soils under cyclic conditions. Detroit, Michigan, pp. 186-197.

Evans, K.M. (1987). A model study of the end bearing capacity of piles in layered carbonate soils. PhD Thesis, Oxford University.

Fioravante, V., Capoferri, Hameury, O., and Jamiolkowski, M. (1995). Deformation characteristics of uncemented carbonate Quiou sand. Proc. Inter. Symp. on Pre-Failure deformation characteristics of geomaterials., IS-Hokkaido, Saporo, Vol. 1, pp. 55-63.

Gajo, A. (1995). The influence of viscous coupling in the propagation of elastic waves in saturated soil. Journ. Geotech. Eng. Div. ASCE. Vol. 121, No. 9, pp. 636-644.

Gajo, A. (1996). The effects of inertial coupling in the interpretation of dynamic soil tests. Geotechnique, Vol. 46, No. 2, pp. 245-259.

Geological Society (1990). Tropical residual soils. Engineering Group working party report. Q. Journ. Eng. Geol. 23, No. 1., pp. 1-101.

Georgiannou, V.N., Rampello, S. and Silvestri, F., (1991). Static and dynamic measurement of undrained stiffness of natural overconsolidated clays. Proc. X ECSMFE, Florence. Vol. 1, pp. 91-96.

Gohl, W.B. and Finn, W.D.L. (1991). Use of piezoceramic bender elements in soil dynamics testing. Proc. Recent advances in instrumentation, data acquisition and testing in soil dynamics. ASCE, Orlando, Florida, pp. 118-132.

Golitghtly, C.R. and Hyde, A.F.L. (1988). Some fundamental properties of carbonate soils. Proc. Int. Conf. Calcareous Sediments, Perth, Vol. 1, pp. 69-78.

Goto, S., Tatsuoka, F., Shibuya, S., Kim, Y.S. and Sato, T., (1991). A simple gauge for local small strain measurements in laboratory. Soils and Foundations, Vol. 31, No. 1. pp. 169-180.

Graham, J. and Houlsby, G.T., (1983). Anisotropic elasticity of natural clay. Geotechnique, Vol. 33, No. 2, pp. 165-180.

Graham, J., Noonan,M.L. and Lew, K.V. (1983). Yield states and stress-strain relationships in a natural plastic clay. Can. Geotech. Journ., Vol. 20, No. 3, pp. 502-516.

Graham, J. and Li, E.C.C. (1985). Comparison of natural and remoulded plastic clay. Journ. Geotech. and Eng. Div., ASCE, Vol. 111, No GT7, pp. 865-881.

Gunn, M. (1993). The prediction of surface settlement profiles due to tunnelling. Proc. of the Wroth memorial Symposium: Predictive soil mechanics. Thomas Telford, London, pp. 304-316.

Hashiguchi, K. (1985). Two and three surface models of plasticity. Proc. V Int. Conf. on Numerical Methods in Geomech., Nagoya, pp. 285-292.

Hardin, B.O. and Richart, F.E. (1963). Elastic wave velocities in granular soils. Journ. of Soil Mech. and Found. Div., No. SM1, pp. 33-65.

Hardin, B.O. and Black, W.L. (1966). Sand stiffness under various triaxial stresses. Journ. of Soil Mech. and Found. Div., ASCE, No. SM2, pp. 27-42.

Hardin, B.O. and Black, W.L. (1968). Vibration modulus of normally consolidated clay. Journ. of Soil Mech. and Found. Div., ASCE, No. SM2, pp. 353-369.

Hardin, B.O. and Black, W.L. (1969). Closure to: Vibration modulus of normally consolidated clay. Journ. of Soil Mech. and Found. Div., ASCE, No. SM3, pp. 1531-1537.

Hardin, B.O. and Drnevich, V.P., (1972). Shear modulus and damping in soils. Measurement and parameter effects. Journ. of Geotech. Eng. Div., ASCE, Vol. 102, No. GT9, pp. 975-978.

Hardin, B.O. (1978). The nature of stress-strain behaviour for soils. Proc. Geotech. Div. Spec. Conf. on Earthquake Eng. and Soil Dynamics., ASCE, Pasadena, Vol. 1, pp. 3-90.

Hardin, B.O. (1985). Crushing of soil particles. Journ. of Geotech. Eng., Vol. 111, No. 10, pp. 1177-1192.

Hardin, B.O. and Blandford, G.E. (1989). Elasticity of particulate materials. Journ. of Geotech. Eng., Vol. 115, No. 6, pp. 788-805.

Hight, D.W. and Higgins, K.G. (1995). An approach to the prediction of ground movements in engineering practice: background and application. Proc. Intern. Symp. on pre-failure deformation characteristics of geomaterials., IS-Hokkaido, Saporo, Vol. 2, pp. 909-947.

Hird, C.C. and Yung, P., (1987). Discussion on: A new device for measuring local axial strain on triaxial specimens by Clayton, C.R.I and Kathrush, S.A., Geotechnique, Vol. 37, No. 3, pp. 413-414.

Hird, C.C. and Yung, P., (1989). The use of proximity transducers for local strain measurements in triaxial tests. Geotech. Testing Journ. Vol. 12, No. 4, pp. 119-133.

Houlsby, G.T., Evans, K.M. and Sweeney, M. (1988). End bearing capacity of model piles in layered carbonate soils. Proc. Int. Conf. on Calcareous Sediments. Perth, Austraila, Vol. 1., pp. 209-214.

Houlsby, G.T. and Wroth, C.P., (1991). The variation of shear modulus of a clay with pressure and overconsolidation ratio. Soils and Foundations, Vol. 31, No. 3, pp. 138-148.

Hryciw, R.D. and Thomann, T.G., (1993). Stress-history based model for G^e of cohesionless soils. Journ. of Geotech. Eng., ASCE, Vol. 119, No. 7, pp. 1073-1093.

Isenhower, W.M. (1979). Torsional simple shear/resonant column properties of San Francisco bay mud. MSc Thesis, University of Texas, Austin.

Isenhower, W.M. and Stokoe, K.H., (1981). Strain rate dependant shear modulus of San Francisco bay mud. Proc. Int. Conf. on Recent Advances in Geotech. Earthquake Eng. and Soil Dynamics, St Luis, Vol. 2, pp. 597-602.

Iwasaki, T., Tatsuoka, F. and Takagi, Y. (1978). Shear moduli of sands under cyclic torsional shear loading. Soils and Foundations, Vol. 18, No. 1, pp. 39-56.

Jamiolkowski, M., Lancellotta, R. and Lo Presti, D.C.F. (1995). Remarks on the stiffness at small strains of six Italian clays. Proc. Intern. Symp. on pre-failure deformation characteristics of geomaterials, IS-Hokkaido, Saporo, Vol. 2, pp. 817-837.

Jardine, R.J., Symes. M.J.R.P. and Burland, J.B. (1984). The measurement of soil stiffness in the triaxial apparatus. Geotechnique, Vol. 34, No. 3, pp. 323-340.

Jardine, R.J., Fourie, A., Maswoswe, J. and Burland J.B. (1985). Field and laboratory measurement of stiffness. Proc. XI Inter. Conf. on Soil Mech. and Found. Eng., San Francisco, Vol. 2, pp. 511-514.

Jardine, R.J. (1985). Investigations of pile-soil behaviour with special reference to the foundation of offshore structures. PhD Thesis, University of London.

Jardine, R.J., Potts, D.M., D.M., Fourie, A.B. and Burland, J.B. (1986). Studies of the influence of non-linear stress-strain characteristics in soil-structure interaction, Geotechnique, Vol. 36, No. 3, pp. 377-396.

Jardine, R.J., Potts, D.M., St.John, H.D. and Hight, D.W., (1991). Some practical applications of a non-linear ground model. Proc. X ECSMFE, Florence, Vol. 1, pp. 223-228.

Jefferies, M.G. (1993). Nor-Sand: a simple critical state model for sand. Geotechnique, Vol. 43, No. 1, pp. 91-103.

Kirkpatrick W.M. and Younger, J.S. (1970). Strain conditions in a compression cylinder. Journ. of the Soil Mech. and Found. Eng. Div., ASCE Vol. 96, No. SM5, pp. 1683-1695.

Kirkpatrick W.M. and Rennie I.A. (1972). Directional properties of consolidated kaolin, Geotechnique, Vol. 22, No. 1, pp. 166-169.

Knox, D.P., Stokoe, K.H., Kopperman, S.E., (1982). Effects of state of stress on velocity of Low amplitude shear wave propagating along principal stress directions in dry sand. Geotech. Eng. Research Rep., GR 82-83. University of Texas at Austin.

Ko, H.Y & Scot, R.F. (1967). Deformation of sand in hydrostatic compression. Journ. of Soil Mech. and Found. Div. ASCE, Vol. 93, No. SM3, pp. 137-156

Lade, P.V. and Nelson, R.B. (1987). Modelling the elastic behaviour of granular materials., Int. Journ. for Numeric. and Analytic. Meth. in Geomech., Vol. 11, pp. 521-542.

Lau, W.H.W. (1988). The behaviour of clay in simple shear and triaxial tests. PhD Thesis, The City University.

Lawrence, F.V. (1963). Propagation of ultrasonic waves through sand. MIT Research report, R 63-08.

Lee, S.H. and Stokoe, K.H. (1986). Investigation of low amplitude shear wave velocity in anisotropic material. Report GR 86-6. University of Texas at Austin.

Lee, I.K., (1991). Mechanical Behaviour of Compacted Decomposed Granite Soil. PhD Thesis, The City University.

Lee, I.K. and Coop, M.R. (1995). The intrinsic behaviour of a decomposed granite soil. Geotechnique, Vol. 45, No. 1, pp. 117-130.

Leroueil, S. and Vaughan, P.R. (1990). The general and congruent effects of structure in natural soils and weak rocks. Geotechnique, Vol. 40, No. 3, pp. 467-488.

Little, J.A., Atkinson, J.H., (1988). One dimensional consolidation characteristics of a glacial till. Q. Journ. of Eng. Geology, Vol. 21, No. 1, pp. 183-199.

Love, A.E.H., (1927). A treatise on the Mathematical theory of elasticity, Cambridge University press.

Lo Presti, D.C.F (1995). General Report: Measurement of shear deformation of geomaterials in the laboratory. Inter. Symp. on Pre-Failure deformation characteristics of geomaterials., IS-Hokkaido, Saporo. Vol. 2, pp. 1067-1088.

Mindlin, R.D., Mason, W.P., Osmer, T.F. and Deresiewcz, H. (1951). Effects on oscillating tangential force on the contact surfaces of elastic spheres. Proc. I US Nationa. Cong. of Applied Mech., pp. 203-208.

Mitchell, J.K. (1976). Fundamentals of Soil Behaviour. John Wiley & Sons. New York.

Mroz, Z., Norris, V.A. and Zienkiewicz, O.C., (1979). Application of an anisotropic hardening model in the analyses of elasto-plastic deformation of soils. Geotechnique, Vol. 29, No. 1, pp. 1-34.

Mroz, Z., Norris, V.A. and Zienkiewicz, O.C., (1981). An anisotropic hardening model for soils and its application to cyclic loading. Int. Journ. Num. Anal. and Math. Meth. in Geomechanics, Vol. 2, pp. 203-221.

Mroz, Z., and Norris, V.A. (1982). Elastoplastic and viscoplastic constitutive models for soils with application to cyclic loading in Pande, G.N. and Zienkiewicz, O.C. (Ed). Soils Mechanics - Transient and Cyclic loads. John Wiley and Sons. London.

Nakagawa K., Soga, K. and Mitchell, J.K. (1996). Pulse transmission system for measuring wave propagation in soil. Journ. of Geotech. Eng., ASCE, Vol. 122, No. 4, pp. 302-308.

Oda, M. (1981). Anisotropic strength of cohesionless sands. Journ. of Geotech. Eng. Div. ASCE, Vol. 107, No. GT9, pp. 1219-1232.

O' Reilly, M.P. and New, B.M. (1982). Settlements above tunnels in the United Kingdom - their magnitude and prediction. Tunnelling' 82. Ed. Jones, M.J., IMM., London, pp. 173-181.

Pane, V. and Burghignoli, A. (1988). Determizione in laboratorio delle cratteristiche dinamiche dell'argilla del Fucino. In Atti del I Convegno del Grup. Naz. di Ing. Geotec. Monselice, Italy, pp. 115-140.

Park, C.S. and Tatsuoka, F. (1994). Anisotropic strength and deformation of sands in plane strain compression. Proc. XIII ICSMFE, New Delhi, Vol. 1, pp. 1-6.

Papa, V., Silvestri, F. and Vinale, F., (1989). Cyclic/dynamic simple shear tests: recent developments. Proc. XII ICSMFE, Rio de Janeiro, Vol. 2, pp. 345-347.

Peck, R.B. (1969). Deep excavations and tunnelling in soft ground. Proc. 7th. Int. Conf. Soil Mech. and Found. Div., Mexico, Vol. 3, pp. 225-290.

Pennigton, D. (1996). Personal Communication

Porovic, E. and Jardine, R.J. (1995). Some observations on the static and dynamic shear stiffness of Ham River sand. Proc. Intern. Symp. on pre-failure deformation characteristics of geomaterials., IS-Hokkaido, Saporo, Vol. 1, pp. 25-31.

Porovic, E. (1995). Investigation of soil behaviour using a resonant column torsional shear hollow cylinder apparatus. PhD Thesis. University of London.

Rampello, S., Viggiani, G. and Georgiannou, V.N. (1993). Strength and dilatancy of natural and reconstituted Vallericca clay. Proc. Int. Symp. on Geotech. Eng. of Hard Soils - Soft Rocks, Athens, Vol. 1, pp. 761-778.

Rampello, S., Silvestri, F., Viggiani, G. (1995a). The dependence of small strain stiffness on stress state and history for fine grained soils: the example of Vallericca clay. Proc. International Symposium on pre-failure deformation characteristics of geomaterials., IS-Hokkaido, Saporo, Vol. 1, pp. 273-279.

Rampello, S., Silvestri, F., Viggiani, G. (1995b). Panellist discussion: The dependence of G_0 on stress state and history in cohesive soils. Proc. International Symposium on pre-failure deformation characteristics of geomaterials, IS-Hokkaido, Saporo, Vol. 2. pp. 1155-1160.

Richart, F.E., Hall, J.R. and Woods, R.D., (1970). Vibrations of soils and foundations. Prentice Hall Inc., New Jersey.

Richardson, D. (1988). Investigation of threshold effects in soil deformations. PhD Thesis, The City university

Roesler, S.K. (1979). Anisotropic shear modulus due to stress anisotropy. Journ. of Geotech. Eng., ASCE, No. 105(7), pp. 871-880.

Roscoe, K.H., Burland, J.B., (1968). On the generalised stress-strain behaviour of "wet" clay. Engineering Plasticity, Cambridge University Press.

Rothenburg, L. and Bathurst, R.J. (1989). Analytical study of induced anisotropy in idealised granular materials. Geotechnique, Vol. 39, No. 4., pp. 601-614.

Rowe, P.W., (1971). Theoretical meaning and observed values of deformation parameters for soils. Proc. Roscoe Memorial Symp. on stress-strain behaviour of soils. pp. 143-194.

Sanches-Salinero, I., Roesset. J.M., Stokoe, K.H., (1986). Analytical studies of body wave propagation and attenuation. Report GR 86-15, University of Texas, Austin.

Schmertman, J.H. (1991). The mechanical aging of soils. The twenty-fifth Karl Terzaghi Lecture. Journ. of Geotech. Eng., Vol. 117, No. 9, pp. 1288-1330.

Schofield, A.N. and Wroth, C.P., (1968). Critical State Soil Mechanics, McGraw-Hill, London.

Scholey, G.K., Frost, J.D., Lo Presti, D.C.F., Jamiolkowski, M. (1995). A review of instrumentation for measuring small strains during triaxial testing of soil specimens. Geotech. Testing Journ., Vol. 18, No. 2, pp. 135-156.

Schulteiss, P.J., (1982). Influence of packing structure on seismic wave velocities in sediments. Ph.D. Thesis. University College of North Wales.

Shirley, D.J. and Hampton, L.D., (1997). Shear-wave measurements in laboratory sediments. Journ. of Acous. Soc. of America, Vol. 63, No. 2, pp. 607-613.

Simpson, B., O'Riordan, N.J. and Croft, D.D. (1979). A computer model for the behaviour of London clay. Geotechnique, Vol. 29, No. 2, pp. 149-177.

Simpson, B., (1992). Thirty second Rankine Lecture: Retaining structures: displacement and design. Geotechnique, Vol. 42, No. 4, pp. 539-577.

Simpson, B., Atkinson J.H., and Jovičić V., (1996). The influence of anisotropy on calculations of ground settlements above tunnels. Proc. Geotechnical Aspects of Underground Construction in Soft Ground, The City University, London, pp. 591-595.

Simić, M. (1996). Personal communication

Skempton, A.W. (1954). The pore-pressure coefficients A and B. Geotechnique, Vol. 4, pp. 143-147.

Skinner, A.E., (1975). The effect of high water pressures on the mechanical behaviour of sediments. PhD Thesis. University of London.

Smith, P.R., Jardine, R.J., and Hight, D.W. (1992). The yielding of Bothkennar clay. Geotechnique, Vol. 42, No. 2, pp. 257-274.

Stallebrass, S.E. (1990a). Stress path tests on undisturbed London clay using local axial strain gauges. GERC report GE/90/22. City University. London.

Stallebrass, S.E (1990b). Modelling the effect of recent stress history on the deformation of overconsolidated soils. PhD Thesis. The City University.

Stallebrass, S.E., Jovičić, V., Taylor, R.N. (1994). Short and long term settlements around a tunnel in stiff clay. Proc. Numer. Meth. in Geotech. Eng., Manchester, pp. 235-240.

Stallebrass, S.E., Jovičić, V., Taylor, R.N. (1995a). The influence of recent stress history on ground movements around tunnels. Proc. Inter. Symp. on Pre-Failure deformation characteristics of geomaterials, IS-Hokkaido, Saporo, Vol. 1, pp. 615-621.

Stallebrass, S.E., Jovičić, V., Atkinson, J.H. (1995b). Influence of geological history on foundation behaviour. Proc. XI ECSMFE, Copenhagen, Vol. 1, pp. 265-272.

Stallebrass S.E., Taylor R.N., (1997). The development and evaluation of a constitutive model for the prediction of ground movements in overconsolidated clay. To be published in Geotechnique.

StJohn, H.J. (1975). Field and theoretical studies of the behaviour of ground around deep excavation in London clay. PhD thesis, University of Cambridge.

Stokoe, K.H.I., Lee, S.H.H. and Knox, D.P. (1985). Shear moduli measurement under true triaxial stresses. Proc. Advances in the Art of Testing Soils Under Cycling Loading Conditions, ASCE Convention, Detroit. pp. 134-142.

Stokoe, K.H., Hwang, S.K., Lee, J.N.K. and Andrus, R.D. (1995). Effects of various parameters on the stiffness and damping of soils at small to medium strains. Proc. Inter. Symp. on Pre-Failure deformation characteristics of geomaterials, IS-Hokkaido, Saporo, Vol. 2, pp. 785-817.

Tavenas, F. and Leroueil, S. (1987). Laboratory and in situ stress-strain-time behaviour of soft clays: a state-of-the-art. Int. Symp. on Geotech. Eng. of Soft soil, Mexico City, pp. 1-46.

Tatsuoka, F., Iwasaki, T., Fukushima, S., Sudo, H., (1979). Stress conditions and stress history affecting shear modulus and damping of sand under cyclic loading. Soils and Foundation, Vol. 19, No. 2, pp. 29-43.

Tatsuoka, F. (1988). Some recent developments in triaxial testing systems for cohesionless soils. Proc. Advanced triaxial testing of soil and rock., ASTM, STP 977, pp. 7-67.

Tatsuoka, F., and Shibuya, S. (1992). Deformation characteristics of soils and rocks from field and laboratory tests. Rep. of the Institute of Industrial Science, The University of Tokyo, Vol. 37, No. 1.

Tatsuoka, F., and Kohata, Y. (1995). Stiffness of hard soils and soft rocks in engineering applications. Proc. Inter. Symp. on Pre-Failure deformation characteristics of geomaterials, IS-Hokkaido, Saporo, Vol. 2, pp. 947-1067.

Taylor R.N. and Coop M.R., (1990). Stress path testing of Boom clay from Mol, Belgium., Proc. 26th Annual Conf. of the Eng. Group of the Geological Soc., Leeds., pp. 89-98.

Timoshenko, S.P., Goodier, J.N., (1951). Theory of elasticity. McGraw-Hill. New York.

Viggiani, G. (1992). Small strain stiffness of fine grained soils, PhD Thesis, The City University.

Viggiani, G. and Stallebrass, S.E., (1994). Shear test data for reconstituted London clay. GERC Report. GE/94/04

Viggiani, G. and Atkinson, J.H. (1995a). The interpretation of the bender element tests. Geotechnique 45, No. 1, pp. 149-155.

Viggiani, G. and Atkinson, J.H. (1995b). Stiffness of fine grained soils at very small strains. Geotechnique 45, No. 2, pp. 249-255.

Vogler, U.W. and Kovari, K. (1978). Suggested methods for determining the strength of rock materials in triaxial compression. Int. Journ. Rock Mech. Min. Sci. Geomech. Abstr. 15, No. 2, pp. 47-51.

Webb, D.L. (1967). The mechanical properties of undisturbed samples of London clay and Pierre shale. PhD Thesis, University of London.

Weiler, W.A., (1988). Small strain shear modulus of clay. Proc. Geot. Eng. Div. Speciality Conf. om Earthquake Eng. and Soil Dynamics., II ASCE. Park City. Utah. pp. 331-345.

Wood, D.M. (1990). Soil behaviour and critical state soil mechanics. Cambridge University Press.

Wood, D.M. (1995). General report: Evaluation of material properties. Proc. Inter. Symp. on Pre-Failure deformation characteristics of geomaterials, IS-Hokkaido, Saporo. Vol. 2, pp. 1179-1199.

Wood, D.M., (1975). Extrapolations of principal stress space with kaolin in a true triaxial apparatus. Geotechnique, Vol. 25, No. 4, pp. 783-797.

Wroth, C.P. (1971). Some aspects of the elastic behaviour of overconsolidated clay. Proc. Roscoe Memorial Symp., Foulis, pp. 347-361.

Wroth, C.P., Randolph, M.F., Houlsby, G.T. & Fahey, M. (1979). A review of engineering properties of soils with particular reference to the shear modulus. OUEL Report 1523/84, University of Oxford.

Wroth, C.P. and Houlsby, G.T., (1985). Soil mechanics, Property characterisation and analysis procedure. Proc. XI ICSMFE. San Francisco, pp. 1-55.

Zytynski, M., Randolph, M.F., Nova R. and Wroth C.P. (1978). On modelling the unloading-reloading behaviour of soils., Int. Journ. for Numeric. and Analytic. Meth. in Geomech., Vol. 2, pp. 87-93.

Parameter	Contacting								Noncontacting	
					Inclinometer Gage					
	X-Ray	Video Tracking	LVDT	Flexible-Strip Radial-Strain Caliper	Electrolevel	Pendulum Gage	Hall Effect Gage	Local Deformation Transducer	Proximity Transducer	Cylindrical Capacitance Device
Direction of measurement	Axial, radial	Axial, radial	Axial, radial	Radial	Axial	Axial	Axial, radial	Axial	Axial, radial	Radial
Operating principle	Discrete X-ray images of deformation of lead-shot grid	Tracking of tracer particles, digital imaging	Inductance	Foil strain gages measure flexible strip deformation	Deformation causes tilt of electrolevel	Strain-gaged pendulum	Hall-effect semiconducting sensor	Bending strain in elastic metal strip	Eddy-current loss principle	Capacitance between two cylindrical capacitors
Output characteristics	X-ray images	Digitized images	Linear	Linear	Nonlinear	Nonlinear	Linear over limited range	Nonlinear	Linear	Non-linear
Commercial availability	No	No	LVDTs-yes	No	Yes	Yes	Yes	No	Yes	No
Relative cost	High	High	Moderate	Not known	Low	Low	Low	Low	Moderate	Moderate
Resolution	Poor	Poor	±0.0001–0.001%	±0.005%	±0.001%	±0.0005%	±0.002%	±0.0001%	2.5×10^{-4} mm (R)	±0.01%
Range	Pre-failure	Pre-failure?	Limited by core-body fracture/ misalignment	Not Known	35%	Post Failure	1.5 mm (R) 2.5 – 7 mm (A)	±1.5 mm	Limited 2.5 mm (R)	Not Known
Accuracy	±0.1–0.2 mm	1%		Not Known	±0.002%			±0.0001%		Not Known
Specimen restrictions	Reconstituted	Reconstituted	None	Stiffer than flexible strip	None	None	None	None	None	Not Known
Cell fluid restrictions	Consider X-ray retardation		Nonconductor	None	None	None	None	None	Not water	Good dielectric properties
Temperature stability	—	—	Stable	Compensated	±3°C	±3°C	Compensated	Compensated	Compensated	±3°C
Pressure stability	—	—	Stable	Not known	Stable	Stable	Stable	Not Known	Stable	Calibration required
Primary publications	Many	Marcus et al.	Many	Holubec & Finn El-Rawaylh	Burland & Symes Jardine et al.	Ackerly et al.	Clayton et al.	Tatsuoka Goto et al.	Many	Mishu
Year introduced	1960s	1993	1970s	1969, 1976	1982, 1984	1987	1986	1988, 1991	1970s	1966
Applications	Research	Research	Research and commercial	Probably redundant	Research and Commercial	Research and Commercial	Research and Commercial	Research and Commercial	Research and Commercial	Research

Table 2.1 Techniques used for the measurement of axial strains inside the triaxial cell (after Scholey et al. 1995)

Table 1. Summary of critical state parameters

Soil	N	Γ	λ	κ	M	ϕ'_{cs}
Dogs Bay Sand	4.80	4.35	0.34	0.008	1.65	40°
Decomposed Granite	2.17	2.04	0.09	0.005	1.59	39°
Ham River Sand	3.17	2.99	0.16	0.014	1.28	32°

Table 2.2 Summary of the critical state parameters for three sands after Coop and Lee 1993

measured quantity	transducer	working range	output voltage at full scale	cell	resolution	noise	error due to hyst., drift and non-lin.
deviatoric force	Wykeham Farrance load cells	5kN	20mV	(B&W)	0.15kPa	±1kPa	±0.8%
		25kN		(HP1)	0.4kPa	±2kPa	
		200kN		(HP2)	3kPa	(1tr)	
pore pressure cell pressure	Druck transducer	0.1MPa	100mV	(B&W)	0.03kPa	±0.8kPa	±0.6%
		6MPa		(HP1)	0.2kPa	±1kPa	
	Maywood transducer	70MPa	210mV	(HP2)	2kPa	(1tr)	

Nomenclature:
(B&W)- Bishop & Wesley triaxial cell
(HP1)- high pressure triaxial cell with a capacity of 5MPa
(HP2)- high pressure triaxial cell with a capacity of 70MPa
(1tr) - less than resolution

Table 3.1a Characteristics of the load cells and pressure transducers

measured quantity	transducer	working range	output voltage at full scale	cell	resolution	noise	error due to hyst., drift and non-lin.
volume change	Imperial College volume gauge + LVDT	35cc (25mm)	±2V	(B&W)	0.0015%	±0.001%	±0.8%
				(HP1)	0.001%		
				(HP2)	0.001%		
external axial displacement	LVDT	25mm	±2V	(B&W)	0.001%	±0.001%	±0.3%
				(HP1)	0.0007%		
local axial displacement	Hall effect transducer	5mm	±1V	(B&W)	0.0003%	±0.003%	±0.9%
				(HP1)			
	LVDT	10mm	±3V	(B&W)*	5E-6%+	±0.00005%	±0.05%

Nomenclature:

(B&W)- Bishop & Wesley triaxial cell

(HP1)- high pressure triaxial cell with a capacity of 5MPa

(HP2)- high pressure triaxial cell with a capacity of 70MPa

+ - at maximum amplification

* - the purpose built system for accurate measurements of local axial displacements

Table 3.1b Characteristics of the volume gauge and axial displacement transducers

sample stiffness	weak (reconstituted)	stiff (natural)	
soil	sands & clays	clay	cemented sand
method	protrusion by pushing	excavation of undersized slots + protrusion	excavation of oversized slots + sealing

Table 3.2 Methods of placing the bender element and the soil sample in contact

Test No.	triax. cell	sample diam. (mm)	P' (MPa)	v_i	v_f	$\underline{v}_f^*$
1db	B&W	38	0.65	2.641	2.515	2.511
3db	HP1	50	4.8	2.685	1.969	1.973
6db	HP1	50	2.0	2.429	2.240	2.237
7db	HP1	50	4.8	2.499	1.951	1.948
8db	B&W	38	0.65	2.350	2.313	2.315
9db	B&W	38	0.63	2.740	2.571	2.575

a) Dogs Bay sand

Test No.	triax. cell	sample diam. (mm)	P' (MPa)	v_i	v_f
1dg	HP1	50	1.5	1.510	1.414
2dg	HP1	50	1.8	1.565	1.417
4dg	HP1	50	2.2	1.490	1.391
5dg	HP1	50	4.8	1.585	1.376
6dg	HP1	50	4.8	1.605	1.406

b) decomposed Granite

Test No.	triax. cell	sample. diam. (mm)	P' (MPa)	v_i	v_f
1hr	HP1	50	4.8	1.717	1.686
2hr	HP1	50	4.8	1.619	1.596
4hr	HP2	50	68	1.689	1.411
5hr	HP2	50	68	1.740	1.448

c) Ham River sand

Nomenclature: v_i- initial specific volume, v_f- final specific volume $\underline{v}_f^*$- calculated from v_i and overall volumetric strain during the test p' (MPa)- maximum isotropic stress reached during the test, B&W- Bishop and Wesley triaxial cell, HP1 - High pressure triaxial apparatus with 5MPa capacity, HP2 - High pressure triaxial apparatus with 70MPa capacity

Table 4.1 Test programme for bender elements tests for the three sands

Test No.	triax. cell	sample. diam. (mm)	P' (MPa)	v_i	v_f
1lgs	HP2	50	69	1.888	1.488
2lgs	HP2	50	25	1.452	1.442
3lgs	B&W	50	0.68	1.450	1.448

Table 4.2 Test programme for bender element tests on Lower Greensand

Test No.	probe No.	triax. cell	sample state	p'_i (kPa)
1sds	sh1	B&W	c	63
	sh2	B&W	c	150
	sh3	B&W	c	195
	sh4	B&W	c	250
	sh8	B&W	oc	150
	sh7	B&W	oc	95
	sh10	B&W	oc	350
	sh13	B&W	oc	450
2sds	sh9	B&W	c	630
	sh12	B&W	oc	350
	sh14	B&W	oc	150
	sh19	B&W	oc	400
3sds	sh15	HP1	c	350
	sh16	HP1	c	1350
	sh17	HP1	c	2150

Nomencalature: p_i'(kPa)- isotropic stress at the start of the shearing probe, B&W- Bishop and Wesley triaxial cell, HP1- High pressure triaxial apparatus with 5MPa capacity, c- compacted state, oc-overconsolidated-compacted state

Table 4.3 Test programme for shearing probes on samples of Dogs Bay sand

Sand	A	n
Dogs Bay sand	3100	0.686
decomposed granite	760	0.884
Ham River sand	3900	0.593
Greensand	4000	0.587

Table 4.4 Material parameters A and n for the four reconstituted sands

Test No.	stress path	v_i	v_f	$\underline{v}_f^*$
2ccsk	η -variable	2.437	1.873	1.878
1ccsk	η=-0.6	2.324	1.983	1.985
3ccsk	η=0.75	2.448	1.987	1.992
4ccsk	η=0	2.447	1.956	1.962

v_i- initial specific volume

v_f- final specific volume

$\underline{v}_f^*$- calculated from v_i and overall volumetric strain during the test

Table 5.1 Test programme for the influence of anisotropic stress state on G_{max} for reconstituted samples of Speswhite kaolin

Test No.	propagation/ polarisation	p'(kPa)	v_i	v_f
6ccsk	hh	400	2.236	2.047
8ccsk	vh	400	2.25	2.041
11ccsk*	hh	550	2.129	2.061
12ccsk*	hh	550	2.129	2.062
13ccsk*	vh	550	2.119	2.084
14ccsk*	hh	250	2.299	2.163
15ccsk*	vh	250	2.289	2.135
16ccsk*	hh	325	2.256	2.092
17ccsk	vh	325	2.287	2.099
18ccsk	hv	325	2.285	2.112

*- Tests carried out by Arnold (1996)

Table 5.2 Test programme for oriented samples of Speswhite kaolin

Test	propagation/ polarisation	p'(kPa)	v_i	v_f
1cclc	vh	400	1.676	1.699
2cclc	hh	400	1.676	-
3cclc	hv	400	-	1.699
4cclc	hh	126	1.742	-
5cclc	hv	126	-	1.747
6cclc	vh	126	1.742	1.741
7cclc	hh	175	1.742	-
8cclc	hv	175	-	1.718
9cclc	vh	175	1.718	1.721
10cclc	hh	272	1.763	-
11cclc	hv	272	-	1.752
12cclc	vh	272	1.750	1.731

Table 5.3 Test programme for undisturbed oriented samples of London clay

Test	propagation/ polarisation	σ_v'(kPa)	p'(kPa)	v_i	v_f
13cclc	hh	400	400	2.007	1.890
14cclc	vh	400	400	2.010	1.906
15cclc	hv	400	400	2.008	1.892
16cclc	hh	1500	3000*	1.800	1.613
17cclc	hh	1500	3000*	1.798	1.613

σ_v'- maximum effective stress in the consolidometer

*- maximum value of p' reached in the triaxial apparatus

Table 5.4 Test programme for reconstituted oriented samples of London clay

model parameters	Materials			
	G45	G90	T08	A15
G	45MPa	90MPa	45MPa	45MPa
κ	0.006	0.006	0.006	0.006
λ	0.097	0.097	0.097	0.097
M	1.0	1.0	1.0	1.0
Γ	2.994	2.994	2.994	2.994
TS	0.2	0.2	0.2	0.2
TT	0.04	0.04	0.08	0.04
ψ	2.5	2.5	2.5	2.5
α	1.0	1.0	1.0	1.5

Table 6.1. Parameters for the 3-SKH model used in the parametric study (nomencalature for the 3-SKH model parameters is given in Section 2.6)

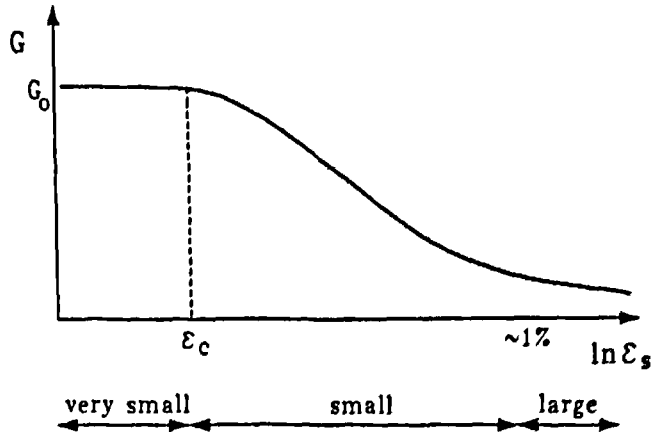

Fig 1.1 An idealisation for the variation of stiffness with strain for soils (after Atkinson & Sallfors, 1991)

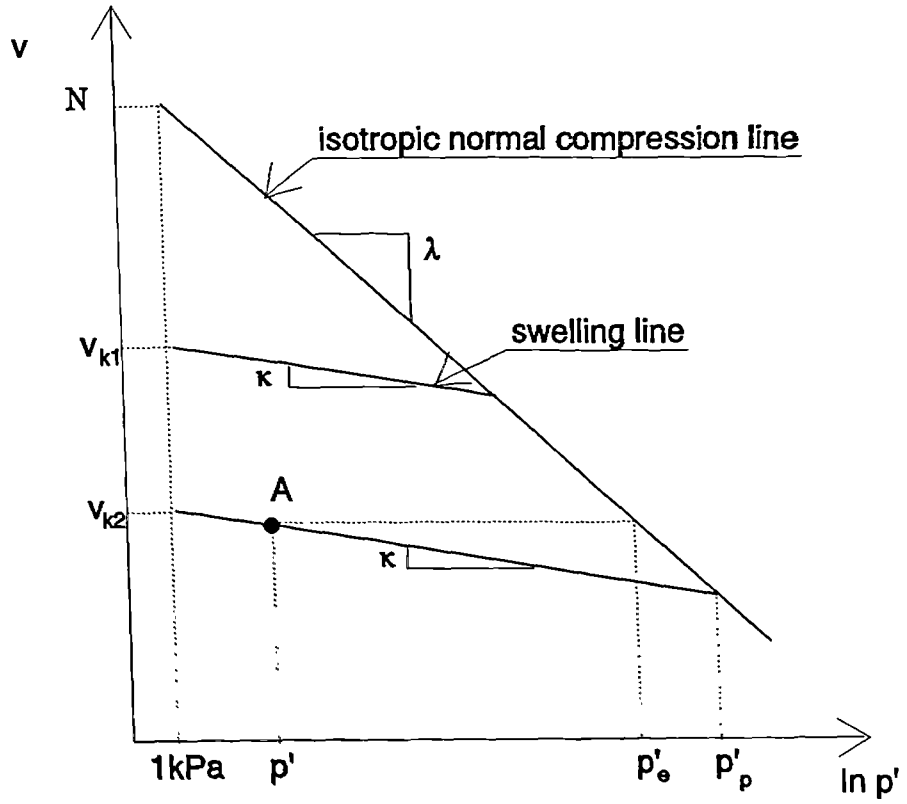

Fig. 1.2 Parameters of isotropic compression for soils

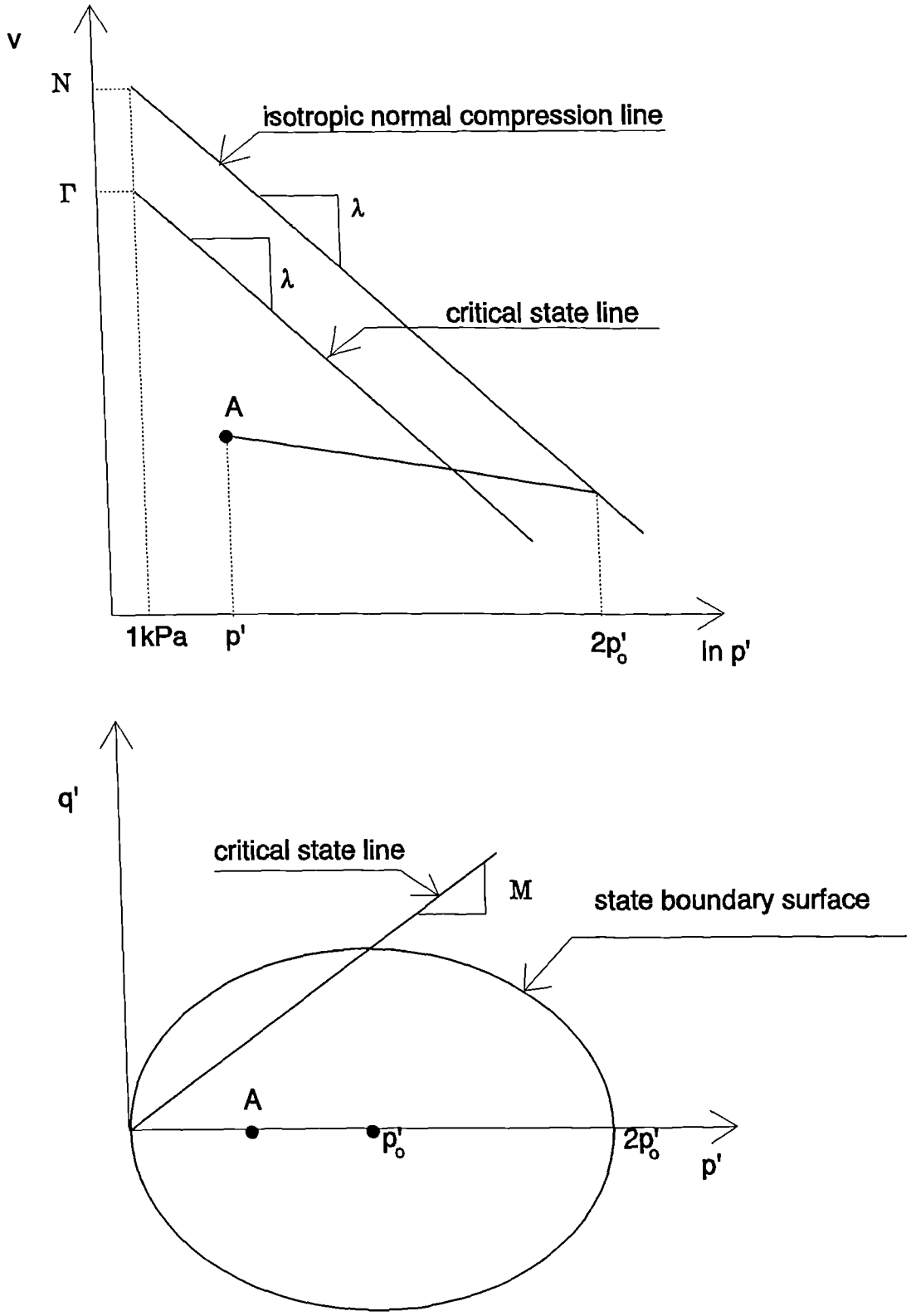

Fig. 1.3 Critical state line and state boundary surface for soils

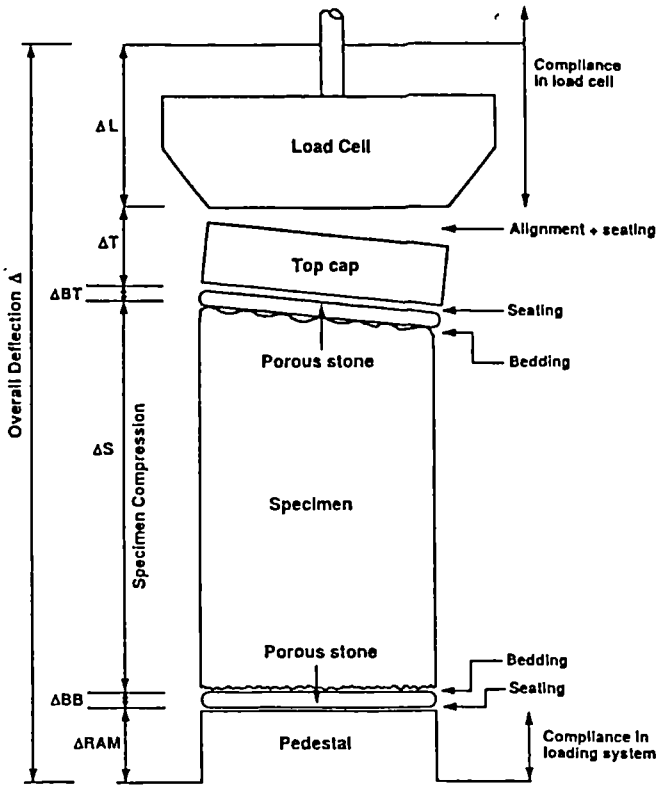

Fig 2.1 Sources of errors in external measurement of axial deformation (after Baldi et al., 1988)

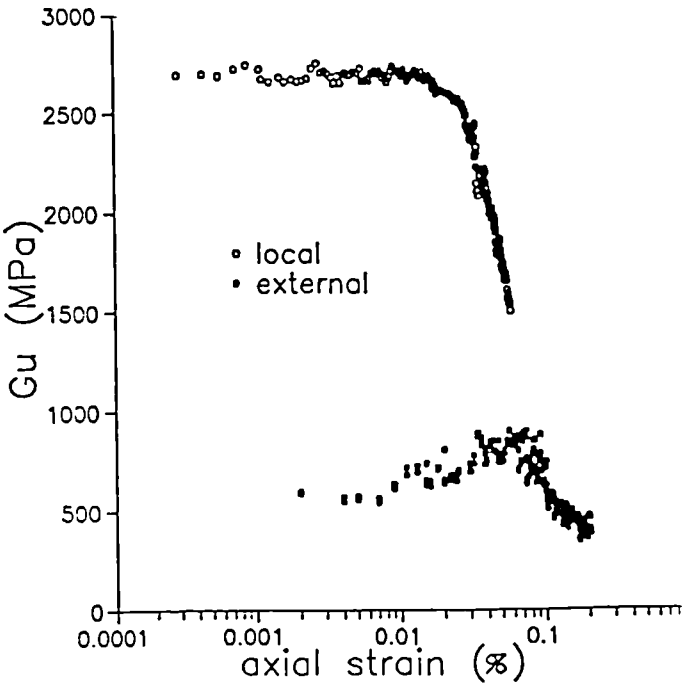

Fig 2.2 Tangent stiffness for an undrained probe on Lower Greensand (Cuccovillo & Coop, 1997)

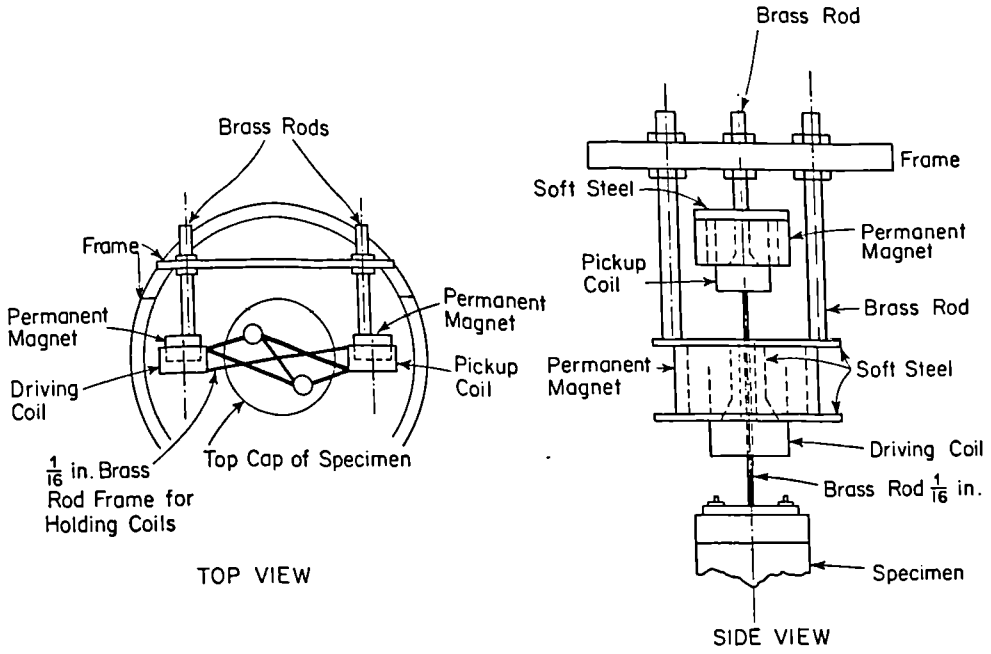

Fig 2.3 Driving and measuring components for a fixed-free resonant-column apparatus (after Richart et al., 1970)

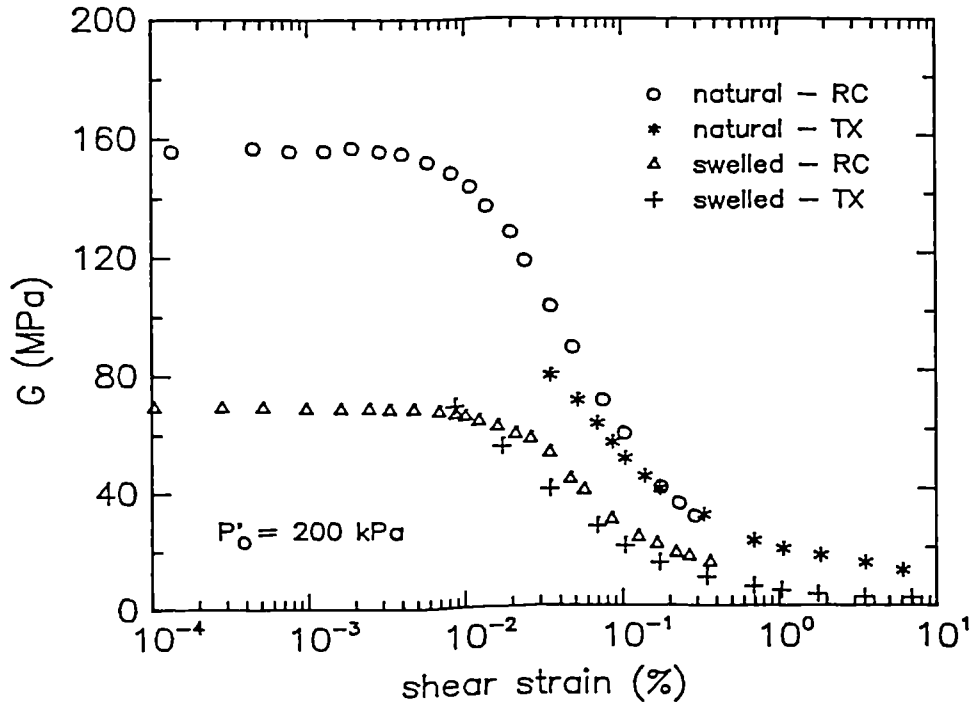

Fig 2.4 Comparative measurement of soil stiffness using dynamic and static methods (after Georgiannou et al., 1991) (TX: triaxial, RC: resonant column)

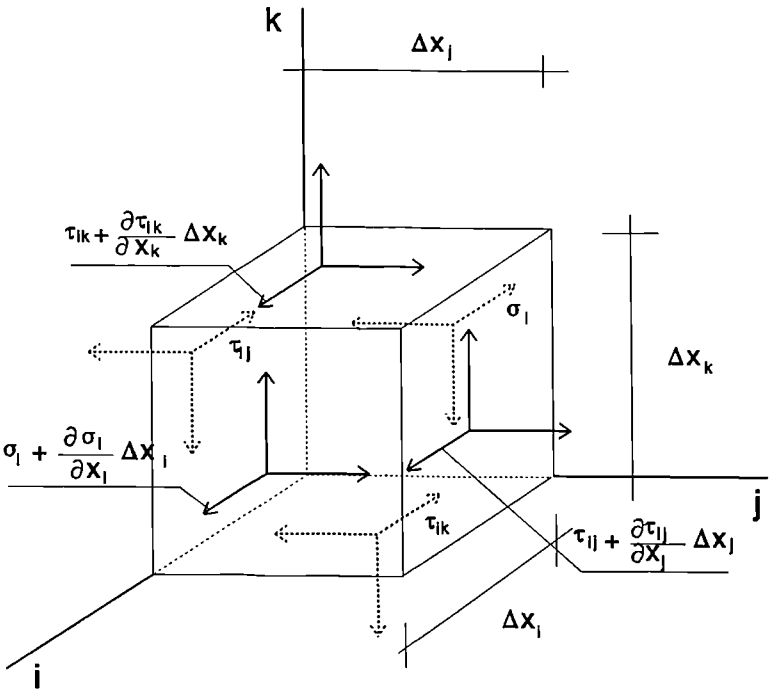

Fig 2.5 Stresses acting on a small element of an infinite elastic medium

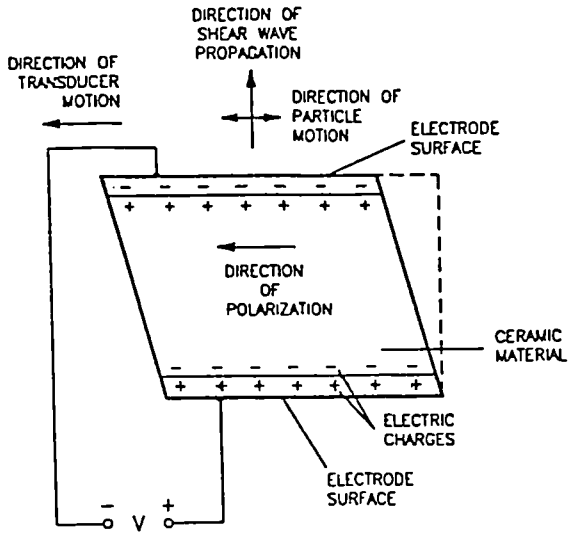

Fig 2.6 Schematic of a shear-plate piezoelectric transducer (after Brignoli et al., 1997)

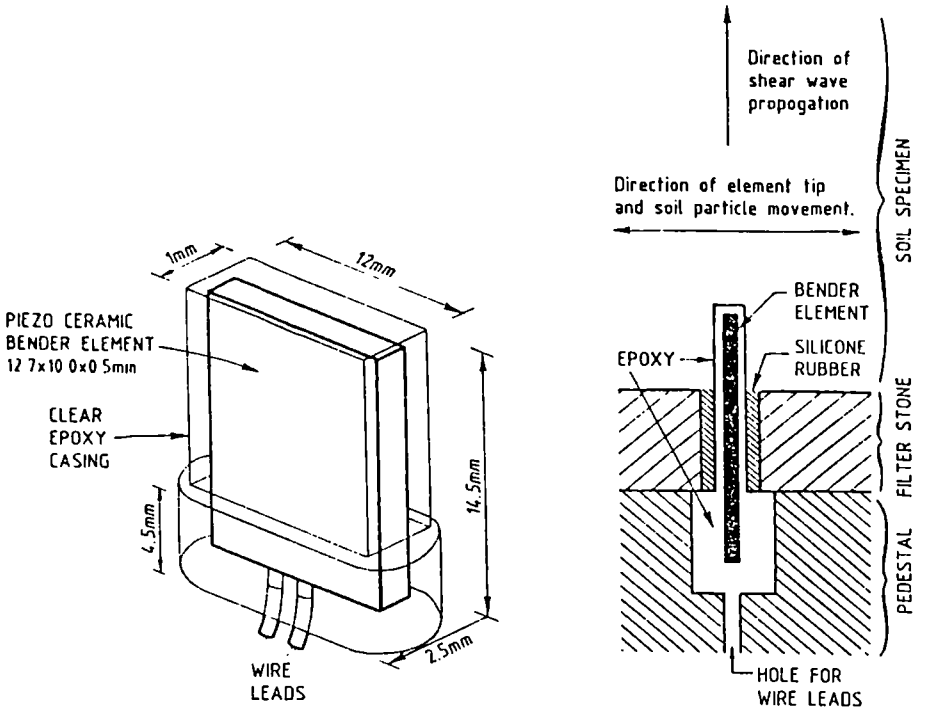

Fig 2.7 Bender element configuration incorporated in a soil testing device (after Dyvik & Madshus, 1985)

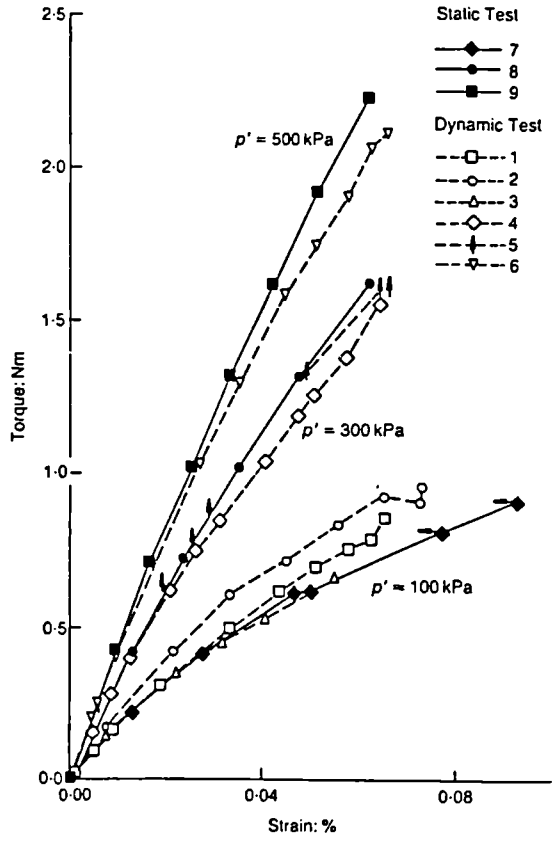

Fig 2.8 Torque-strain curves at different frequencies for Leighton Buzzard sand (after Bolton & Wilson, 1989)

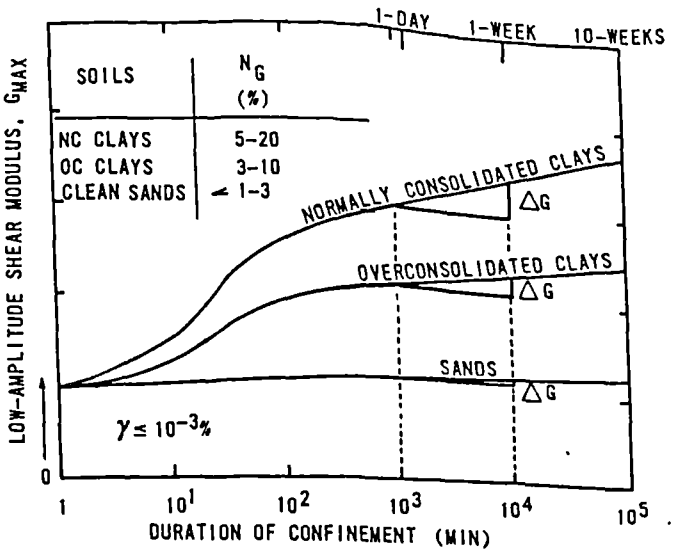

Fig 2.9 Effect of confinement time on shear modulus (after Anderson & Stokoe, 1979)

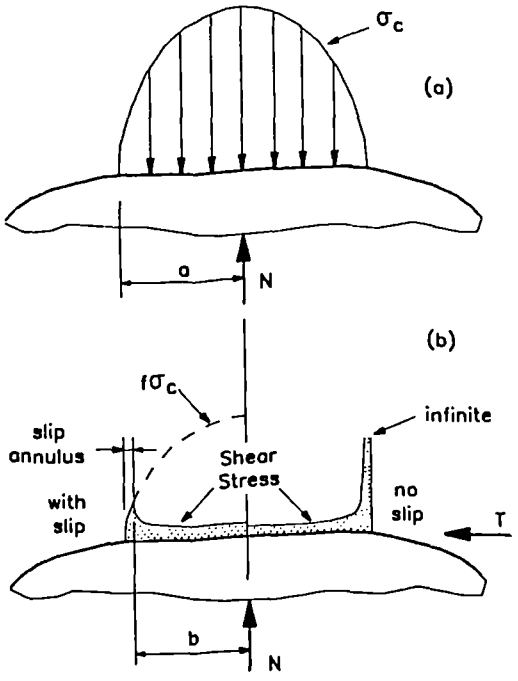

Fig 2.10 Contact stresses between spherical particles (after Mindlin et al., 1951)

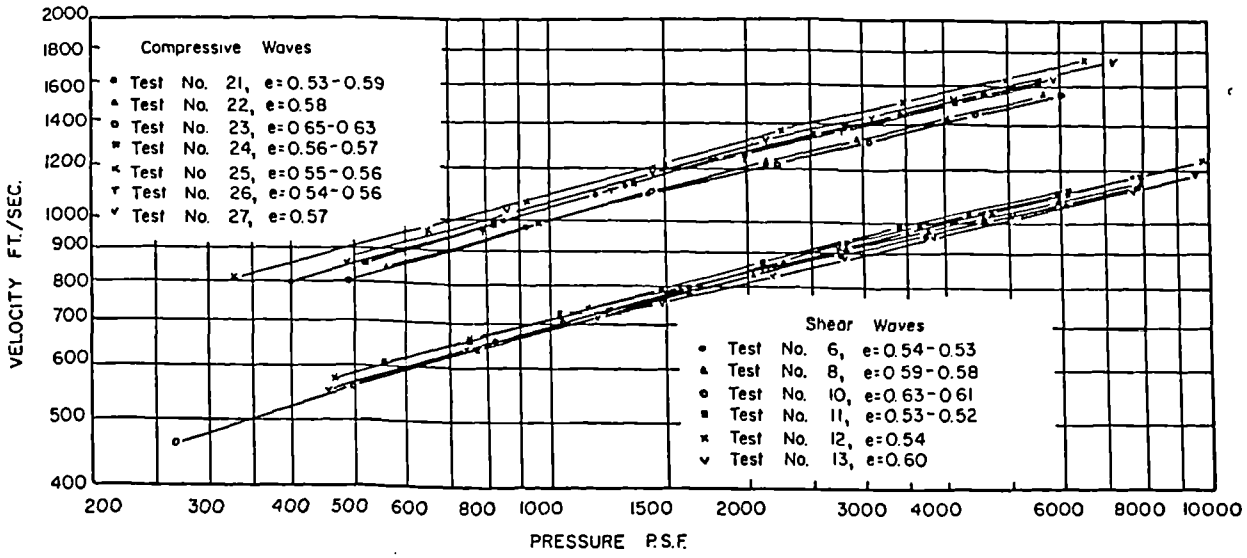

Fig 2.11 Variations of shear and compressive wave velocity with confining pressure and void ratio for dry Ottawa sand (after Hardin & Richart, 1963)

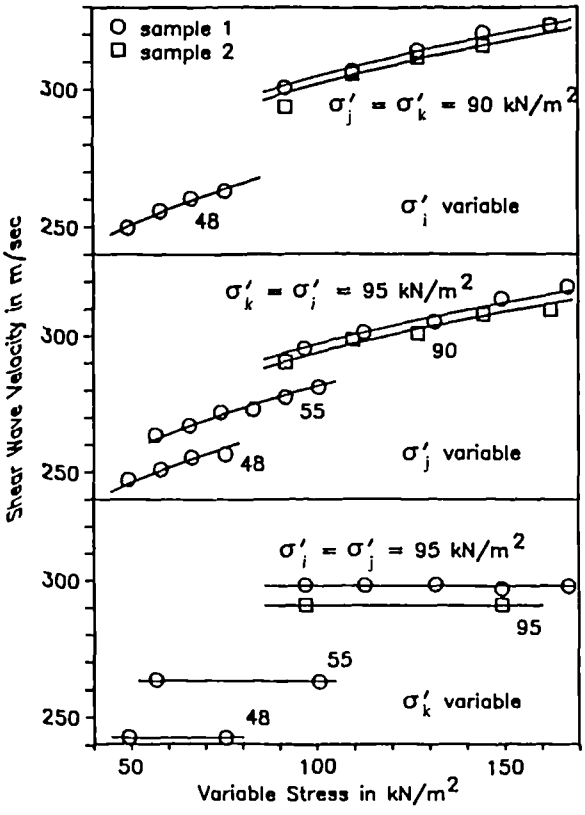

Fig 2.12 Variation of shear wave velocity due to independent variations of three principal stresses (after Roesler, 1979)

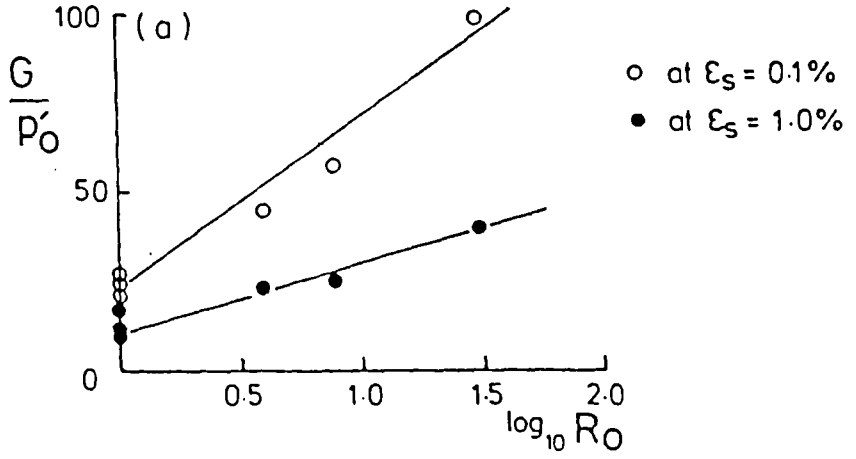

Fig 2.13 Variation of tangent stiffness with overconsolidation ratio for undrained triaxial tests on a glacial till (after Little & Atkinson, 1988)

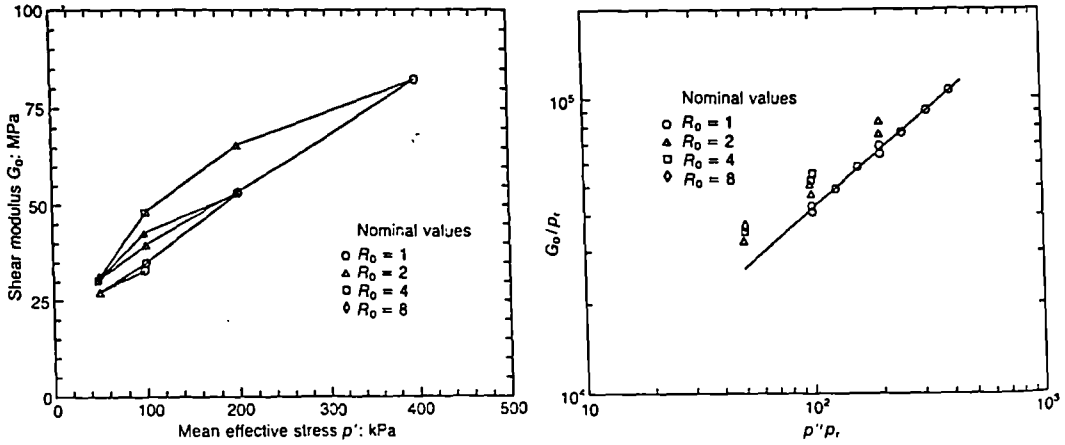

Fig 2.14 Variation of G_{max} (G_0) with stresses and overconsolidation for reconstituted samples of speswhite kaolin (after Viggiani & Atkinson, 1995b)

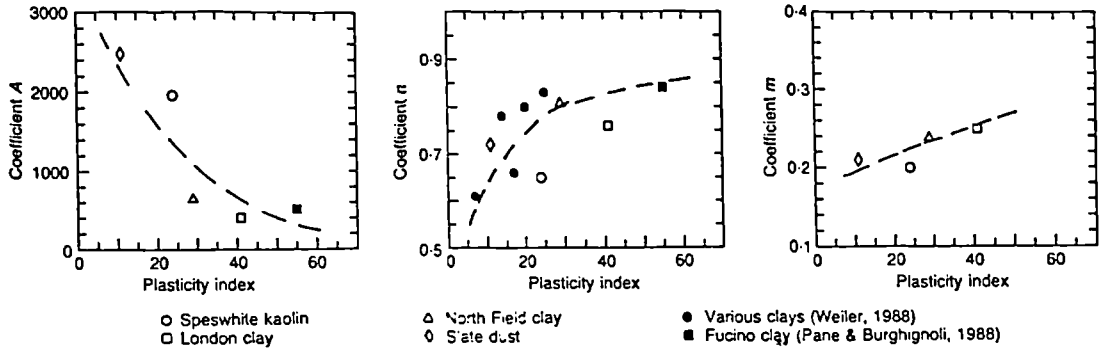

Fig 2.15 Variation of stiffness parameters for G_{max} with plasticity index (after Viggiani & Atkinson, 1995b)

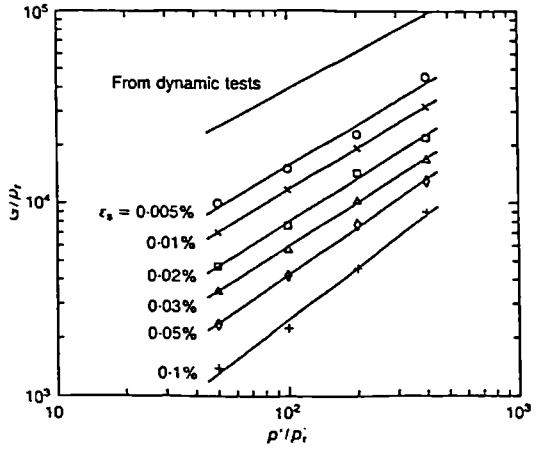

Fig 2.16 Variation of G with mean effective stress at different strain levels for constant p' drained tests on kaolin (after Viggiani & Atkinson, 1995b)

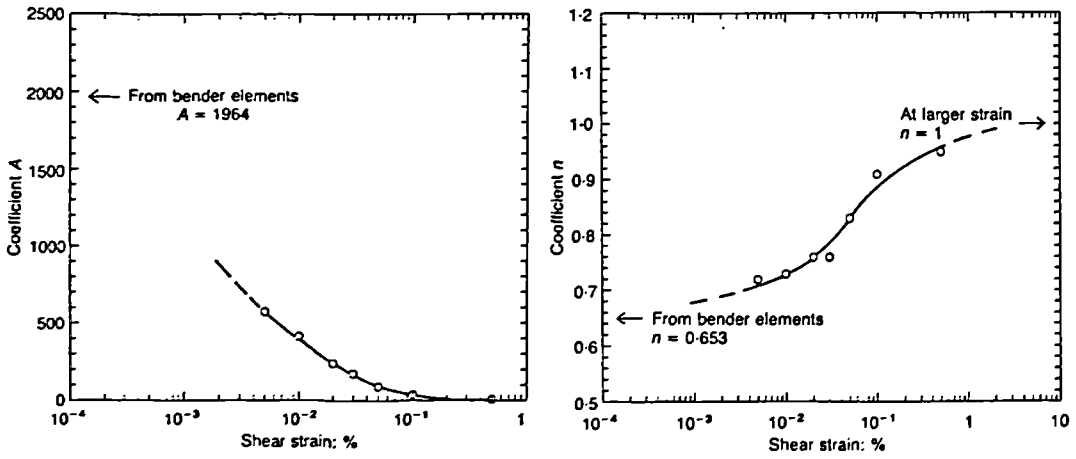

Fig 2.17 Variation of the parameters A and n versus shear strain for constant p' drained tests on kaolin (after Viggiani & Atkinson, 1995b)

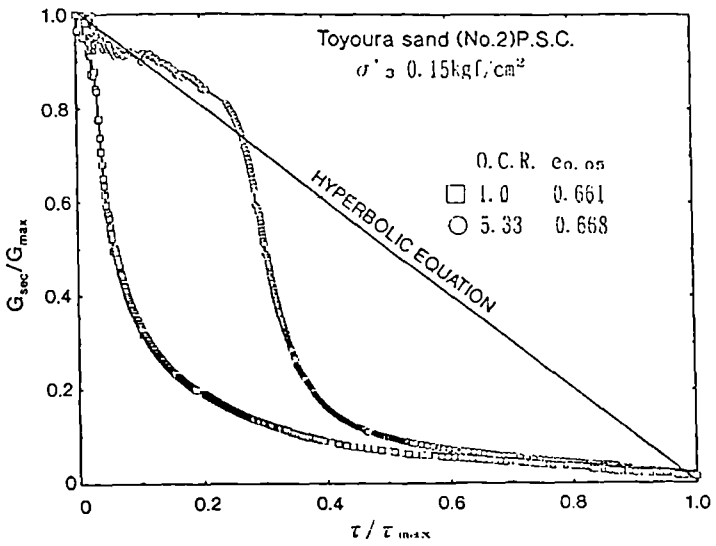

Fig 2.18 Variation of normalised stiffness with normalised shear stress for Toyoura sand (after Tatsuoka & Kohata, 1995)

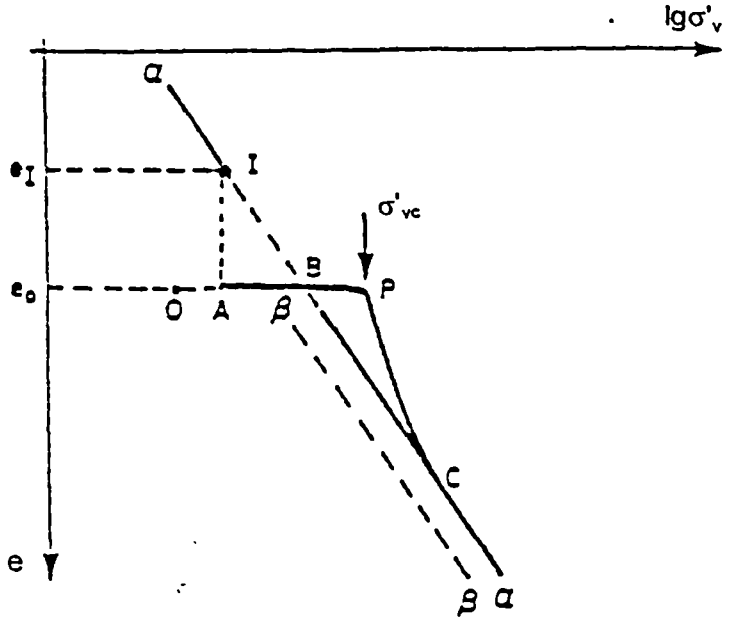

Fig 2.19 Schematic description of the consolidation of a natural clay deposit (after Tavenas & Leroueil, 1987)

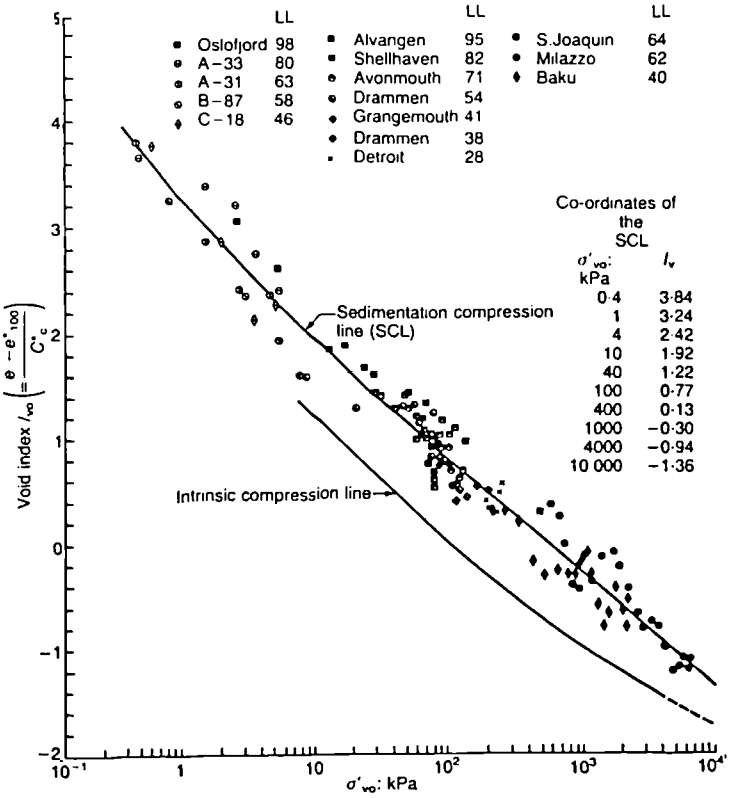

Fig 2.20 Relationship between void index and logσ'_v for normally consolidated clays (after Burland, 1990)

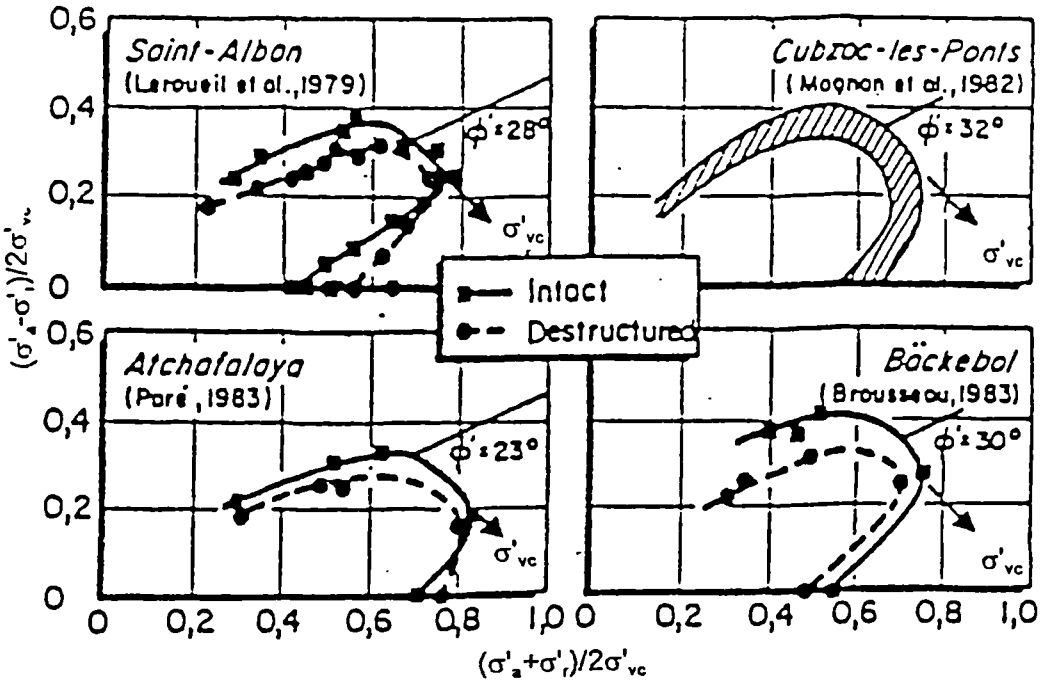

Fig 2.21 State boundary surfaces for intact and destructured clays (after Tavenas & Leroueil, 1995)

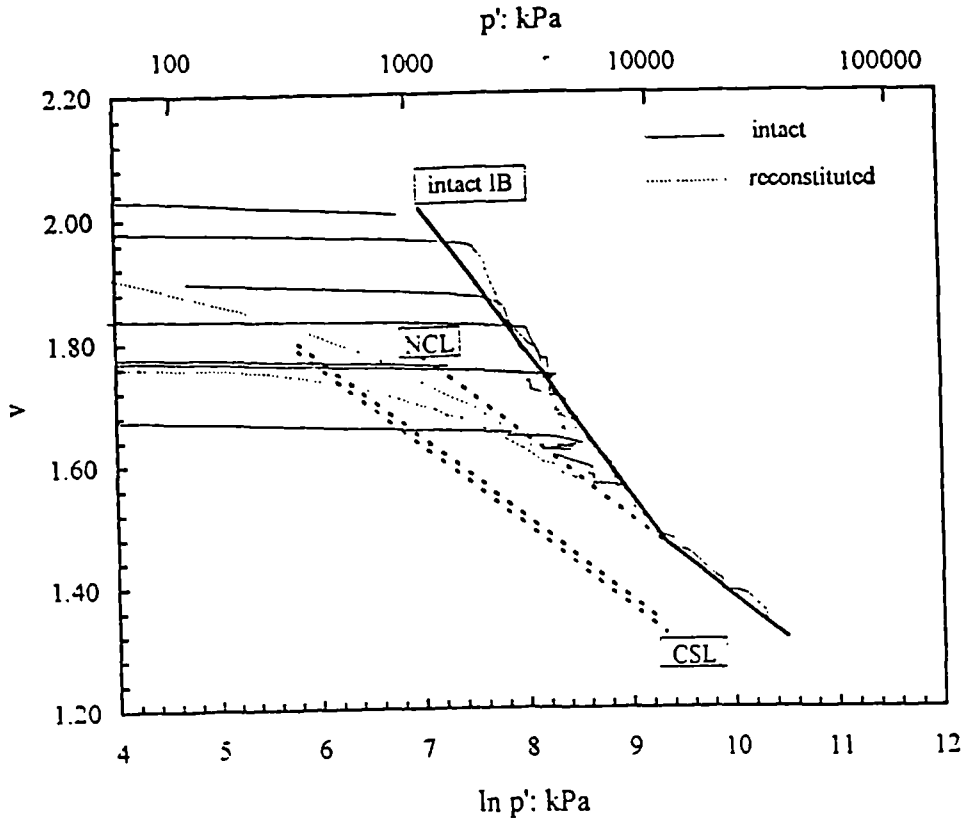

Fig 2.22 Isotropic boundary for the intact samples of calcarenite (after Cuccovillo, 1995)

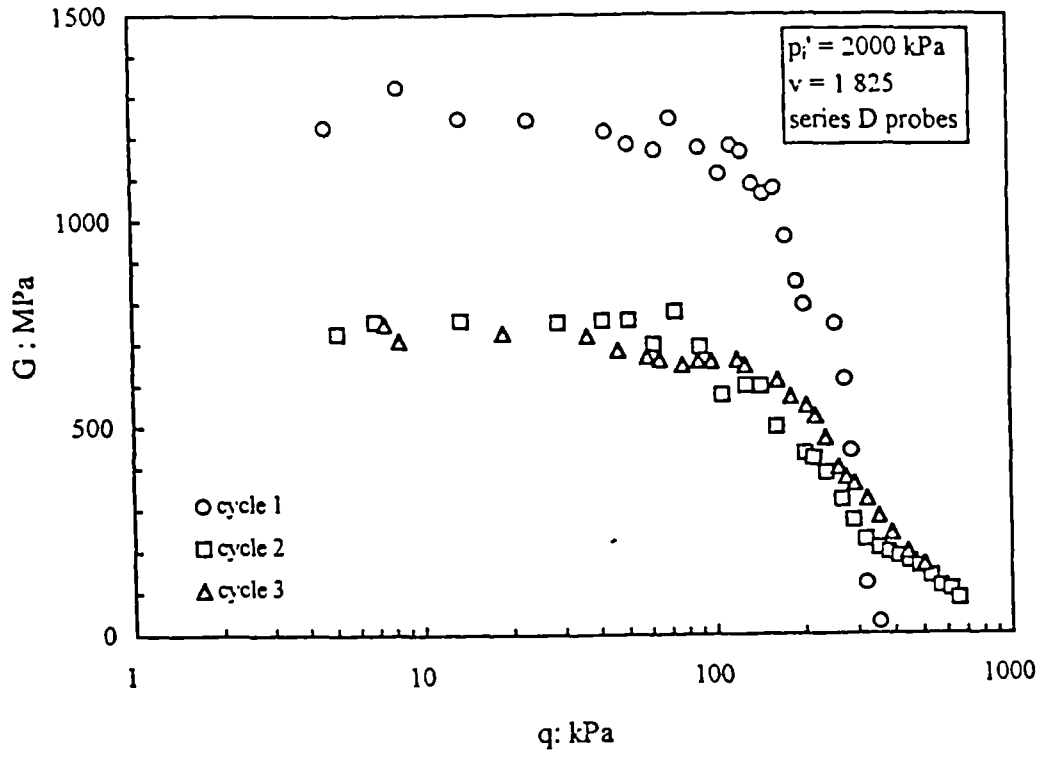

Fig 2.23 Variation of the tangent shear moduli with deviator stress for undrained loading probes on calcarenite (after Cuccovillo, 1995)

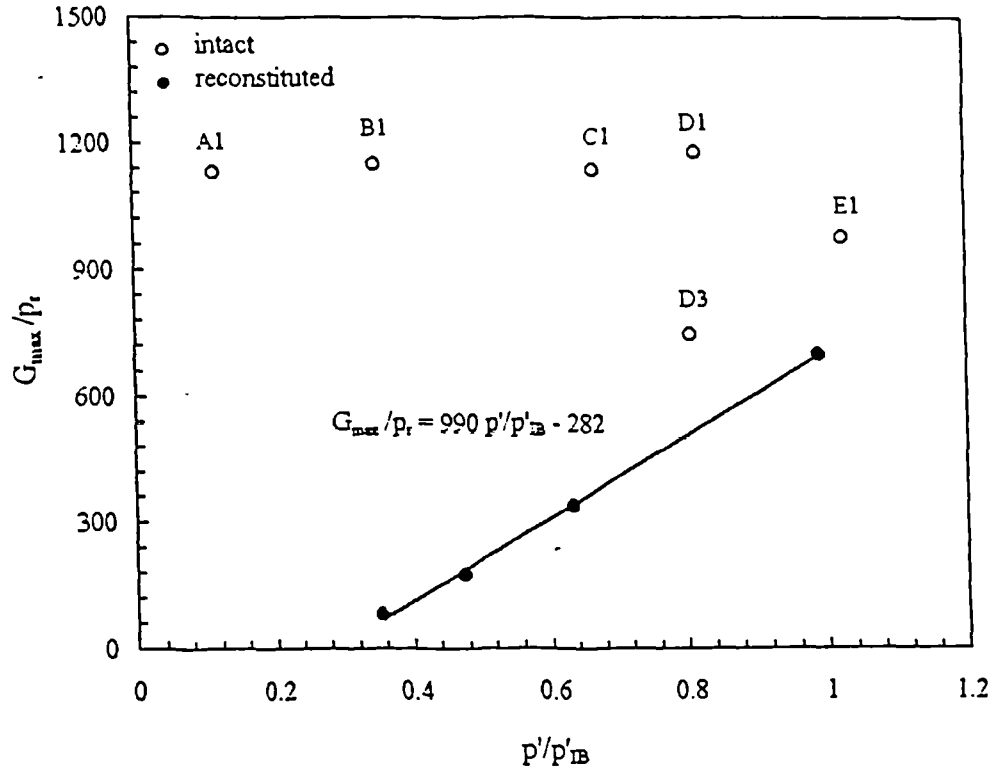

Fig 2.24 G_{max} for intact and reconstituted calcarenite as a function of the normalized state p'/p'_{IB} (after Cuccovillo, 1995)

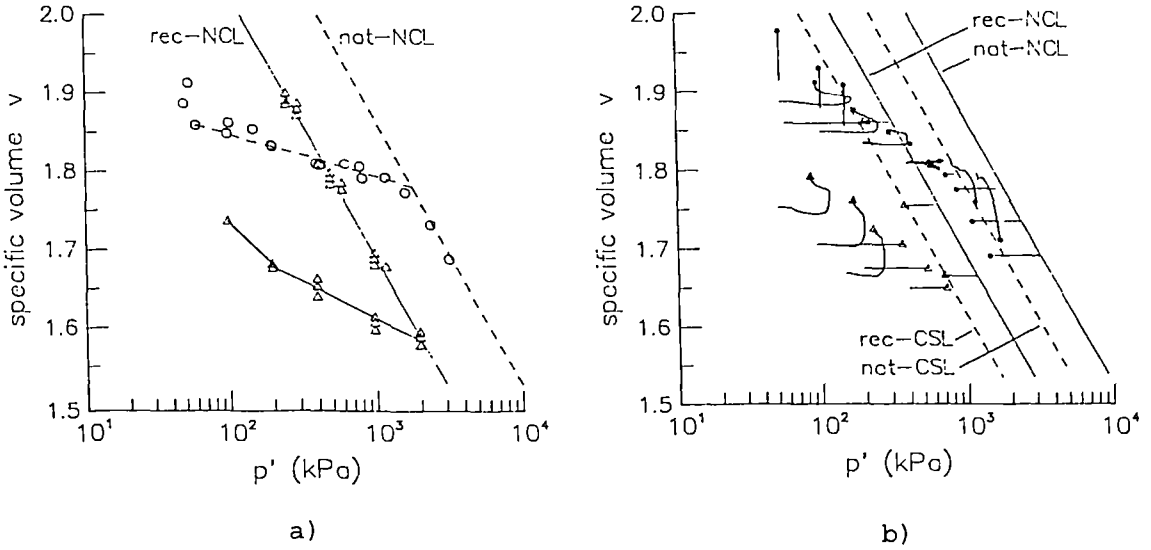

Fig 2.25 Comparison between natural and reconstituted Vallericca clay: a) isotropic compression b) stress-volume paths during shearing (after Rampello et al., 1993)

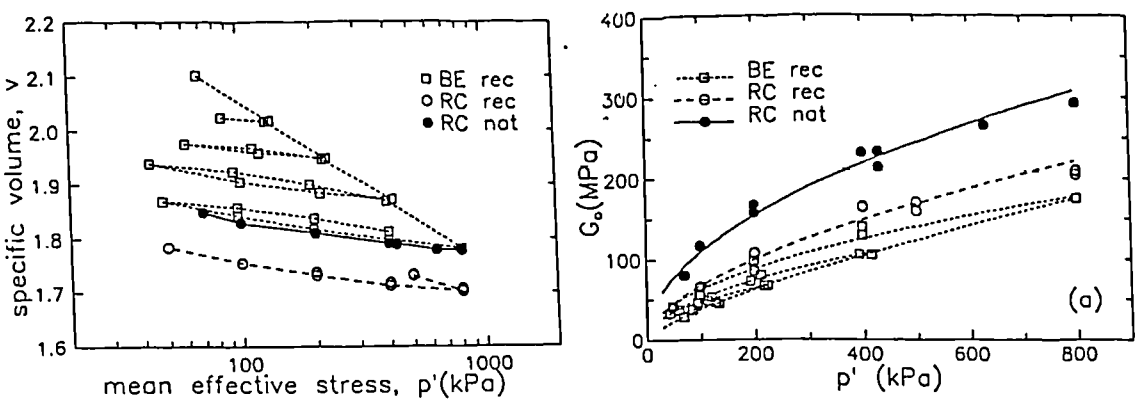

Fig 2.26 Intact and reconstituted samples of Vallericca clay: a) isotropic compression and swelling b) G_0 versus mean effective stress (after Rampello et al., 1995a)

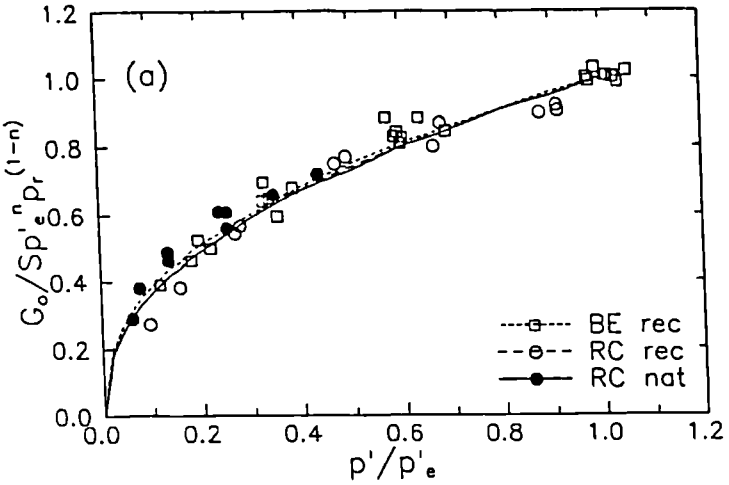

Fig 2.27 Normalized small strain stiffness for Vallericca clay (after Rampello et al., 1995a)

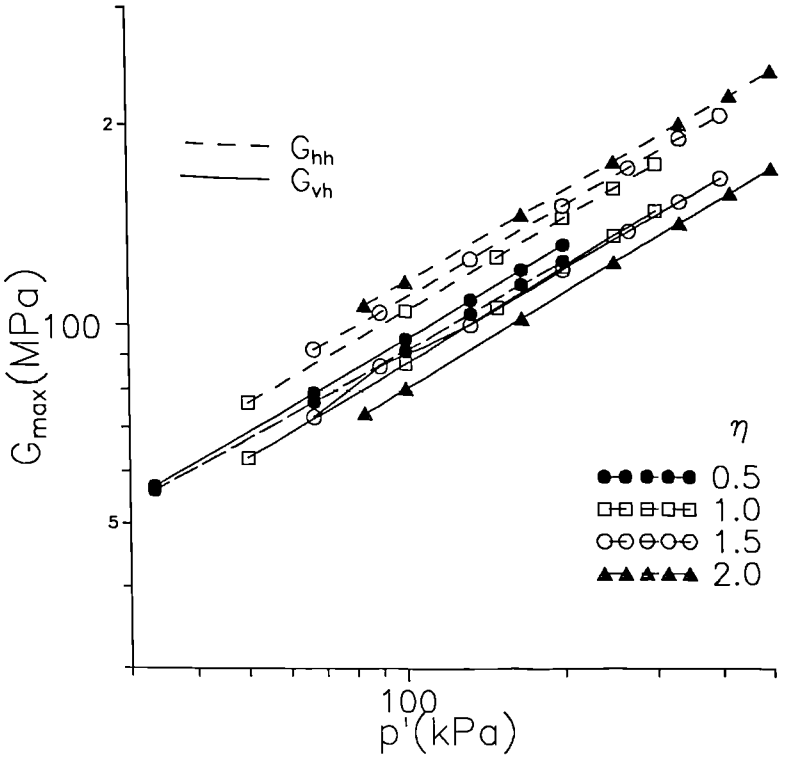

Fig 2.28 Variation of G_{vh} and G_{hh} with mean effective stress for Ticino sand (adapted from Bellotti et al., 1996)

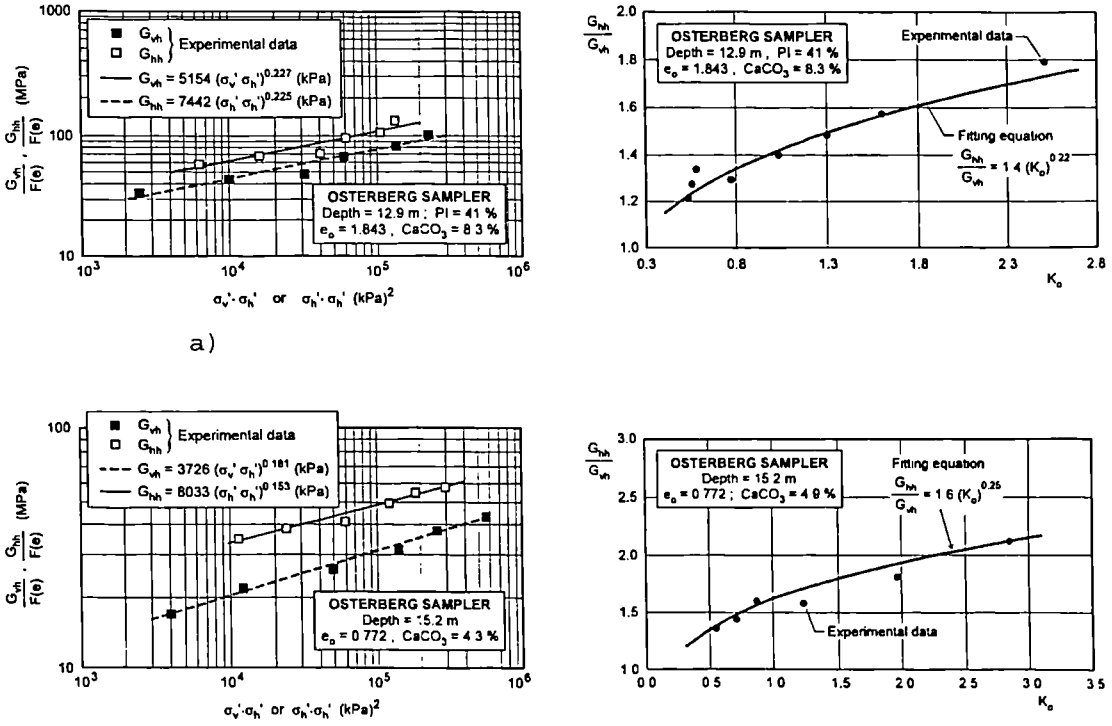
Experimental data
G_{vh} = 5154 ($\sigma_v'\cdot\sigma_h'$)$^{0.227}$ (kPa)
G_{hh} = 7442 ($\sigma_h'\cdot\sigma_h'$)$^{0.225}$ (kPa)
OSTERBERG SAMPLER
Depth = 12.9 m ; PI = 41 %
e_o = 1.843 , $CaCO_3$ = 8.3 %
$\sigma_v'\cdot\sigma_h'$ or $\sigma_h'\cdot\sigma_h'$ (kPa)^2
OSTERBERG SAMPLER
Depth = 12.9 m , PI = 41 %
e_o = 1.843 , $CaCO_3$ = 8.3 %
Experimental data
Fitting equation
$\frac{G_{hh}}{G_{vh}} = 1.4\,(K_o)^{0.22}$
K_o
a)
Experimental data
G_{vh} = 3726 ($\sigma_v'\cdot\sigma_h'$)$^{0.181}$ (kPa)
G_{hh} = 8033 ($\sigma_h'\cdot\sigma_h'$)$^{0.153}$ (kPa)
OSTERBERG SAMPLER
Depth = 15.2 m
e_o = 0.772 , $CaCO_3$ = 4.3 %
$\sigma_v'\cdot\sigma_h'$ or $\sigma_h'\cdot\sigma_h'$ (kPa)^2
OSTERBERG SAMPLER
Depth = 15.2 m
e_o = 0.772 ; $CaCO_3$ = 4.9 %
Fitting equation
$\frac{G_{hh}}{G_{vh}} = 1.6\,(K_o)^{0.25}$
Experimental data
K_o
b)

Fig 2.29 The influence of effective consolidation stresses on normalized shear moduli for: a) Pisa clay b) Panagaglia clay (after Jamiolkowski et al., 1995)

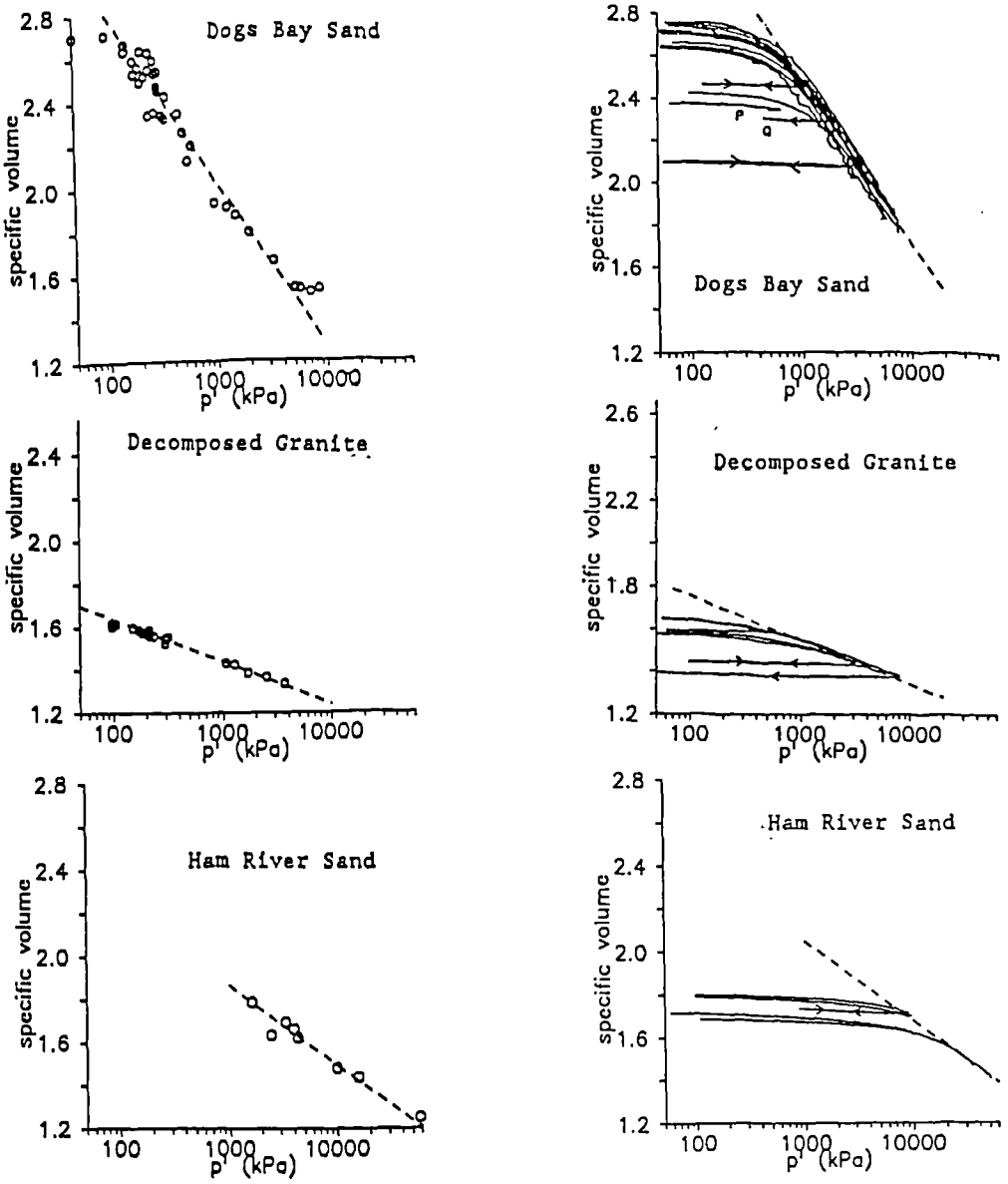

Fig 2.30 Isotropic compression lines and critical state lines for three different sands (after Coop & Lee, 1993)

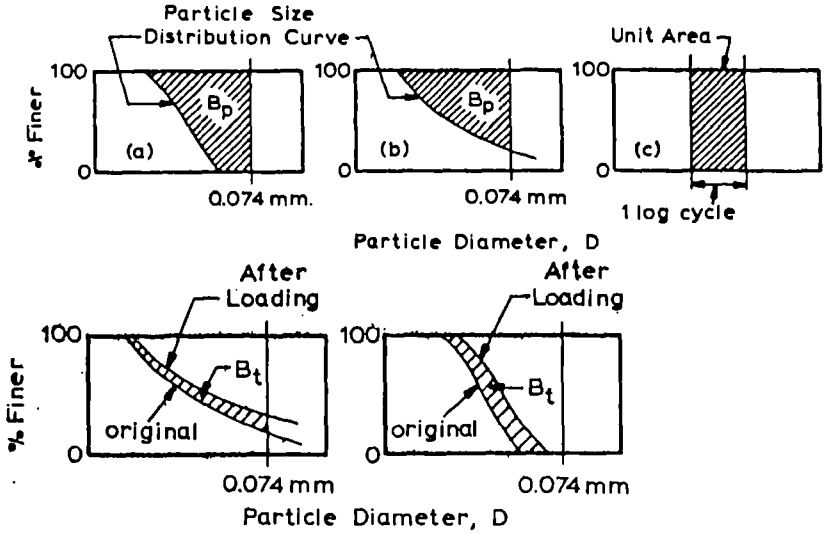

Fig 2.31 Definition of breakage potential and total breakage (after Hardin, 1985)

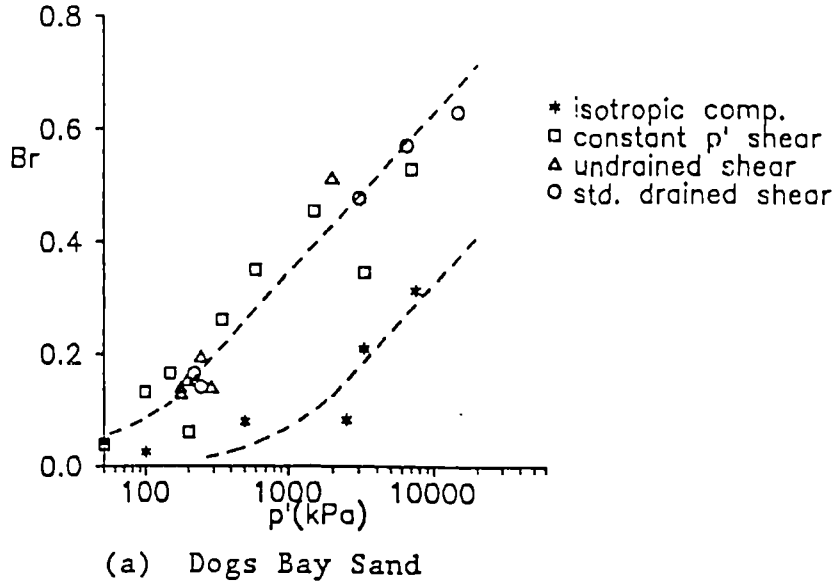

Fig 2.32 Variation of relative breakage with mean effective stress (after Coop & Lee, 1993)

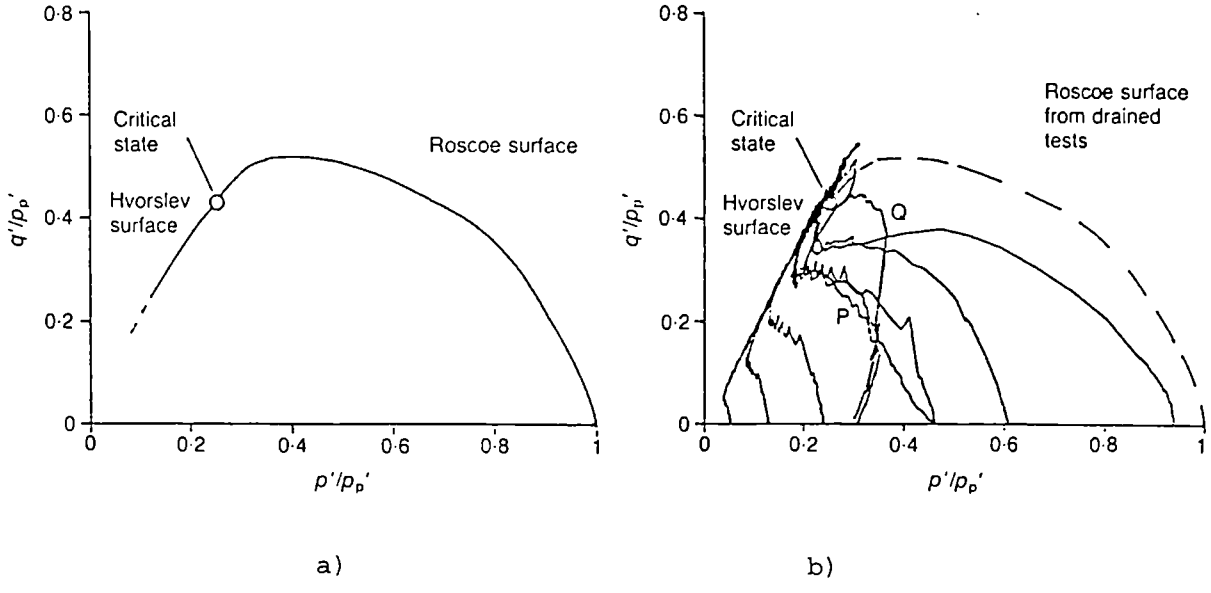

Fig 2.33 Normalized triaxial stress paths: a) interpretation of a drained test b) undrained tests (after Coop, 1990)

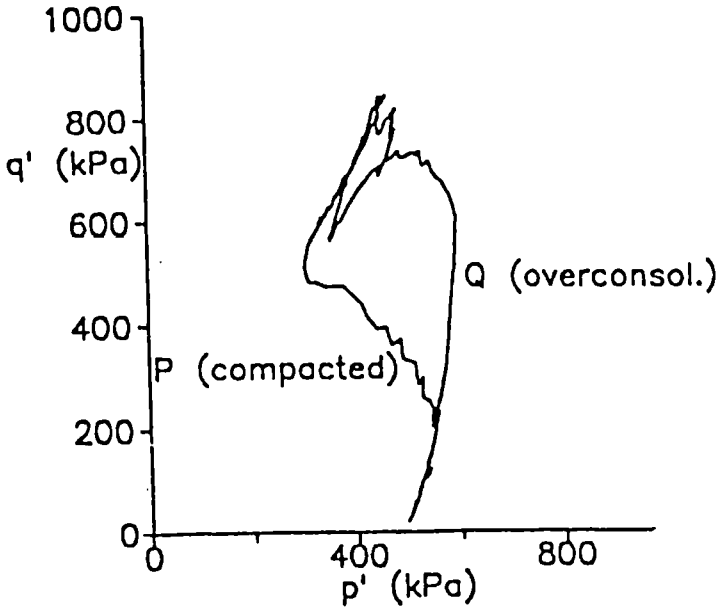

Fig 2.34 Stress paths for compacted and overconsolidated samples of Dogs Bay sand (after Coop, 1990)

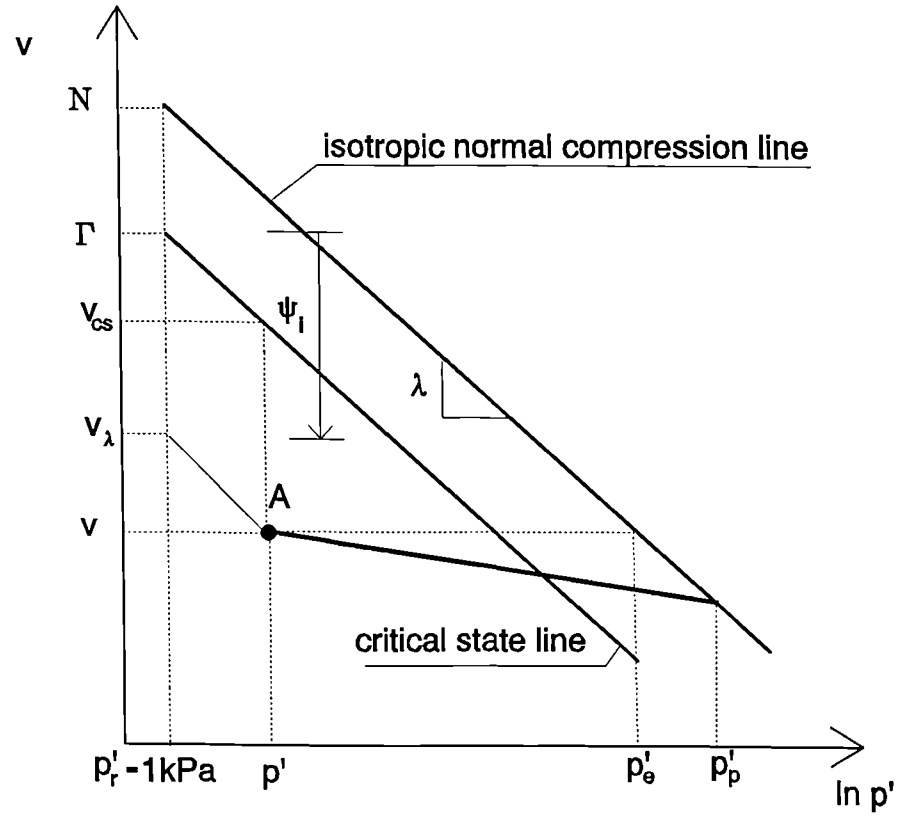

Fig 2.35 State variables for sands

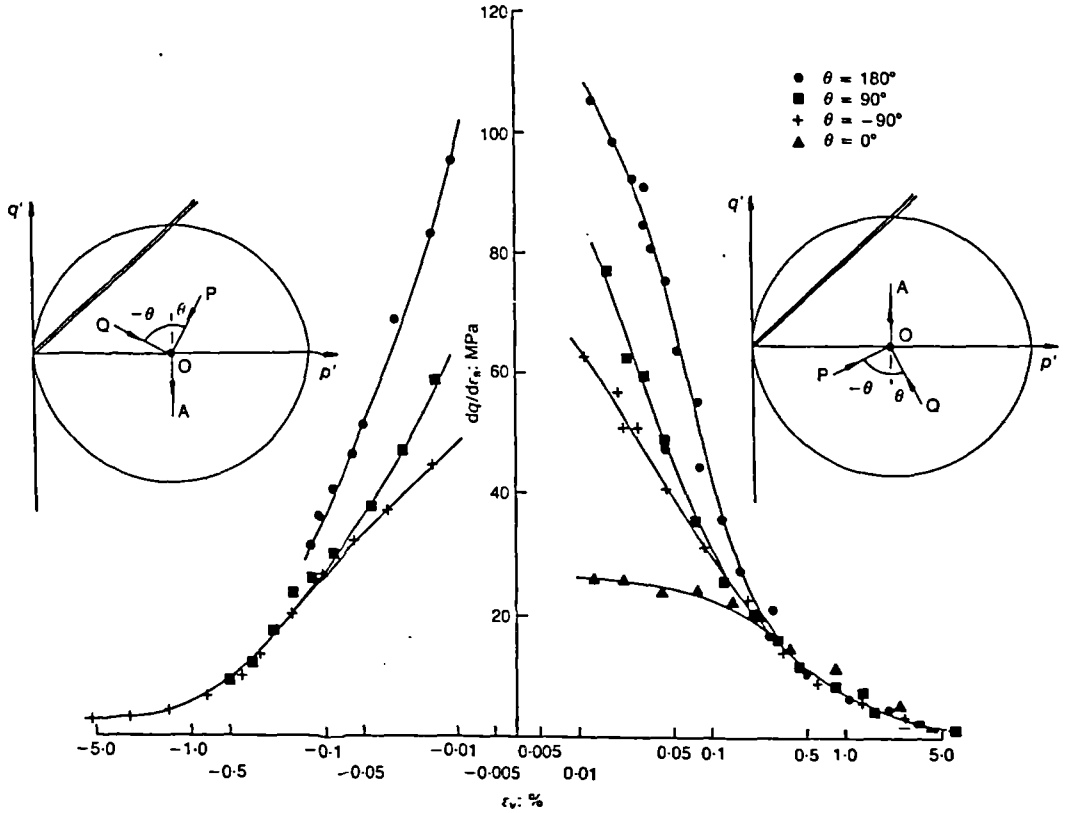

Fig 2.36 Influence of recent stress history on the stiffness of reconstituted London clay (after Atkinson et al., 1990)

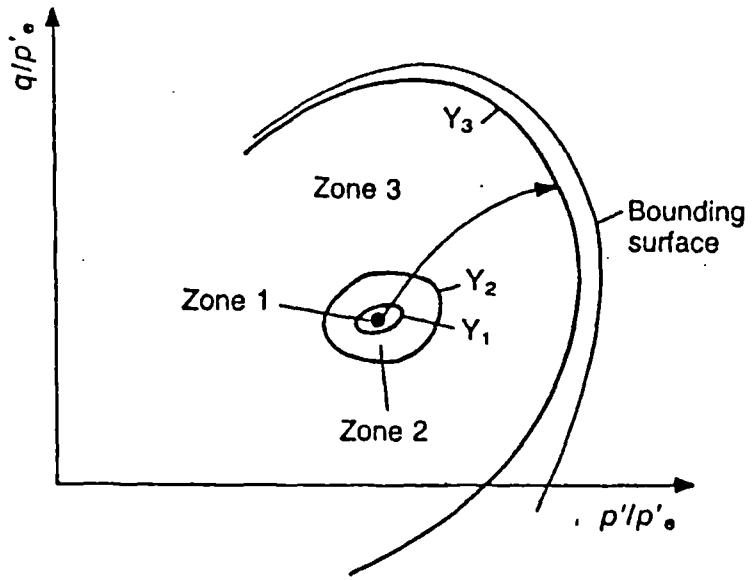

Fig 2.37 Framework for the yielding behaviour of natural clays (after Jardine et al., 1991)

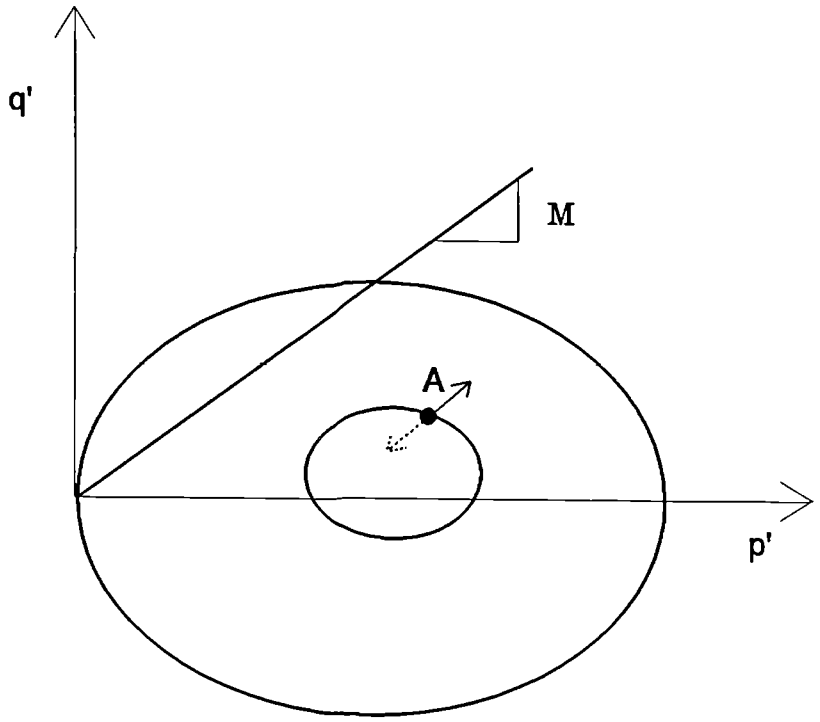

Fig 2.38 Bubble extension of the Modified Cam Clay model (after Al Tabbaa & Wood, 1989)

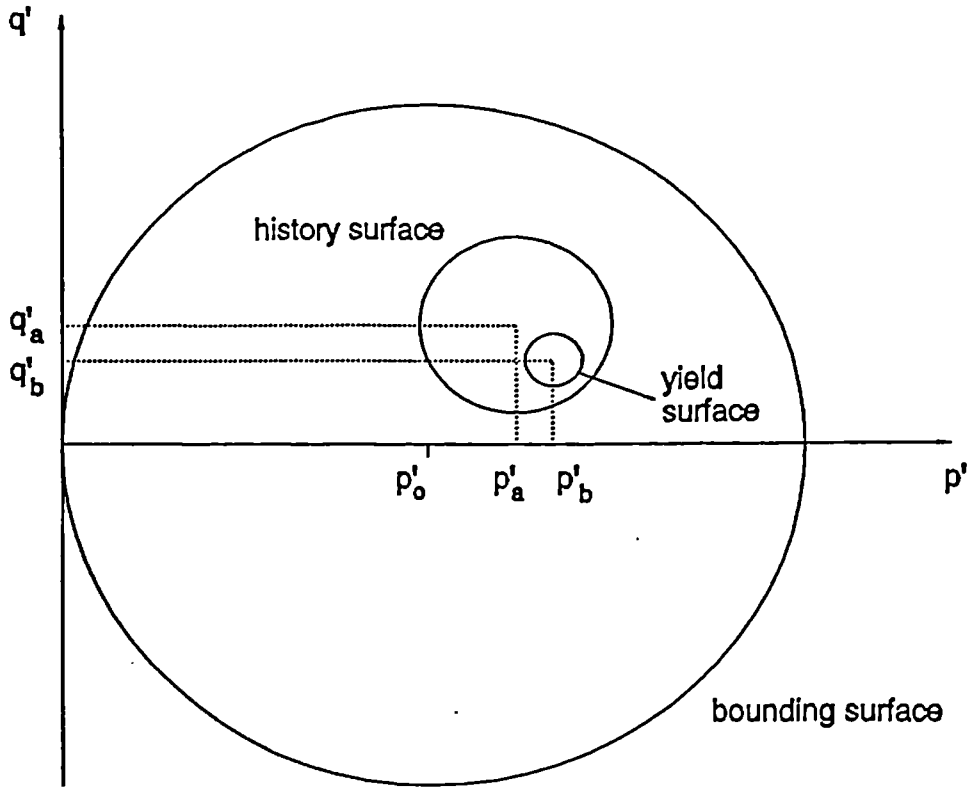

Fig 2.39 The three surface kinematic hardening model in triaxial stress space (after Stallebrass, 1990b)

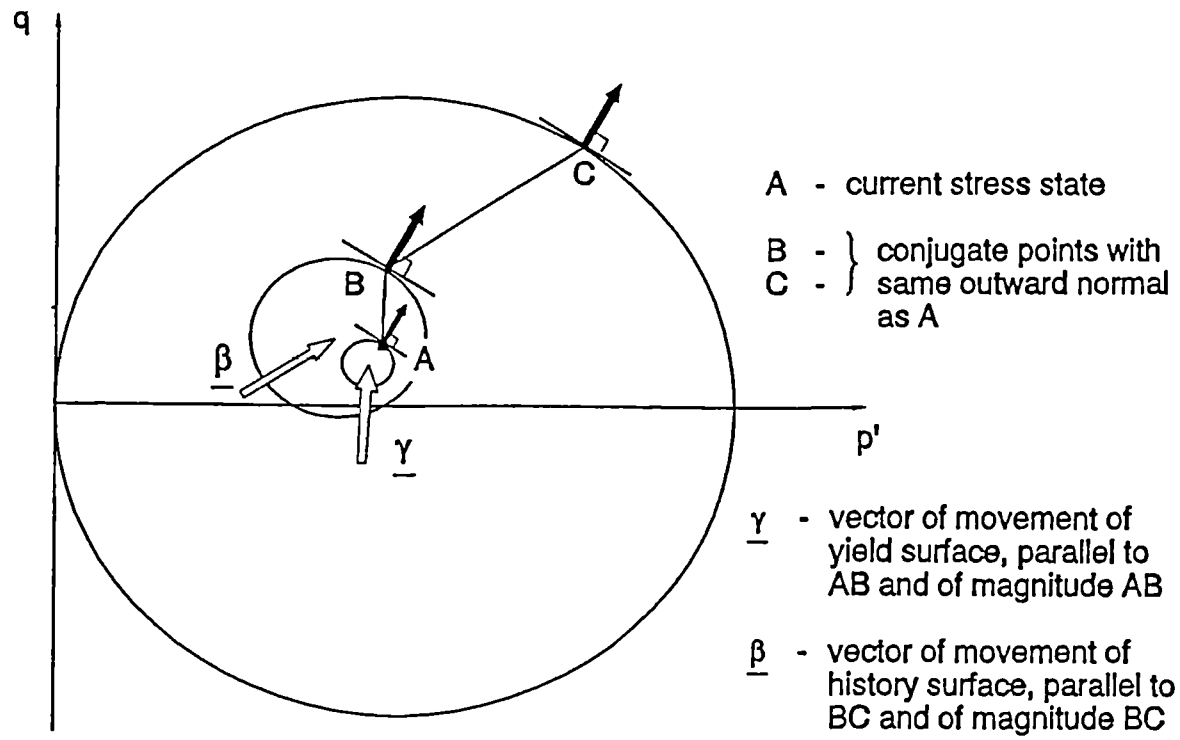

Fig 2.40 Principle of translation rule for kinematic surfaces in the 3-SKH model (after Stallebrass, 1990b)

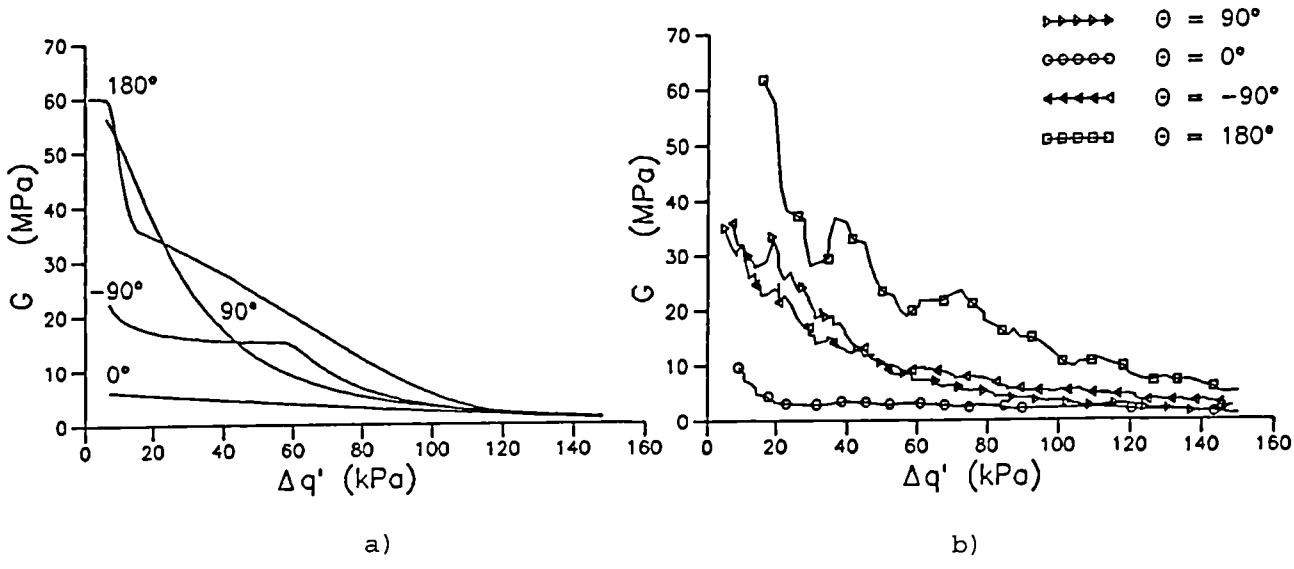

Fig 2.41 Comparison between stiffness data computed from: a) single element simulation and b) test results (after Stallebrass, 1990b)

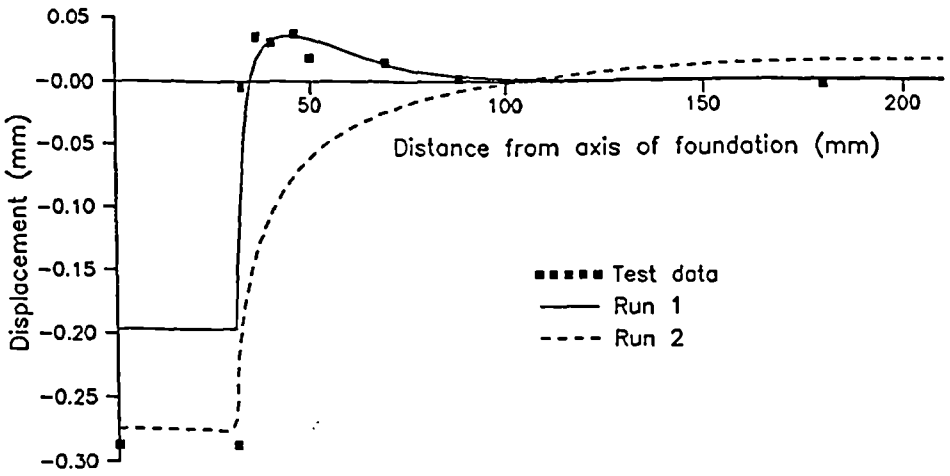

Fig 2.42 Comparison between centrifuge test data and computed settlement profiles for a circular foundation in kaolin (after Stallebrass & Taylor, 1997) (Run1: the 3-SKH model, Run2: the Modified Cam Clay model)

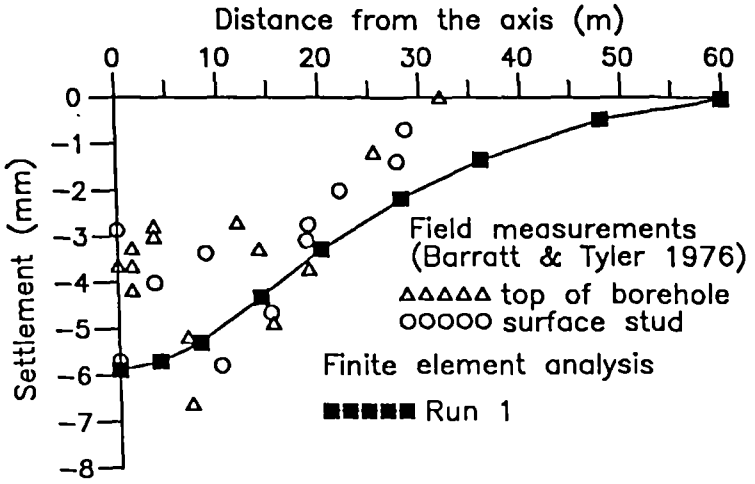

Fig 2.43 Computed surface settlement profiles above a tunnel in London clay compared to field data (after Stallebrass et al., 1994)

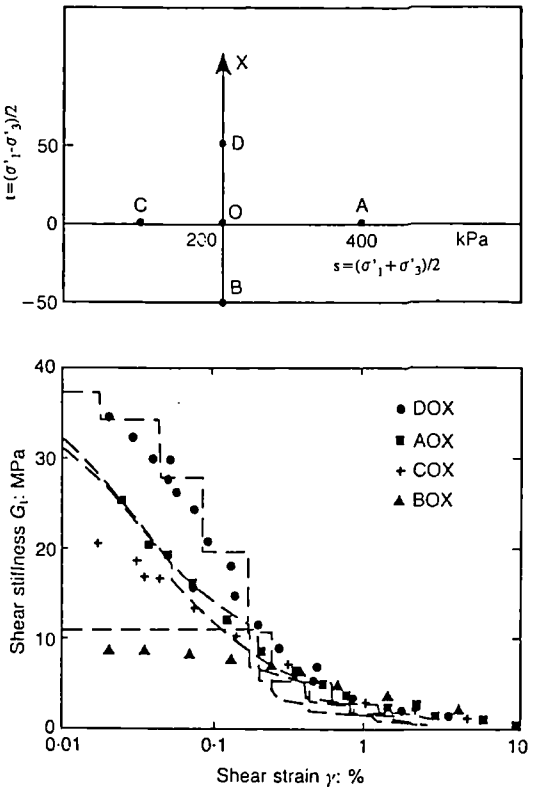

Fig 2.44 Prediction of the recent stress history effect using the brick and string model (after Simpson, 1992)

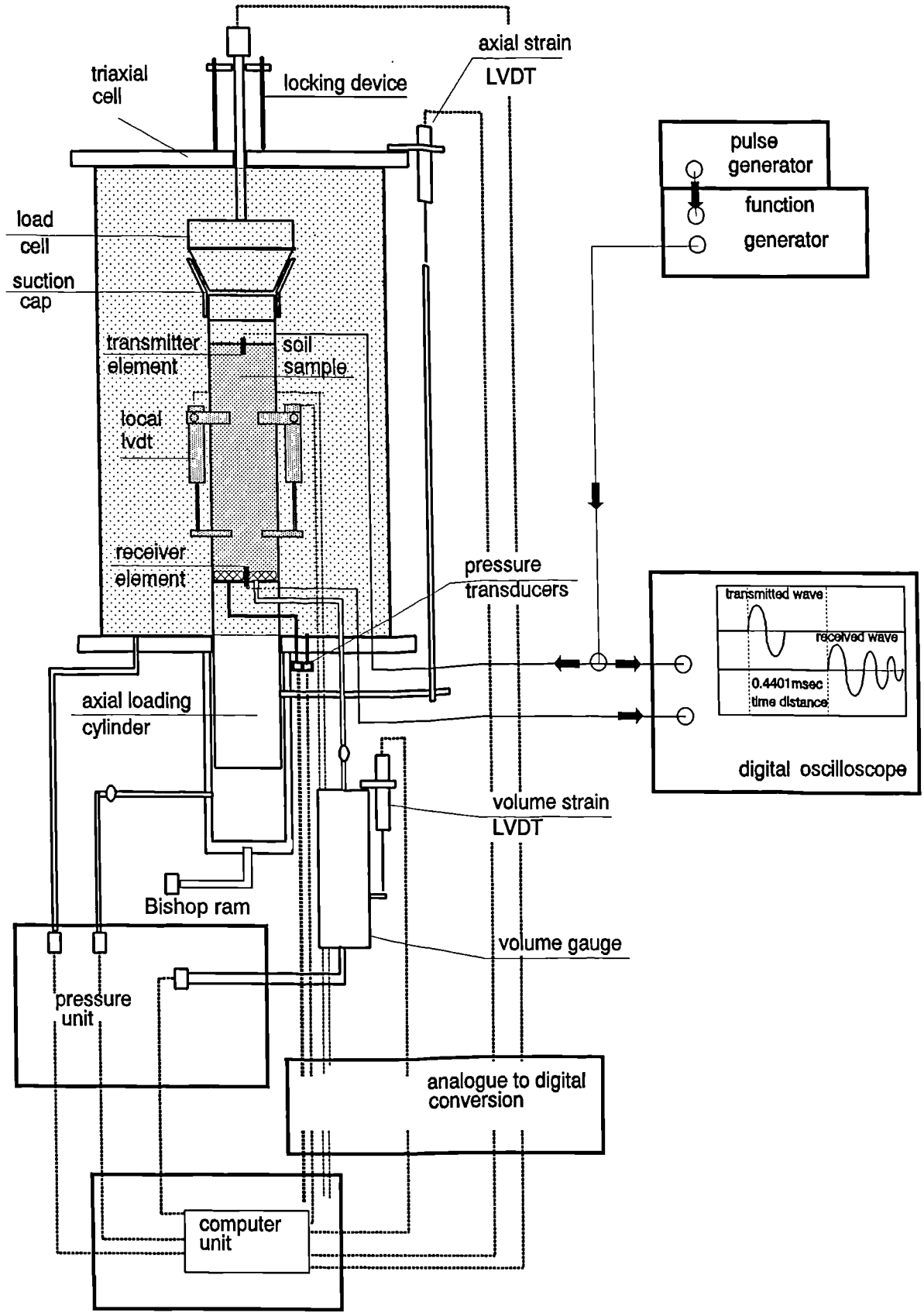

Fig. 3.1 Bender element configuration in a triaxial apparatus

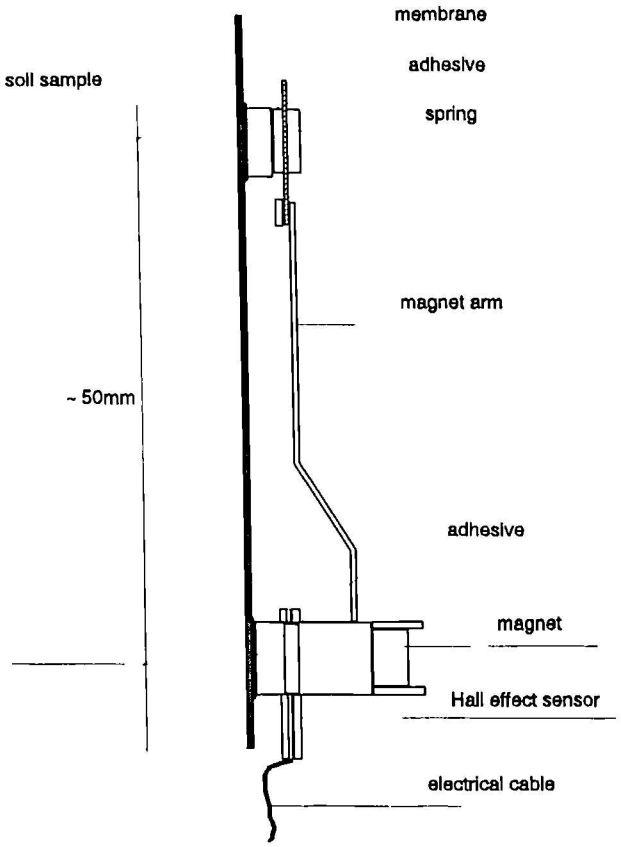

a)

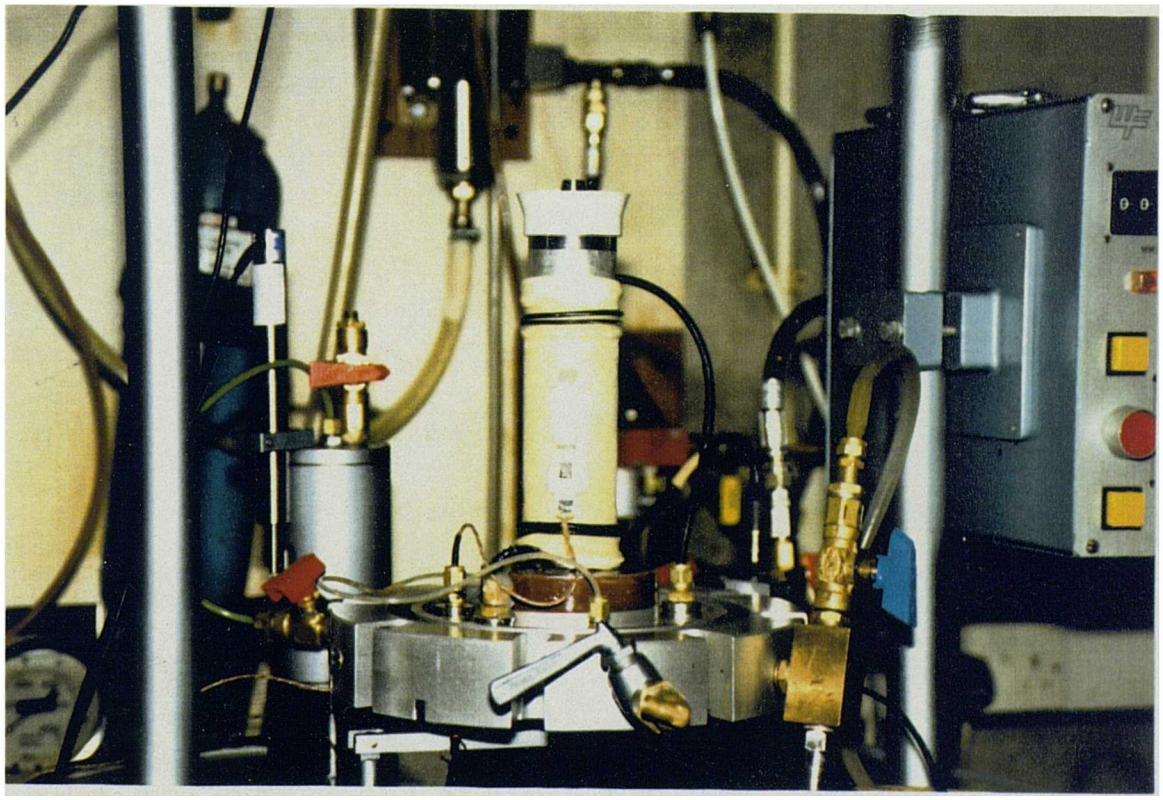

b)

Fig. 3.2 The Hall effect transducers: a) schematic b) mounted on a triaxial sample

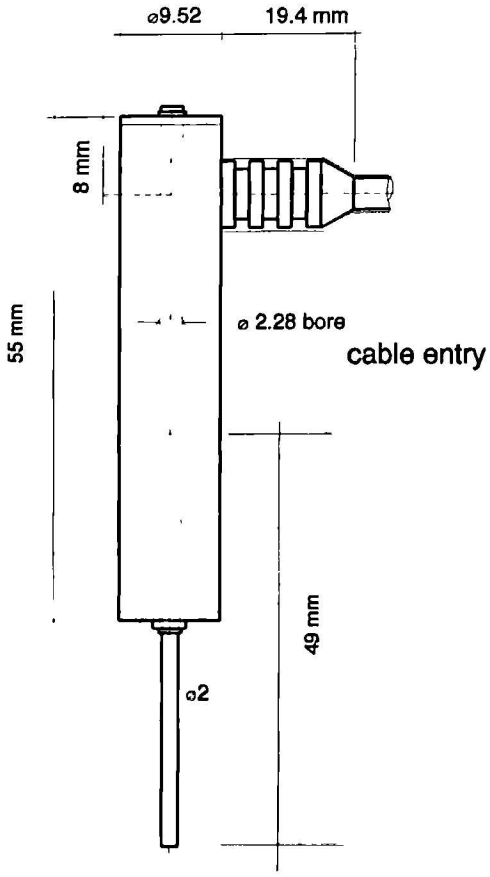

a)

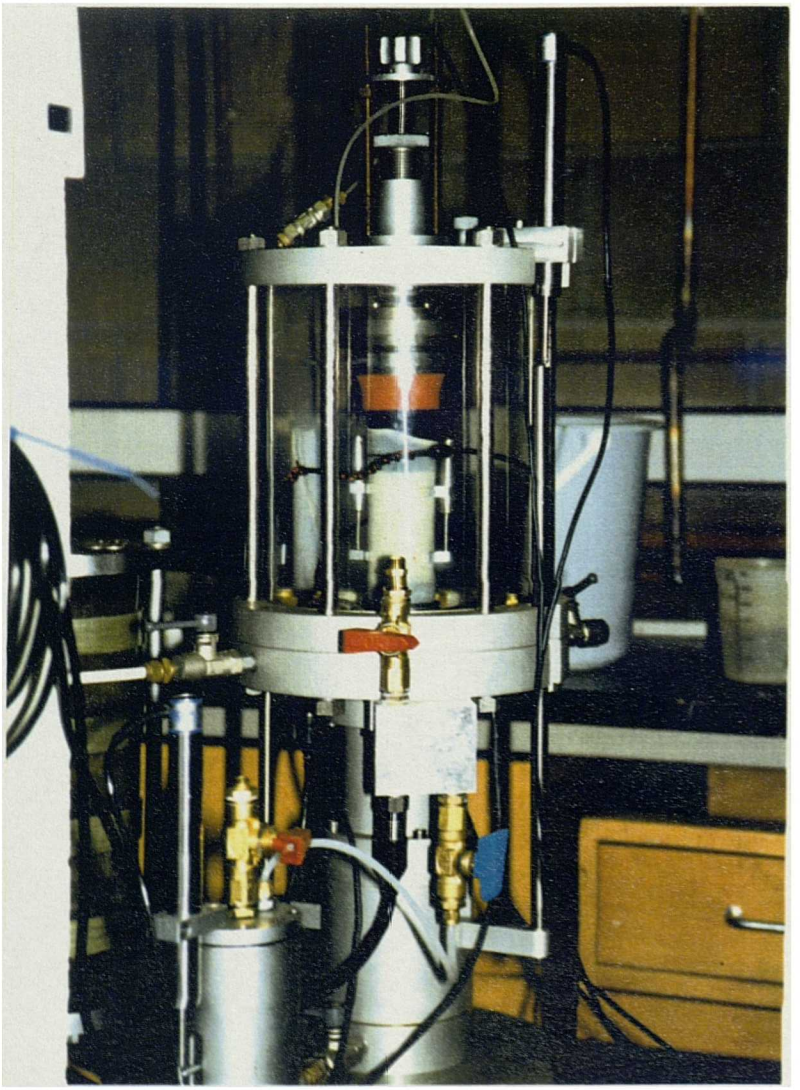

b)

Fig 3 3 LVDT (RDP D5/200): a) schematic b) mounted on a triaxial sample

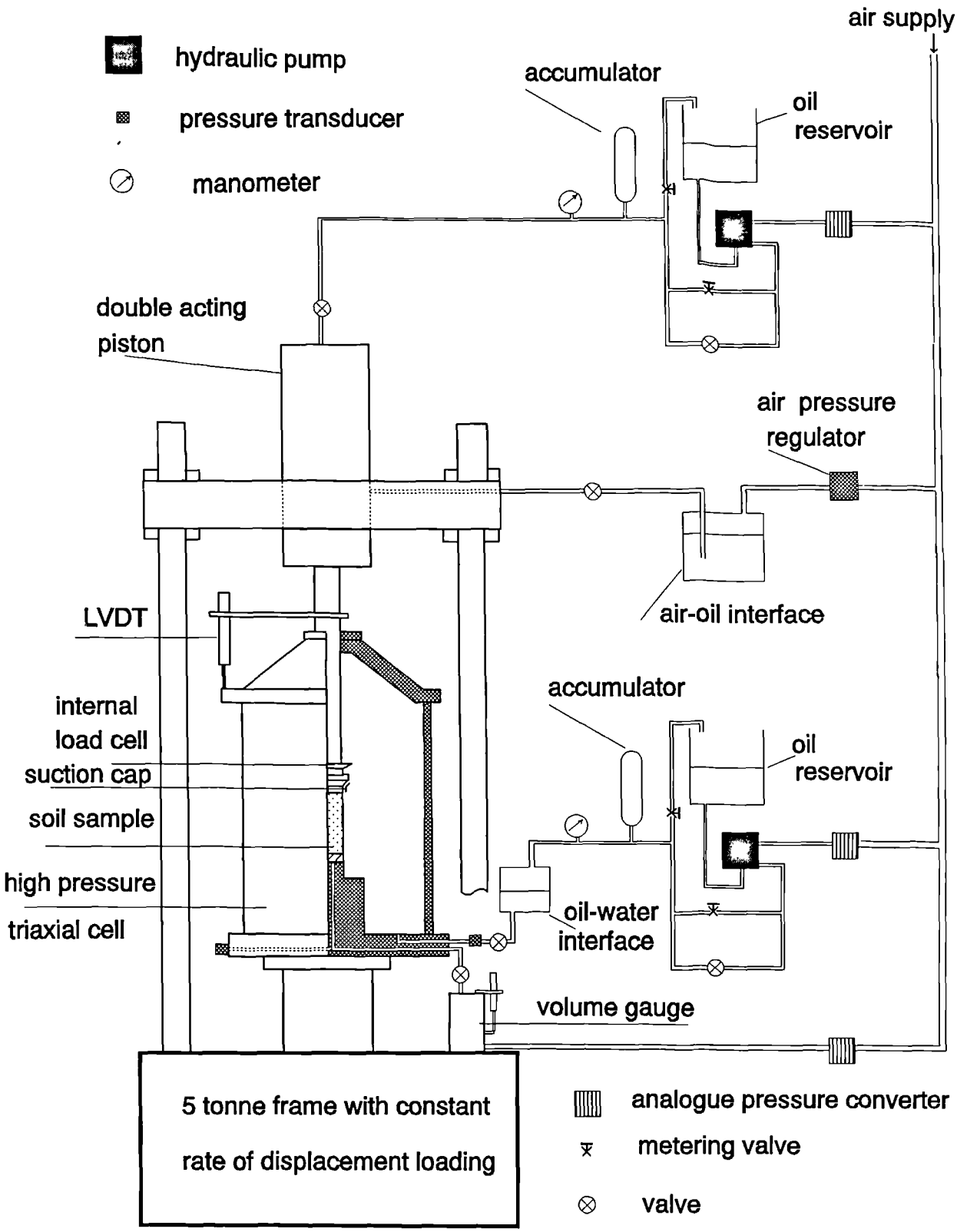

Fig. 3.4 The high pressure triaxial apparatus with a capacity of 5MPa

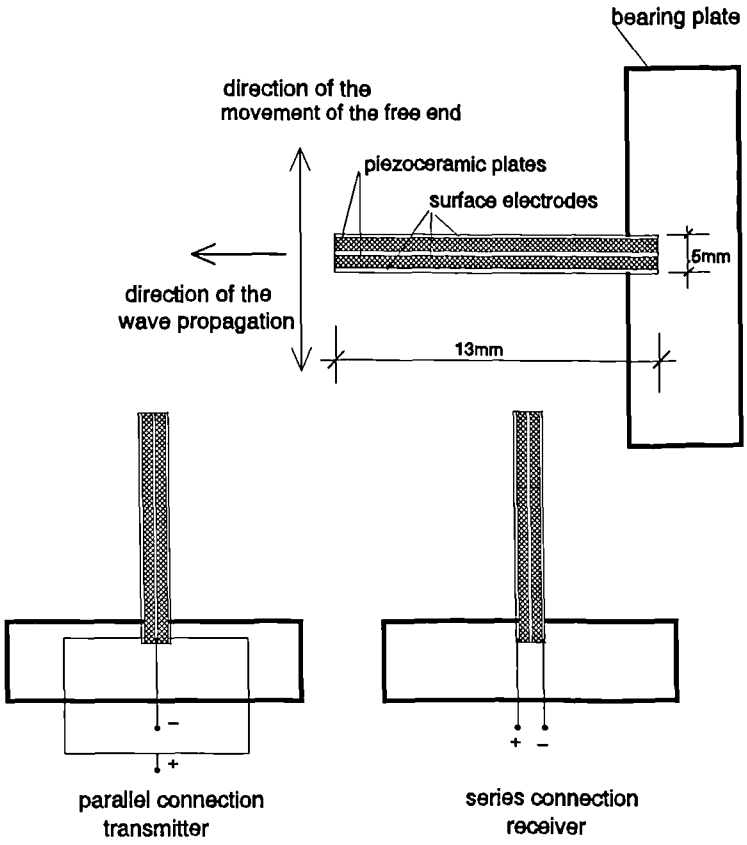

Fig. 3.7 Schematic of a bender element

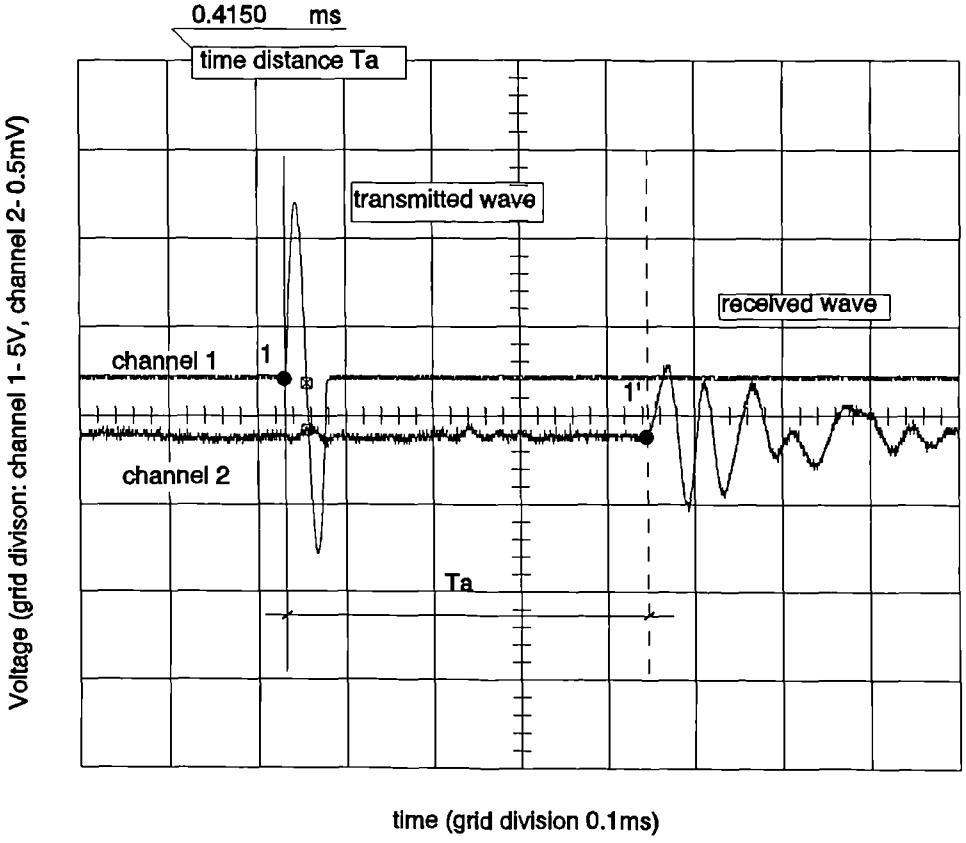

Fig. 3.8 Characteristic points of measurement of the arrival time from the screen of the oscilloscope

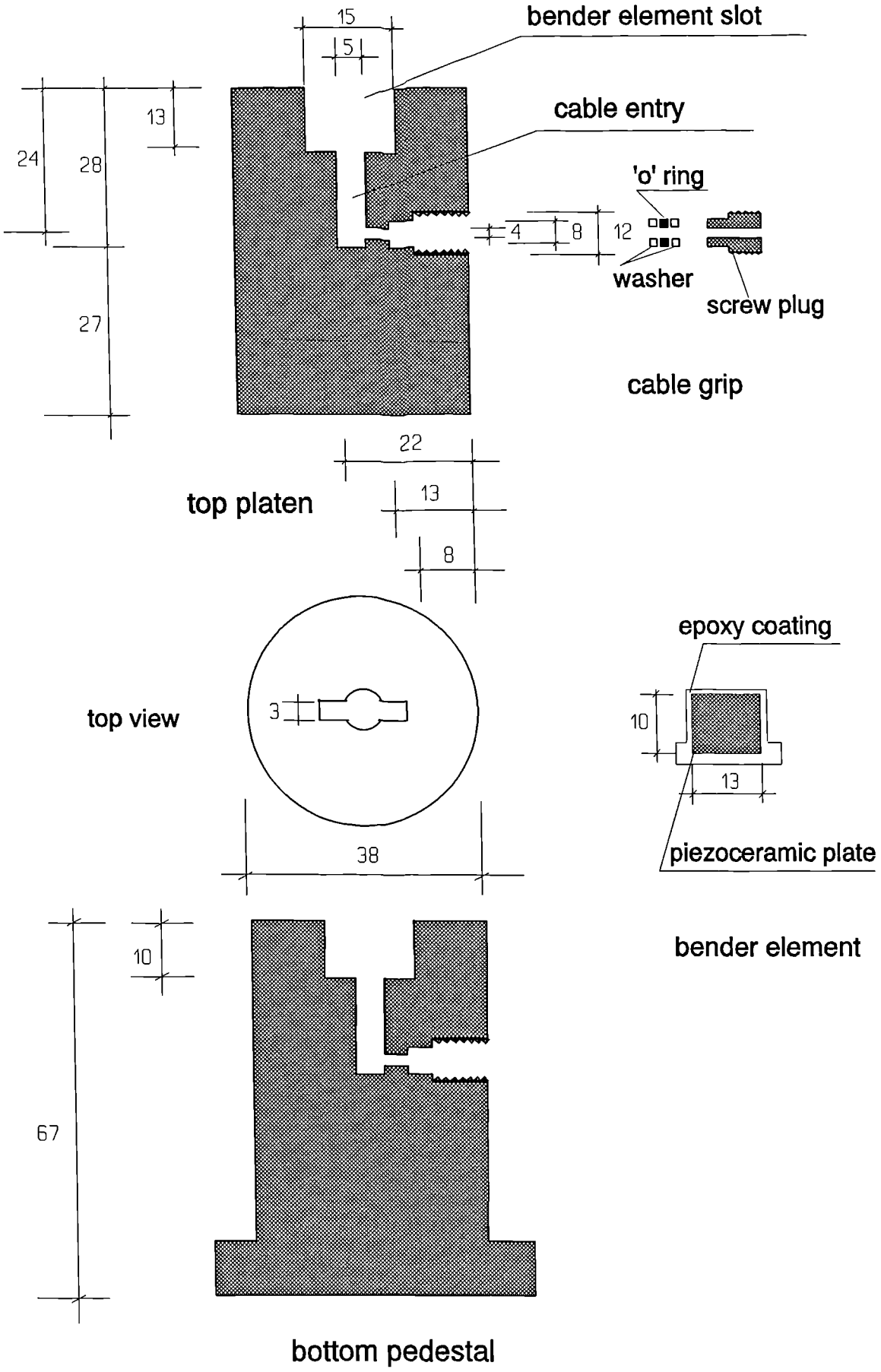

Fig. 3.9 Design details of the top cap and the bottom pedestal (dimensions in mm)

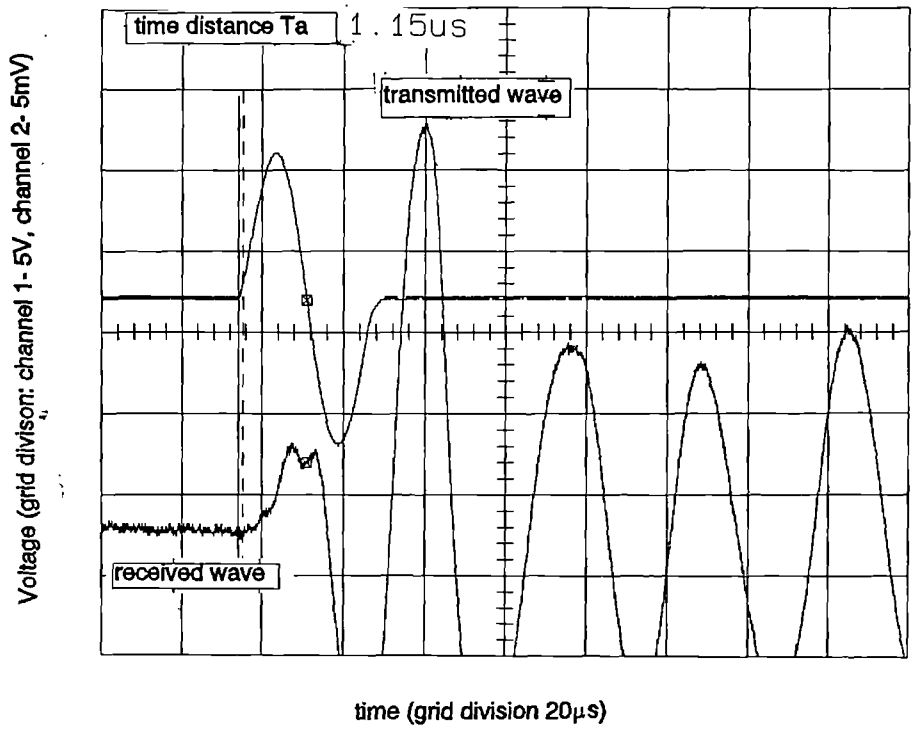

a)

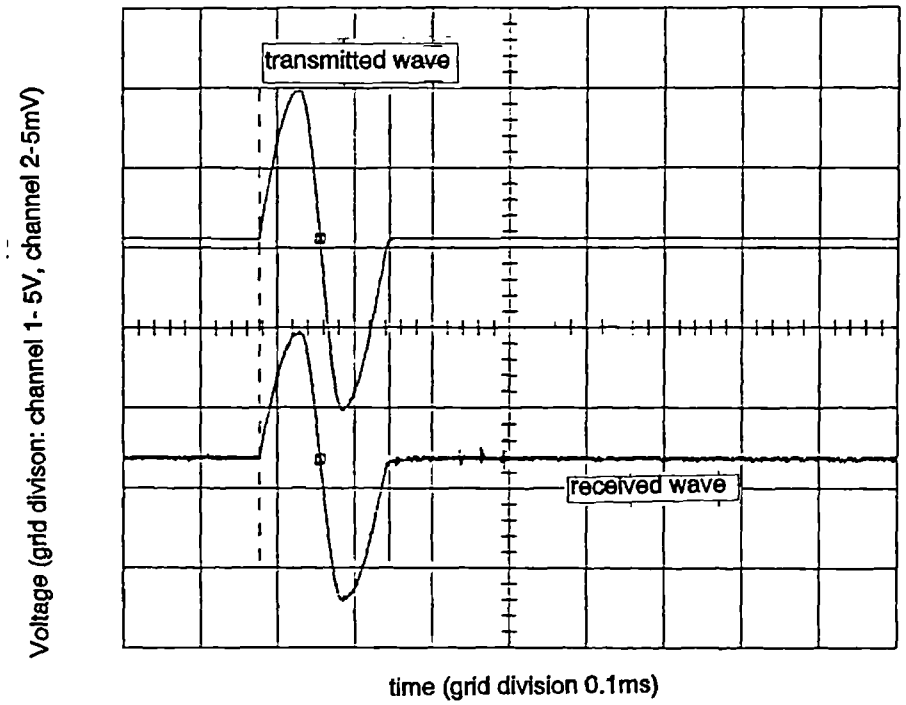

b)

Fig. 3.10 Preliminary checks of the receiver rising time: a) elements in contact, b) self-monitoring element

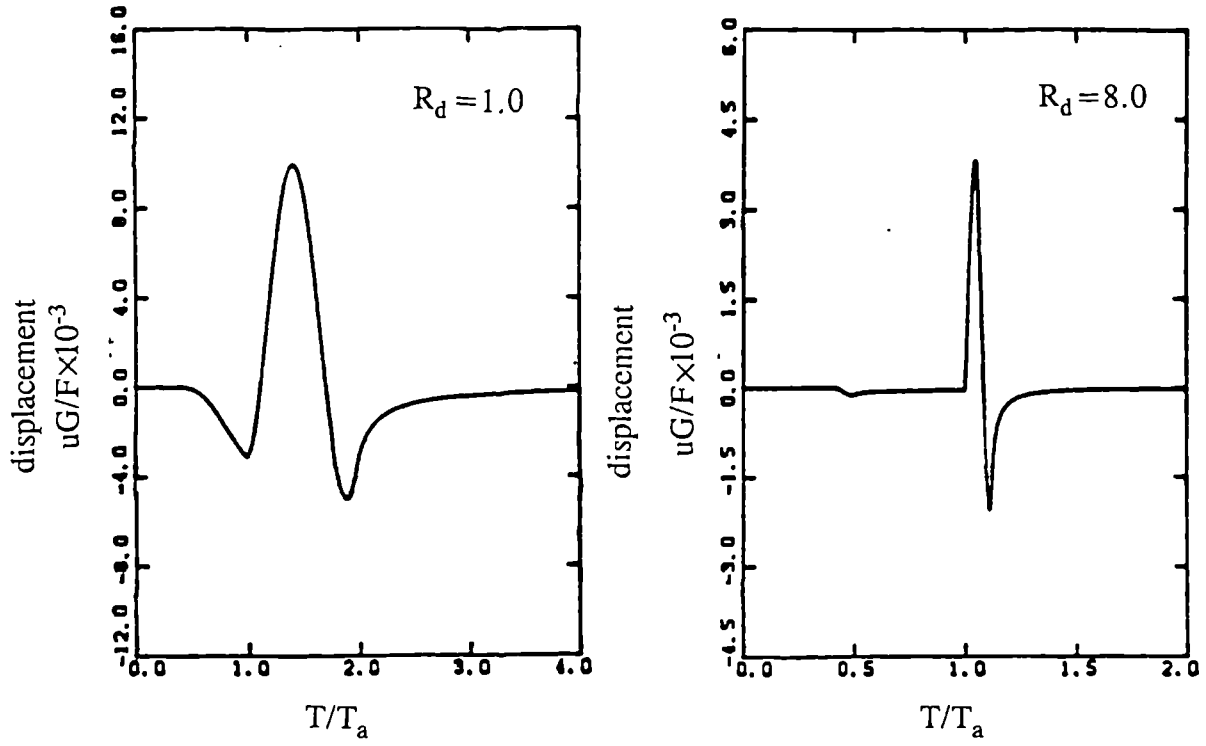

Fig. 3.11 Analytical solution for the motion at the monitoring point (After Sanches Salinero at al., 1986), (u= particle displacement, F=amplitude of loading force)

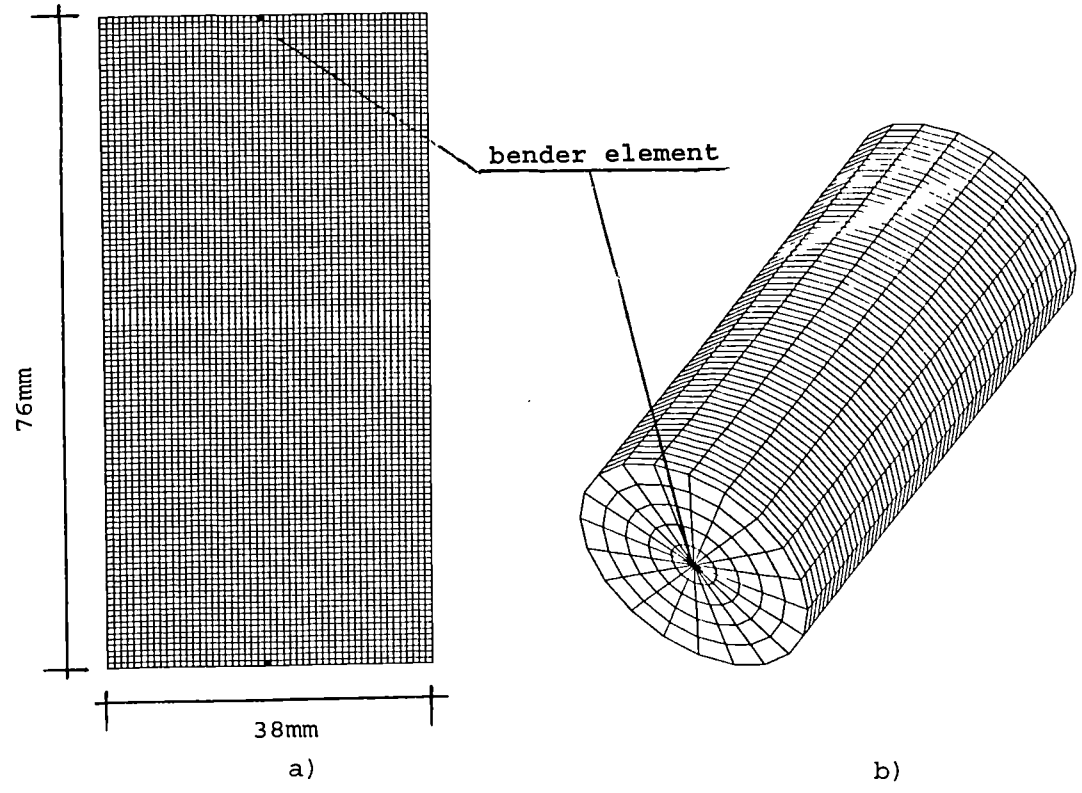

Fig. 3.12 Finite element mesh for: a) 2D analysis, b) 3D analysis

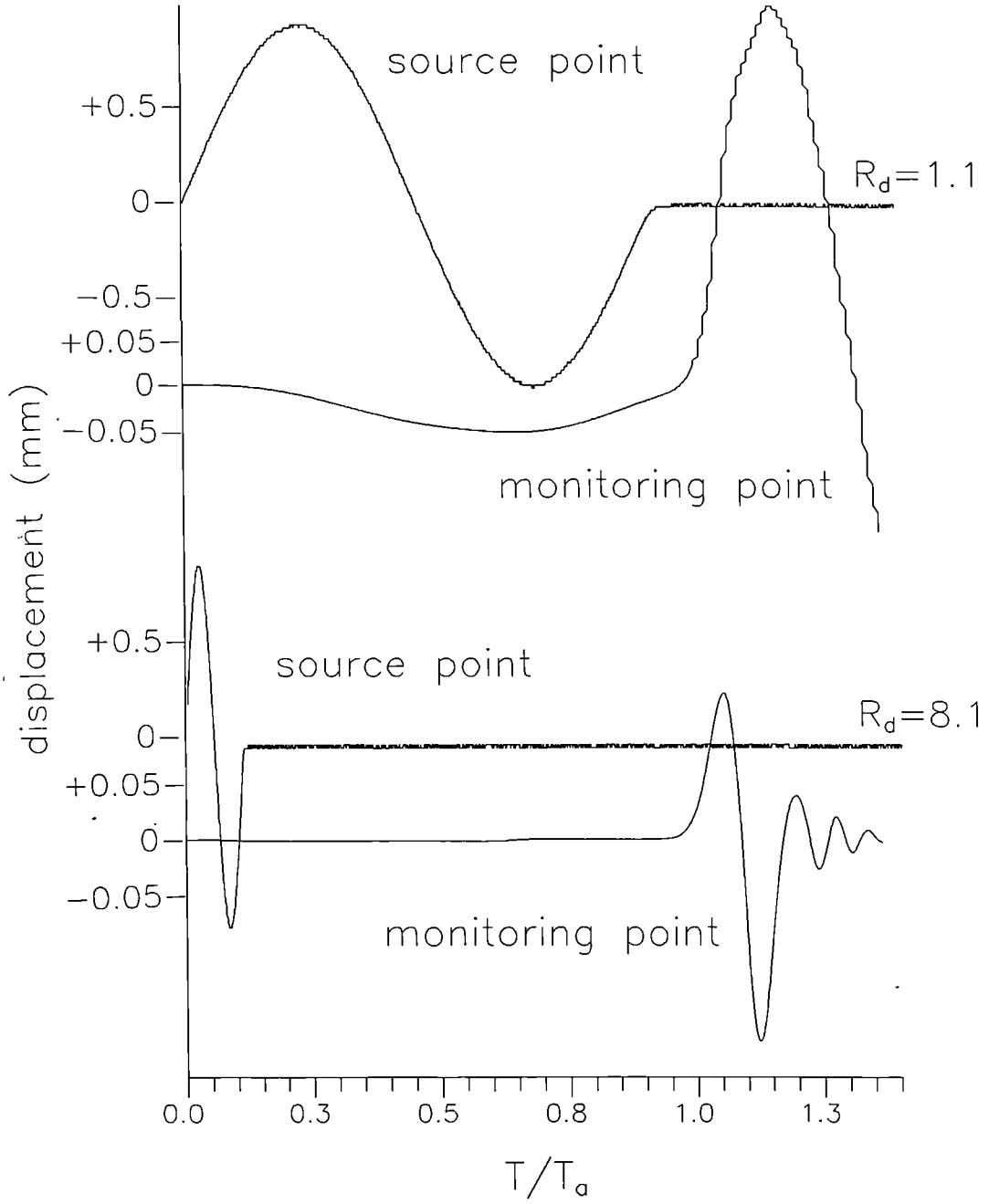

Fig. 3.13 Finite element solutions for the motion at the monitoring node (2D analysis)

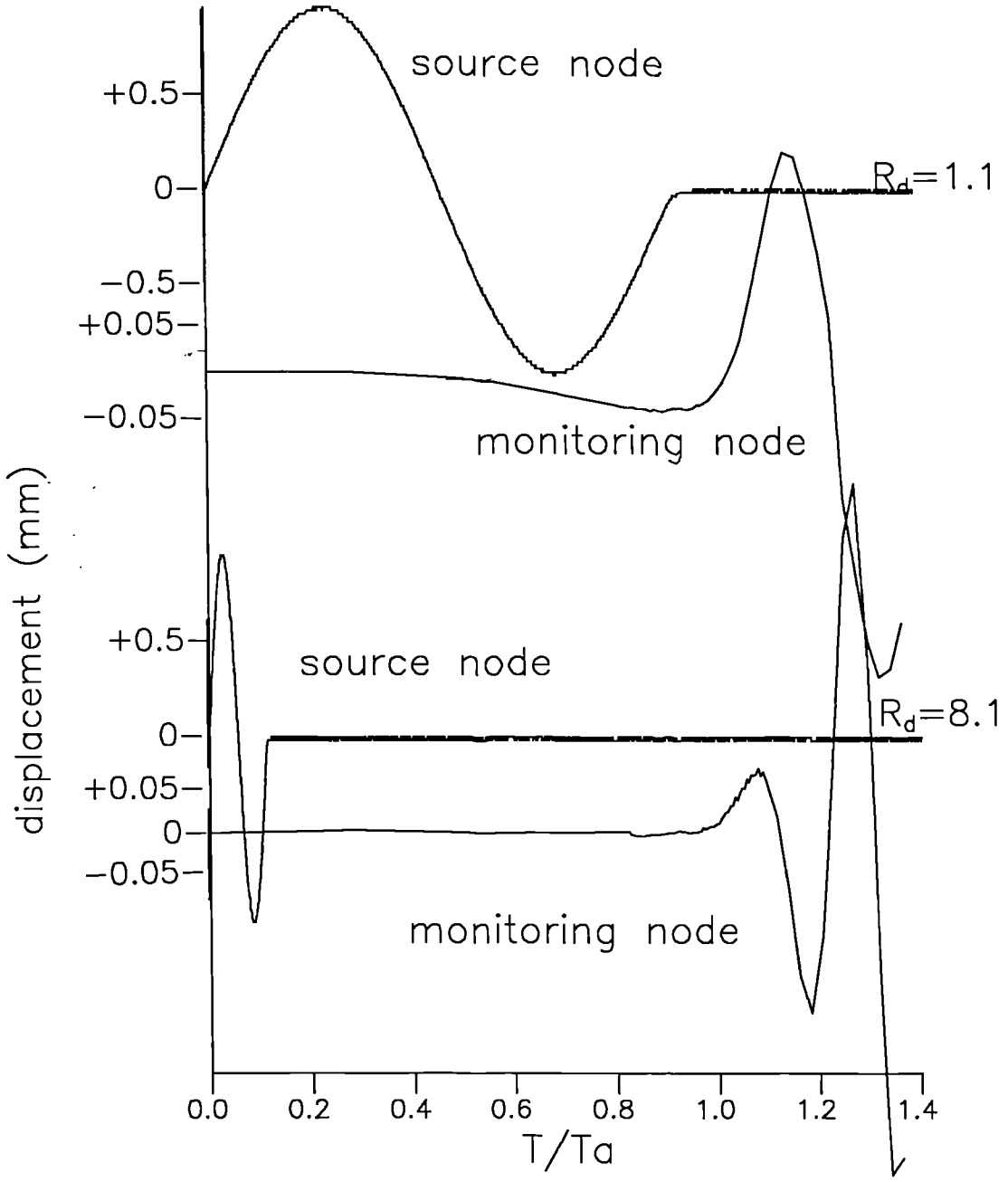

Fig. 3.14 Finite element solutions for the motion at the monitoring node (3D analysis)

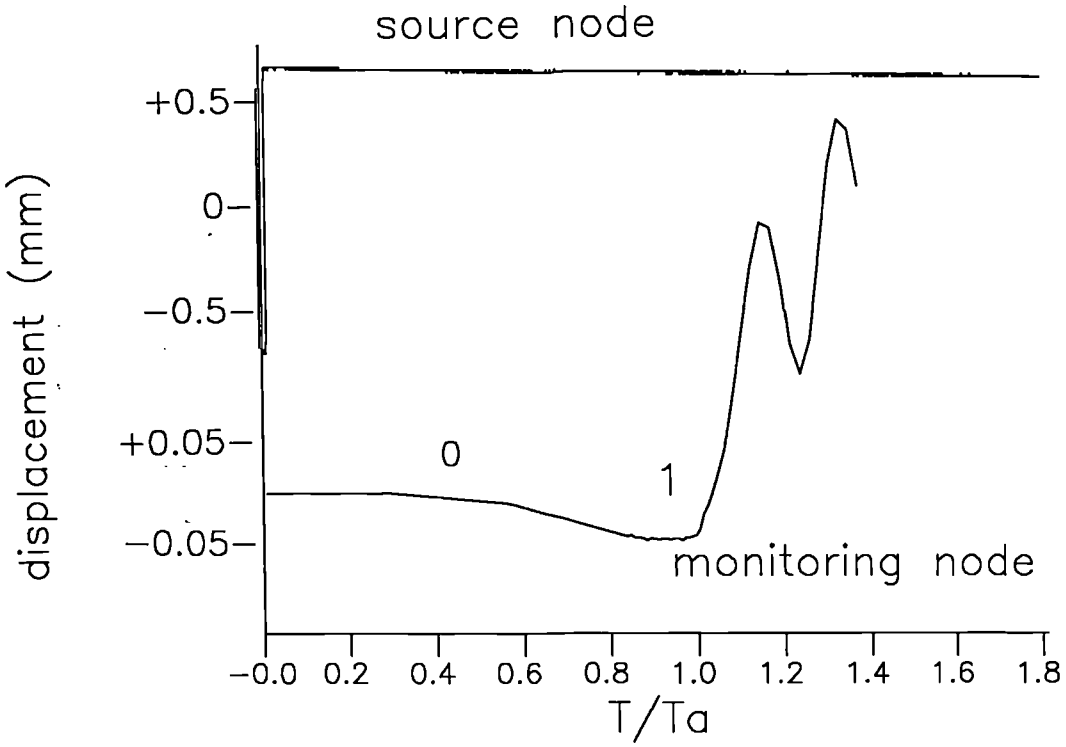

Fig. 3.15 Finite element solution for the motion at the monitoring node for a square wave at the source (3D analysis)

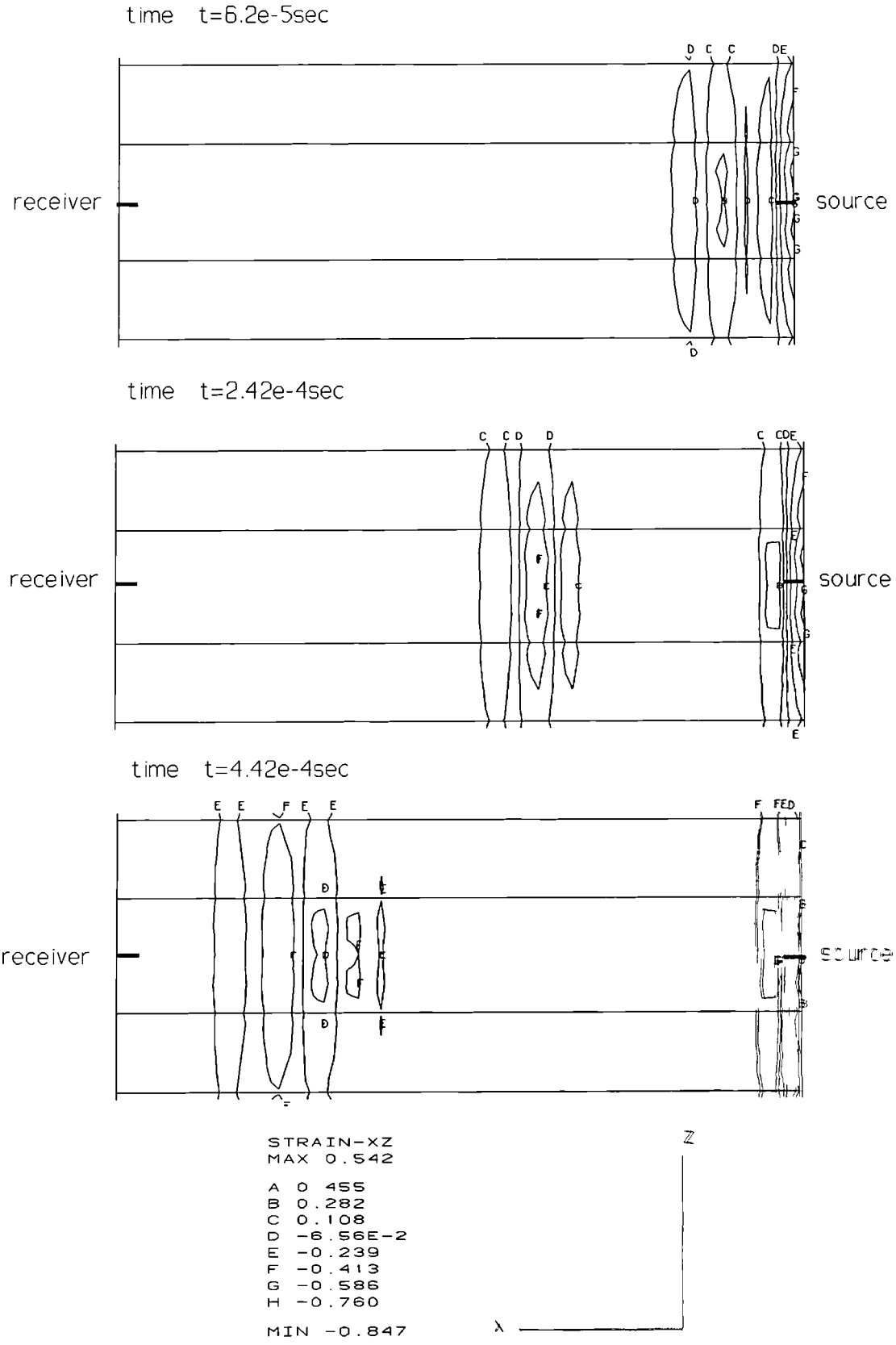

Fig. 3.16 Finite element solution for strain contours in the plane of the motion

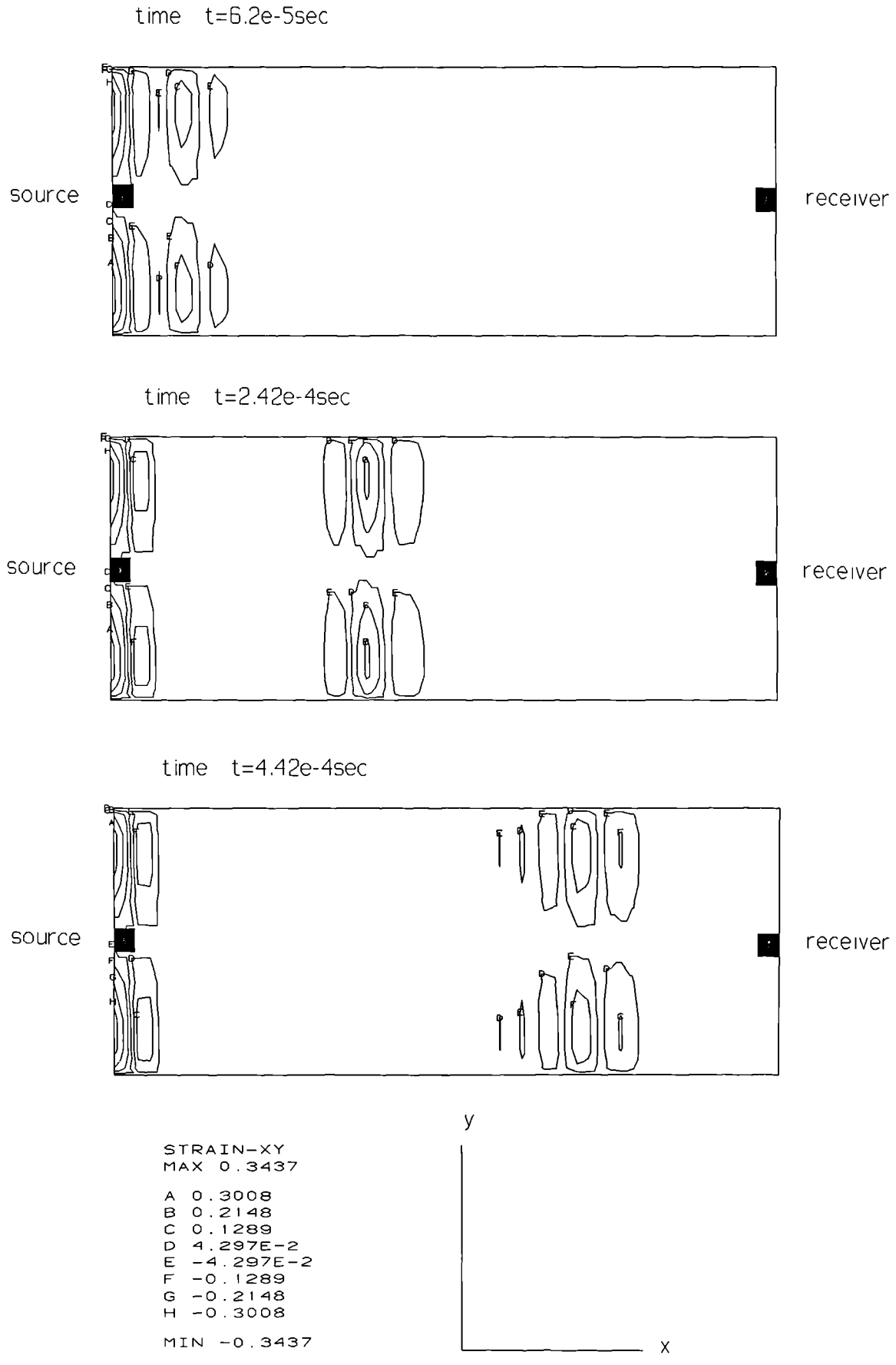

Fig. 3.17 Finite element solution for strain contours in the plane perpendicular to the motion

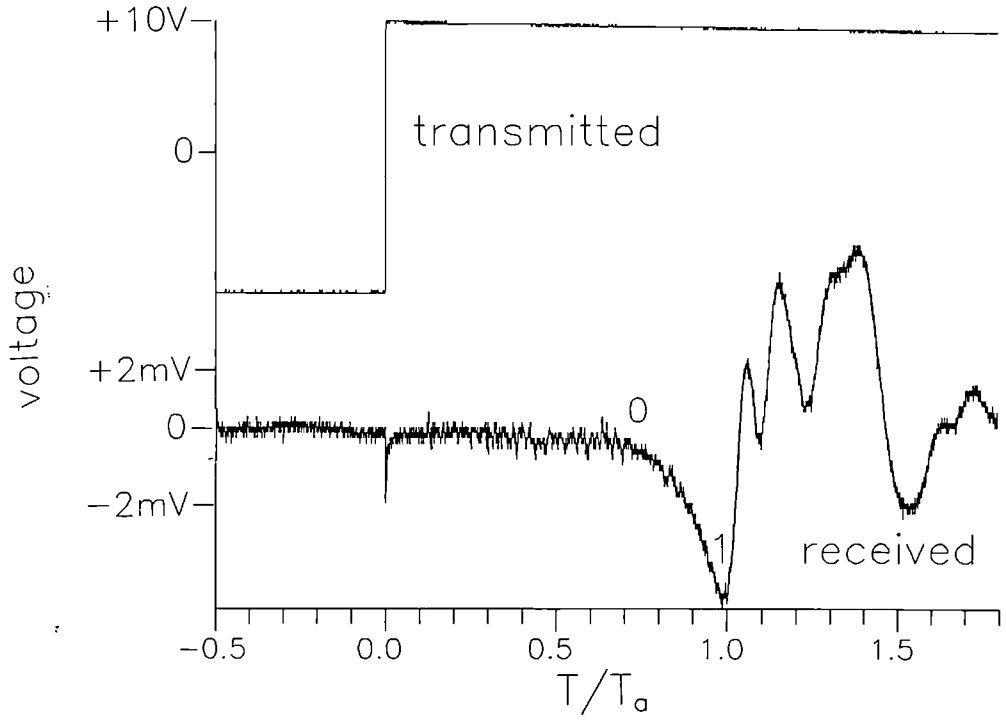

Fig. 3.18 Typical test data for a square input wave

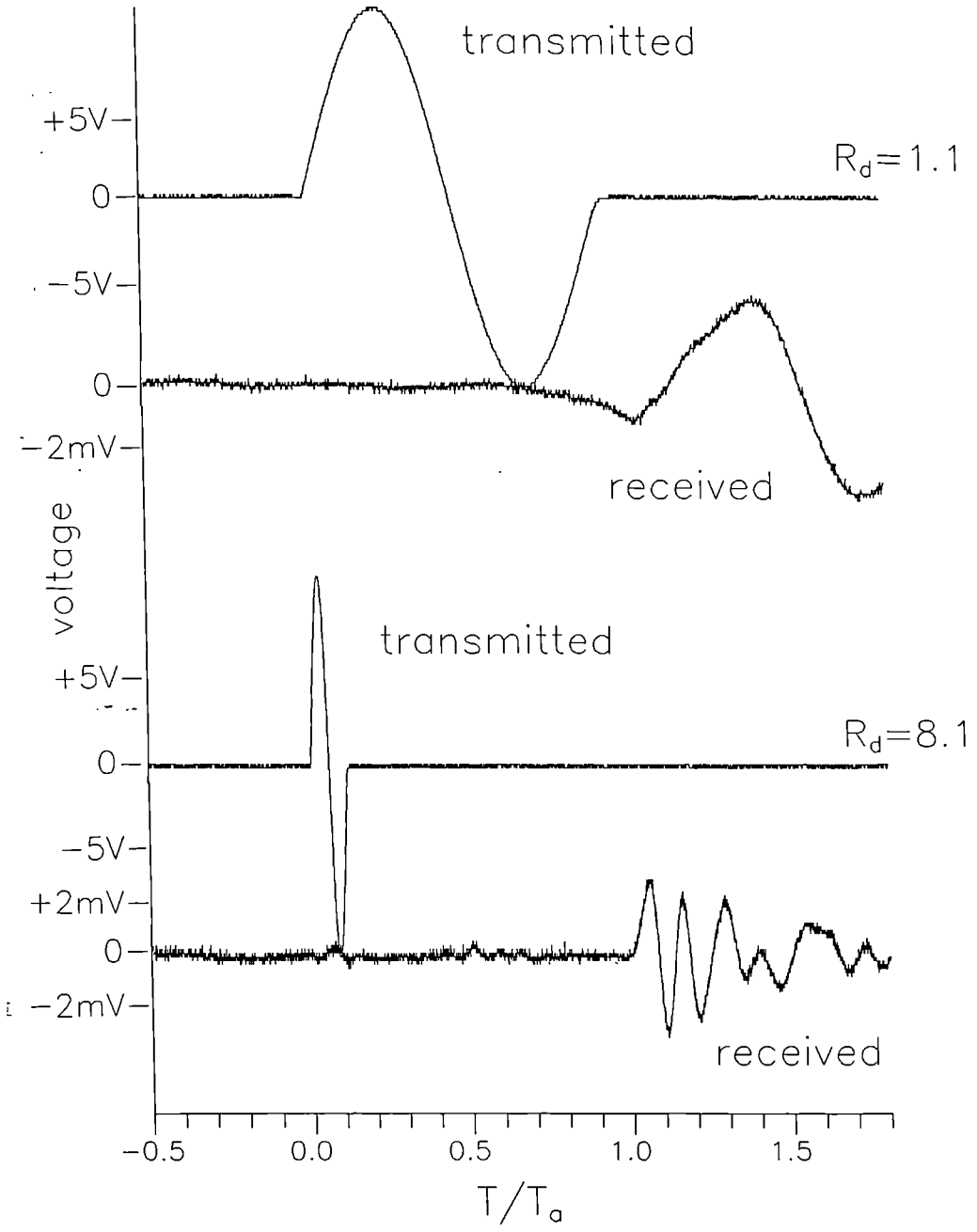

Fig. 3.19 Typical test data for a sinusoidal input wave

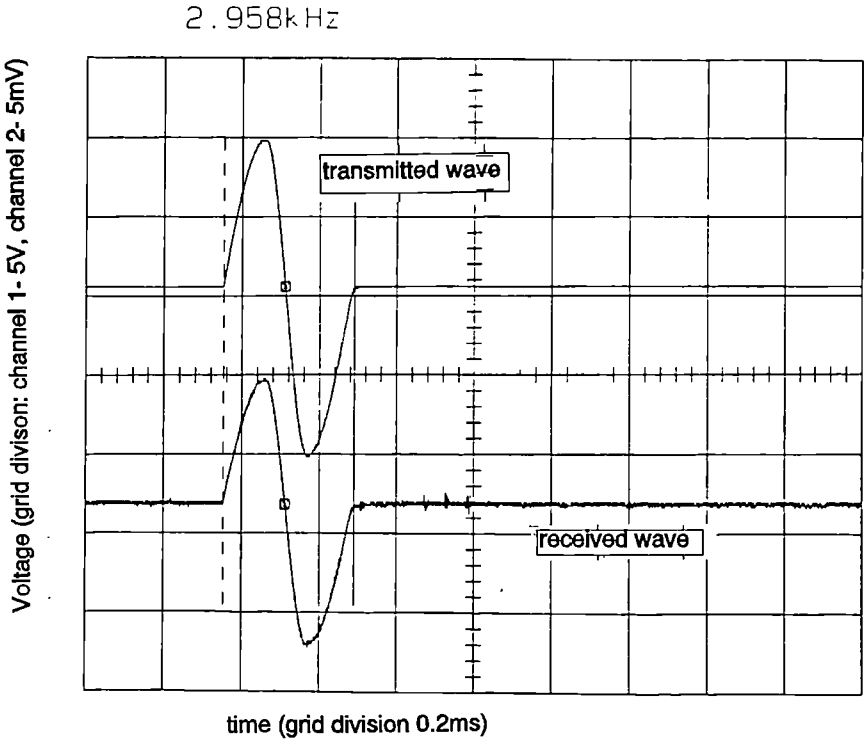

a) Frequency of the input wave f=2.96kHz

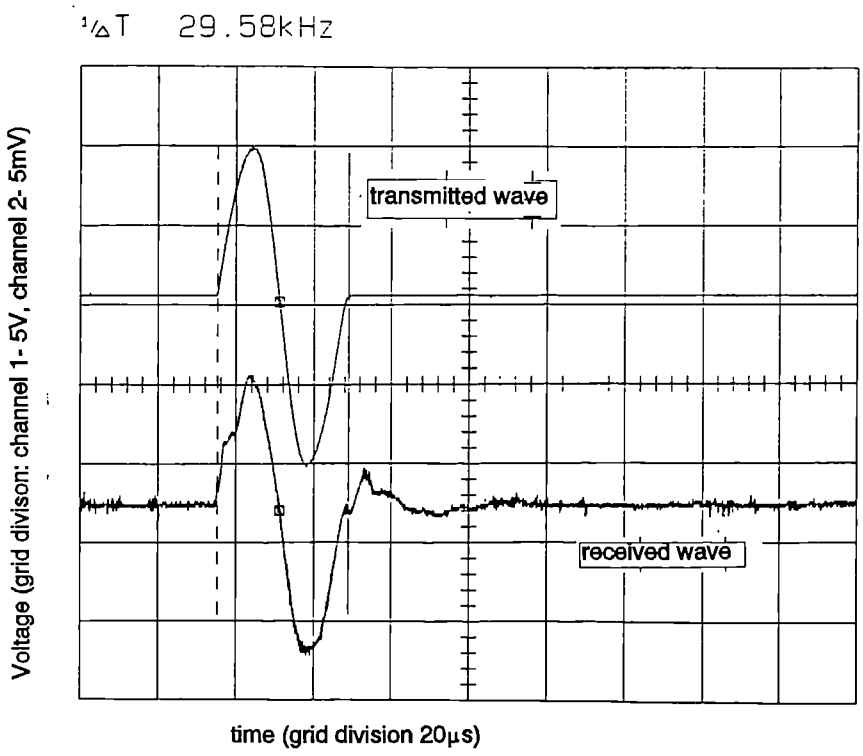

b) Frequency of the input wave f=29.6kHz

Fig. 3.20 Oscilloscope traces from a self-monitoring element in a cemented sand

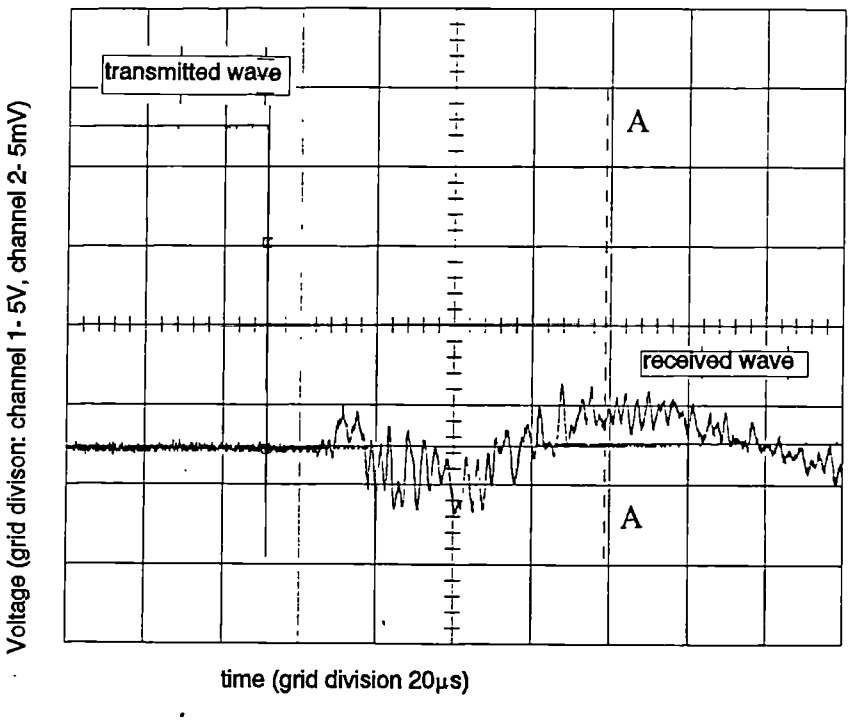

Fig. 3.21 Oscilloscope trace showing overshooting for a square wave in soft rock

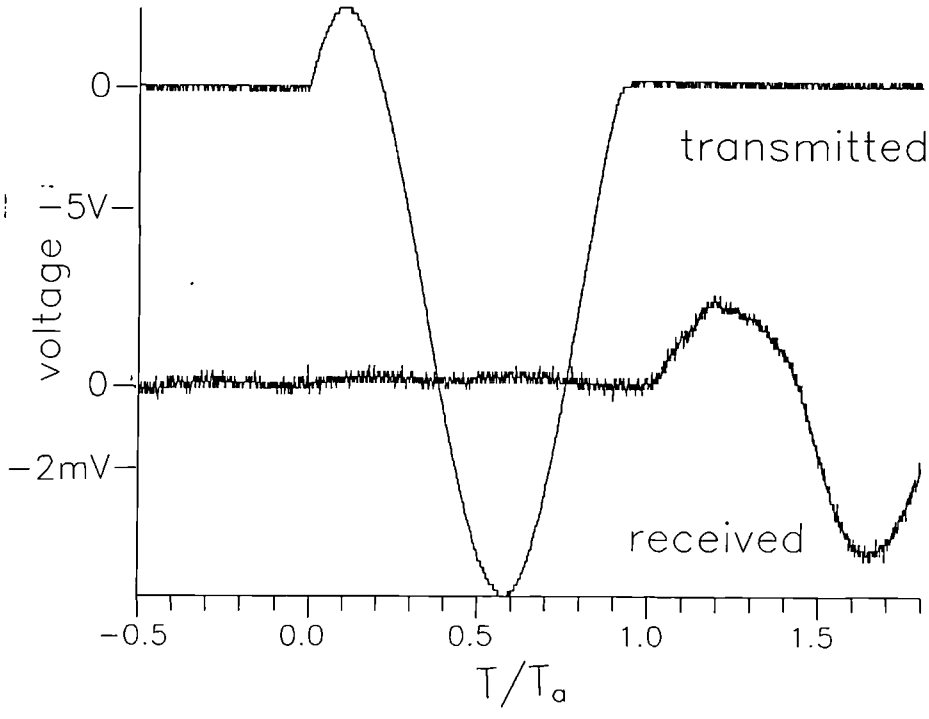

Fig. 3.22 Cancelling the near field effect with a modified sine wave

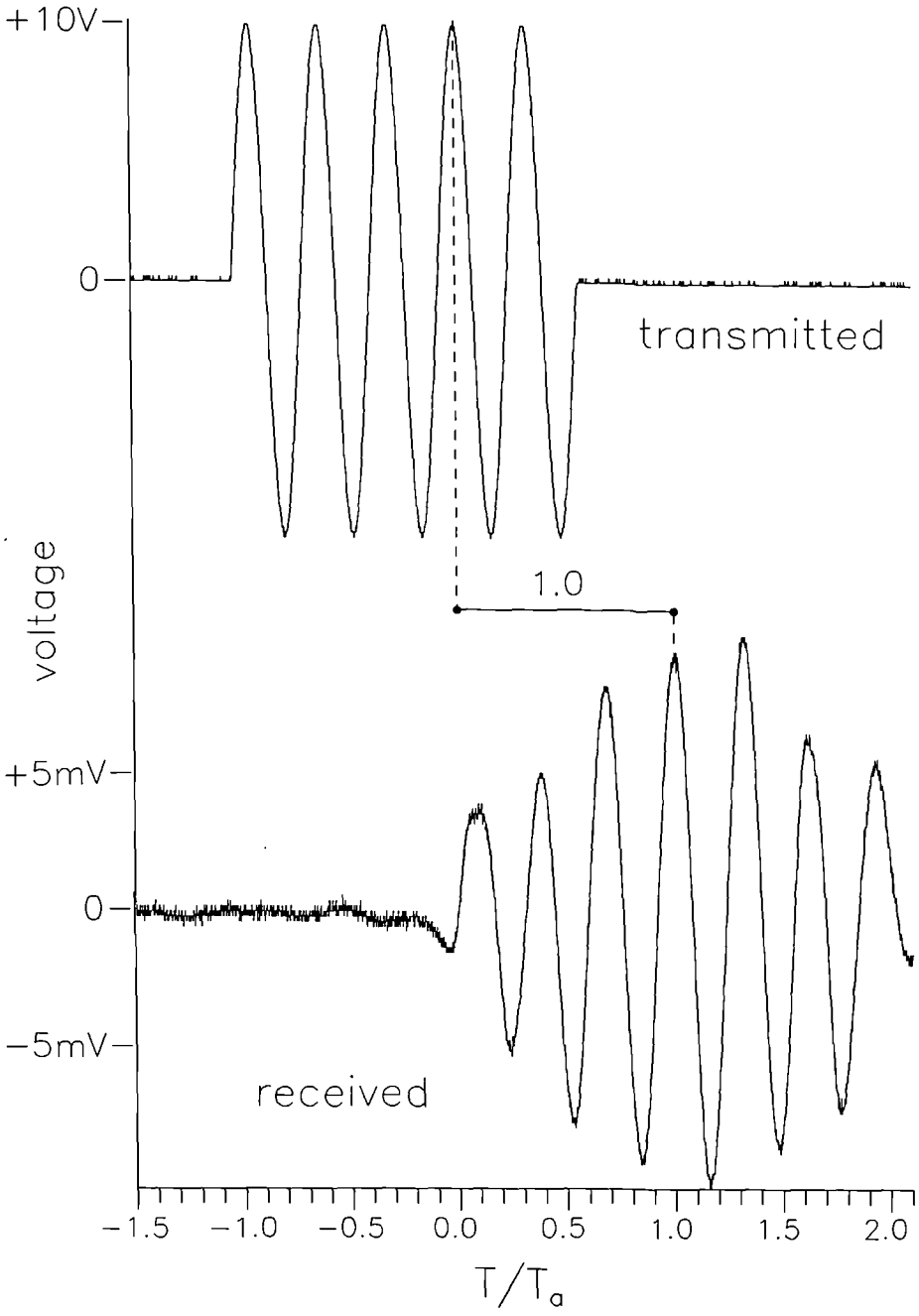

Fig. 3.23 Resonance of the receiving element

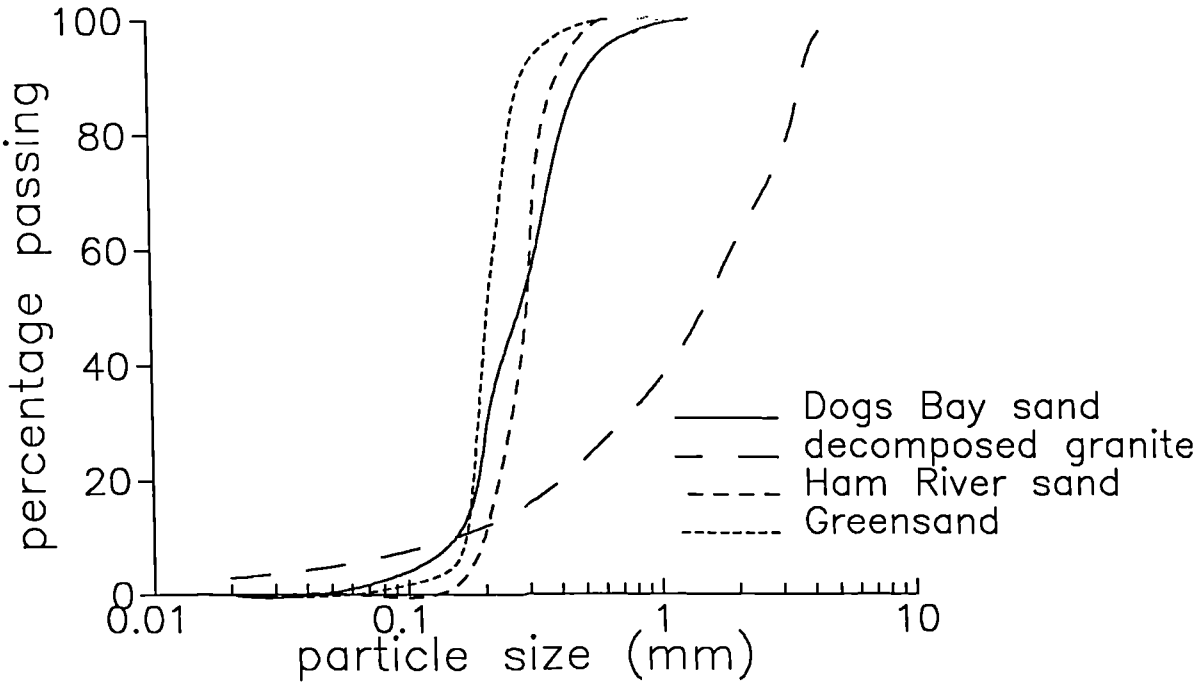

Fig. 4.1 Gradings curves for the four reconstituted sands (adapted from Coop & Lee, 1993 and Cuccovillo, 1995)

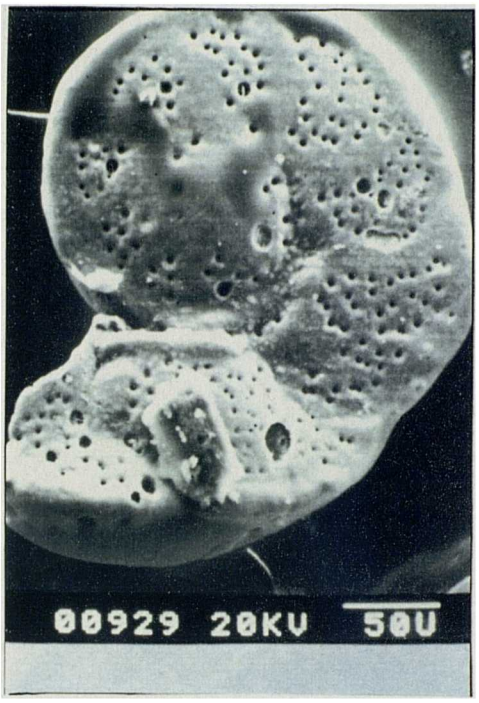

a) Dogs Bay sand

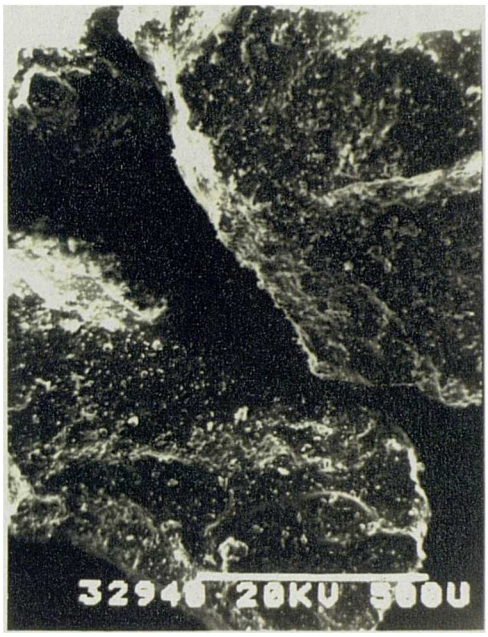

b) decomposed granite

c) Ham River sand

d) Lower Greensand

Fig. 4.2 Scanning electron micrographs of typical soil particles for the four sands (micrograph of Greensand after Cuccovillo, 1995)

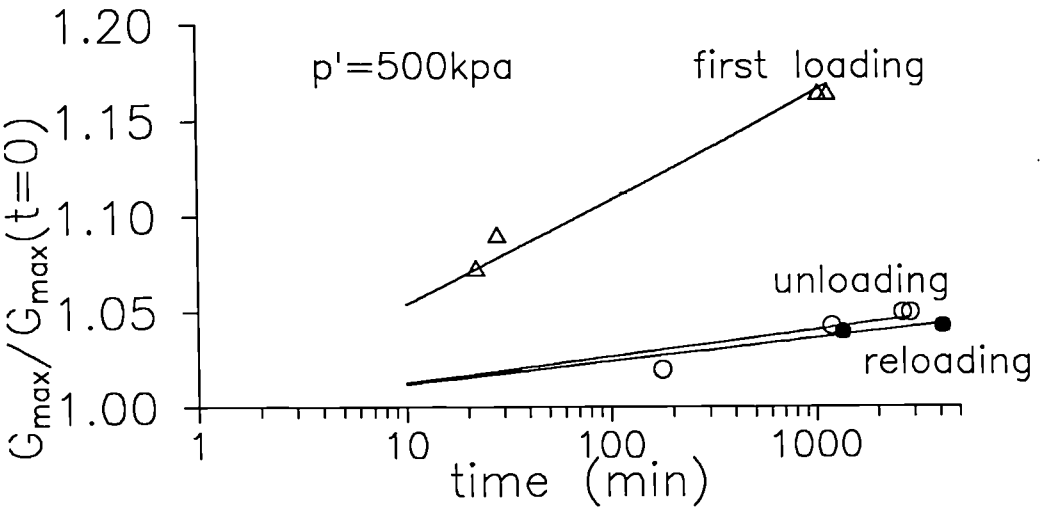

a) influence of current loading direction

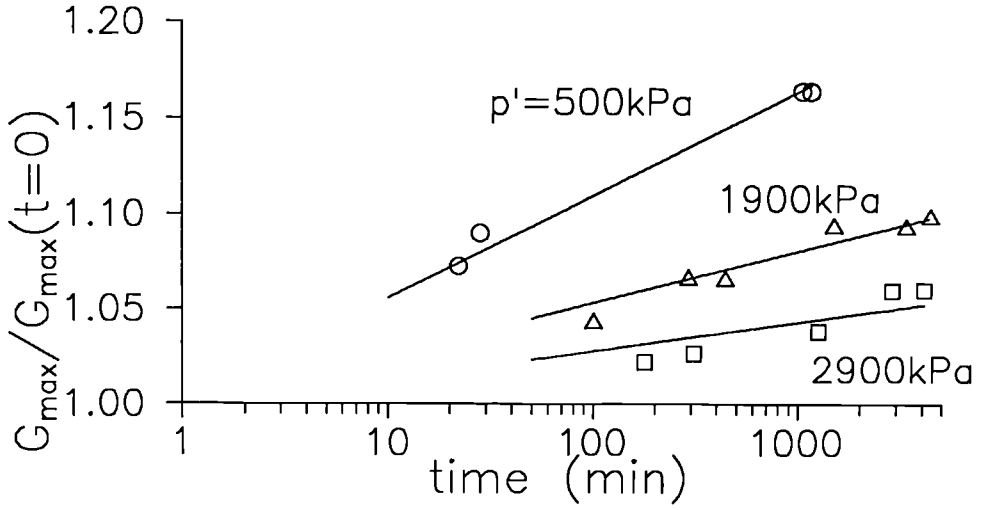

b) influence of confining stress

Fig. 4.3 Creep test data for Dogs Bay sand

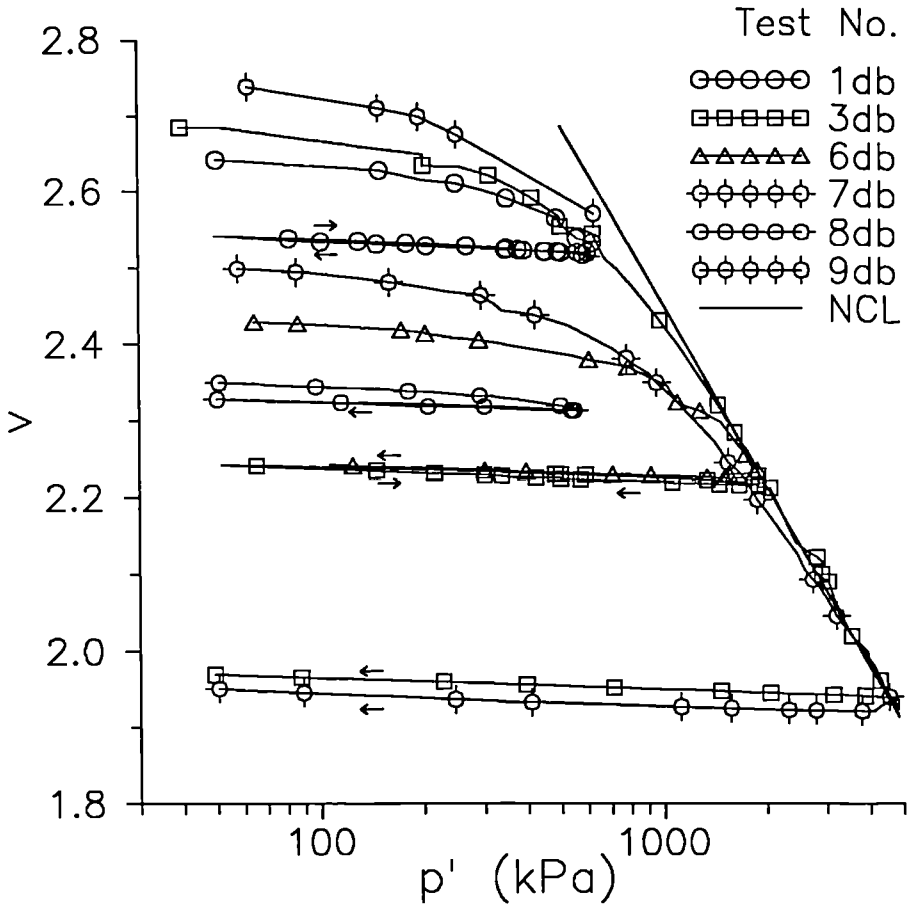

Fig. 4.4 Volumetric paths during isotropic compression and swelling of samples of Dogs Bay sand

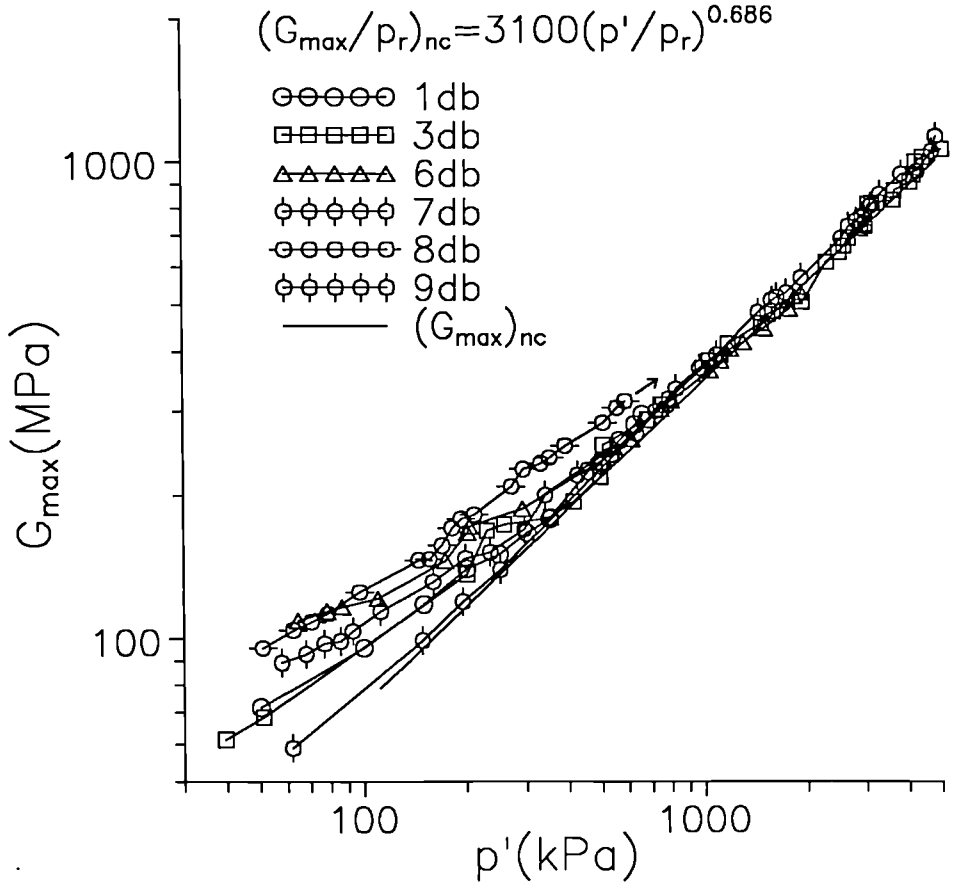

Fig. 4.5 Variation of G_{max} with isotropic stress p' for samples of Dogs Bay sand under first loading

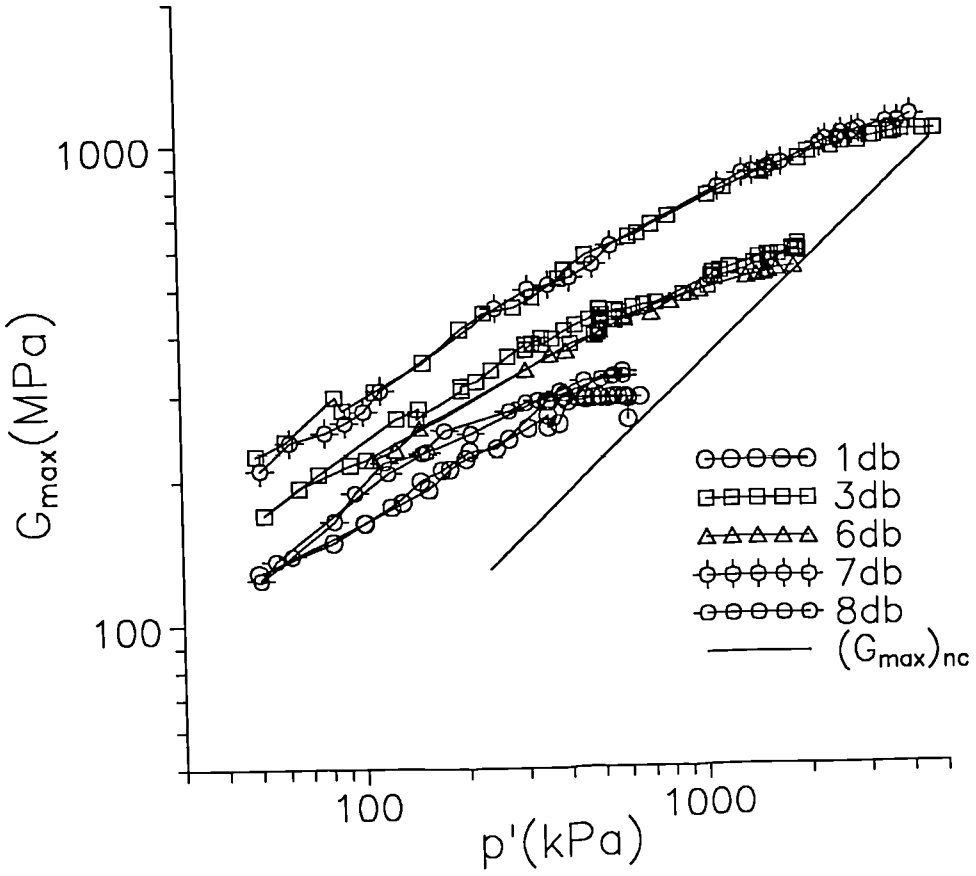

Fig. 4.6 Variation of G_{max} with isotropic stress p' for samples of Dogs Bay sand unloaded from the normal compression line

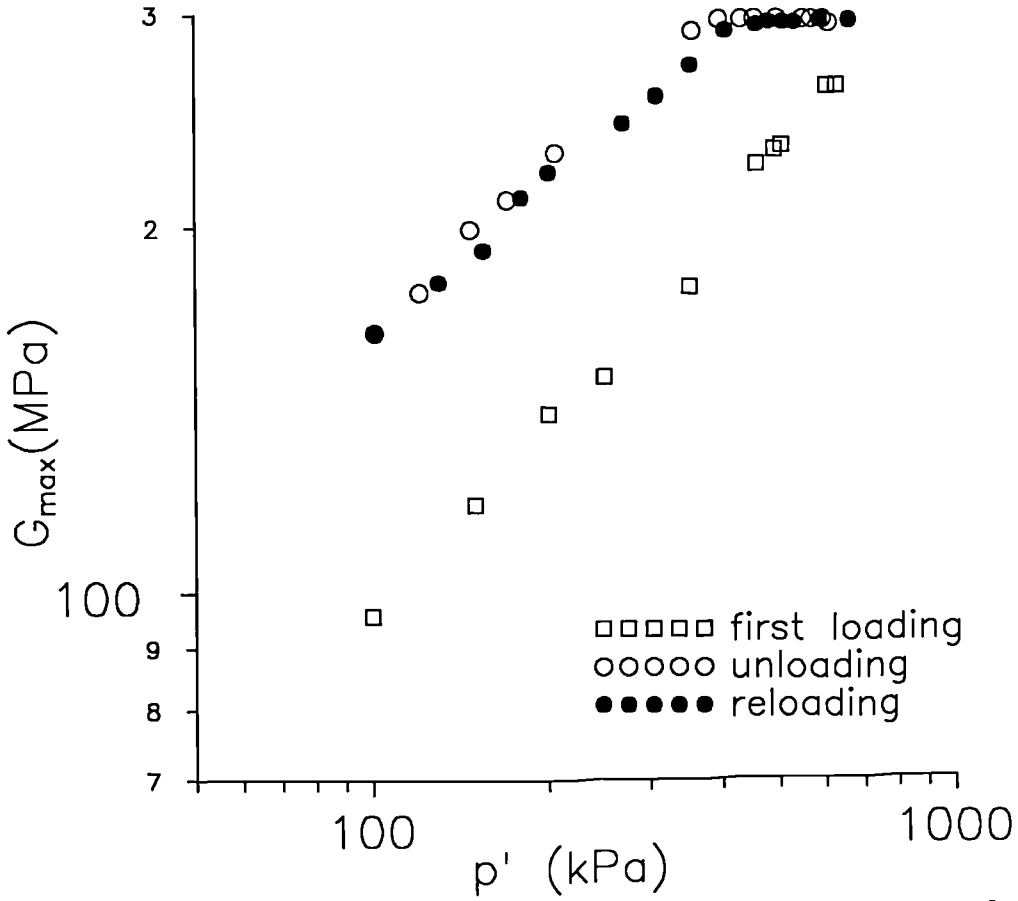

Fig. 4.7 Variation of G_{max} for isotropic swelling of a sample of Dogs Bay sand affected by creep (sample No. 1db)

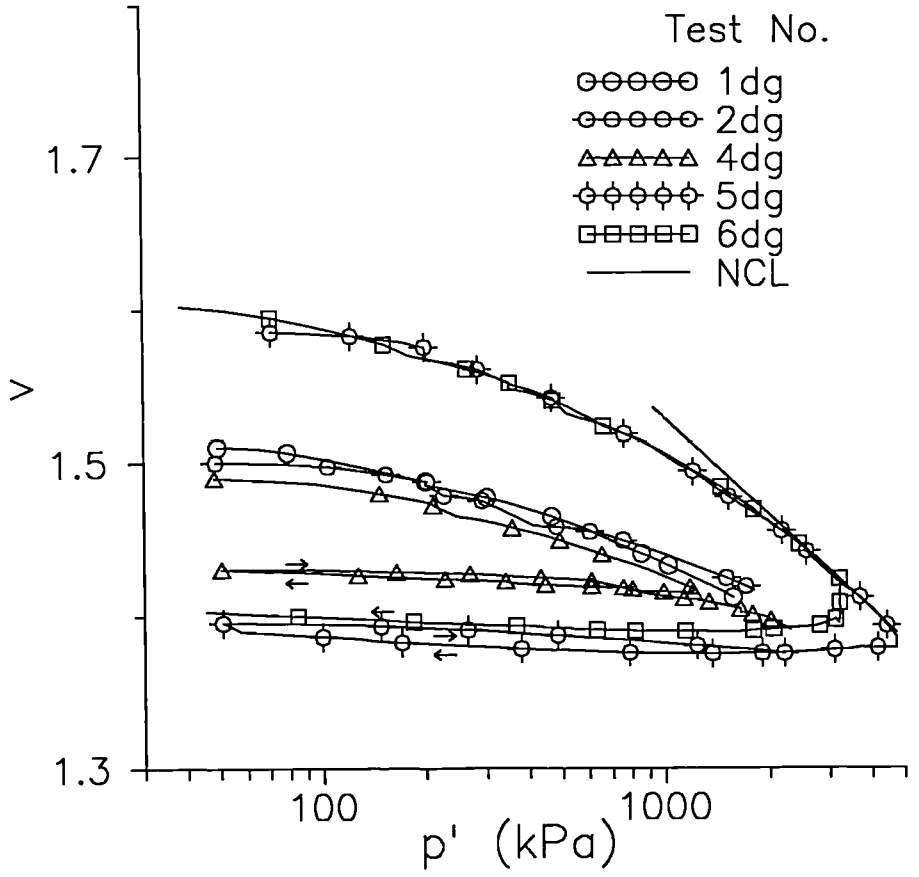

Fig. 4.8 Volumetric paths during isotropic compression and swelling of samples of decomposed granite

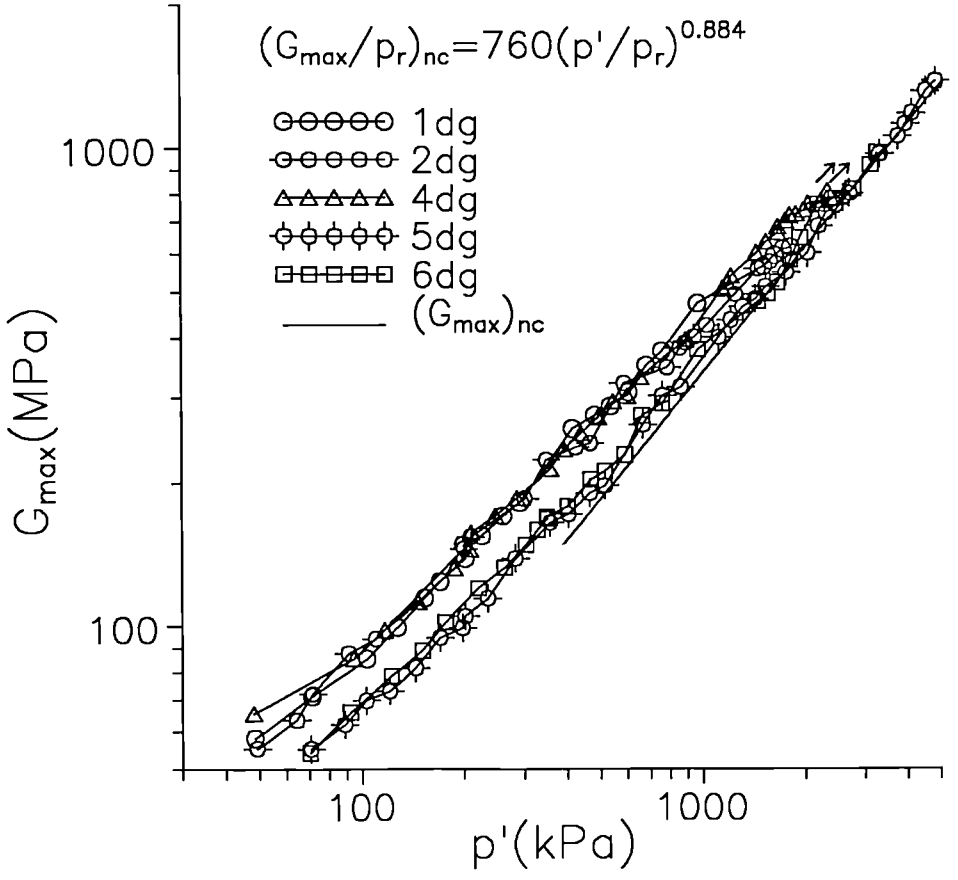

Fig. 4.9 Variation of G_{max} with isotropic stress p' for samples of decomposed granite under first loading

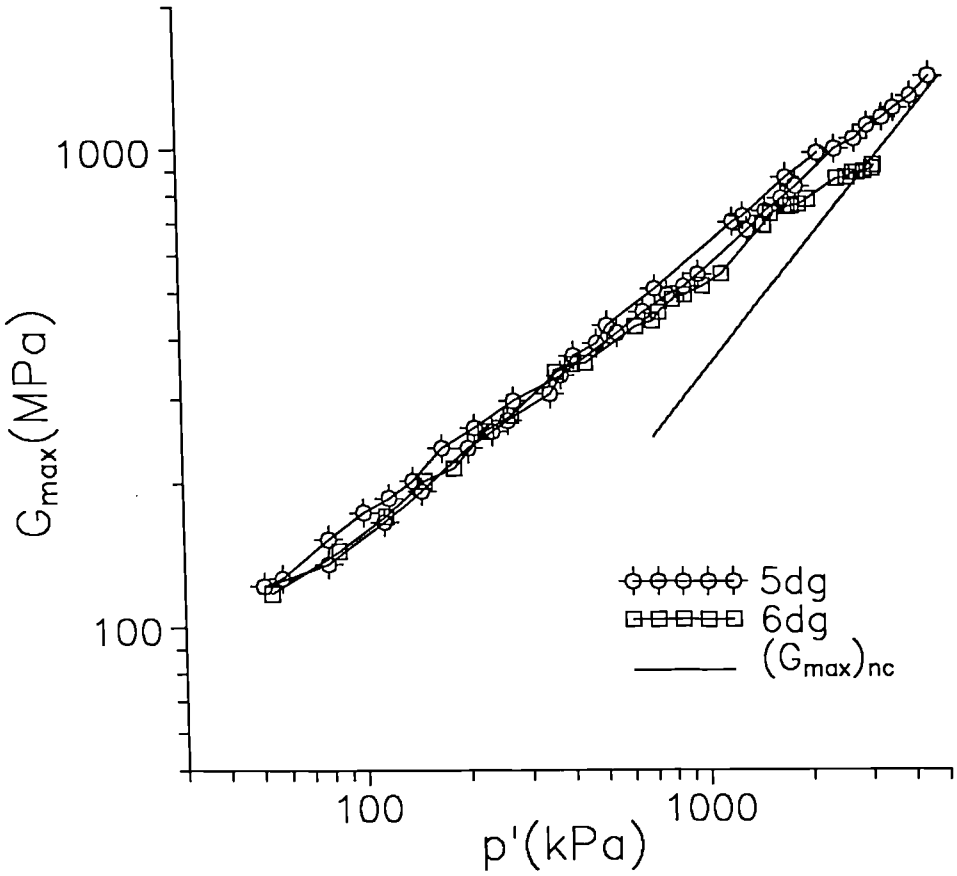

Fig. 4.10 Variation of G_{max} with isotropic stress p' for samples of decomposed granite unloaded from the normal compression line

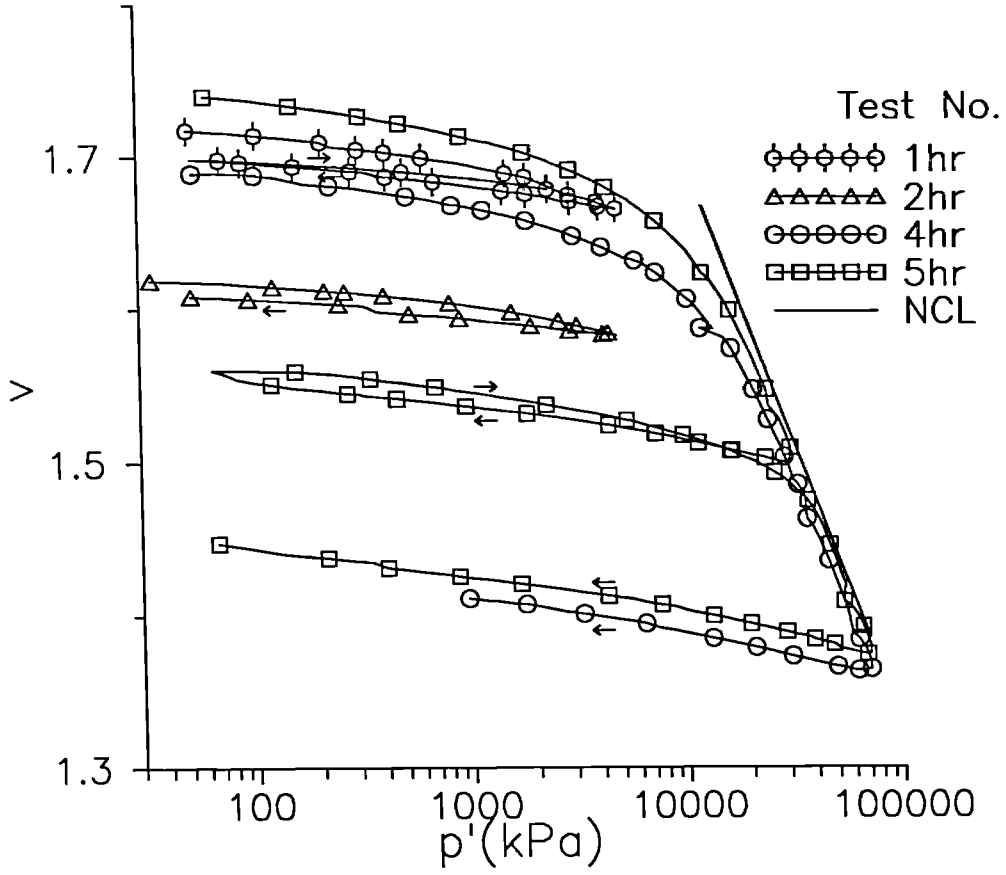

Fig. 4.11 Volumetric paths during isotropic compression and swelling of samples of Ham River sand

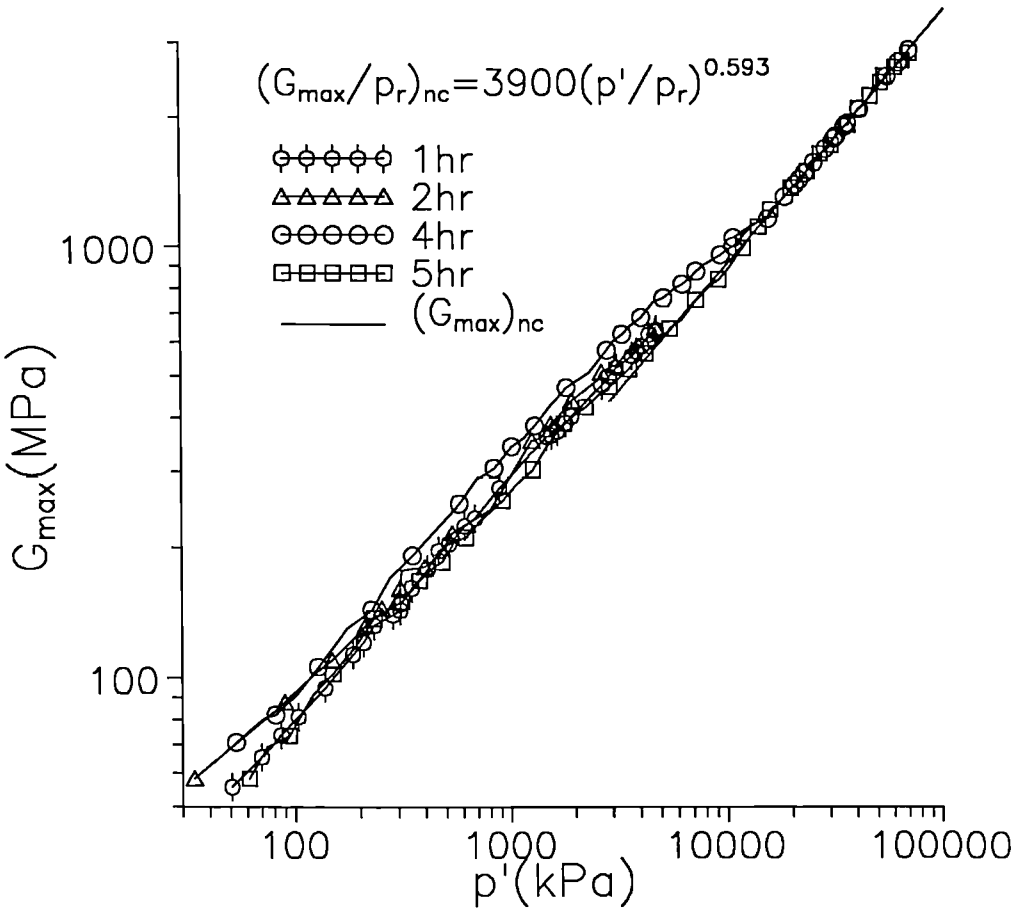

Fig. 4.12 Variation of G_{max} with isotropic stress p' for samples of Ham River sand under first loading

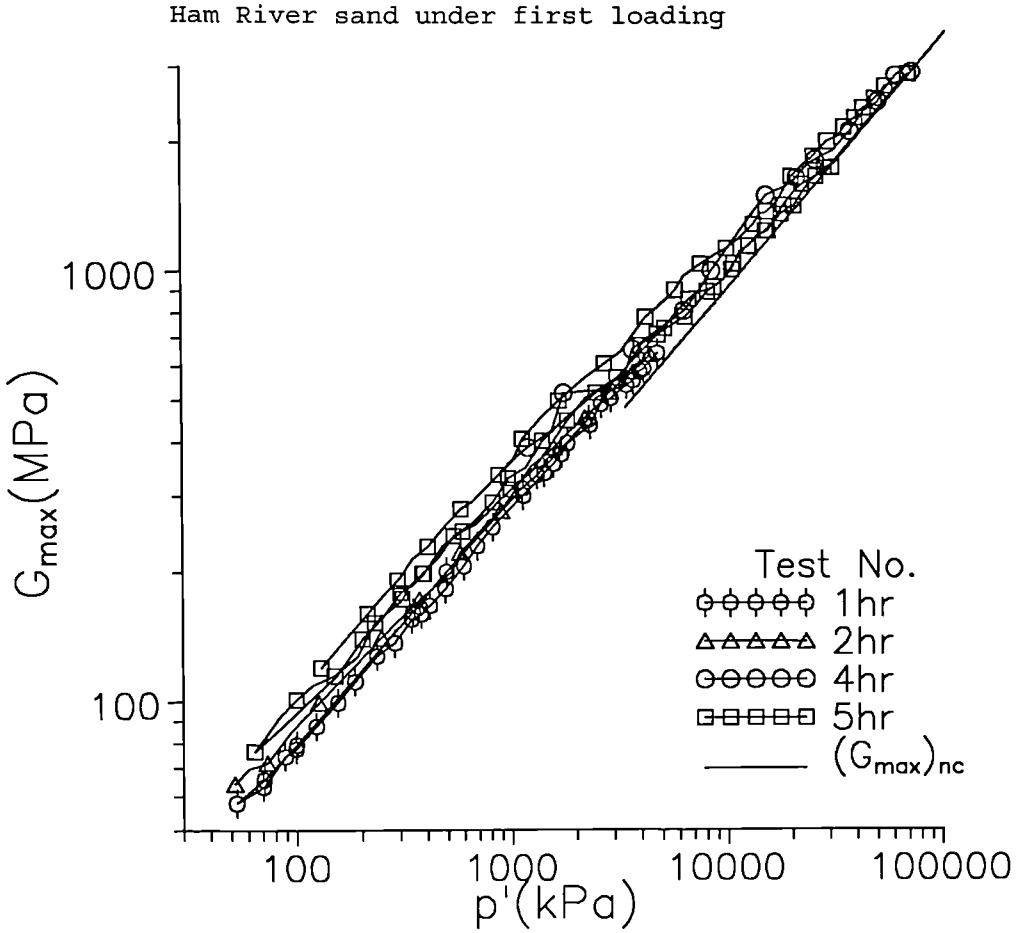

Fig. 4.13 Variation of G_{max} with isotropic stress p' for samples of Ham River sand unloaded from the normal compression line

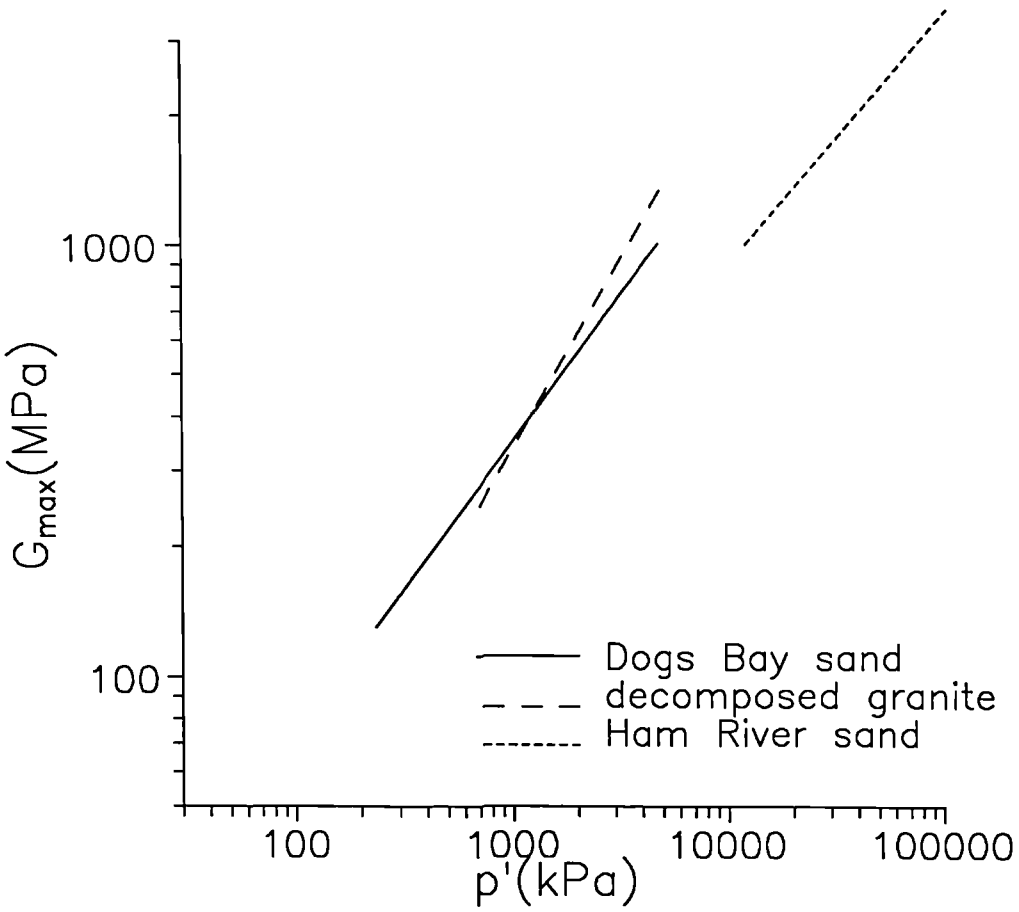

Fig. 4.14 Comparison of the $(G_{max})_{nc}$ lines for the three sands

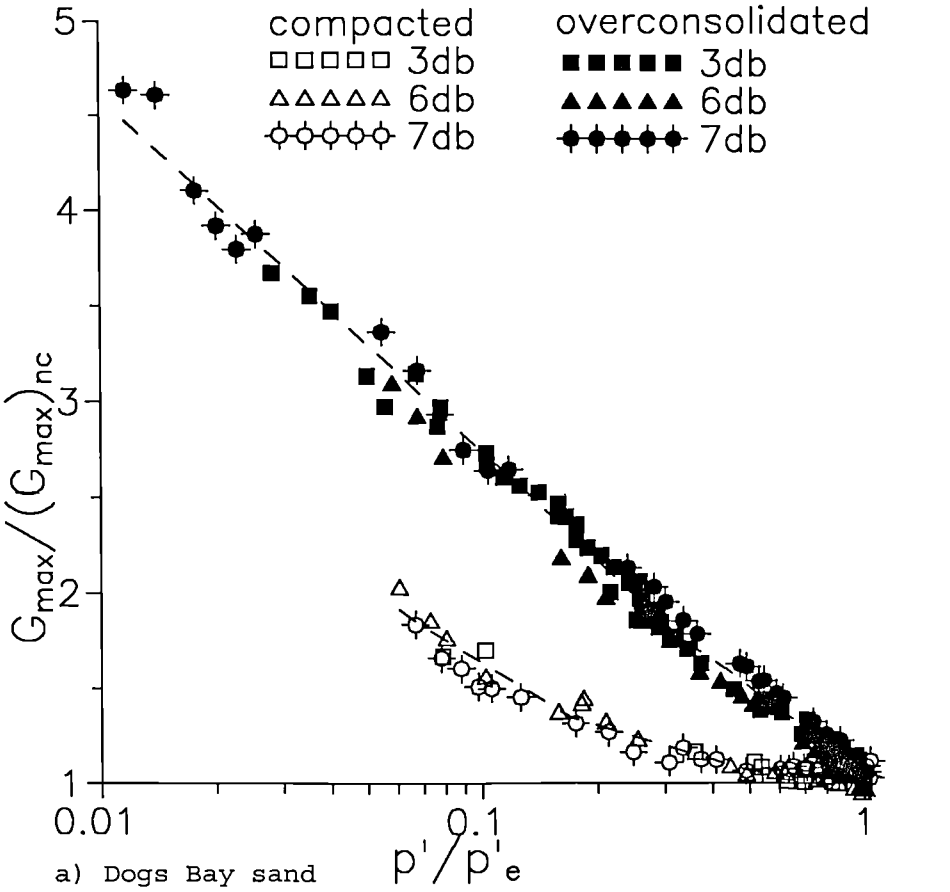

a) Dogs Bay sand

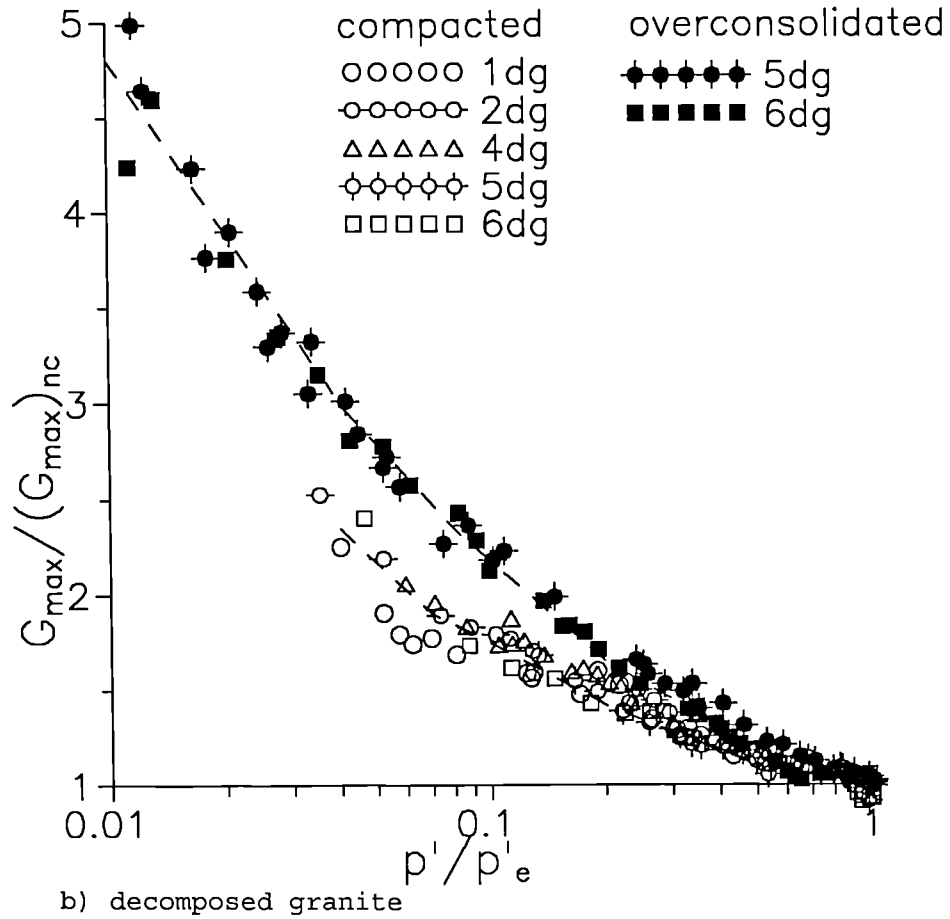

b) decomposed granite

Fig. 4.15 Variation of normalised stiffness with normalised volumetric state for compacted and overconsolidated samples of the three sands

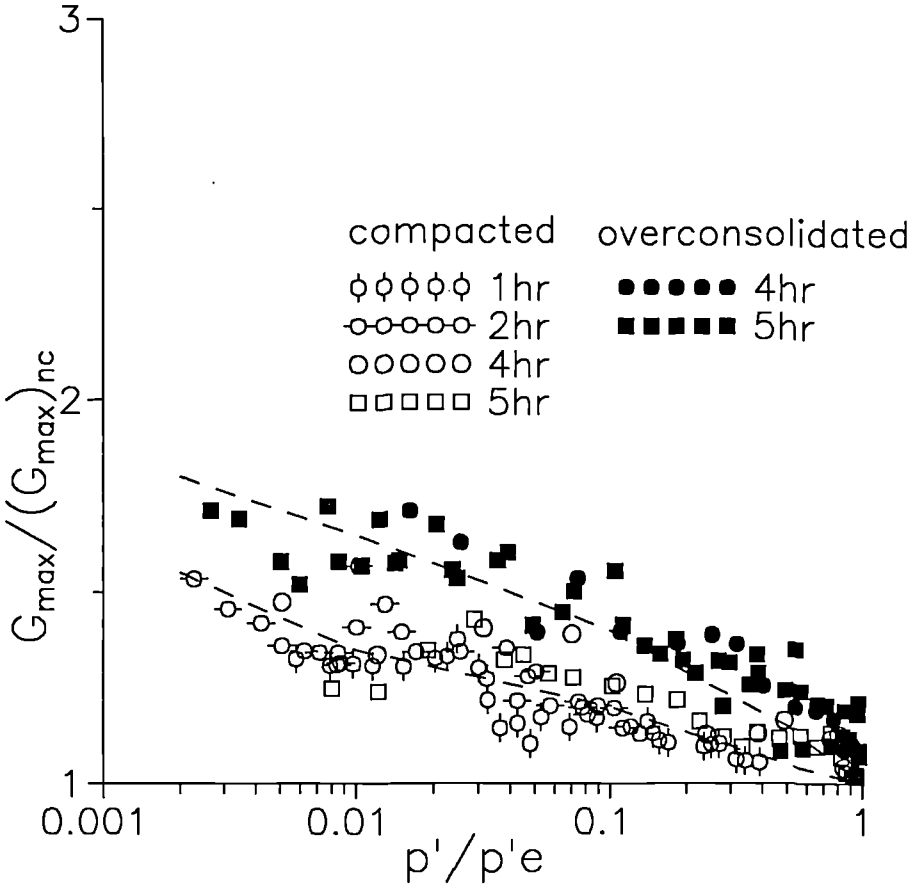

c) Ham River sand

Fig. 4.15 Variation of normalised stiffness with normalised volumetric state for compacted and overconsolidated samples of the three sands

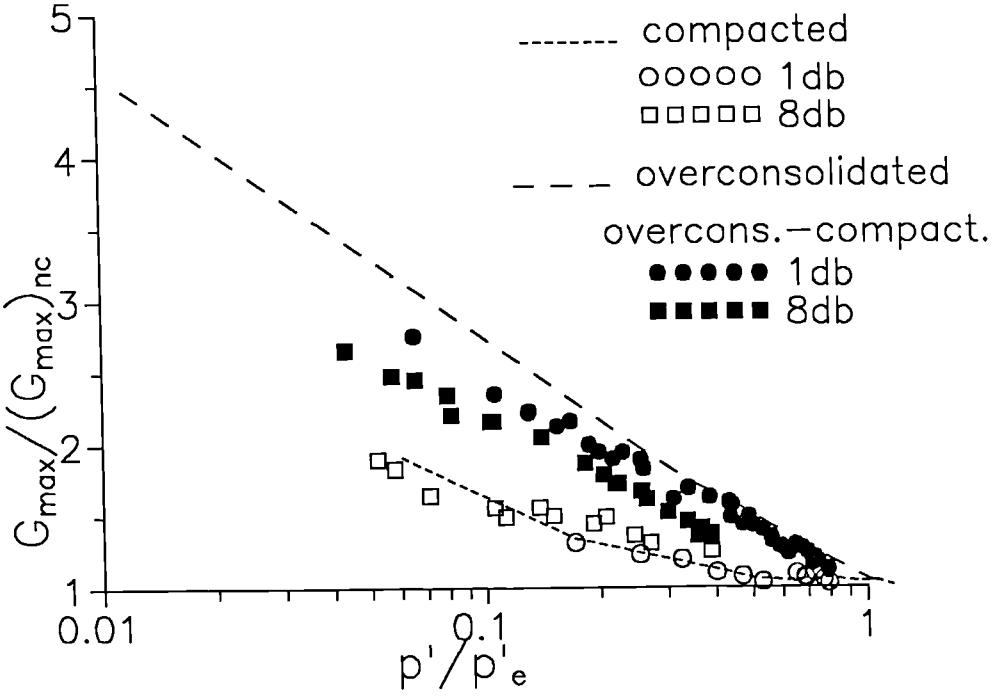

Fig. 4.16 Variation of normalised stiffness with normalised volumetric state for overconsolidated-compacted samples of Dogs Bay sand

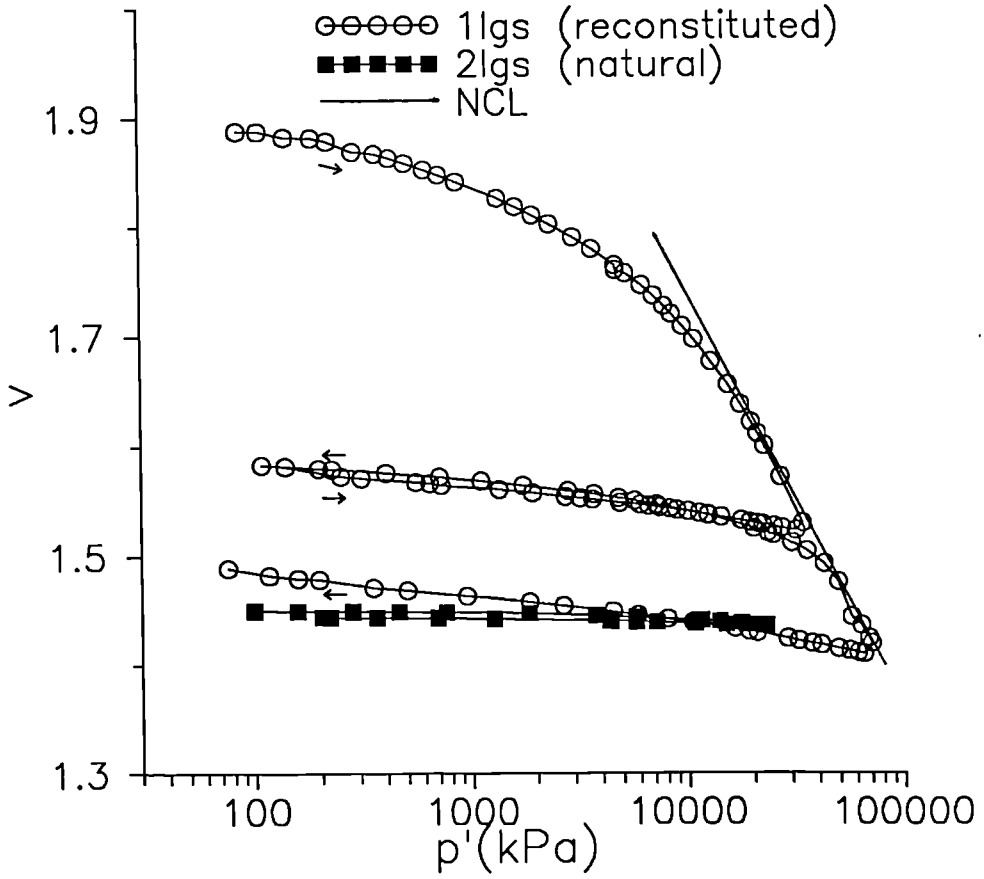

Fig. 4.17 Volumetric paths during isotropic compression and swelling of natural and reconstituted samples of Greensand

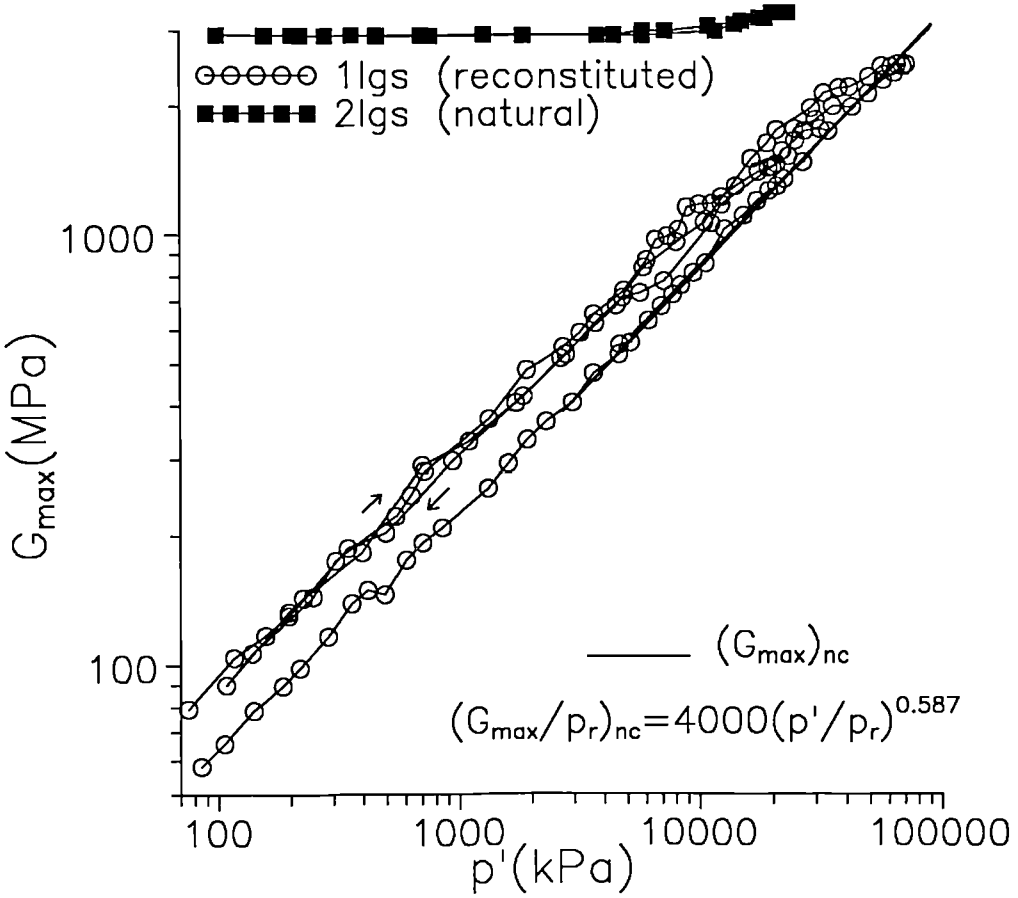

Fig. 4.18 Variation of G_{max} with isotropic stress p' for reconstituted and natural samples of Greensand

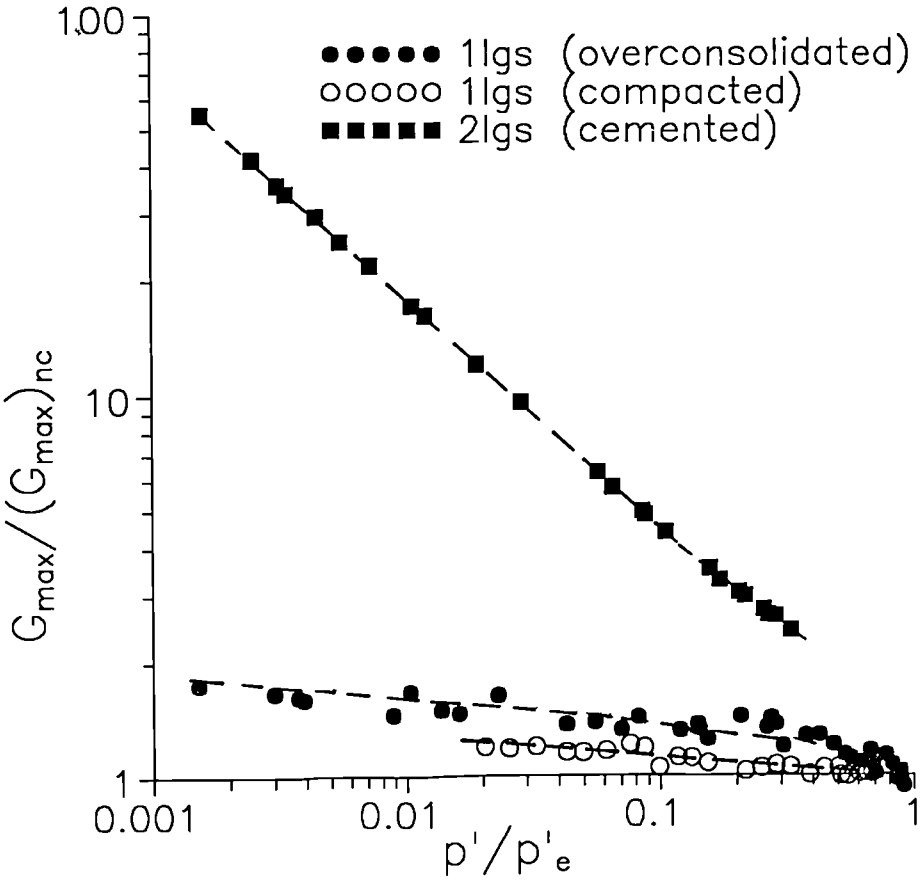

Fig. 4.19 Variation of normalised stiffness with normalised volumetric state for reconstituted and natural samples of Greensand

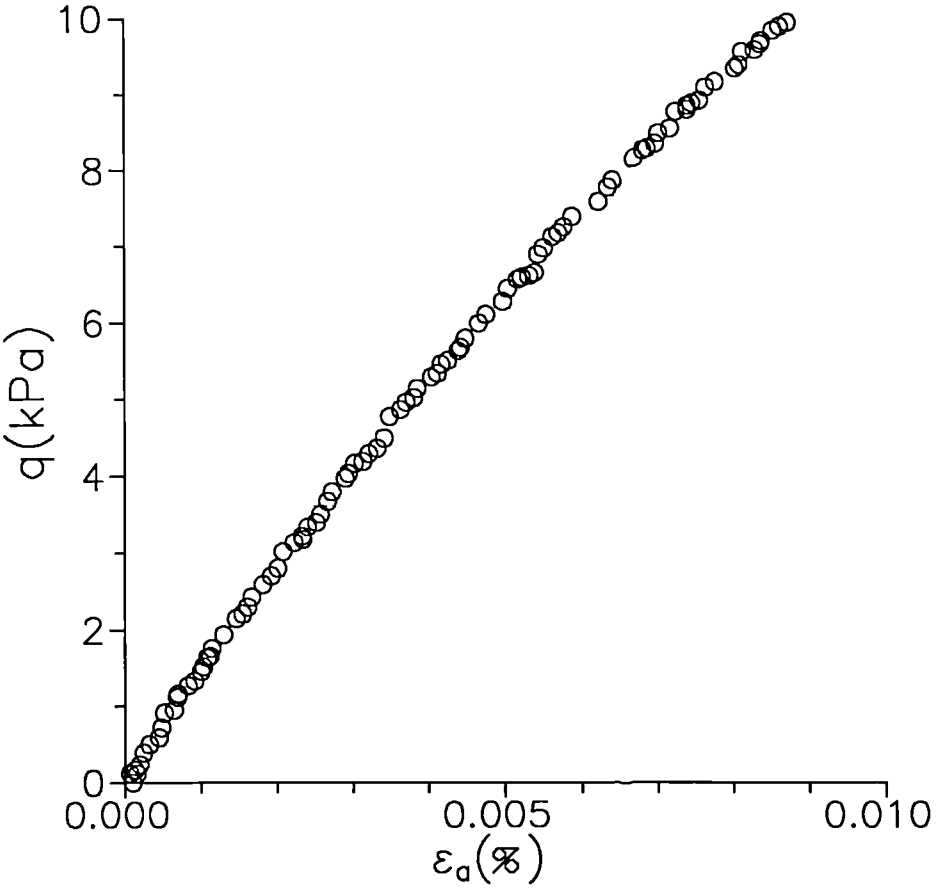

a)

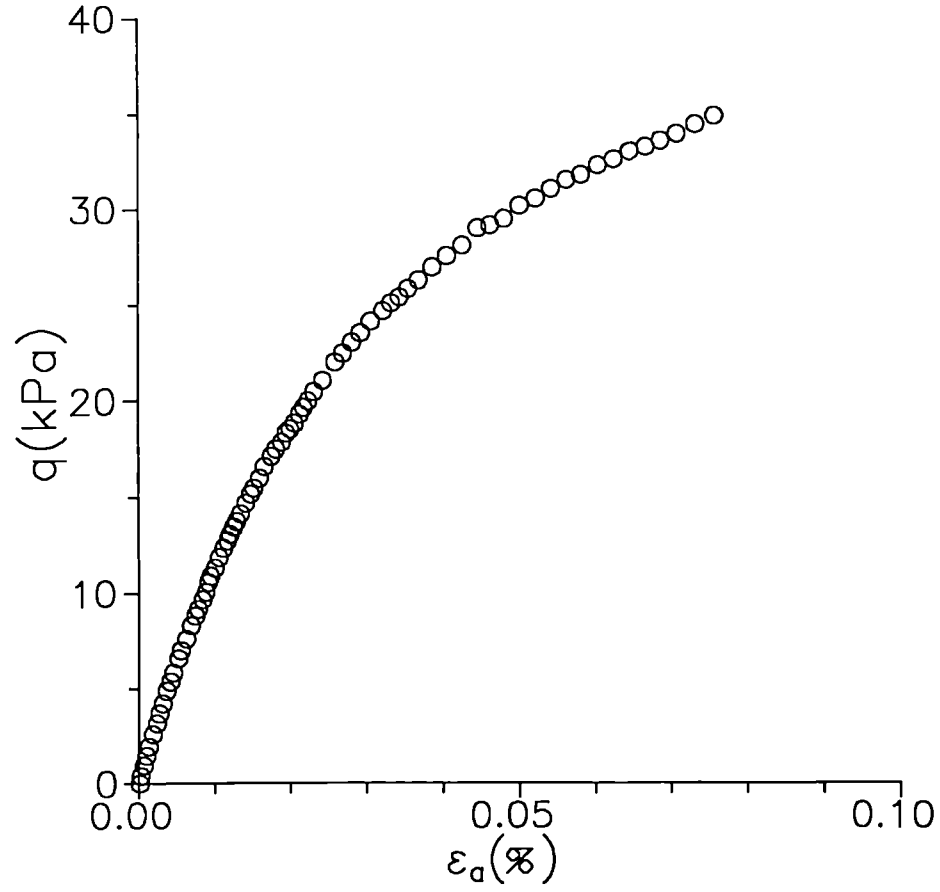

b)

Fig. 4.20 A typical stress-strain curve for an undrained shearing probe on Dogs Bay sand

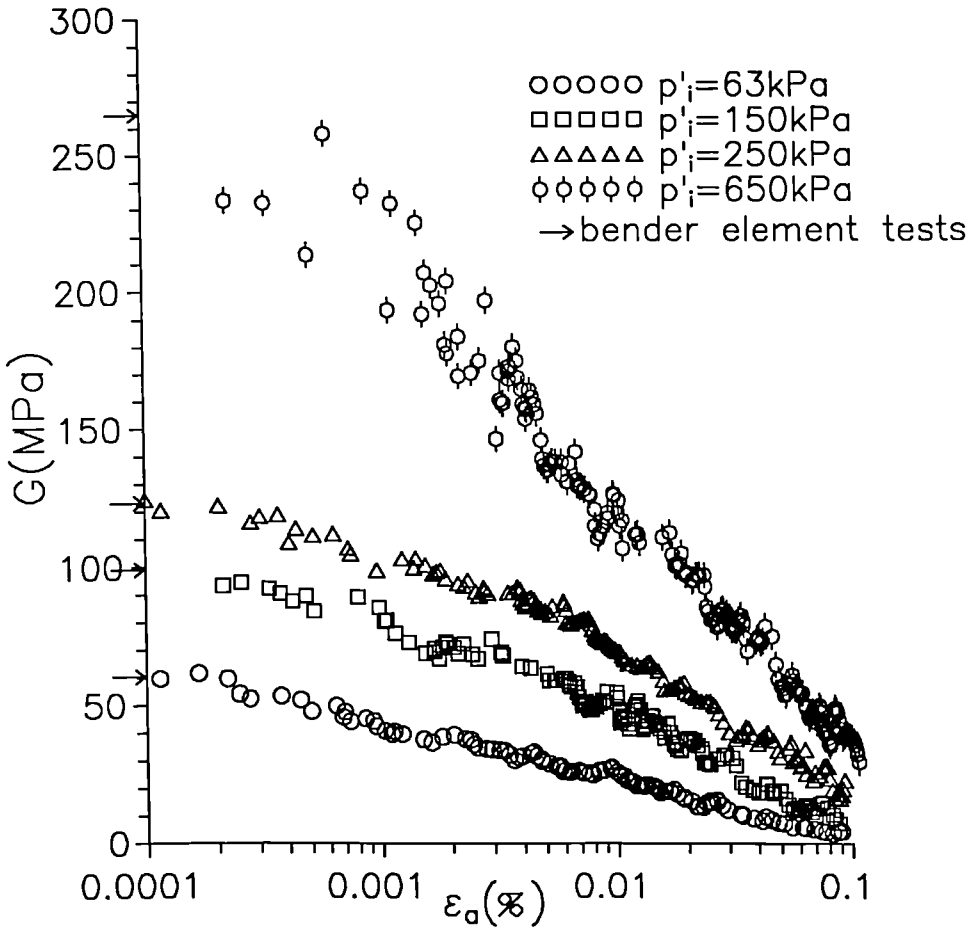

Fig. 4.21 Variation of tangent stiffness with strain for a set of undrained shearing probes on compacted samples of Dogs Bay sand

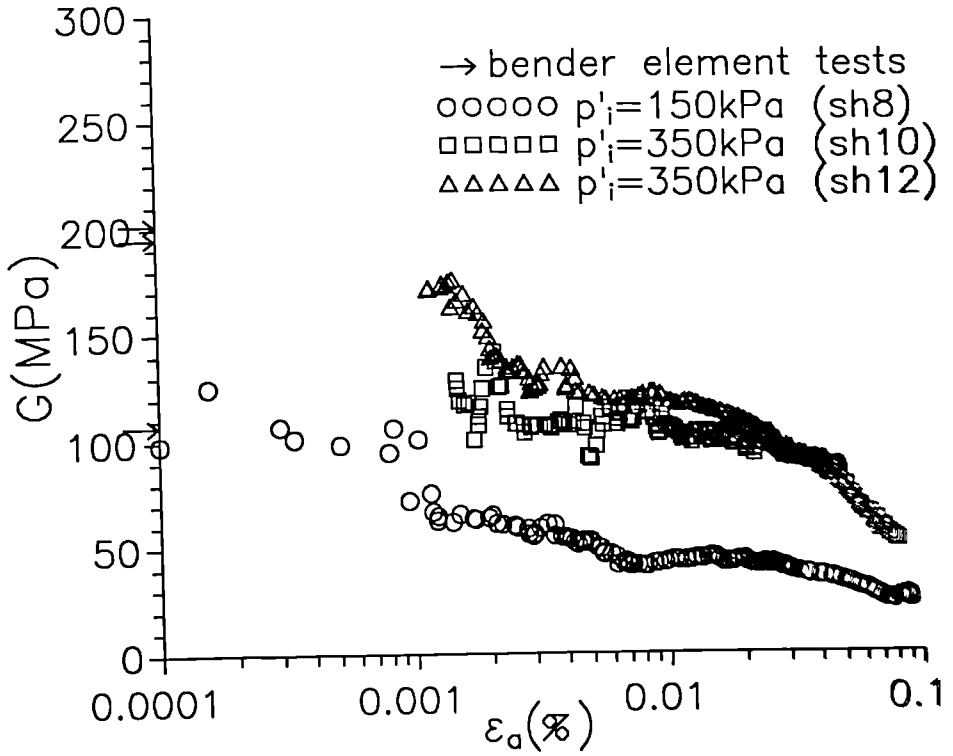

Fig. 4.22 Variation of tangent stiffness with strain for a set of undrained shearing probes on overconsolidated-compacted samples of Dogs Bay sand

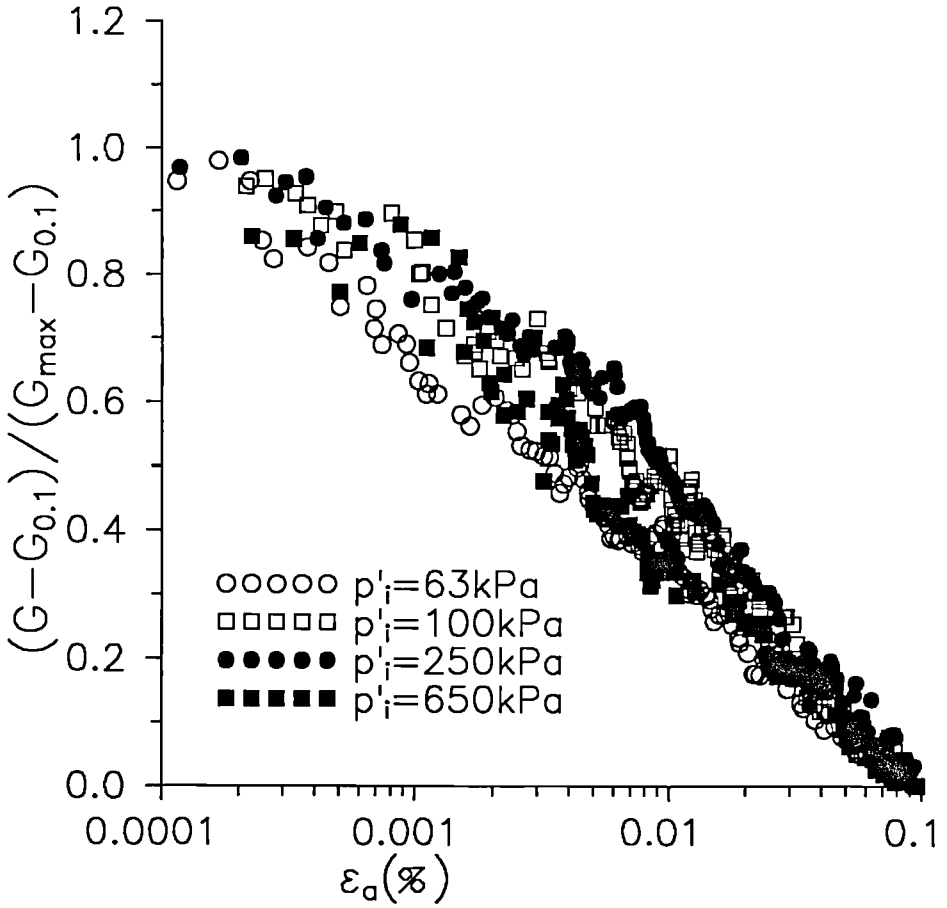

Fig. 4.23 Normalised stiffness-strain curves for compacted samples of Dogs Bay sand

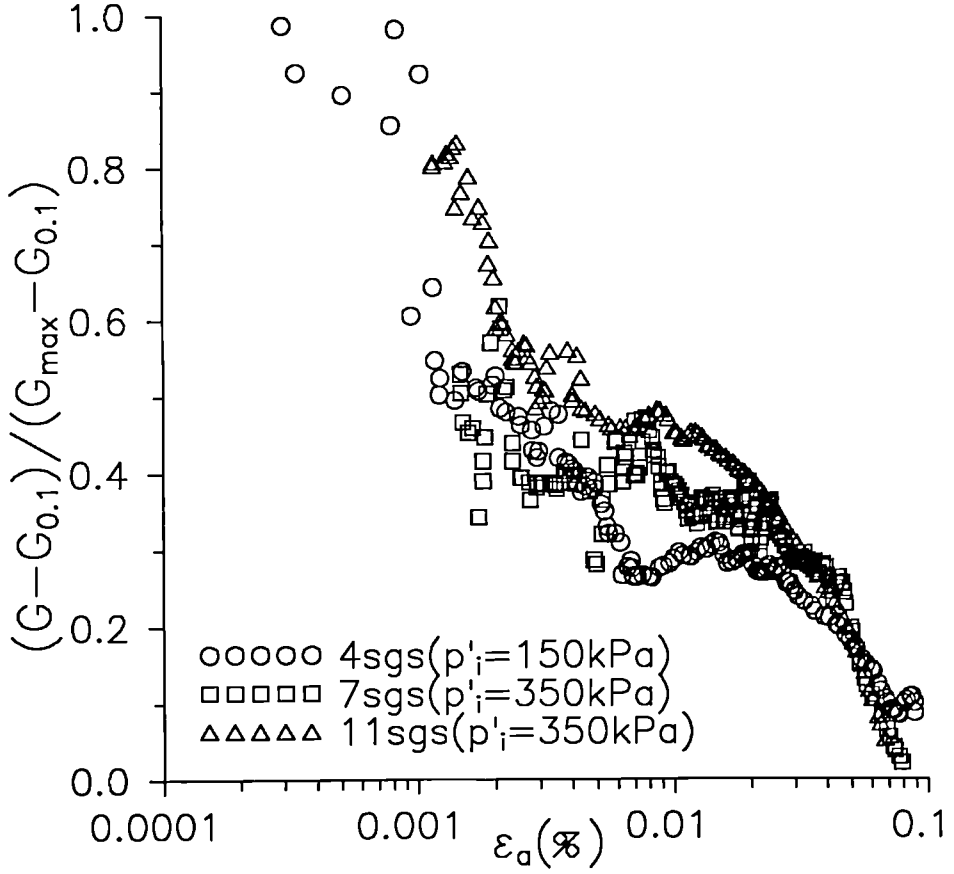

Fig. 4.24 Normalised stiffness-strain curves for overconsolidated-compacted samples of Dogs Bay sand

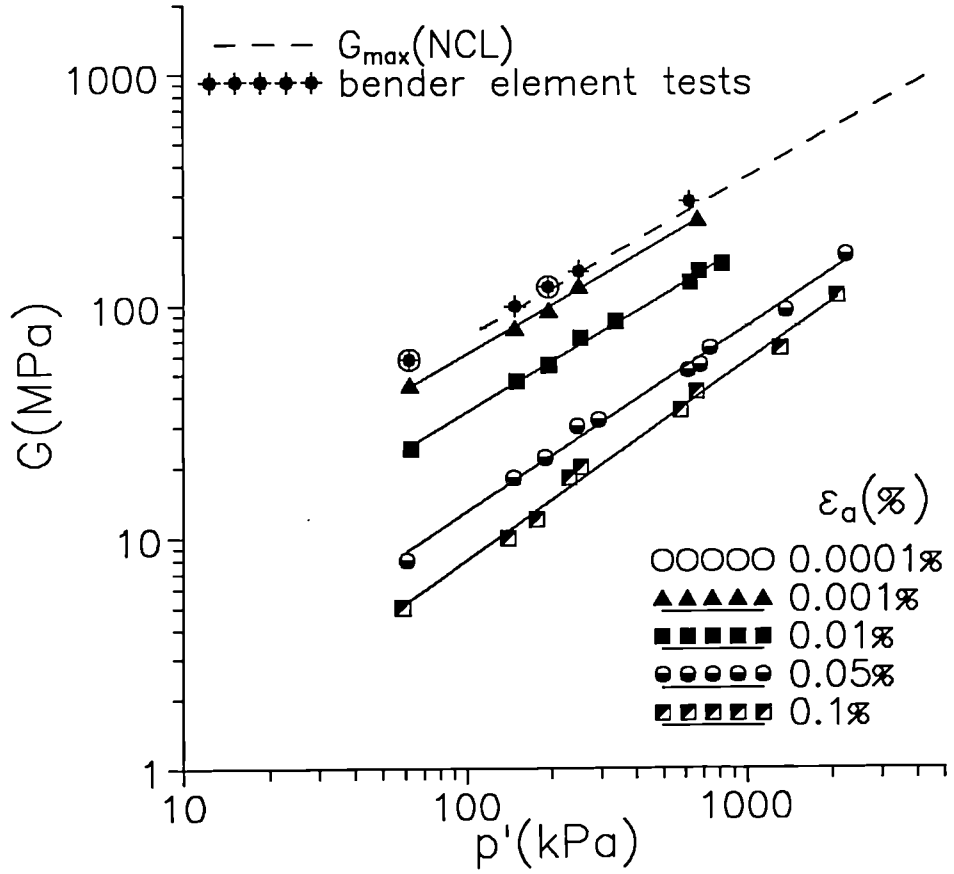

Fig. 4.25 Variation of tangent stiffness with stress and strain level for compacted samples of Dogs Bay sand

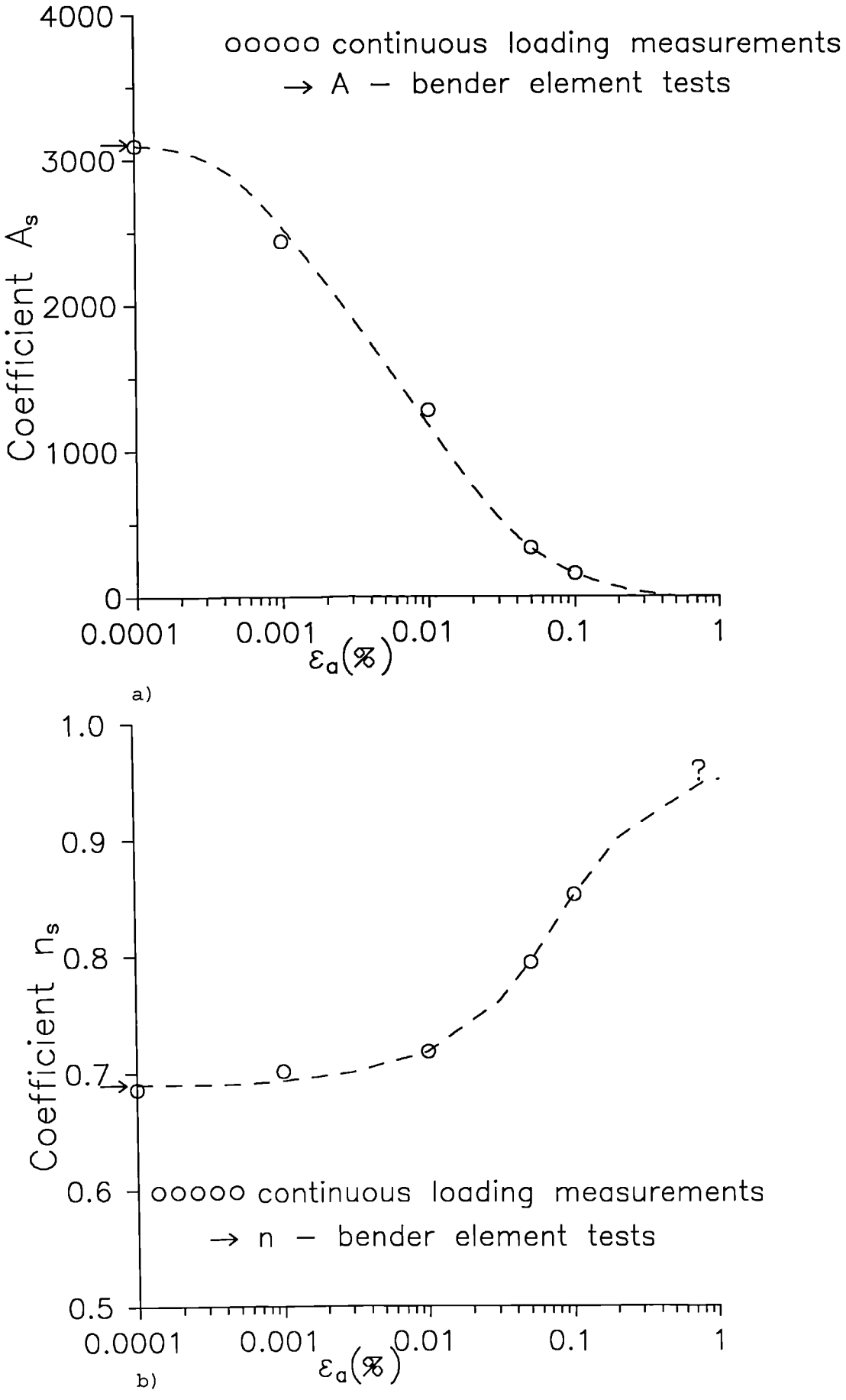

Fig. 4.26 Variation of the parameters A_s and n_s with strain level for Dogs Bay sand

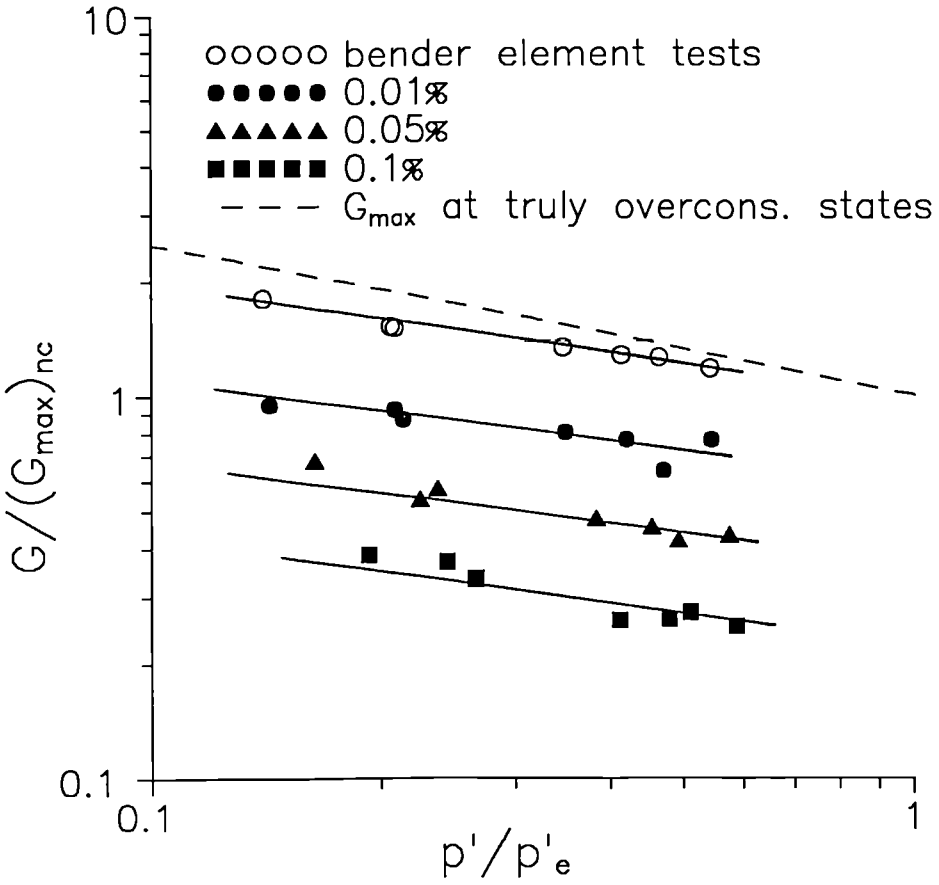

Fig. 4.27 Variation of normalised tangent stiffness with normalised volumetric state for overconsolidated-compacted samples of Dogs Bay sand

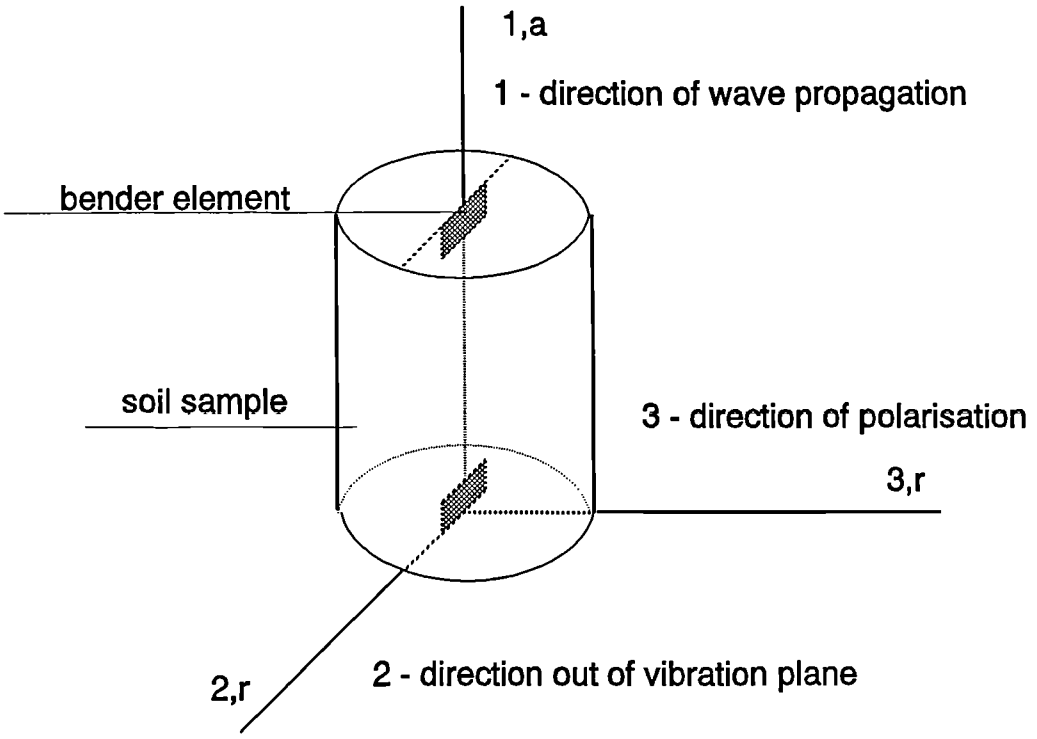

Fig. 5.1 The standard configuration of bender elements in the triaxial apparatus

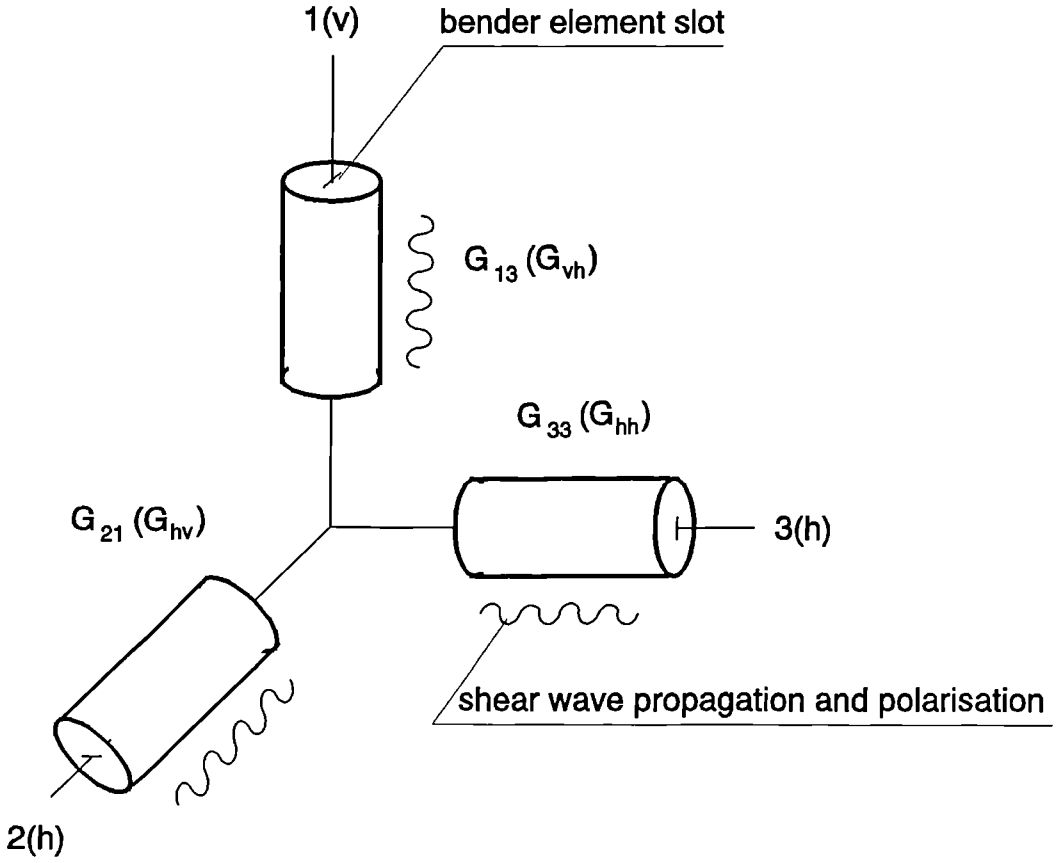

Fig. 5.2 Notation for measurement of stiffness of cross-anisotropic soil using bender elements

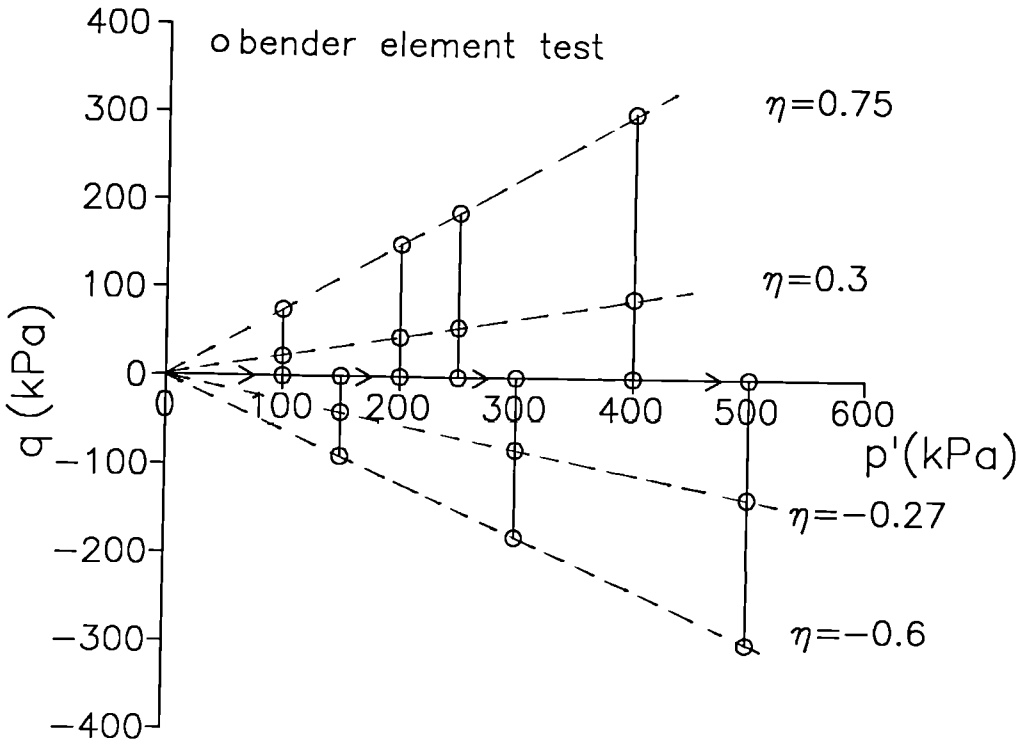

a)

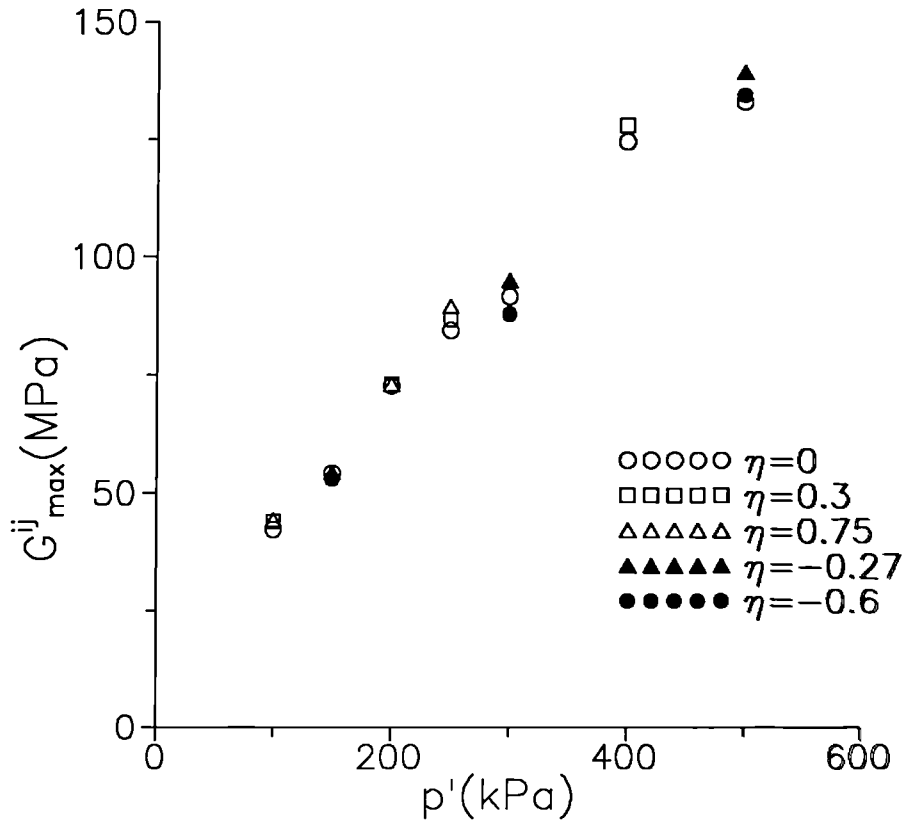

b)

Fig. 5.3 Bender element tests on a sample of reconstituted kaolin following constant p' stress paths: a) test programme b) test results

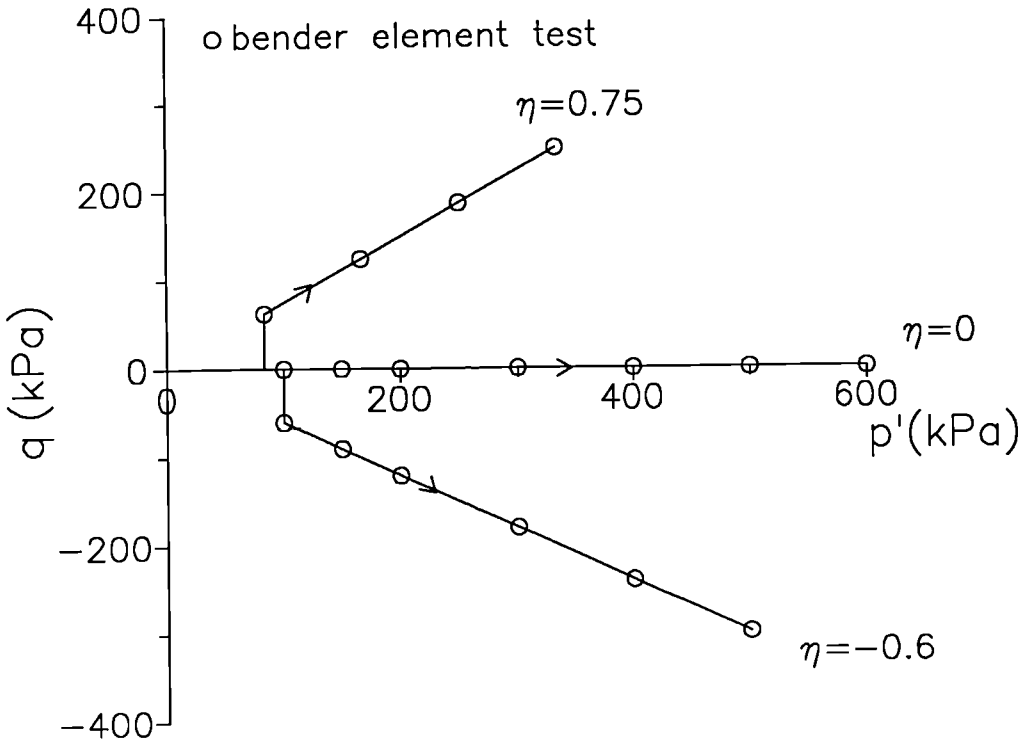

a)

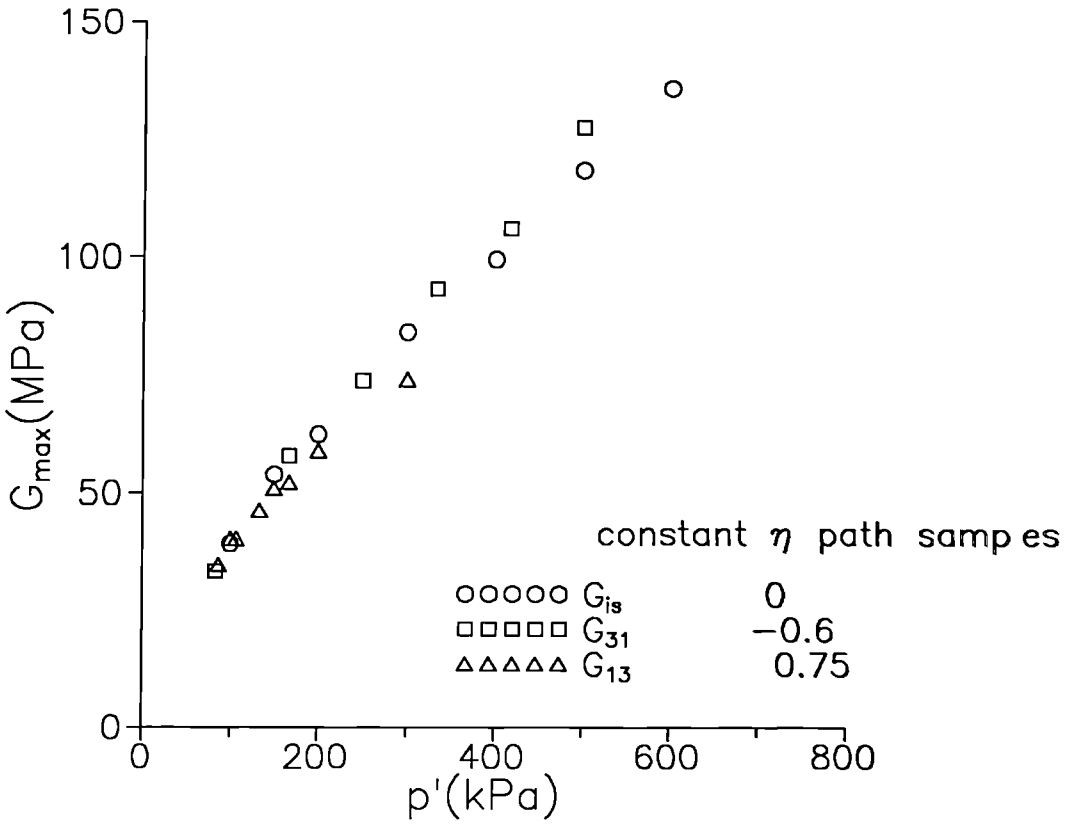

b)

Fig. 5.4 Bender element tests on reconstituted kaolin samples following constant η stress paths: a) test programme b) test results

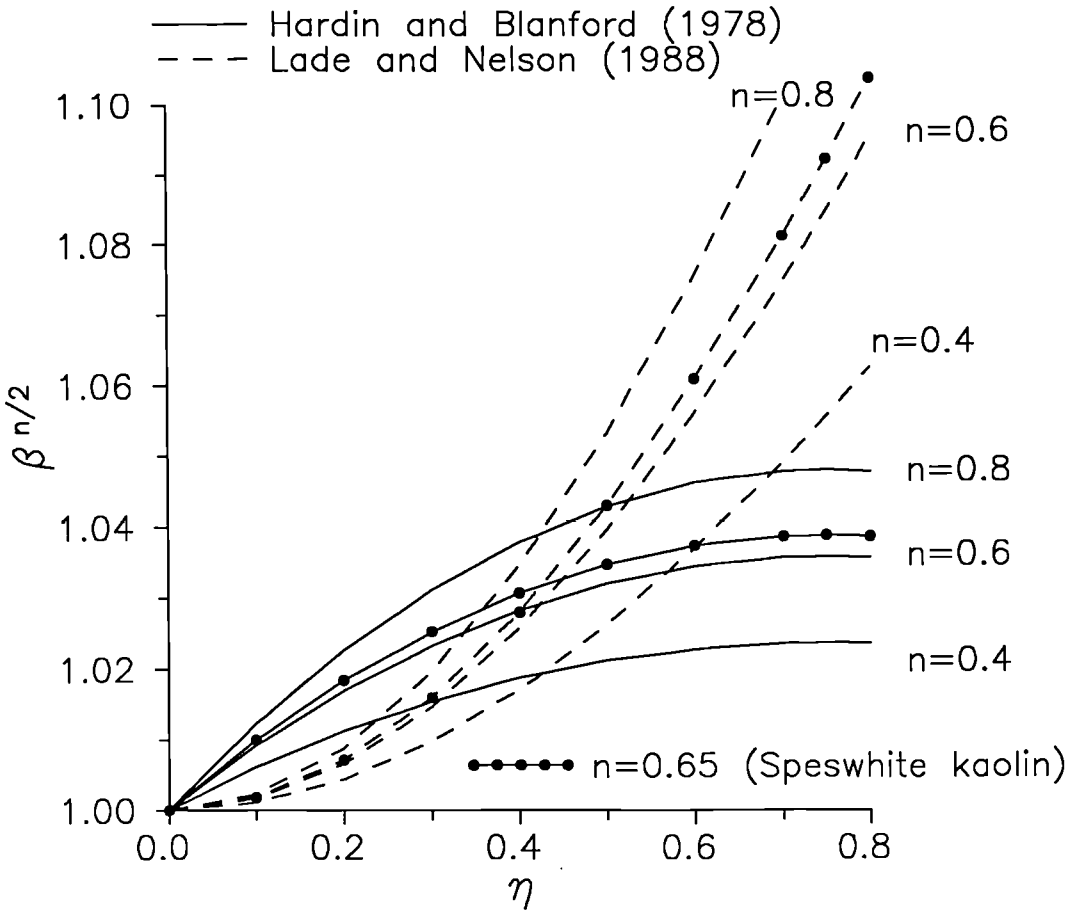

Fig. 5.5 Theoretical and empirical evaluations of the magnitude of stress induced anisotropy of G_{max}

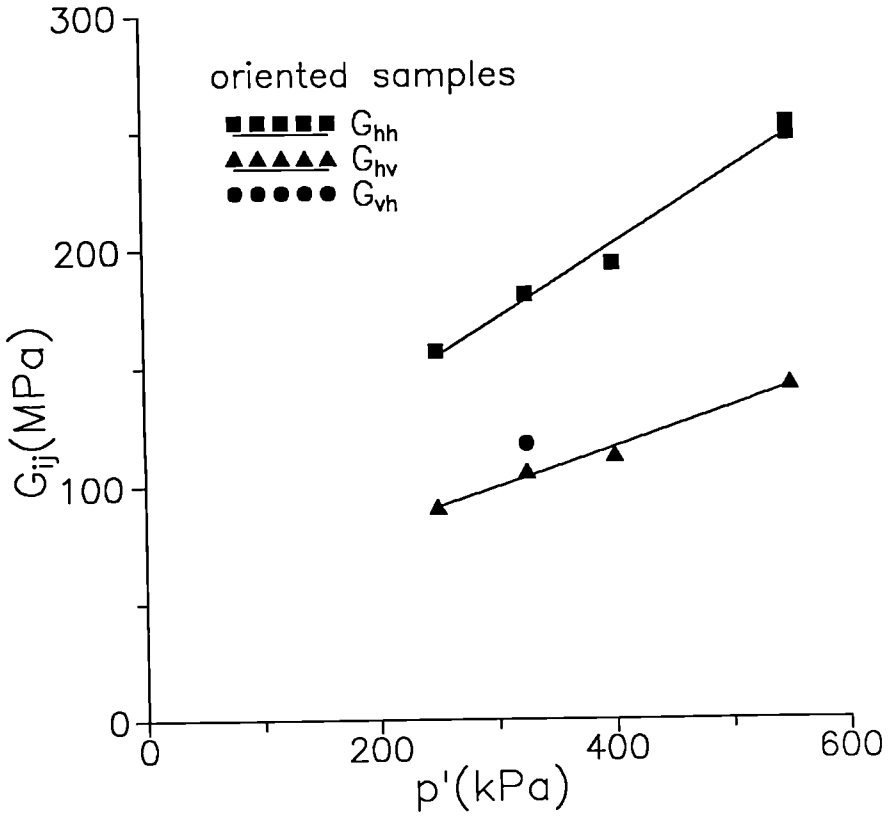

Fig. 5.6 Bender element tests on oriented samples of reconstituted Speswhite kaolin

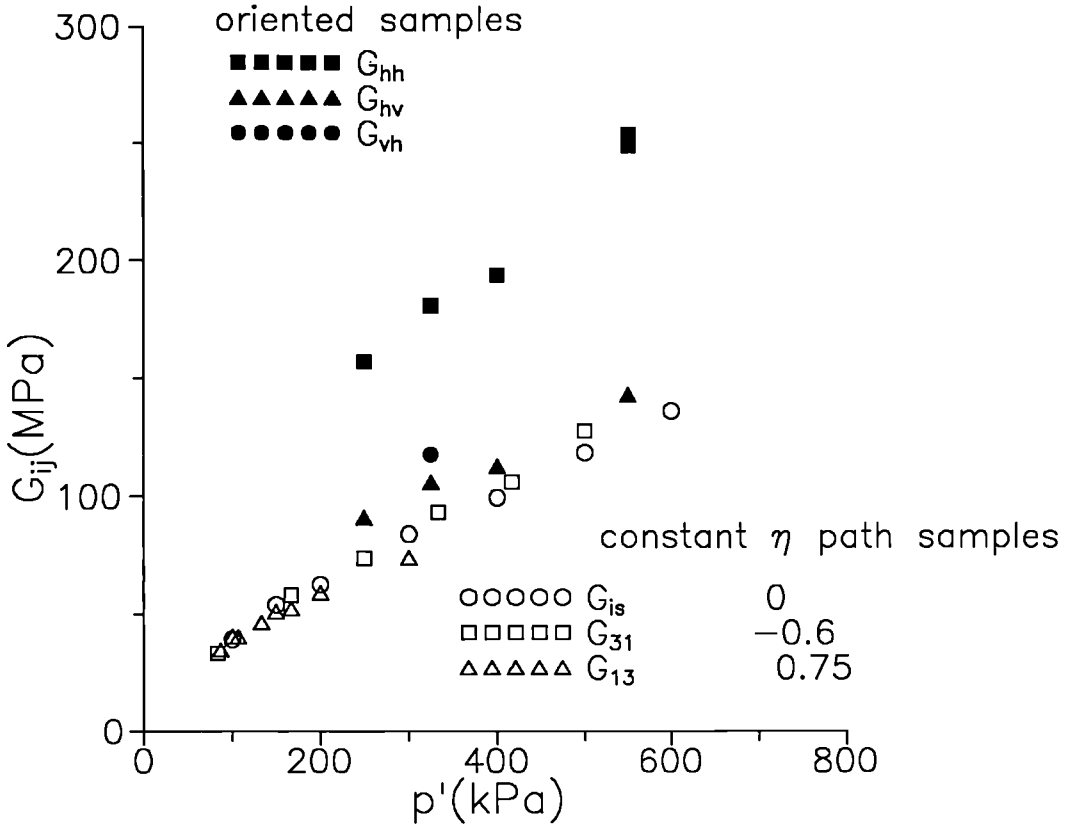

Fig. 5.7 Comparison between stress induced and strain induced anisotropy of reconstituted Speswhite kaolin

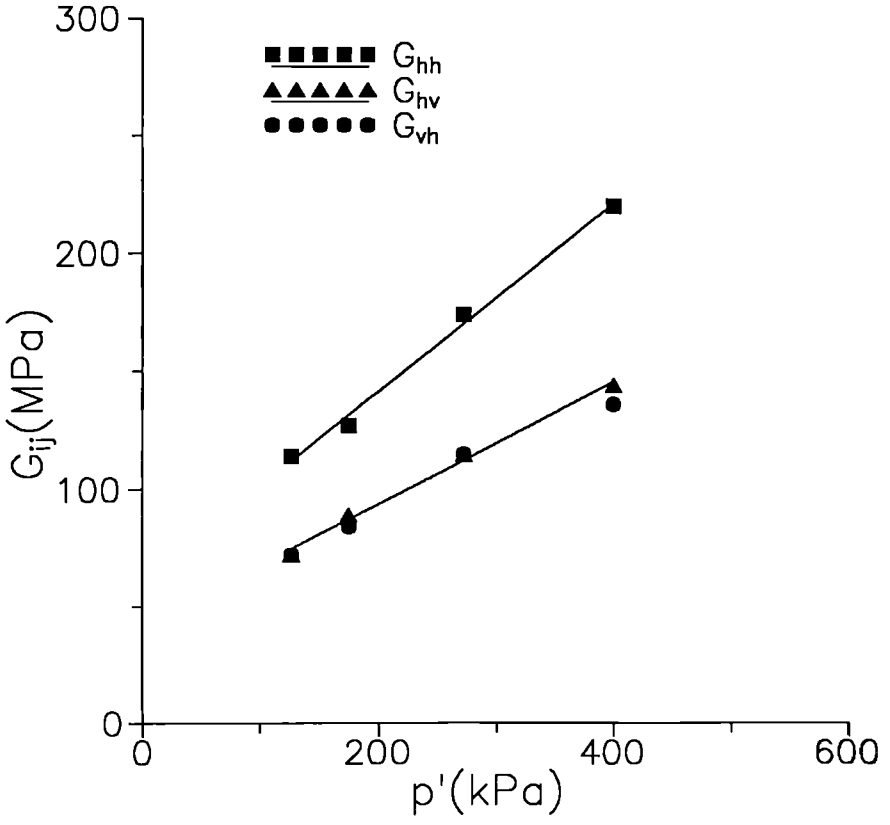

Fig. 5.8 Bender element tests on oriented samples of undisturbed London clay

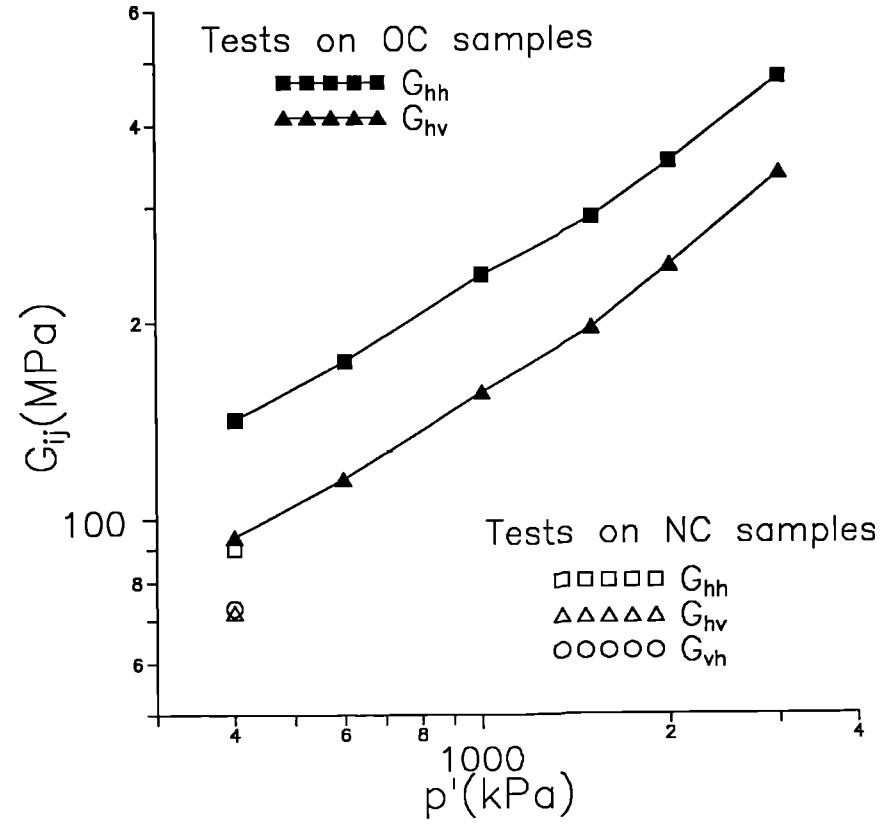

a)

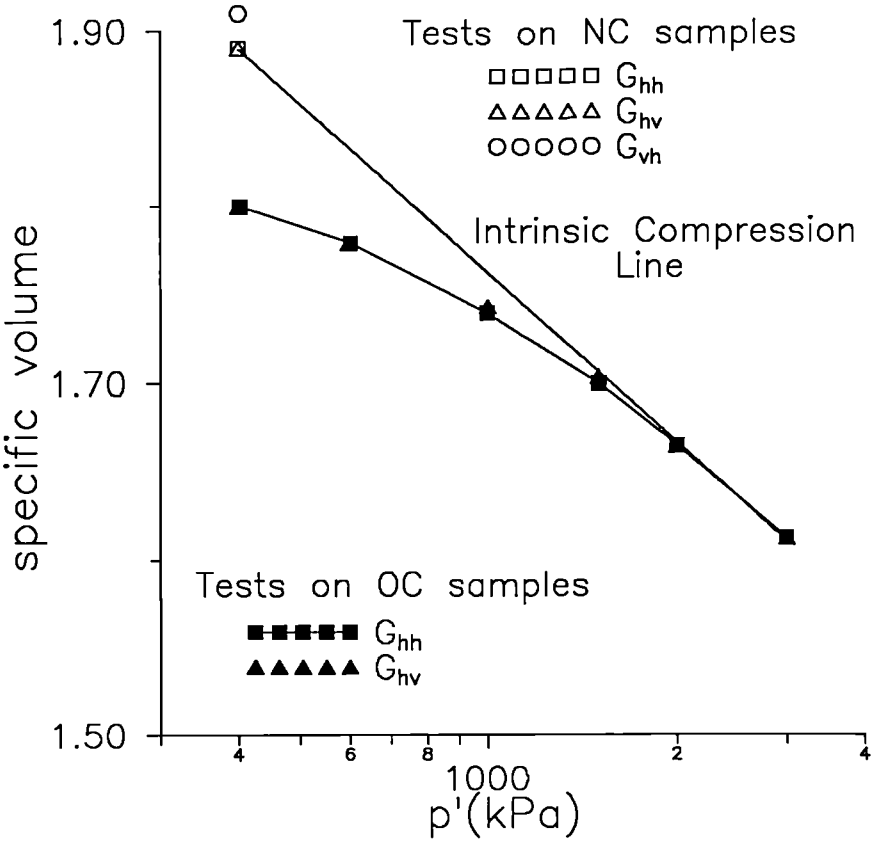

b)

Fig. 5.9 Bender element tests on oriented samples of reconstituted London clay

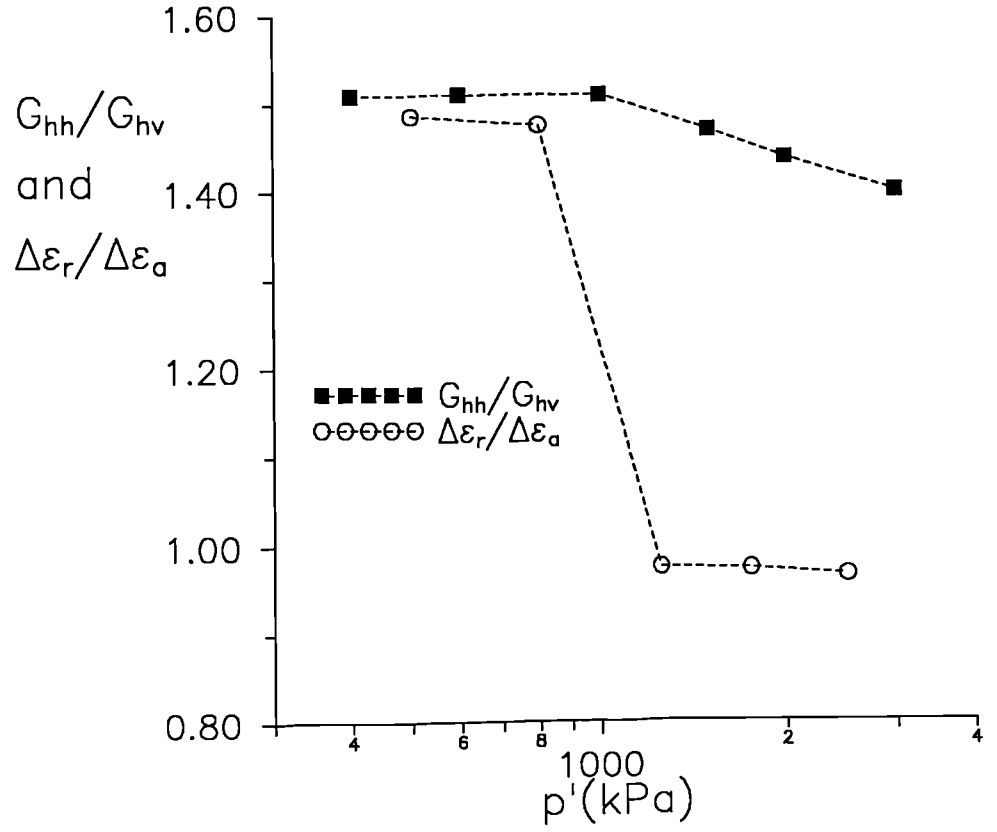

a)

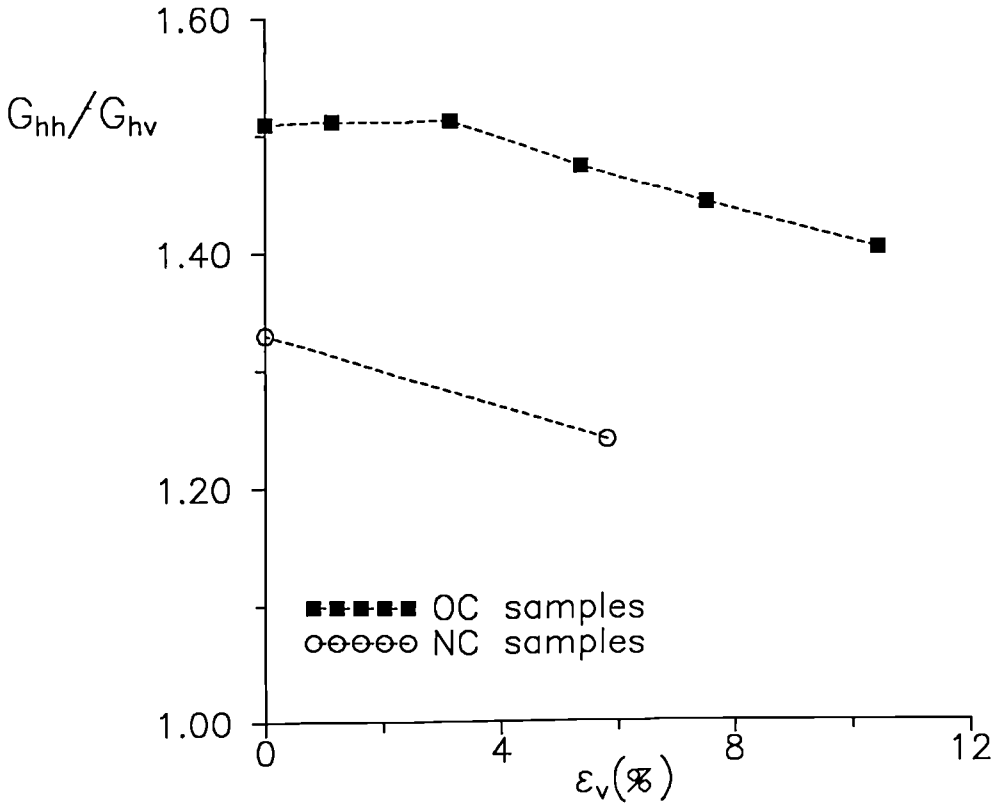

b)

Fig. 5.10 Variation of the degree of anisotropy and strain increment strain ratio with a) mean effective stress and b) volumetric strain ratio for reconstituted London clay

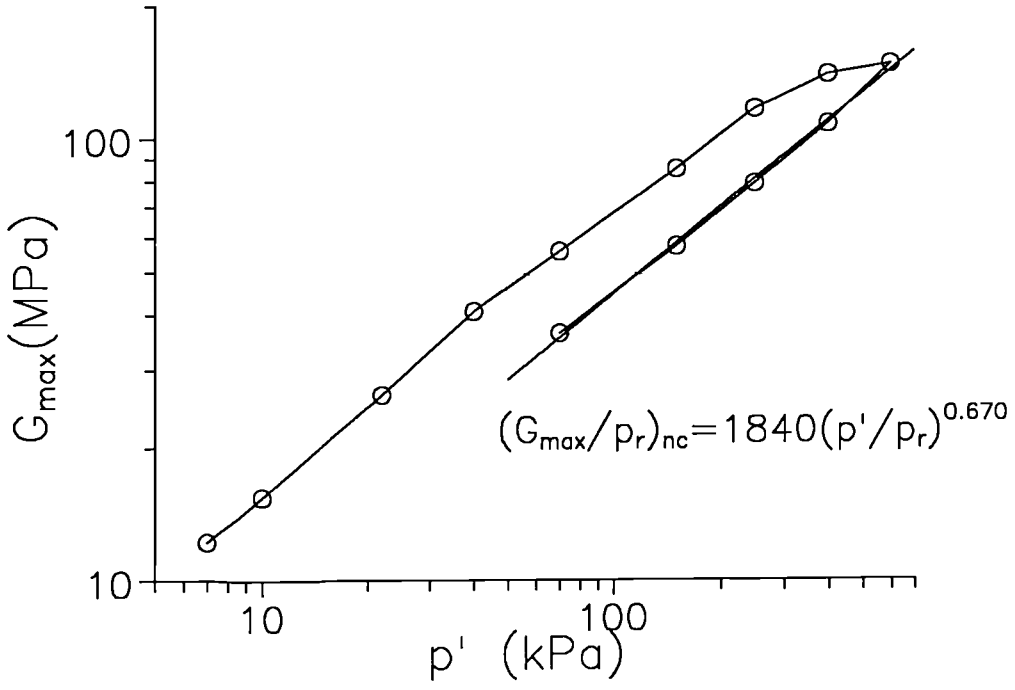

a)

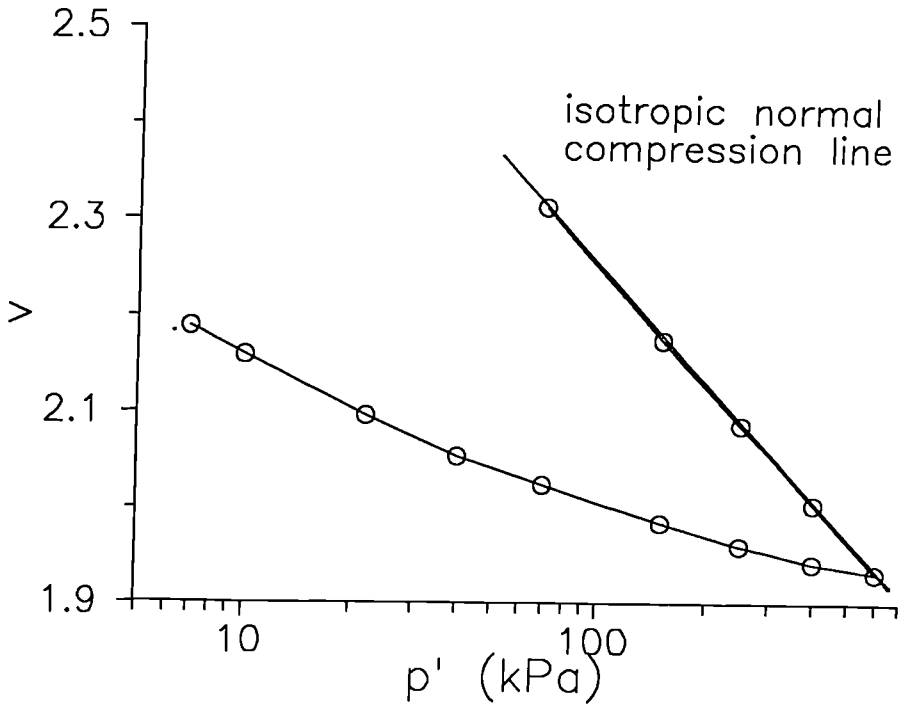

b)

Fig. 5.11 Variation of G_{max} and specific volume with p' during isotropic compression and swelling of reconstituted Speswhite kaolin

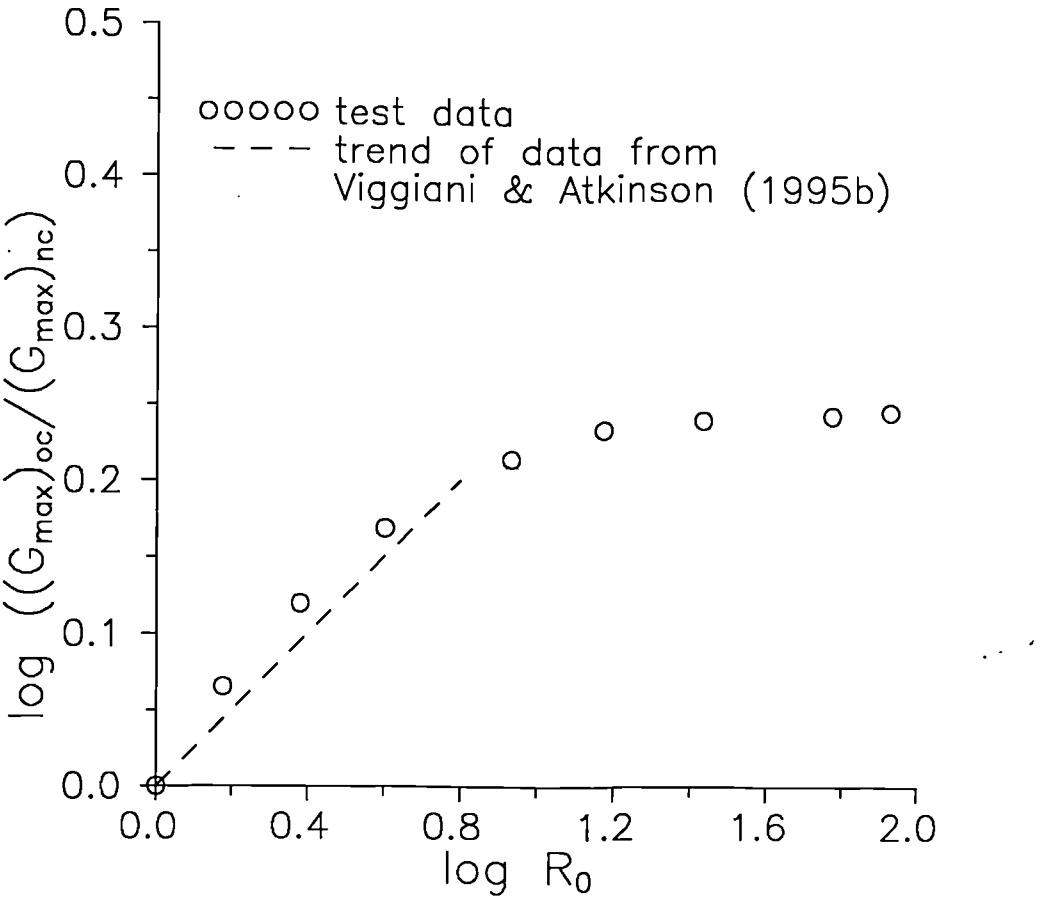

Fig. 5.12 Variation of normalised stiffness with overconsolidation ratio for reconstituted Speswhite kaolin

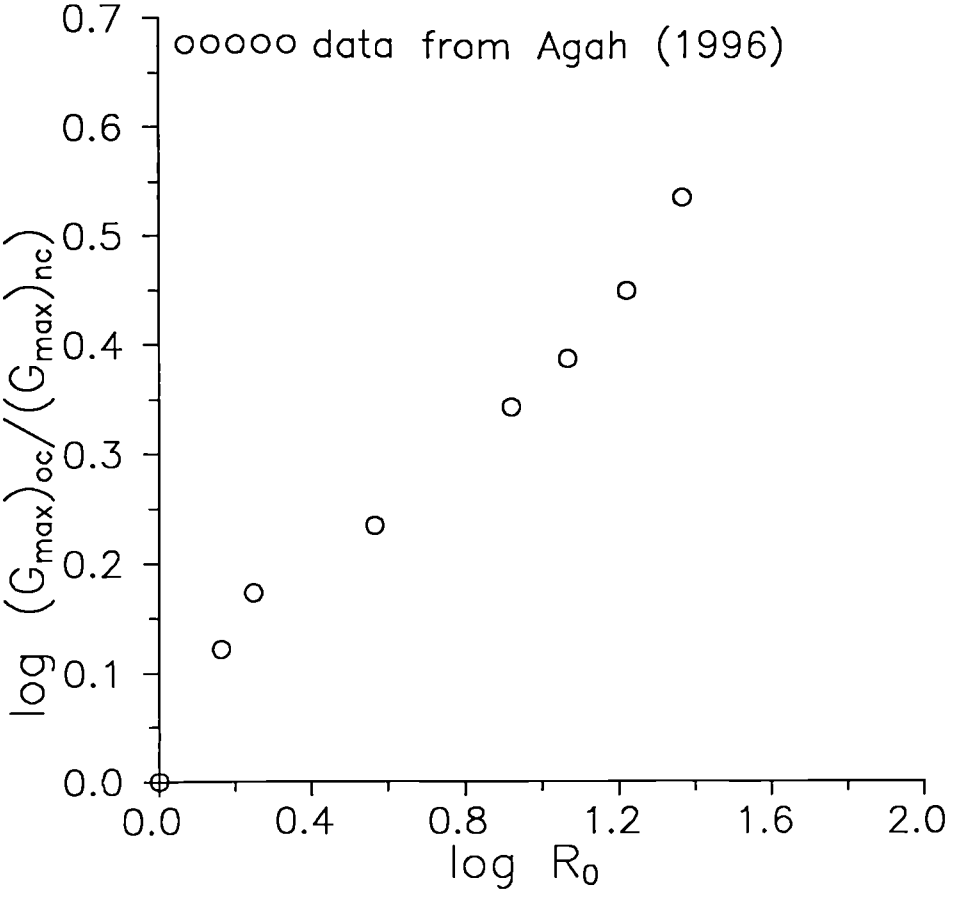

Fig. 5.13 Variation of normalised stiffness with overconsolidation ratio for reconstituted Boom clay

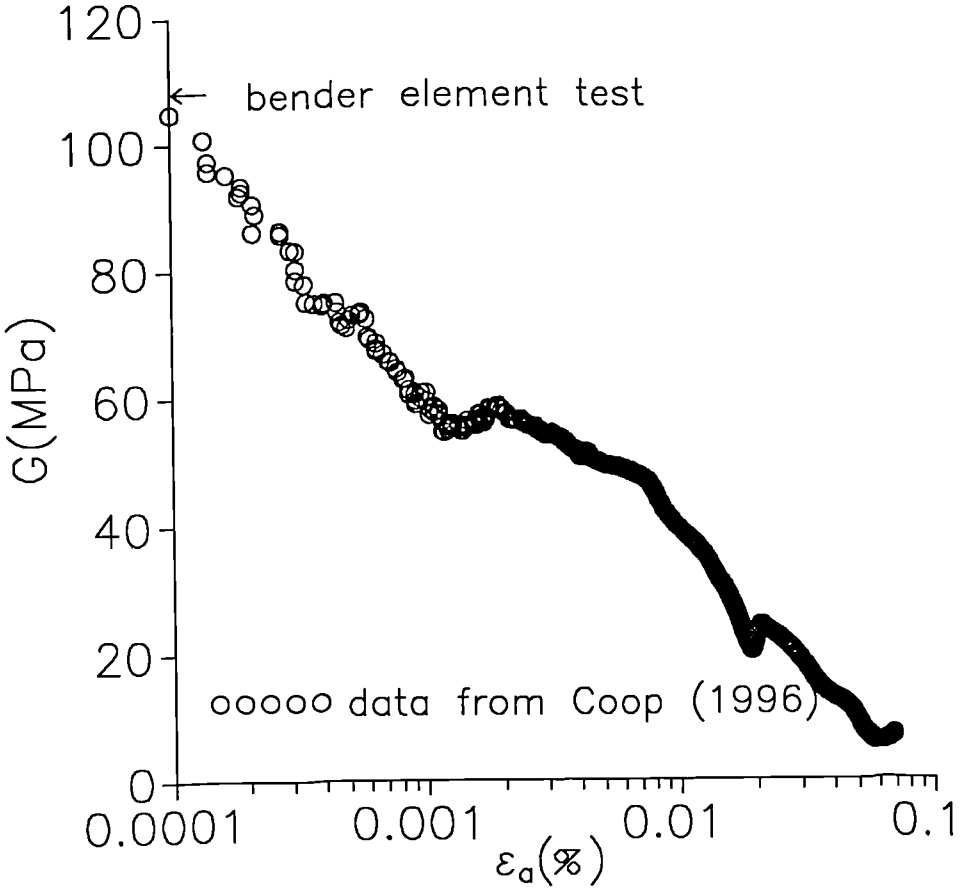

Fig. 5.14 Typical stiffness-strain curve for undrained shearing of normally consolidated kaolin

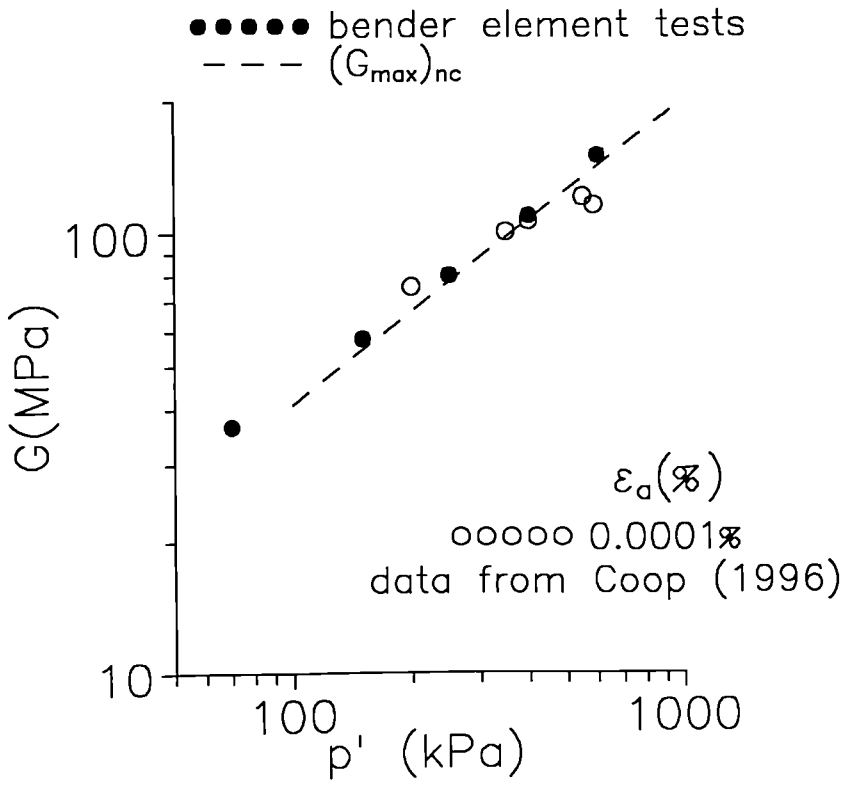

Fig. 5.15 Bender element and LVDT stiffnesses for normally consolidated kaolin

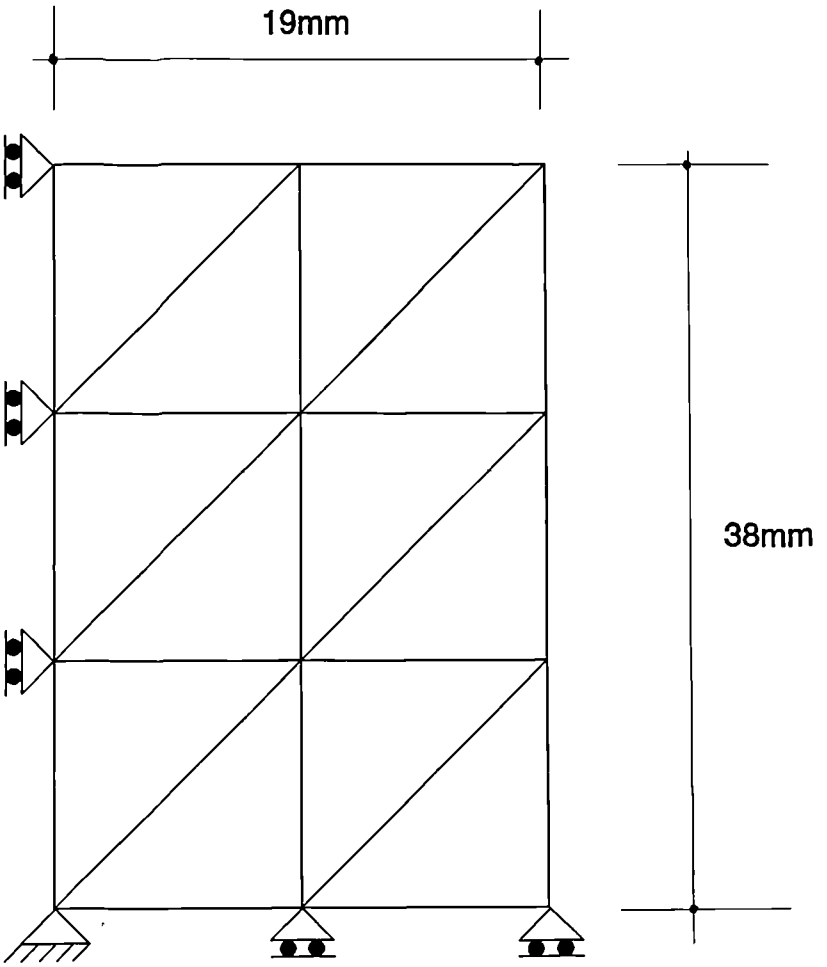

Fig 6.1. Geometry and boundary conditions of the finite element mesh representing a triaxial sample

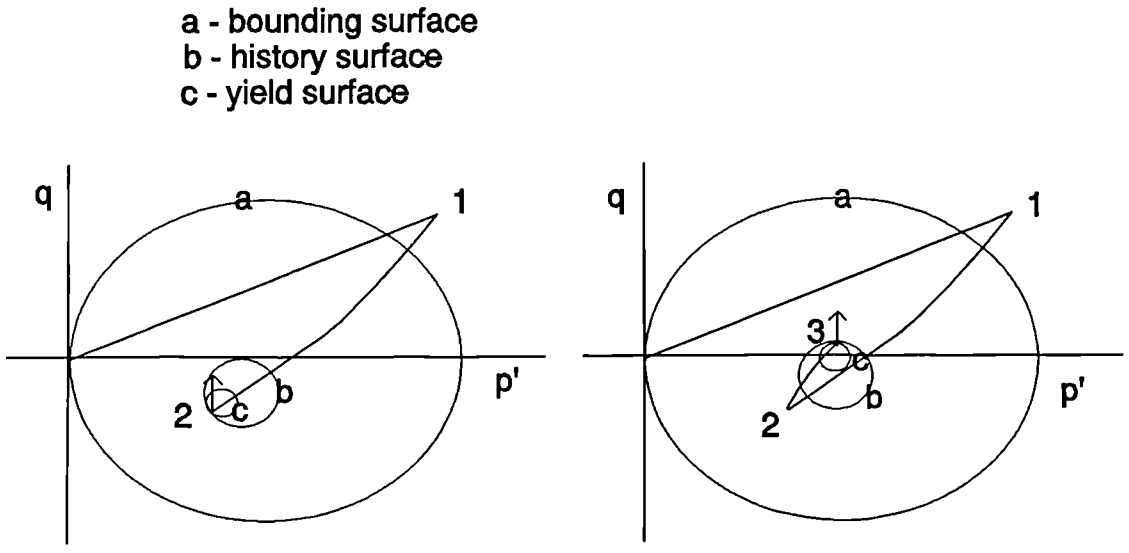

a) History 1 b) History 2

Fig 6.2. Typical stress paths for an overconsolidated soil deposit

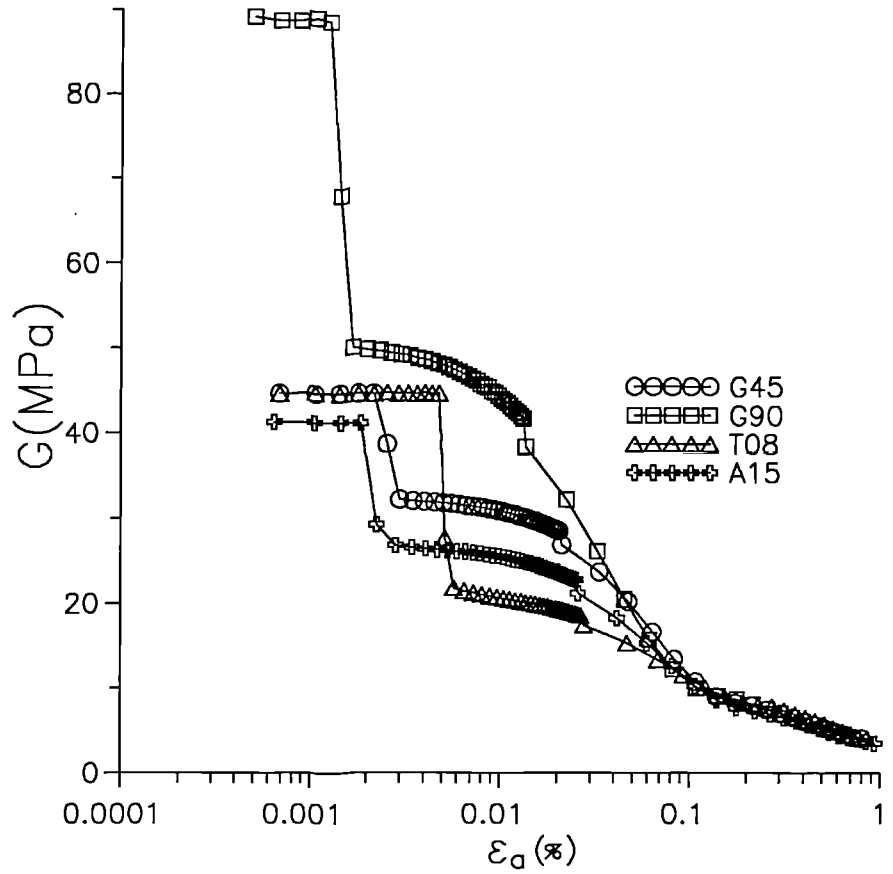

a) after History 1

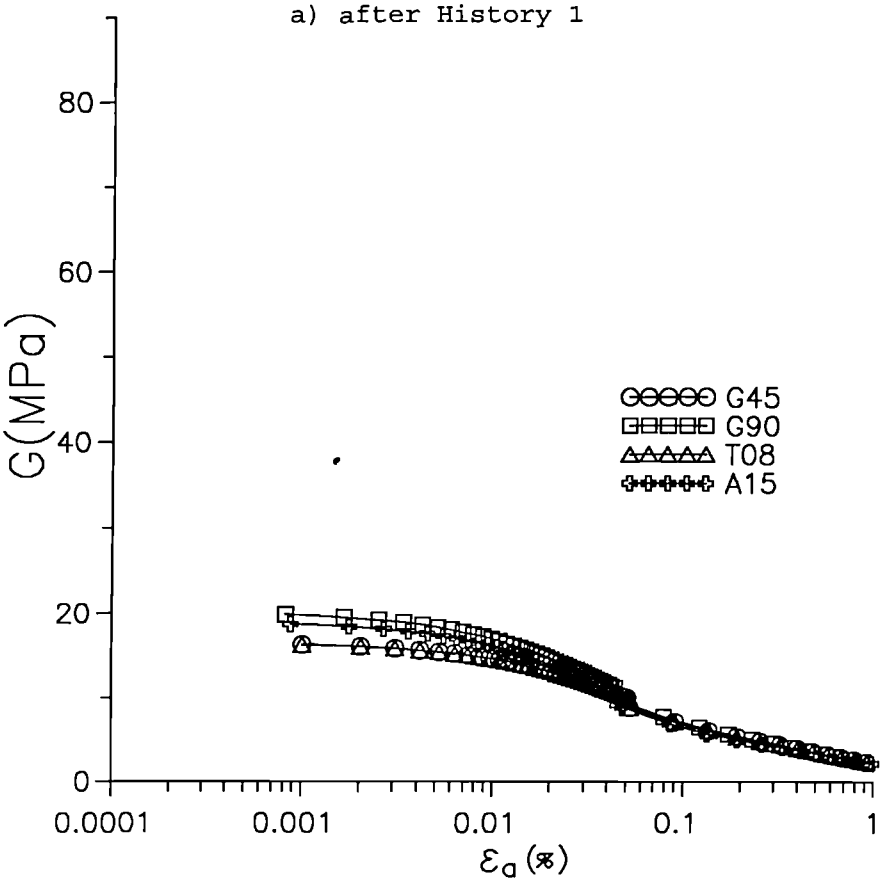

b) after History 2

Fig 6.3. Calculated tangent stiffnesses for undrained triaxial compression

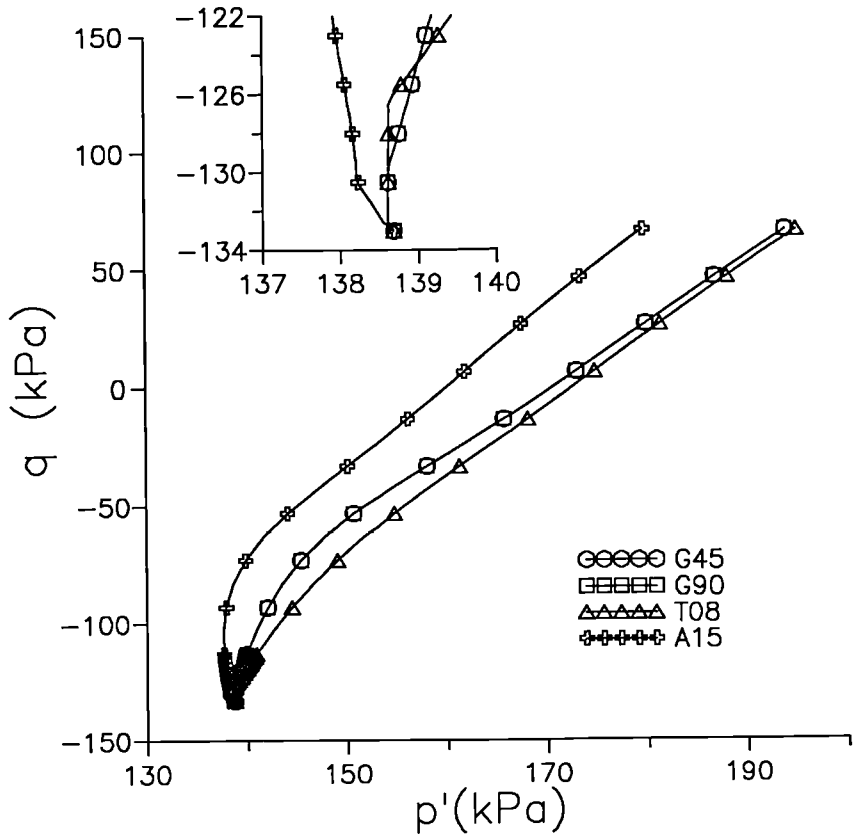

a) after History 1

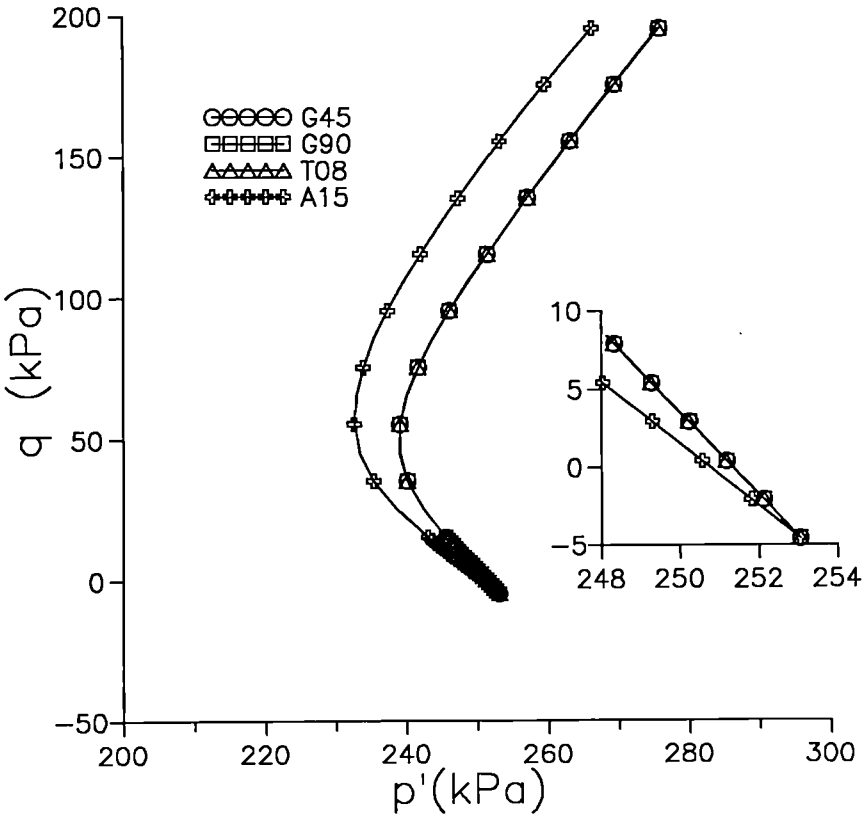

b) after History 2

Fig 6.4. Mobilised stress paths during undrained triaxial compression (note that the q and p' grid is distorted)

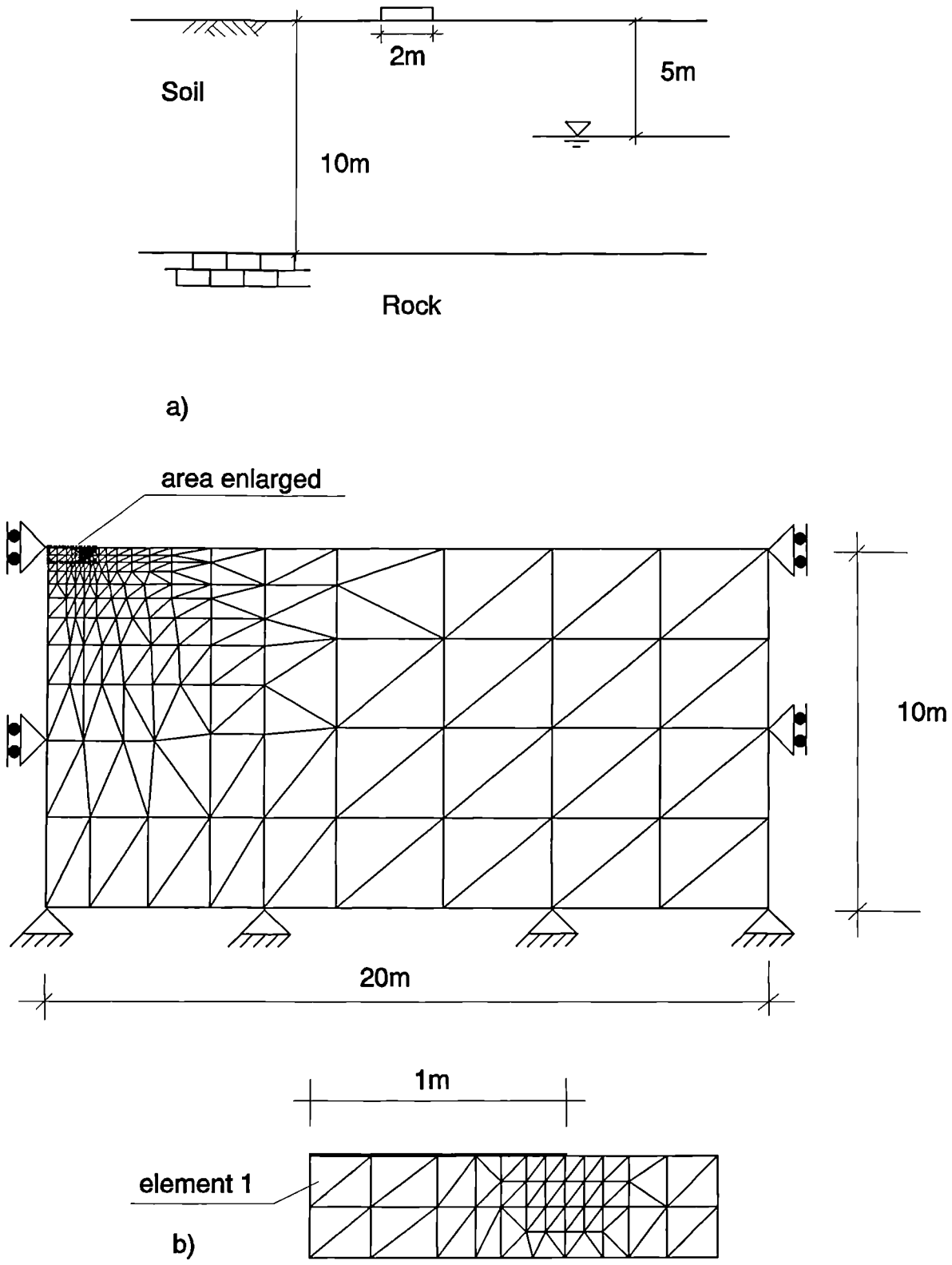

Fig 6.5. Geometry of the boundary value problem of the rigid foundation: a) ground conditions, b) finite element mesh

a - bounding surface

b - history surface

c - yield surface

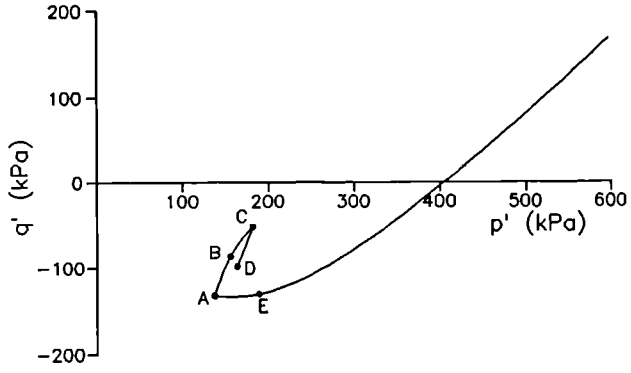

a) stress paths corresponding to 5m deep soil layer

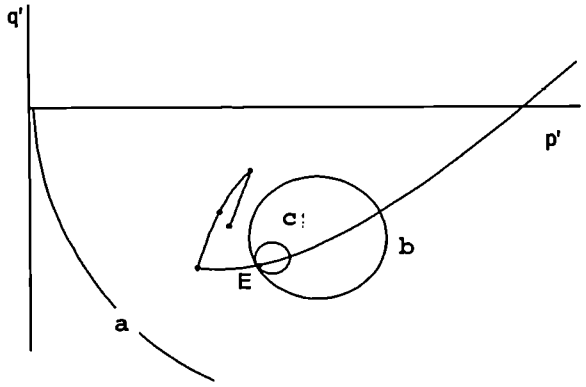

b) History E

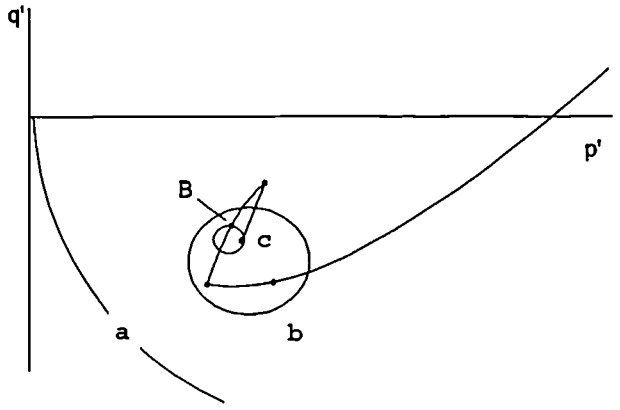

c) History B

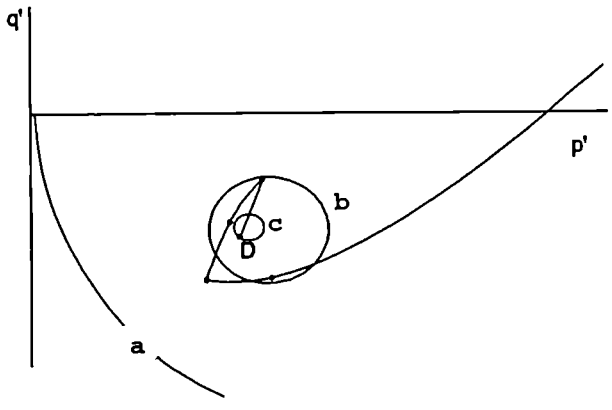

d) History D

Fig 6.6. Characteristic stress histories of an overconsolidated layer of London clay

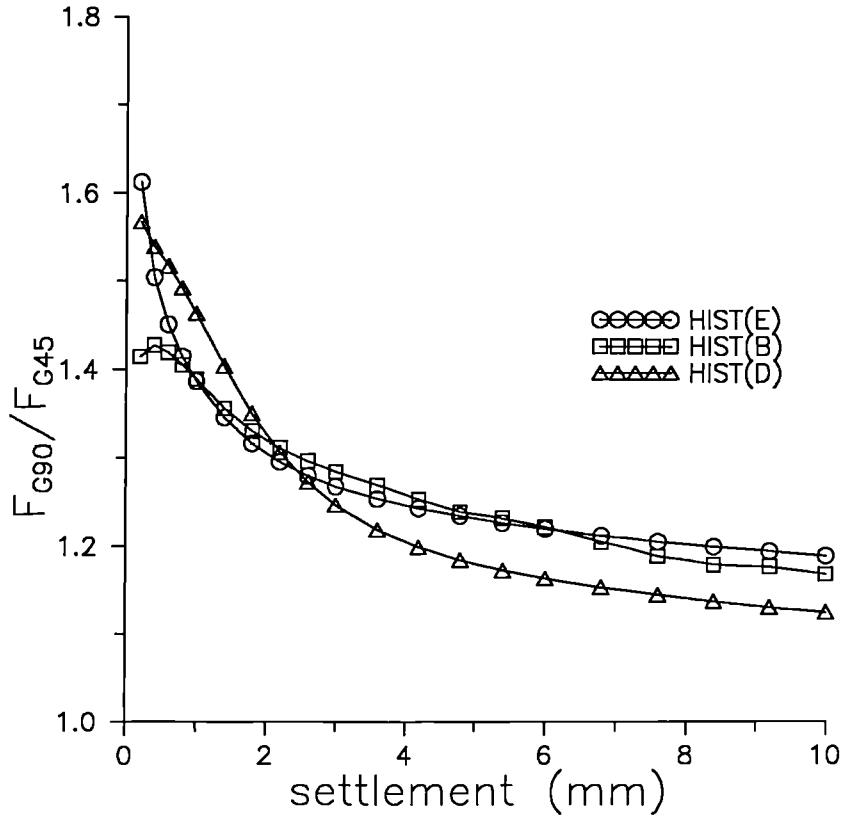

Fig 6.7. Comparison of mobilised foundation loads for materials G45 and G90

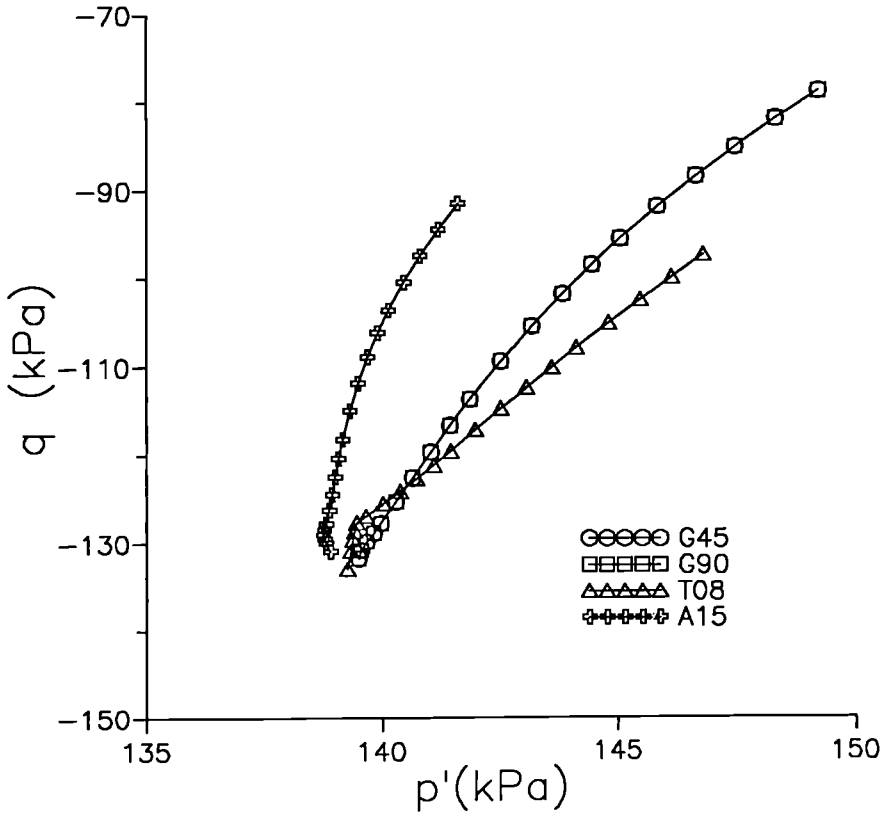

Fig 6.8. Mobilised stress paths in element 1 caused by foundation loading after History E (note that the q and p' grid is distorted)

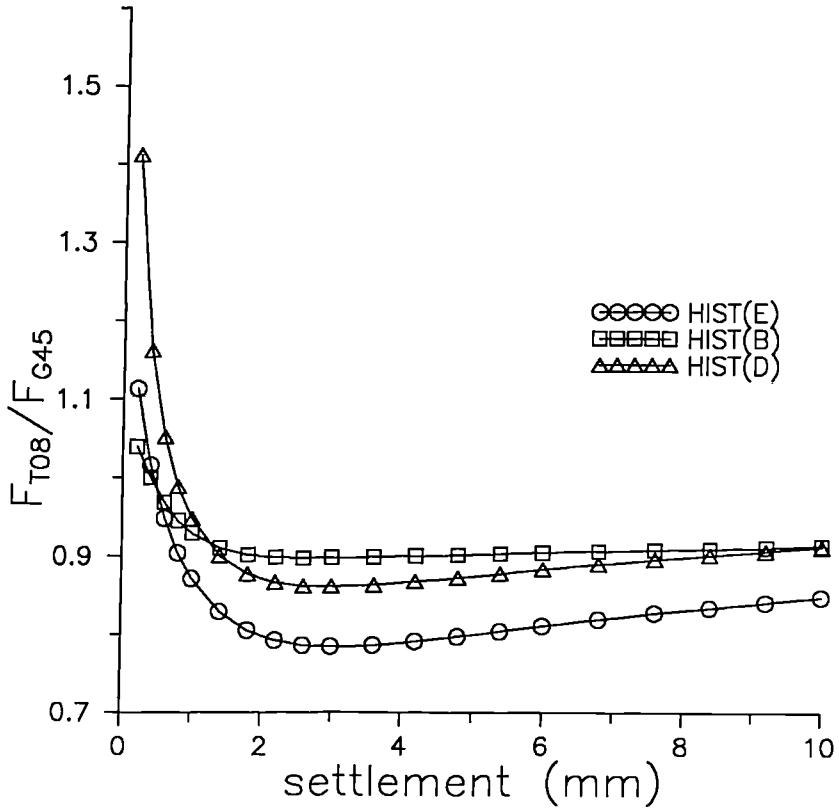

Fig 6.9. Comparison of mobilised foundation loads for materials G45 and T08

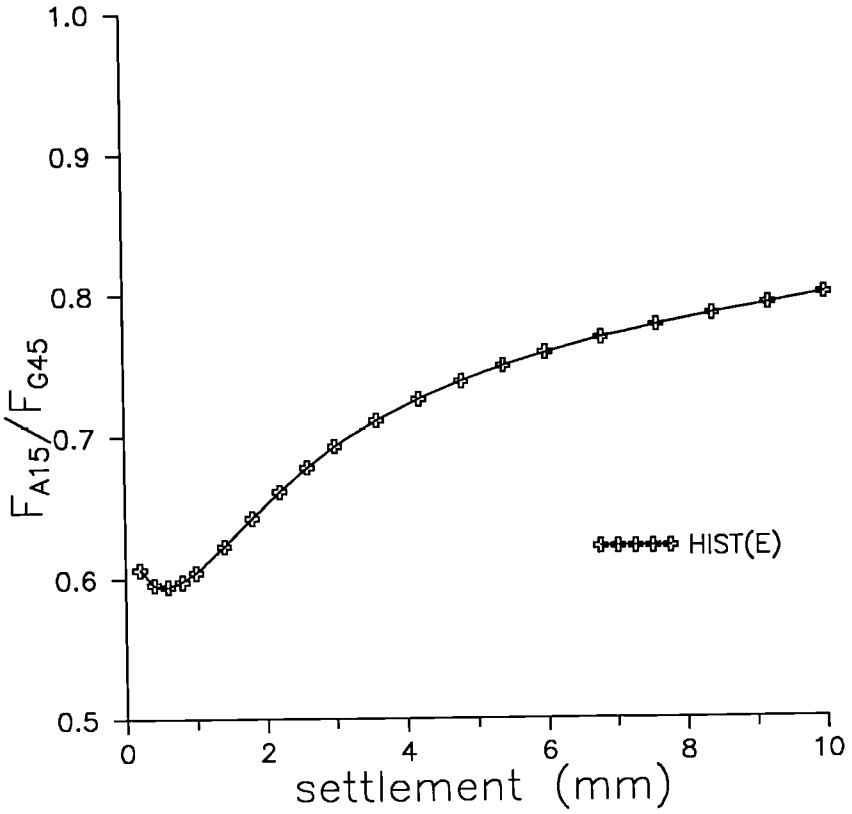

a) load ratio

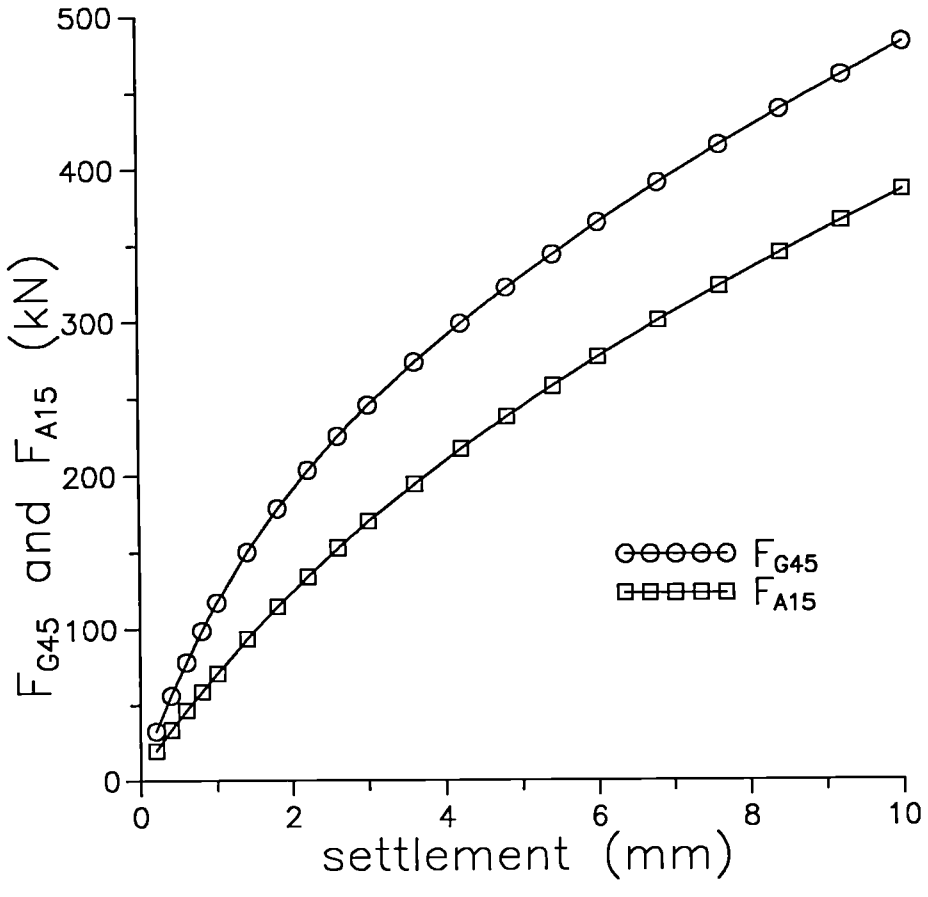

b) foundation loads

Fig 6.10. Comparison of mobilised foundation loads for materials G45 and A15

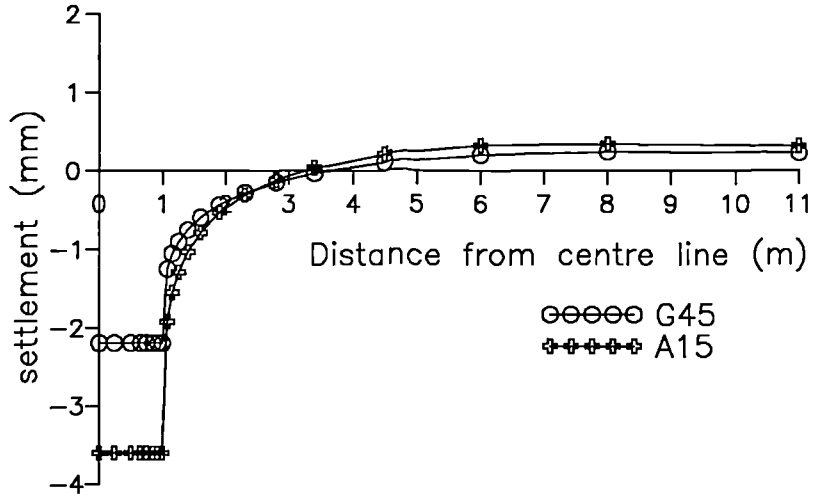

a) at the same foundation load

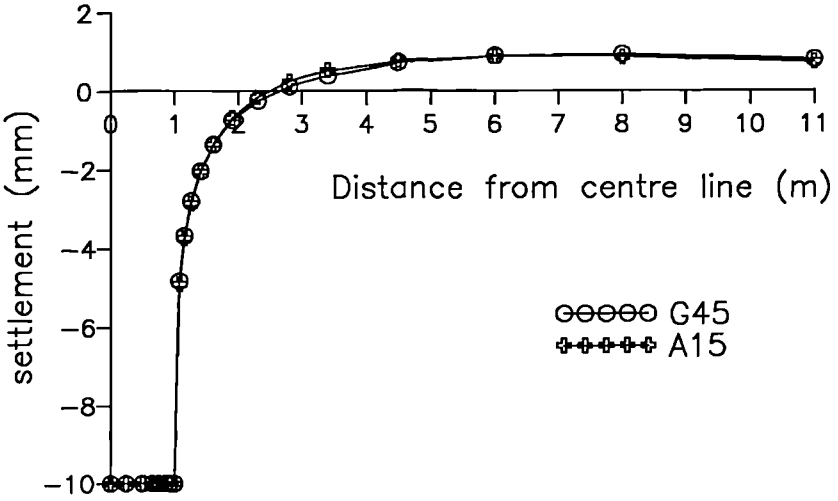

b) at the same settlement

Fig 6.11. Comparison of settlement profiles for materials G45 and A15: a) at the same foundation load, b) at the same settlement

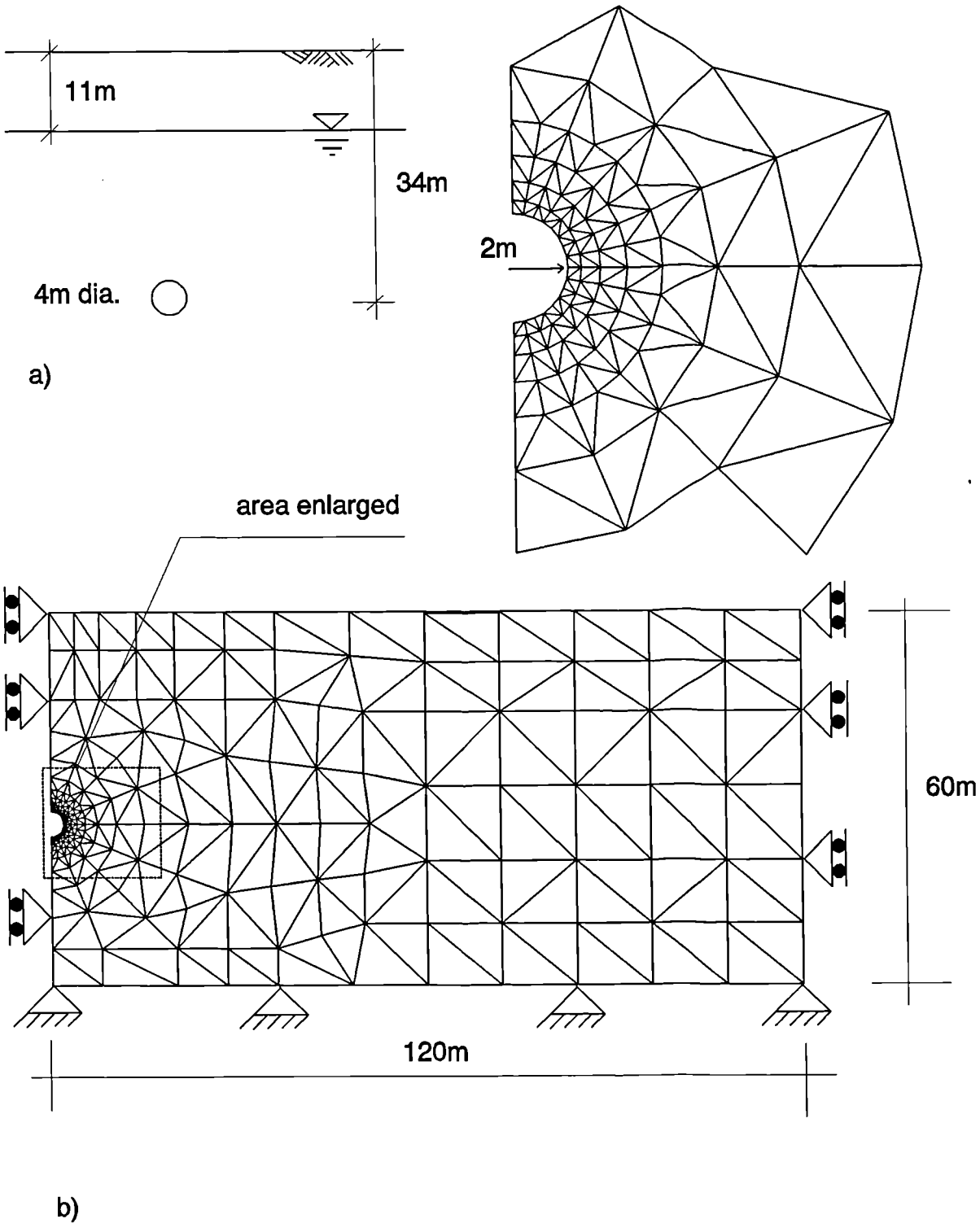

Fig 6.12. Geometry of the boundary value problem for the deep tunnel: a) ground conditions, b) finite element mesh

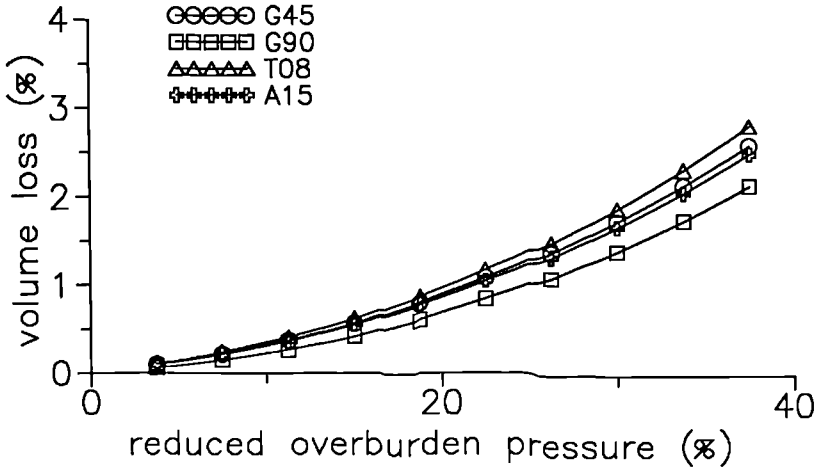

a) after recent stress history DTI1

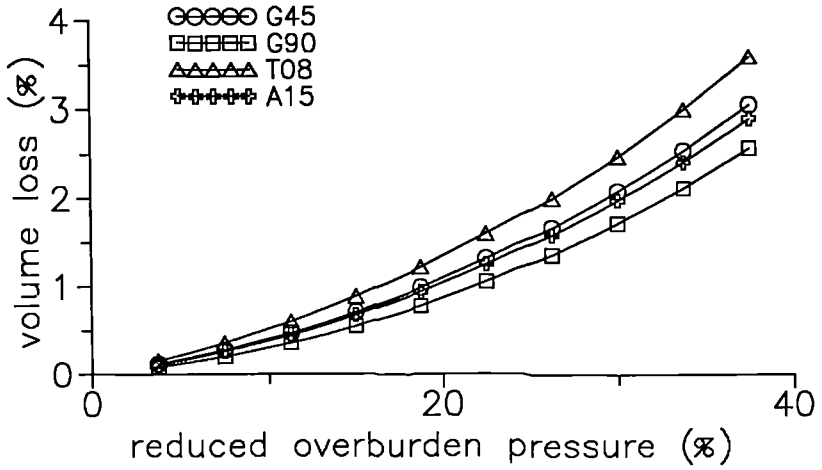

a) after recent stress history DTI2

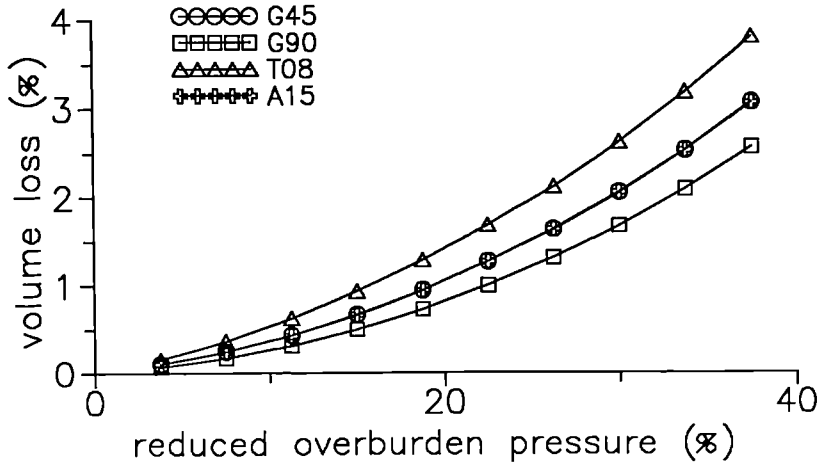

b) after recent stress history DTI4

Fig 6.13. Comparison of calculated volume loss against reduced overburden pressure for all materials

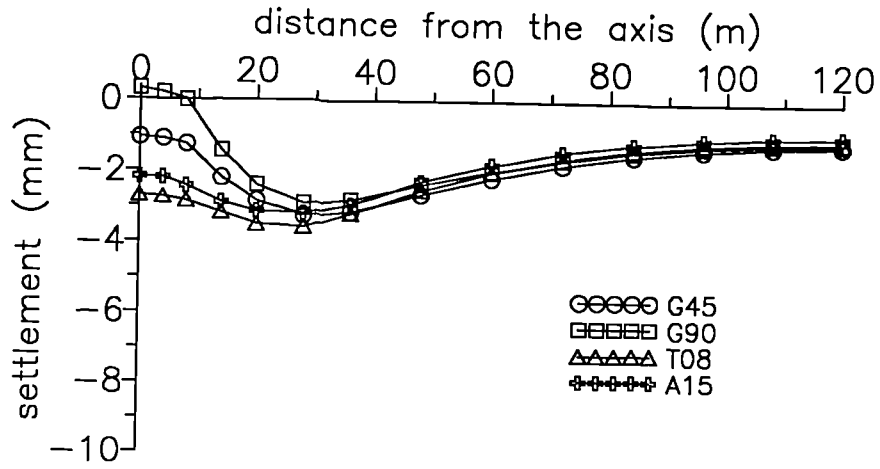

a) after recent stress history DTI1

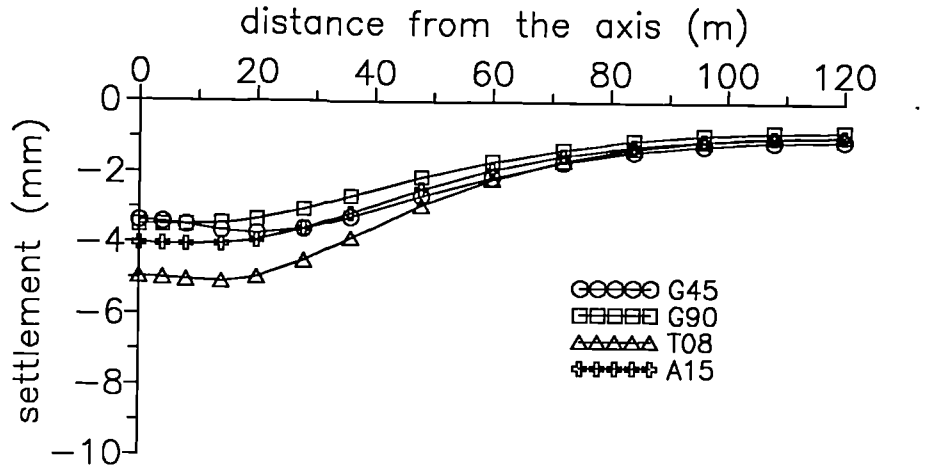

b) after recent stress history DTI2

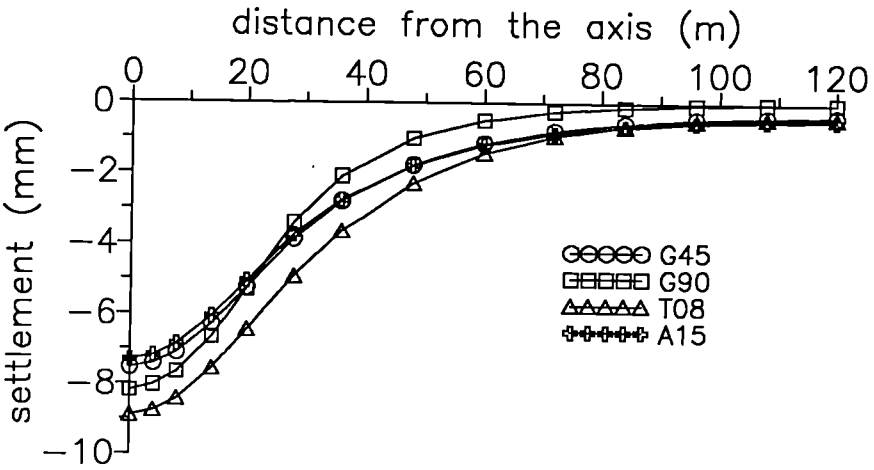

c) after recent stress history DTI4

Fig 6.14. Comparison of settlement profiles for all characteristic materials

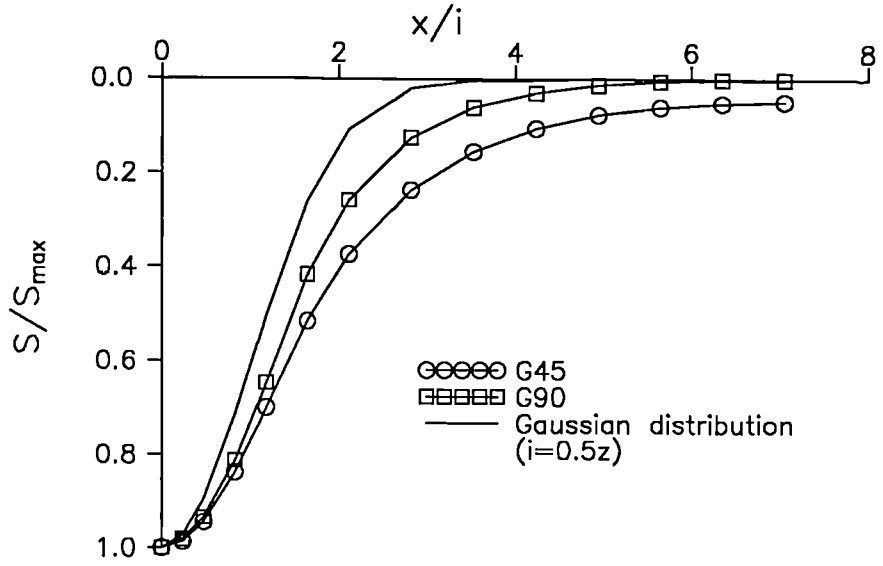

Fig 6.15. Normalised settlement profiles for materials G45 and G90 compared to Gaussian distribution for i=0.5z